UNIVERSITAT JAUME·I

DEPARTMENT DE QUÍMICA INORGÀNICA i ORGÀNICA

SUPRAMOLECULAR METALLOGELS FOR APPLICATION IN CATALYSIS

Metalogeles supramoleculares para su aplicación en catálisis

PhD thesis

Marco Filipe Cerqueira Araújo

Supervisor:

Beatriu Escuder Gil

Castellón de la Plana, June 2016

UNIVERSITAT JAUME·I

DEPARTAMENT DE QUÍMICA INORGÀNICA I ORGÀNICA

Beatriu Escuder Gil, Associate Professor at the Department of Inorganic and Organic Chemistry, Universitat Jaume I.

CERTIFY that the PhD thesis entitled "Supramolecular metallogels for application in catalysis" presented by Marco Araújo, has been developed under her supervision at the Organic Chemistry Section of the Department of Inorganic and Organic Chemistry, Universitat Jaume I.

Castelló, June 2016

Beatriu Escuder Gil

This work has been financed by the EU (Marie Curie ITN-Smartnet). Marco Araújo thanks EU for an ESR Marie Curie contract.

The main part of this work has been published up to date in the following papers:

Triazolyl-based molecular gels as ligands for autocatalytic 'click' reactions. M. Araújo, S. Díaz-Oltra, B. Escuder, *Chem. Eur. J.* - under press. DOI: 10.1002/chem.201600594

Tandem catalysis of an aldol-'click' reaction system within a molecular hydrogel. M. Araújo, I. Muñoz Capdevilla, S. Díaz-Oltra, B. Escuder. *Molecules* - Submitted

AKNOWLEDGEMENTS

Foram 3 anos em que coloquei todas as minhas forças para poder terminar com sucesso esta tese. No entanto, não sei se o conseguiria se não tivesse a ajuda dos mais próximos, que ainda que longe, me conseguiram sempre apoiar neste difícil e árduo objectivo. Quero agradecer assim a toda a minha família, sem excepção (pais, primos, tios, avós, irmãos) pelo apoio e preocupação, pelos momentos divertidos que tenho passado ao vosso lado e que sempre me ajudaram a recuperar a auto-estima e a ir buscar forças onde não tinha para terminar este trabalho. Não os consigo enumerar a todos senão tinha que escrever mais 3 páginas e passaria a chamar-se testamento em vez de agradecimentos. Agradeço também à minha namorada por me aturar nos momentos mais complicados, naqueles em que este trabalho me esgotava e eu desatava a resmungar, ou que me retirava todo o tempo e não sobrava nenhum para lhe dedicar. Aos meus amigos de Portugal, e vocês sabem todos quem são, um muito obrigado por sempre me suportarem, suportarem as minhas brincadeiras, as minhas desavenças, os meus exageros (sempre na brincadeira) e sobretudo, a minha hiperactividade característica!

Pido perdón por el primero párrafo de los agradecimientos estar en Portugués, ahora continuaré en un idioma intermedio entre el portugués y el español. Gracias a todos los que conocí entre Castellón y Vilafamés, dentro y fuera de la UJI. Gracias Juan y Bea, por me elegir para realizar este proyecto, por compartieren vuestro conocimiento y experiencia que me ayudaron a escribir esta tesis…AH, y por la parrillada organizada en el día de mi entrevista, que nunca me olvidaré. Bea, a ti un mucho "Obrigado" por siempre estar a mi lado y por todo el apoyo e consejos, sea a nivel personal o a nivel de trabajo, principalmente en los momentos más difíciles en que nada me salía. Gracias a mis colegas de laboratorio, Juanjo (Que espectáculo de pelotas, pero mejor aún son las "Girls in their summer clothes"), Carles (me debes unas colss…y lo sabes!), Jorge (el Gallego), Silviiiia ("La euskera"), Saaaanti (que pedazo de paciencia no?!), César (el compañero extranjero), Nishant (nos debes agradecer por enseñar al mondo la India, sino no estarías aquí), no olvidando la recién-llegada Ana Torres, por todos los momentos que hemos pasado durante estos tres años, tanto en el Laboratorio como en las comidas! Juanjo y Carles….Aiii Santa Barbara, sois el Patrimonio Mundial! Marta, que ahora estas lejos, gracias por aguantar-me durante todo el tiempo que te machaqué en el laboratorio, de verdad, no lo sé como no me pegaste una paliza…pero ya me conoces…soy portugués, non hay mucho que hacer! Compañeros de otros laboratorios, Ana, Raúl, Andreu, que aguantaron este personaje durante todo este tiempo, lo sé que muchas veces soy

insoportable pero así también tengo la certeza que nunca me olvidaran! Raúl y Ana, gracias por las caminatas y por los paisajes inolvidables, aunque el Gerês hay que visitarlo…pero todos juntos! Y a Paula, por la pelota y la bolsa del Vilareal, y por me aguantar forzosamente. Fabrizzio perché?? Voglio mi Panetone!!

A Tiago, João, e Nuno, el trio Portugués de Castellón, mis compatriotas, vos agradezco por todo menos por las noches del submarino!! Nuno, a ti, gracias por las "francesinhas" y por los momentos del café en que hablamos de tudo. Una frase para vos definir: Somos do Norte e basta carago!

A las personas que he conocido en Vilafamés, António, Helena, Javier, Rosa, gracias por todo el importante soporte que me han dado al largo de estos tres años en los cuales, aunque poco tiempo, he estado también con vosotros. Judith, José, Ana, Yolanda, Tony, David, Carlos, Jesús, Javi, Vicky, Inés, Rosa, Abel, gracias por me acoger con vuestra simpatía y compañerismo, por me ayudaren a pasar parte de las mañanas y me proporcionaren momentos de risa. A mi amicci de Italia: Annalisa, Arianna, Filippo, Giada, Saer, Marco, Luca, Andrea Cioni, Valentina, Parisa…Grazie mille a tutti e per tutto! Que lindo!!!

For the people of SMARTNET, thank you for the unforgettable moments at the meetings, everything finishes…but the best things will always stay! Jorge thank you for showing me the always incredible Pirineo..and for the "pollo con caracoles"! And specially, I would like to thank all the people from Bordeaux that was with me during the secondment. For the supervisors, Dr. André Del Guerzo, Guillaume, and my colleagues Kaars de Vet y Philip Schaffer, thank you for helping me with all the burocracies and with the always complicated microscope, without you my thesis would not be so long. Also from Bordeaux but out of the lab, thank you Frank, Pedro, Leire, Mathias, Philip and Kaars, for that funny lunches at the canteen, for that funny nights at the "Last Resort", and for all the unforgettable moments…Don't let this special group die!

Empecé en Portugués y voy terminar en portugués con un agradecimiento especial. Avô, a ti dedico este trabalho, obrigado por todo o suporte que me deste até aos dias de hoje, agora espero retribui-lo neste momento em que mais precisas!

Coragem meu Avô!

At the end of every hard earned day

people find some reason to believe.

Bruce Springsteen – Reason to Believe

TABLE OF CONTENTS

ABBREVIATIONS

1D	one dimensional
3D	three dimensional
abs	Absorption
Asc	Ascorbate
BnN_3	Benzylazide
BTTES	2-[4-{(bis[(1-tert-butyl-1H-1,2,3-triazol-4-yl)methyl]amino)methyl}-1H-1,2,3-triazol-1-yl]ethyl hydrogen sulfate
BTP	2,6-bis(1,2,3-triazol-4-yl)pyridine
Cagg	Concentration of aggregated material
Csol	Concentration of soluble material
CD	Circular dichroism
Cbz	Carboxybenzyl
° C	Centigrade degrees
Cu/C	Copper on charcoal
CuAAC	Copper(I) catalyzed azide-alkyne cycloaddition
DBC	Dibenzoyl-(*L*-)-cystine
DCC	Dicyclohexylcarbodiimde
DCU	Dicyclohexylurea
DDOA	2,3-didecyloxyanthracene
DIPEA	*N*,*N*-diisopropylethylamine
DNA	Deoxyribonucleic acid
DMS	Dimethylsulfate
DMSO	Dimethylsulfoxide
DYSA	Dynamic self-assembly

EtOAc	Ethyl acetate
EDS	Energy-dispersive X-ray spectroscopy
EDC·HCl	N-(3-dimethylaminopropyl)-N’-ethylcarbodiimide hydrochloride (EDC)
eq	equivalents
Exc	Excitation
Em	Emission
EtOH	Ethanol
FTIR	Fourier transform infrared spectroscopy
FRET	Förster resonance energy transfer
G’	Elastic (storage) moduli
G’’	Viscous (loss) moduli
GDP	Guanosine diphosphate
GNF	Glycosyl-nucleoside fluorinated amphiphiles
GTP	Guanosine-5’-triphosphate
h	hours
His	Histidine
HEPES	(4-(2-hydroxyethyl)-1-piperazineethanesulfonic acid)
HOMO	Highest occupied molecular orbital
ICP-MS	Inductively coupled plasma-mass spectrometry
LMW	Low-molecular-weight
LUMO	Lowest unoccupied molecular orbital
max	Maximum
m.g.c.	Minimum gel concentration
MeI	Methyl iodide
MeCN	Acetonitrile
MeOH	Methanol
MOF	Metal organic frameworks

NMR	Nuclear magnetic resonance
NHS	*N*-hydroxysuccinimide
OAc	acetate
overn.	Overnight
OctOH	Octanol
pKa	acidity constant
PB	Phosphate buffer
Pd/C	Palladium over charcoal
RNA	Ribonucleic acid
rt	Room temperature
STEM	Scanning transmission electron microscopy
SAXS	Small-angle x-ray scattering
SANS	Small-angle neutron scattering
S_N2	Bimolecular nucleophilic substitution
SEM	Scanning electron microscopy
T_2	Transversal relaxation time
TNA	Threose nucleic acid
t-BuOH	*tert*-buthanol
TBTA	tris[(1-benzyl-1H-1,2,3-triazol-4-yl)methyl]amine
TEM	Transmission electron microscopy
THF	Tetrahydrofuran
T_{gel}	Temperature of gelation
TRIS	2-Amino-2-hydroxymethyl-propane-1,3-diol
T_{sol}	Temperature of solubilisation
Tz	Triazole
UV-VIS	Ultraviolet-visible
XRD	X-ray diffraction

WAXD	Wide-angle X-ray diffraction

SYNTHESIZED GELATORS

CHAPTER 3 AND CHAPTER 4

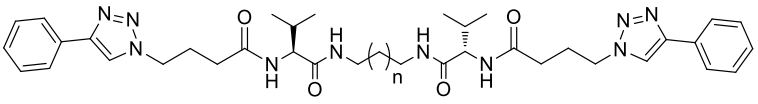

PhTzVal$_3$: n=1
PhTzVal$_6$: n=4
PhTzVal$_8$: n=6

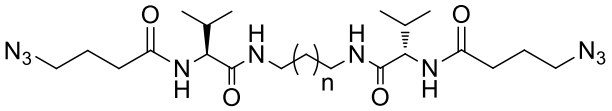

N$_3$Val$_3$N$_3$: n=1
N$_3$Val$_6$N$_3$: n=4
N$_3$Val$_8$N$_3$: n=6

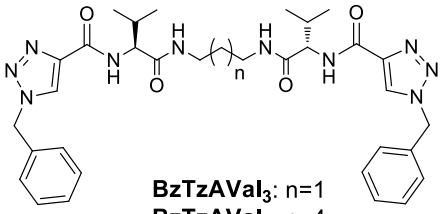

BzTzAVal$_3$: n=1
BzTzAVal$_6$: n=4
BzTzAVal$_8$: n=6

CHAPTER 5 AND CHAPTER 6

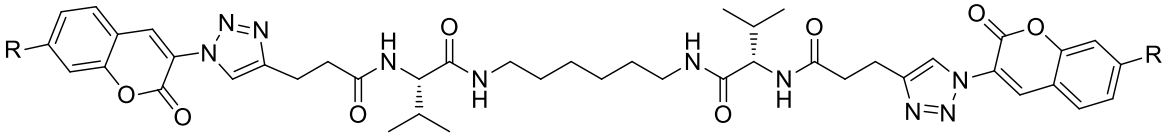

Et$_2$NAzTzVal$_6$: R= Et$_2$N
HOAzTzVal$_6$: R= OH

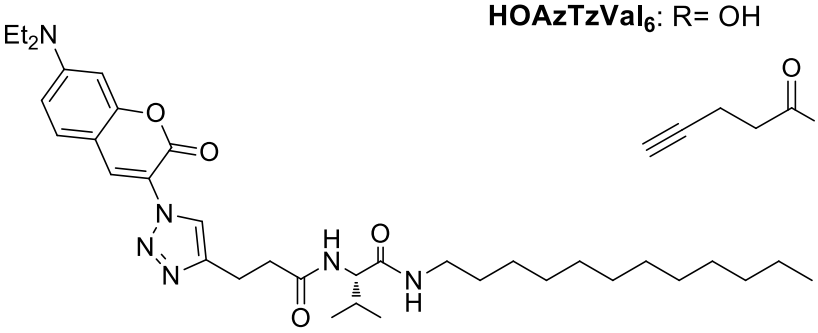

Et$_2$NAzTzVal$_{12}$

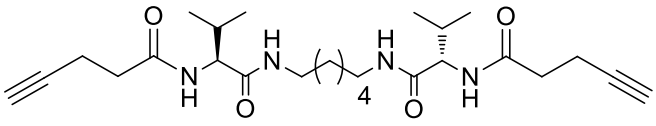

AlkyVal$_6$

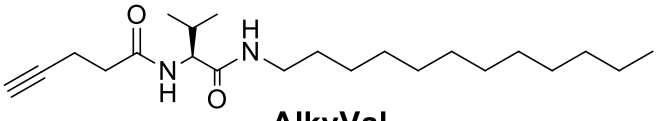

AlkyVal$_{12}$

RESUMEN

La tesis se enfoca a la aplicación de geles como catalizadores heterogéneos de la reacción de cicloadición 1,3-dipolar de Huisgen. Desde el descubrimiento del cobre (I) como catalizador de esta reacción, originando regioselectivamente triazoles 1,4-disubstituidos, la cicloadición azida-alquino catalizada con cobre (CuAAC) ha ganado bastante importancia en los campos de la ciencia farmacéutica y de materiales. La creciente importancia de la reacción en el campo industrial se debe tanto de las condiciones suaves de síntesis como a su robustez, originando los productos pretendidos con buen rendimiento y sin necesidad de purificación adicional.

Geles son materiales blandos metaestables con aspecto sólido y que no fluyen, siendo mayoritariamente líquidos en su composición. Estos materiales han atraído un gran interés científico debido a la posibilidad de ser obtenidos a partir de fuentes naturales o utilizando sencillos métodos de síntesis. Los geles están presentes en nuestro día a día, y engloban un considerable número de aplicaciones. Desde cosméticos, agricultura, espesantes de comida o constituyentes biomédicos, hasta telecomunicaciones o baterías, estos versátiles materiales blandos vienen ganando una gran preponderancia en el mundo actual. Dependiendo de las fuerzas que soportan su estructura auto-ensamblada, estos materiales pueden ser subcategorizados como geles químicos o geles físicos. Los últimos, específicamente los gelantes orgánicos de baja masa molecular (o geles moleculares), los cuales se auto-ensamblan con la intervención de interacciones no covalentes, figuran como el principal enfoque de esta tesis, atendiendo a su reversibilidad y su capacidad de responder a estímulos externos.

La tesis empieza con una introducción (Capítulo 1) que da una idea general de la definición, clasificación, propiedades y caracterización de geles. Ejemplos de aplicaciones generales de este tipo de materiales son también discutidos. Este capítulo prosigue con una breve definición de la química ‘click’ enfocada a la reacción de cicloadición 1,3-dipolar de Huisgen. El reciente descubrimiento de la variante catalizada por cobre (I) y su correspondiente mecanismo son presentados.

Los motivos que nos llevaron a la realización de esta tesis están enunciados en el Capítulo 2, con especial atención para las ventajas ambientales proporcionadas por la utilización de catalizadores heterogéneos. La parte principal de esta tesis está formada por cuatro capítulos enfocados a la aplicación de geles de baja masa molecular como catalizadores de la CuAAC.

El capítulo 3 describe el diseño y la síntesis de geles moleculares bolaanfifílicos funcionalizados con fragmentos catalíticos de feniltriazol (**PhTzVal$_n$**) o benciltriazol (**BzTzAVal$_n$**).

La influencia del fragmento catalítico en las propiedades de los geles y su actividad catalítica constituyen los principales temas de discusión. Los gelantes funcionalizados con el fragmento catalítico feniltriazol, separado del núcleo central derivado de *L*-valina por una cadena alquílica compuesta por cuatro átomos de carbono, exhiben una mejor capacidad de gelación en comparación con los gelantes en los cuales el fragmento catalítico benciltriazol se encuentra acoplado directamente al mismo núcleo central, siendo capaces de formar tanto organogeles en varios disolventes con diferente polaridad, como hidrogeles. Ambos tipos de gelantes demuestran capacidad para complejar el cobre (I), resultando en un aumento de sus propiedades mecánicas. Las propiedades termotrópicas y viscoelásticas dependen del el tamaño de la cadena de carbono del núcleo central derivado de *L*-valina. El gel bolaamfifílico que contiene 3 átomos de carbono como separador central de los fragmentos de *L*-valina presenta una mayor T_{sol} (definida como la temperatura necesaria para promover la transición gel → disolución) y mejores propiedades mecánicas, acompañadas de una mejor habilidad para gelar en disolventes polares. Además, los compuestos funcionalizados con el fragmento catalítico feniltriazol demuestran capacidad para catalizar su propia síntesis. Dentro de estos, el gelante que contiene una cadena de 3 átomos de carbono separando los dos grupos de *L*-valina que componen el núcleo central exhibe una peor actividad autocatalítica debido a su diferente empaquetamiento tanto durante el proceso de auto-ensamblaje como durante la reacción.

El Capítulo 4 trata de la aplicación del metalogelante funcionalizado con el fragmento de feniltriazol y conteniendo 3 átomos de carbono como separador central (**Cu(I)-PhTzVal$_3$**) y presentado en el Capítulo anterior, en la catálisis de un sistema multicomponente de las reacciones tándem aldol-'click'. El metalogel de cobre (I) demuestra capacidad para catalizar la reacción "one-pot" 'click'-aldol en un proceso auto-tándem, obteniéndose conversiones de 62% en dos días de reacción. La reacción puede ocurrir por dos vías distintas, dependiendo de la cantidad inicial de reactivos y de la competitividad de las dos reacciones del sistema. El mecanismo catalítico propuesto está basado en el comportamiento de las aldolasas tipo II, aunque la acidez de uno de los sustratos pueda contribuir positivamente para la catálisis de esta reacción de tres componentes. Este hidrogel catalítico puede ser utilizado como un catalizador heterogéneo tándem para sistemas de reacciones 'click'-aldol.

En el Capítulo 5 se describe el diseño y la síntesis de gelantes fluorescentes funcionalizados con azidocumarinas. Utilizando dos azidocumarinas sustituidas con un grupo dietilamino o hidroxilo, se ha intentado seguir la formación y auto-ensamblaje de un gel fluorescente utilizando la técnica de microespectroscopia confocal de fluorescencia. La reacción entre la azidocumarina que contiene el grupo dietilamino como sustituyente, y una red de dos componentes formada por un gel

alquino derivado de *L*-valina y un gel catalítico fluorescente que emite en la región azul del espectro electromagnético, resulta en la formación de un gel fluorescente que emite en la región del ciano. Se demuestra que el gel obtenido se forma exactamente sobre las fibras de la red catalítica, probablemente en los puntos de intersección entre el gel reactivo y el gel catalítico de la red de dos componentes. Sin embargo, el proceso de auto-ensamblaje es difícil de seguir por microespectroscopia confocal de fluorescencia en virtud de la fuerte emisión del fondo. Este sistema podría ser utilizado en la síntesis de materiales funcionales formados por una red de geles de dos componentes.

Finalmente, el Capítulo 6 está relacionado con la actividad catalítica de un gelante fluorescente anfifilico, derivada de su auto-ensamblaje dinámico. Los reactivos fenilacetileno y bencilazida son utilizados como "fuel" para activar el metalogel, promoviendo su desensamblaje y consecuente migración hace a la disolución. Este comportamiento dinámico se revela determinante para su actividad catalítica en la reacción 'click' modelo entre la bencilazida y el fenilacetileno, obteniéndose conversiones de 71% en apenas 3 h y en presencia de únicamente 1 mol% de catalizador. El rendimiento de la reacción puede ser seguido visualmente, una vez que el gel vuelve a su estado estacionario cuando se alcanza un rendimiento en torno al 50%. La posterior adición de "fuel" promueve la reactivación del gel en su forma catalítica. Según los experimentos de reutilización, el metalogel puede ser utilizado en dos ensayos consecutivos manteniendo su actividad catalítica sin necesidad de ser aislado entre cada ciclo catalítico. Este sistema disipativo puede ser aplicado como un catalizador dinámico heterogéneo para reacciones 'click'.

La tesis termina con un capítulo donde se describen las conclusiones generales extraídas de este proyecto de doctorado. Los gelantes de la familia **PhTzVal$_n$** demostraron capacidad para catalizar su propia síntesis, originando un sistema 'click' sostenible. El gelante **PhTzVal$_3$** merece especial atención debido a su capacidad para catalizar un sistema 'click'-aldol tándem. Entre los gelantes sintetizados, es importante destacar el gelante presentado en el Capítulo 6, el cual presenta mejor actividad catalítica para la reacción modelo 'click' que los gelantes bolaanfifilicos descritos en el Capítulo 3, aunque su reciclabilidad debería ser mejorada.

SUMMARY

This thesis focuses on the application of gels as heterogeneous catalysts for the Huisgen 1,3-dipolar cycloaddition. Since the discovery of that copper(I) could catalyse this reaction, producing regioselectively 1,4-dissubstituted triazoles, the copper(I) catalysed azide-alkyne cycloaddition (CuAAC) has been gaining a growing interest in the field of pharmaceuticals and materials science. The mild conditions and robustness of the reaction, giving the desired products in high yields and without the need of further purification are determinant characteristics for the increasing importance of this reaction in the industrial field.

Gels are metastable soft materials with a solid-like appearance which do not flow, being predominantly liquid in composition. These materials have attracted a tremendous scientific interest due to the possibility of obtaining them from natural sources or by simple synthetic methods. Gel materials are present in our daily life, covering a wide range of applications. From cosmetics to agriculture, food thickeners or biomedical constituents to telecommunications and batteries, these versatile soft materials have been gaining a growing preponderance in today's world. Depending on the forces responsible for their formation, these materials can be subcategorized in chemical or physical gels. Physical gels, specifically low molecular organic gelators (or molecular gels), which are commonly formed by non-covalent interactions that confer them with stimuli-responsive behaviour, are the main focus of this thesis.

The thesis starts with an introduction (Chapter 1) which provides a wide overview on the definition, classification, properties and characterization of gels. Examples of the general applicability of these soft materials in catalysis are also discussed. It proceeds with a brief definition on 'click' chemistry with a special focus on the Huisgen 1,3-dipolar cycloaddition reaction. The recent discovery of the copper(I) catalysed version of this reaction is presented together with its mechanistic catalytic pathway, as well as the its contribution in the synthesis of new materials is described.

The reasons that motivated the execution of this project are described in Chapter 2, with special focus on the environmental advantages brought by the use of heterogeneous catalysts. The main part of the thesis is composed by four chapters focusing the catalytic application of *L*-valine derived low molecular weight gelators to the copper(I) catalysed azide-alkyne cycloaddition.

Chapter 3 describes the design and synthesis of amino acid derived bolaamphiphilic molecular gels functionalized with phenyltriazole (**PhTzVal$_n$**) or benzyltriazole (**BzTzAVal$_n$**)

catalytic fragments. The influence of the catalytic fragment on the properties of the gels is discussed, as well as their catalytic performance towards the model 'click' reaction between benzylazide and phenylalkyne. The compounds bearing a phenyltriazole fragment separated from the central core by an alkyl chain with four carbons exhibit a better gelation ability in comparison with the ones bearing a benzyltriazole directly attached to the *L*-valine central core, being able to form organogels in a wide range of solvents with different polarity, as well as hydrogels. Both kinds of gels are able to coordinate copper(I), reinforcing the structure of the gels and allowing them to recover upon gel breaking. The thermotropic and viscoelastic properties of the gels change depending on the length of the carbon spacer on the *L*-valine central core. A higher T_{sol}, defined as the temperature needed to promote the transition gel → solution, together with an increased gel strength, as well as a greater tendency for the formation of gels in polar solvents is observed for the gel having a three carbon spacer in its structure. Furthermore, the phenyltriazole functionalized compounds present self-replicating behaviour, being able of catalysing their own synthesis. The gelator exhibiting three carbons as a spacer in the *L*-valine central core (**Cu(I)-PhTzVal$_3$**) showed the poorest autocatalytic activity, which was attributed to to its different structural packaging during the self-assembly process and during the reaction.

Chapter 4 refers to the application of this phenyltriazole metallogel bearing three carbon spacer (**Cu(I)-PhTzVal$_3$**), studied in the previous chapter, on the catalysis of a multicomponent aldol-'click' system. The copper(I) metallogel successfully catalyse the "one-pot" 'click'-aldol addition reaction in an auto-tandem like process, achieving conversions of 62% within 2 days reaction. The reaction may proceed through two different mechanistic pathways, depending on the competitiveness of the reactions. The proposed mechanistic pathway follows a biomimetic approach similar to that of type II aldolases, although the acidity of one of the substrates can also positively contribute to the catalysis of this three-component reaction. We therefore believe that catalytic hydrogel can be applied as a heterogeneous tandem catalyst for similar 'click'-aldol reaction systems.

On Chapter 5, the design and synthesis of azidocoumarine functionalized fluorescent gels is reported. Using two different azidocoumarines functionalized with diethylamino or hydroxyl groups, we tried to monitor the formation and self-assembly of a fluorescent gel by confocal fluorescent microspectroscopy. The coupling of the diethylamino substituted azidocoumarine through a 'click' reaction to a two-component gel network, composed by a *L*-valine derived alkyne gel and a fluorescent catalytic gel emitting in the blue region of the electromagnetic spectrum, results in the formation of a fluorescent gel emitting in the cyano region. It is demonstrated that the

newly formed gel grow exactly on the fibers of the catalytic network, certainly in the intercrossing points of the two-component reactant-catalyst networks. However, the process of self-assembly is difficult to follow by confocal fluorescent microspectroscopy due to the high emission coming from the background. Nevertheless, a two-component hybrid organic-inorganic material emitting on cyano and blue regions has been successfully obtained. This system can be used for the synthesis of functional two-component gel systems through 'click' reactions.

Finally, Chapter 6 deals with the dynamic self-assembly derived catalytic activity of a fluorescent amphiphilic gelator. The reactants phenylacetylene and benzylazide are used as fuels to activate the metallogel by promoting its disassembly and migration to solution. Such dynamic behaviour provide the gel with catalytic activity for the model 'click' reaction between benzylazide and phenylacetylene, achieving conversions of 71% in just 3 hours in the presence of 1 mol% catalyst. The yield of the reaction can be visually monitored, since the gel return to its steady state by a reassembly process when the yield of reaction is around 50%. Further addition of the fuel provide the reactivation of the gel into its catalytic form. Recycling experiments show that the metallogel can be used for two consecutive runs without any loss of catalytic activity and without the need of being isolated. This dissipative system can be applied as a dynamic heterogeneous catalyst for 'click' reactions.

The thesis ends with a chapter describing the general conclusions extracted from this doctoral project. The overall objectives of this thesis, which are specially focused on the synthesis of heterogeneous gel catalysts with activity for the Huisgen 1,3-dipolar cycloaddition were satisfactorily accomplished. The gelators from **PhTzVal$_n$** family showed ability to catalyse their own synthesis in a sustainable self-replicating 'click' reaction. Special attention is given to **PhTzVal$_3$**, which was able to catalyse a tandem 'click'-aldol system. Between the synthesized gelators, it is also important to highlight the amphiphilic gelator from **Chapter 6**, which presented better catalytic performance for the model 'click' reaction than the bolaamphiphilic ones presented in **Chapter 3**, although its recyclability should be improved.

Chapter 1

Introduction

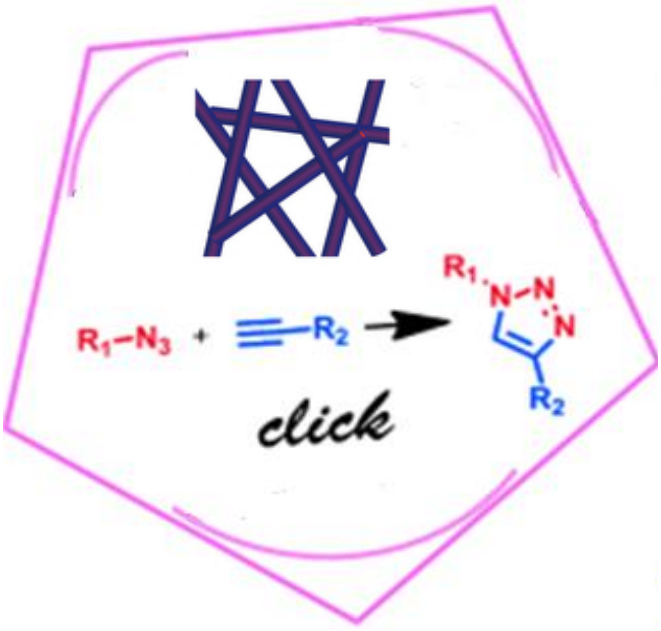

This introductory Chapter gives an overview of molecular gels and 'click' chemistry. It ends with a brief overview on the application of Huisgen 1,3-dipolar cycloaddition to supramolecular chemistry.

1.1. Gels: Definition, Classification and Formation

Among the materials that are present in our everyday life, gels occupy a prominent position. From foodstuffs such as confectionary to cosmetic products and lubricating greases, we are all familiar with the look and feel of jelly-like materials. Gels have a solid-like appearance and do not flow, being predominantly liquid in composition (**Figure 1**).

Figure 1. Examples of gels present in everyday life.

One of the most important and comprehensive definitions of gels was introduced by Paul Flory in 1974, who defined a gel as a two component colloidal dispersion exhibiting a continuous microscopic structure with macroscopic dimensions, which is permanent on time scale of analytic experiments, and that is solid-like in its rheology behaviour below a certain stress limit, despite of being mostly liquid.[1] Although not all the gel systems are colloidal in nature, one can consider that all the gels consist of a solid three-dimensional matrix, which is constructed by the crosslinking of polymeric strands of (macro) molecules by physical or chemical forces, in the presence of bulk gas or liquid phases.[2] The viscoelastic, solid-like macroscopic appearance of a gel is the result of the entrapment of the bulk gas or liquid phase (solvent) in the interstices of the 3D elastic network of gelator molecules through surface tension and capillary forces.[3]

In analogy to folded proteins, the fibrous network of the gels can be divided into primary, secondary and tertiary structures. The primary structure (Å-nm scale) derives from the anisotropic aggregation of gelator molecules in 1D architectures. The formation of primary rod-like structures (1D aggregates) is determined by molecular level recognition and their characteristics depend on the influence of the ratio of cross-sectional areas of hydrocarbon chain (if present), polar moiety of the gelator and polarity of the solvent. These primary structures further self-assemble to form aggregates (nm-µm scale) that might acquire several morphologies, such as sheets, ribbons, vesicles, micelles, fibres. The transition from the secondary to tertiary structure (µm-mm scale),

which occurs through the formation of an extended network that entraps the solvent, is dependent on the strength and type of interactions between the individual aggregates. Factors affecting gelation include solvent nature, polarity, molecular shape of the gelator, temperature, and the possible participation of co-surfactants. These factors are determinant to describe the gelation process.[4,5]

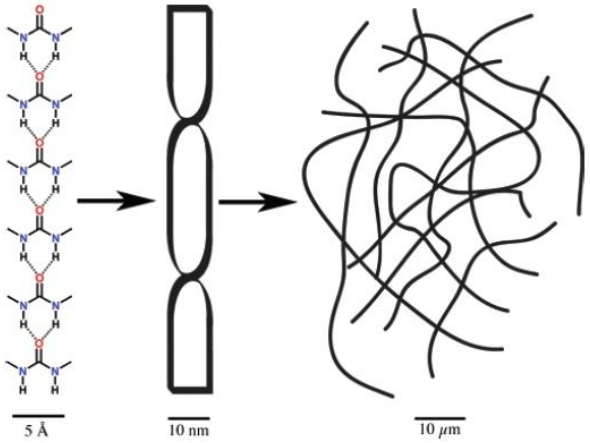

Figure 2. The primary, secondary and tertiary structures of a self-assembled physical gel.[4]

Gels may be classified either according to their source (natural or artificial), or according to the solvent entrapped by the 3D porous gel network. Regarding the solvent, a gel may be formed in water (hydrogel), in an organic solvent (organogel) or in air (aero- or xerogel).

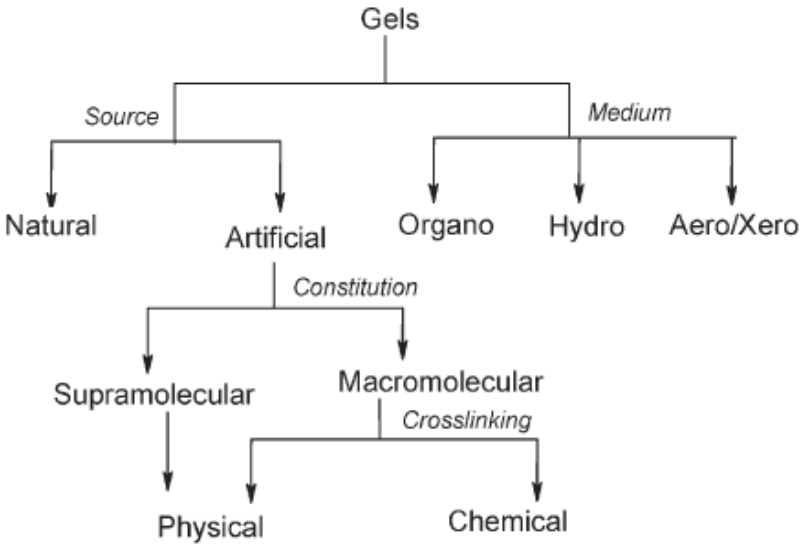

Figure 3. Classification of gels.

The non-covalent interactions required to promote gelation are also dependent on the solvent. Thus, while in the case of organogels gelation is commonly achieved by dipolar interactions, such as specific and directional hydrogen bonding or metal coordination, in hydrogels the solvophobic effect is reiterative the main driving force for gelation.[6]

The strength and type of interactions that assist the self-assembly allow the classification of these soft-like materials into two types: chemical gels and physical gels. In chemical gels, the formation of the 3D network occurs through covalent crosslinking of its components, usually resulting in a permanent network structure (crosslinked polymer gels). Although in some vinyl polymers such as polystyrene and poly(methylmethacrylate) with high stereoregularity the final structure may be reversible, this represent very rare cases in literature and their gelation ability is relatively low.[7]

On the other hand in physical gels, the self-assembling process is driven by non-covalent forces, such as hydrogen-bonding, Van der Waals, charge transfer, dipole-dipole, π-π stacking and coordination interactions. In this group, it is important to define molecular gels, which are nanostructured soft materials formed by anisotropic aggregation of low-molecular-weight (LMW) molecules into 1D architectures, that further self-assemble into 3D fibrillar networks (supramolecular polymers) that percolate the solvent, and supramolecular polymer gels, which are resultant from the physical aggregation of polymer chains.[8,9]

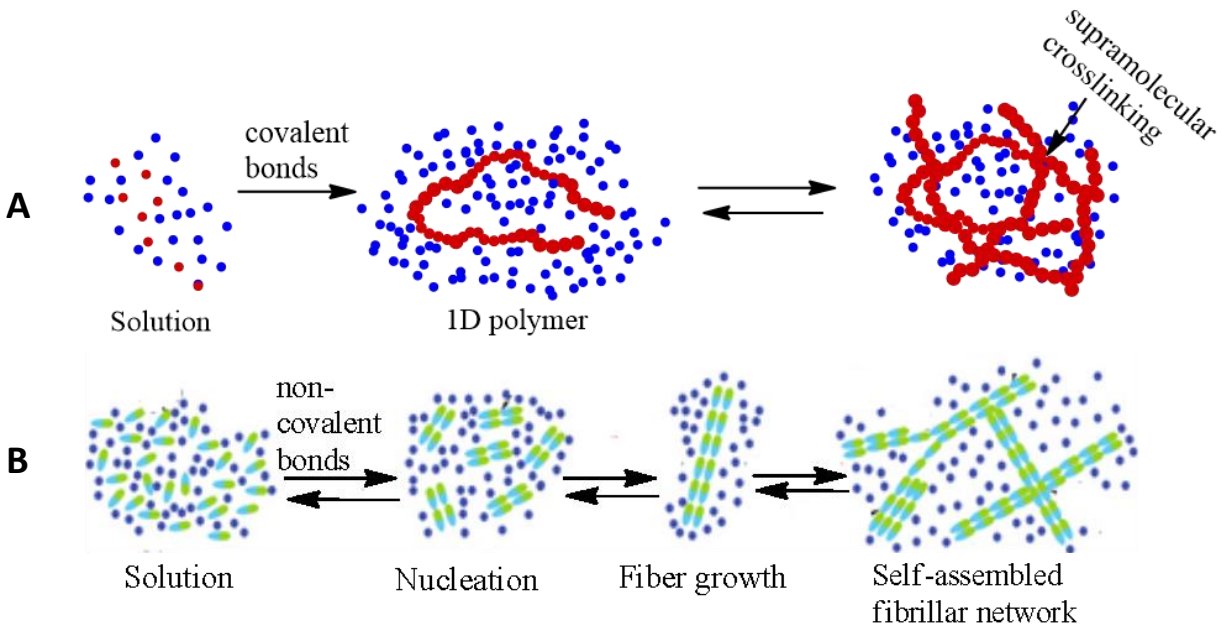

Figure 4. Formation of a polymer gel (A) and molecular gel (B).

In the last decade, gels derived from LMW compounds (M < 3000 Da) have attracted great interest due to several reasons:[10]

- Big diversity of gelator-structures is accessible by standard synthetic methods.
- Many gelators derive from natural sources (proteins, amino acids, sugars…) and thus, are potentially biocompatible and biodegradable. The non-covalent forces that sustain their

three dimensional network is also determinant for their biocompatibility and biodegradability.

- Molecular gels are thermo-reversible, exhibiting a reversible sol-to-gel transition and providing the possibility of re-establishing internal monomeric bonds after chain rupture.
- Very low minimum gelation concentrations can be found.
- High tolerance towards the addition of salts and other additives.
- May be thixotropic – show reversible sol-gel transition under isothermal sharing stress followed by rest.

Between all these properties, the facile functionalization of these compounds by common synthetic chemistry is regarded as a key feature towards the fabrication of advanced smart materials. Many gelating agents that incorporate photo-sensitive, pH-sensitive or molecular recognition moieties may be directed to high-tech applications ranging from regenerative medicine to electronic devices. Controlled drug release, optoelectronics, regenerative medicine, catalysis, molecular recognition and sensing are just few examples of the wide range of fields that can be attained by self-assembled supramolecular nanostructured gel materials.[11,12]

1.2. Molecular gels: Self-assembly, Properties and Characterization

The usual method for the formation of molecular gels comprises dissolution of the gelator in hot solvent and subsequent cooling to a given temperature, obtaining a supersaturated solution. While cooling, such supersaturation causes a rapid assembly of the molecules into elongated fibres of dimensions around 5-100 nm diameter, which further aggregate into a 3D entangled network.[13] Although this constitutes the most common procedure of gelation, other stimuli including ultrasound, pH-gradient or the use of enzymes may also be applied to obtain such self-assembled structures.[14]

During the standard process of gel formation, poorly organized metastable aggregates can be formed upon cooling, which in turn can be corrected into thermodynamically more stable and highly organized gels or crystals. Because the resultant materials may contain large crystals in coexistence with fibrous network, gelation is often regarded as a kind of frustrated crystallization. The fact that the formation of molecular gels is not directly related with the minimum energy that the gelator/solvent mixture can exhibit allow us to describe gels as metastable solid-like materials, whose formation is governed by kinetics and thermodynamics.[15,16]

In the case of a fibrous network, the fibre formation by self-assembly of small molecular building blocks occurs via a crystallization mechanism, which involves a phase separation, followed

by nucleation and growth steps.[17] For example, kinetic studies on an organogel derived from glutamic acid reveal that the mechanism involves nucleation-growth-branching-growth-branching, meaning that the end of each branch acts as a nucleation site from which *n* branches grows out.[18]

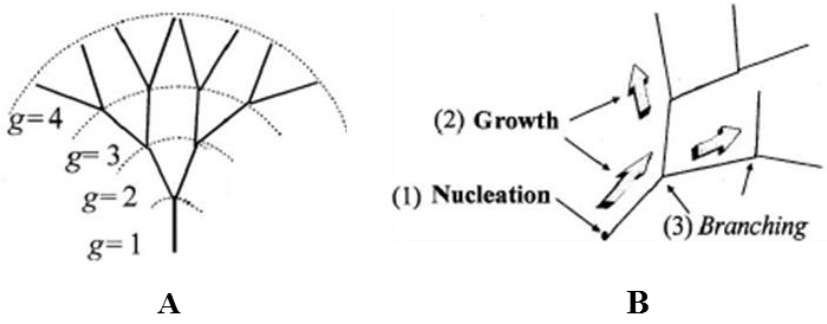

Figure 5. Illustration of the usual Cayley fractal tree, characterized by branches of length ξ exhibiting a distance l (A) and representation of fractal growth mechanism of organogel nanofibers from a glutamic acid derived organogelator (B).[18]

Thus, it can be considered that the elongated shape of fibres arise from a strong anisotropic growth process. The difference between the surface free energy of fibres and crystals, derived from the large interfacial area of fibrous network, together with the difference in lattice energy arising from fiber defects or different packing within fibres are on the basis of the metastable character of the gels.[18]

The different superposition of the fibres and the resultant network morphology may highly influence the thermal and viscoelastic properties of the final gel materials. The thermoreversibility of gels formed by the standard heating-cooling method allows the identification of characteristic temperatures related with the assembly and disassembly processes. By applying simple visual inspection techniques, such as dropping ball technique, bubble motion or the popular inverted test tube method, characteristic viscosity points such as the temperature at which the gel is formed (T_{gel}) and the one at which the gel loses its structural integrity (T_{sol}) may be identified. These temperatures are dependent on the structure of the gel, nature of the solvent and total concentration of the gelator.[19]

The mentioned methods may also be applied to determine the minimum amount of gelator required to achieve the formation of a gel network capable of entrapping a specific solvent, defined as the minimum gelation concentration (m.g.c.). This parameter is the result of two different contributions, namely the concentration of material required for the formation of 3D network (C_{agg}) and the concentration of gelator molecules that remain in solution (C_{sol}). The later (C_{sol}), may be determined by ^{1}H NMR, using a concentric tube with an internal reference of known concentration.[20]

Another important characteristic of a gel is related with its mechanical stability, which can be assessed by rheology. Rheology is defined as the science of deformation and flow behaviour, and is related with the response of a material to an applied stress.[21] In rheological experiments, the gel is subjected to an oscillatory stress, and the response of the material is measured in terms of elastic (storage) *G'* and viscous (loss) moduli *G"*. This technique gives an insight on the relaxation and lifetime of the non-covalent bonds between gelator molecules, allowing to distinguish between hard gels, where $G' >> G"$ at all frequencies, and soft gels, where $G' > G"$ at high frequencies and $G' < G"$ at low frequencies (larger time scales). The gel point, defined as the point at which *G'* starts to exceed *G"*, may be also determined by using rheology.[5,22]

Rheology studies may be also complemented with microscopy techniques such as scanning electron microscopy (SEM) or transmission electron microscopy (TEM) in order to relate the viscoelastic properties of the gel with the morphology of the fibre network.

Crystallographic techniques such as small angle X-ray scattering (SAXS), small angle neutron scattering (SANS) or single-crystal X-ray diffraction may also give an insight on the size, morphology and supramolecular arrangement of the fibres.[23] However, the presence of defects on the fibres or the difficulty on obtaining a crystal highly limits the use of such methods. As a result, powder X-ray diffraction (XRD) of lyophilized gels is commonly used to obtain some information on the structure of a gel and organization of the fibres, allowing the assignment of simple phases such as lamellar or hexagonal phases. Furthermore, if the WAXD patterns of the crystalline and gel states are comparable, it can be concluded that they acquire a similar supramolecular organization, allowing the construction of a crystal structure that represent the structural arrangement of the gel upon self-assembly.

Additionally, Fourier transform infrared (FTIR) and Raman spectroscopies also provide information about the supramolecular arrangement of the gel, by allowing the study of hydrogen-bonding interactions. NMR may also be used for this purpose, although in the gel phase very broad signals are obtained due to the large correlation time of the assemblies and very short transversal relaxation times T_2.[24]

1.3. Molecular gels in catalysis

Catalysis is regarded as an indispensable tool in the synthesis of both simple and highly complex molecules and polymers, ranging from milligram lab scale to multiton industrial processes.[25] In the field of catalysis, the use of heterogeneous catalytic systems is regarded as a greener and environmentally friendly alternative to homogeneous catalysts attending to their

characteristic recyclability.

Among the wide range of materials applied in heterogeneous catalysis, gels have attracted great interest as reaction containers and catalytic systems. The heterogeneous two-phase nature of gels provides a large and highly active surface area between gel fibres and entrapped solvent, which may make the functional catalytic groups more accessible to substrates. Furthermore, the high porosity of the 3D network provides viscoelastic and dynamic support, and facilitates the accessibility of small reactants to the highly solvated network, allowing fast diffusion of the substrates to the catalytic active sites.[26] Additionally, the organization of the multiple catalytic sites in the fibre surface could generate additional catalytic features, such as multivalent interactions, neighbouring effects and cooperativity. On the other hand, the high degree of molecular order may induce regio- and stereoselective transformations.[26] Another interesting feature of gels is that the differences in polarity between the solvent pools and inner regions of the fibres may lead to substrate selectivity.[27] Finally, the amphiphilic nature of the gel environment may provide better solubility and separation of substrates and products.[28]

The well-defined way of self-assembly of molecular gels and possibility of tuning this process, together with their dynamic nature providing reversible gel-to-sol phase transitions, constitute major advantages over polymer gels, potentiating their application in catalysis. Miravet, Escuder and their co-workers demonstrated this concept by tuning the *pKa* of stimuli-responsive molecular gels through sol-to-gel phase transition. Such highly organized self-assembly process allowed control of the orientation of existing reactive or catalytic groups, bringing them into critical proximity. Such feature could have a strong impact in reactivity when compared to homogeneous phase or less structured polymer-based gels.[29]

Focusing on their application in catalysis, molecular gels can be classified into two categories, depending whereas the catalytic centre is a metal (metallocatalyst) or just an organic catalytic fragment (organocatalyst). Regarding metal loaded gels (metallogels), they can be divided into three different groups depending both on the influence of the metal on the aggregation process and on the initial presence/absence of metal. The metal may constitute the main driving force for self-assembly (self-supported metallogels) or may be posteriori added to a fibrillary network constructed with free ligand sites (supramolecular multitopic ligands), or alternatively may be already present in the gel structure (organometallic gelators).

A relevant example of organocatalytic gels has been reported by *Guler et al.*, who described a His-containing peptide that formed a hydrogel capable of catalysing ester hydrolysis reaction.[30] In this work, the authors have shown that the nanofibers had an important role in the catalytic process, due to the high density of catalytic sites on their surface. Since then, important achievements in the

application of amino acid-based gelators to catalysis have been reported by the group of Miravet and Escuder. One of their most relevant works is related with the preparation of molecular gels with pendant *L*-proline moieties attached to a *L*-valine based gelator scaffold and their application as efficient catalysts in the base catalysed Henry nitroaldol reaction between nitromethane or nitroethane and 4-nitrobenzaldehyde or 4-chlorobenzaldehyde (**Figure 6**).[31]

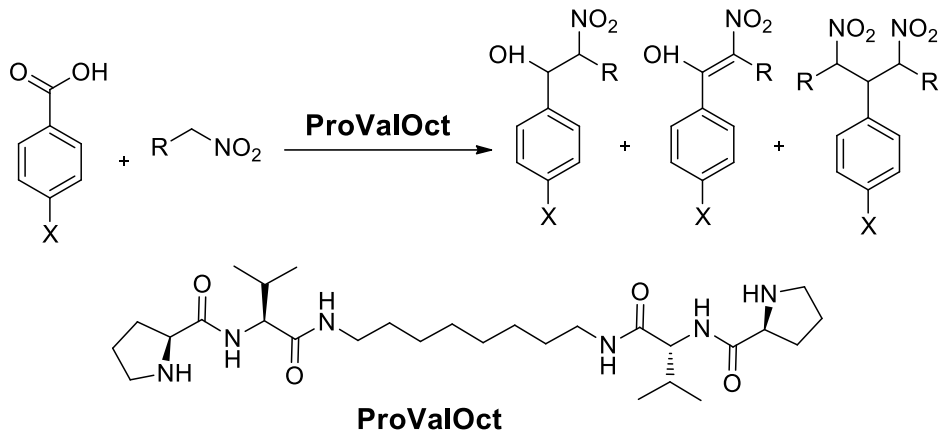

Figure 6. Henry nitroaldol reaction and structure of the bolaamphiphilic catalytic gelator.

The authors observed that in the presence of the gel the *L*-proline fragment acted as a basic catalyst, promoting the nitroaldol reaction by an ionic pair type mechanism, which is initiated by nitroalkane deprotonation (**Figure 7**). In this work, a quantitative conversion of the aldehyde to the corresponding nitroalkane was achieved only in the presence of the gel, whereas in solution low conversions and presence of byproducts resultant from dehydration and conjugated addition to nitroalkane have been detected. It was found that the self-assembly of these bolaamphiphilic gelators produced an enhancement in basicity, probably due to cooperation of *L*-proline moiety.

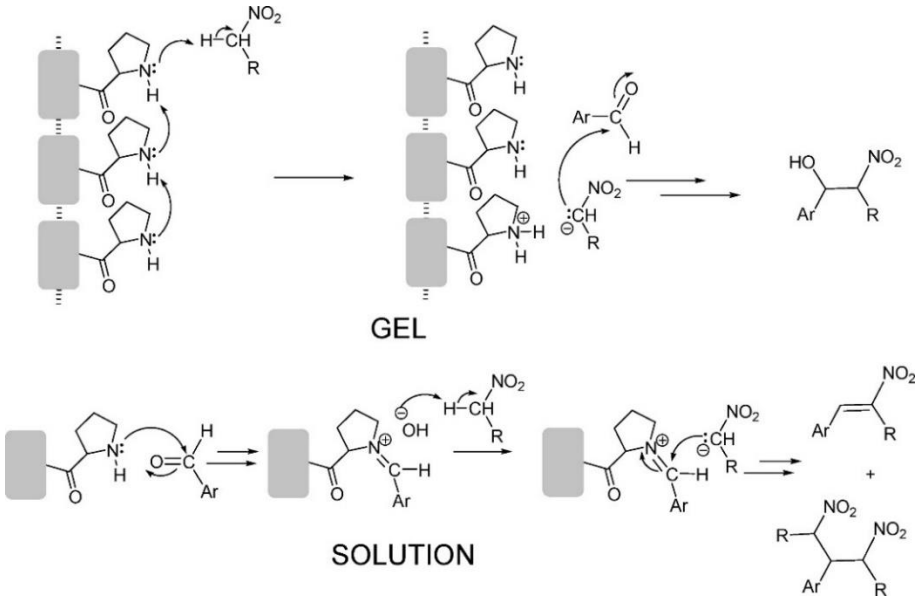

Figure 7. Proposed catalytic mechanism followed by the self-assembled gel and in solution.[31]

Taking advantage of the catalytic ability of *L*-proline in aldol reactions, the same group described the synthesis of a *L*-proline functionalized amphiphilic gelator and its application as an efficient heterogeneous catalyst in the direct aldol reaction between cyclohexanone and 4-nitrobenzaldehyde, obtaining the desired product with high stereoselectivity. The gel catalyst could be recycled and used up to three runs without significant loss of catalytic activity.[32]

In the field of metallocatalysis, the first gel systems developed were based on pyridine based ligands. Exploring the high affinity of pyridine ligands to coordinate palladium, *Xu et al.* developed a series of catalytic metallogels which were formed irreversibly in DMSO *via* the creation of cross-linked three dimensional coordination polymer networks promoted by the coordination of multidentade ligands to the Pd(II) centre.[33] These coordination polymer gels were successfully applied as catalysts for the aerobic oxidation of benzyl alcohol to benzaldehyde, being able of increasing the reaction rate two fold in comparison with the same reaction carried in the presence of the palladium salt $Pd(OAc)_2$. The reason for this higher catalytic performance was attributed to the higher stability of the gel-Pd(II) catalysts. Pyridine-based molecular gels have also been developed as supramolecular multitopic ligands, in which the fibrillary network can be constructed either in the presence of the metal or before its introduction. An interesting example of this kind of gelators was reported by Miravet, Escuder and co-workers, who developed *L*-valine derived gelators functionalized with a pyridine fragment, which were able to form organogels and pH-responsive hydrogels supported by the formation of a dimmer structure stabilized by four intermolecular hydrogen bonds (**Figure 8**).[34]

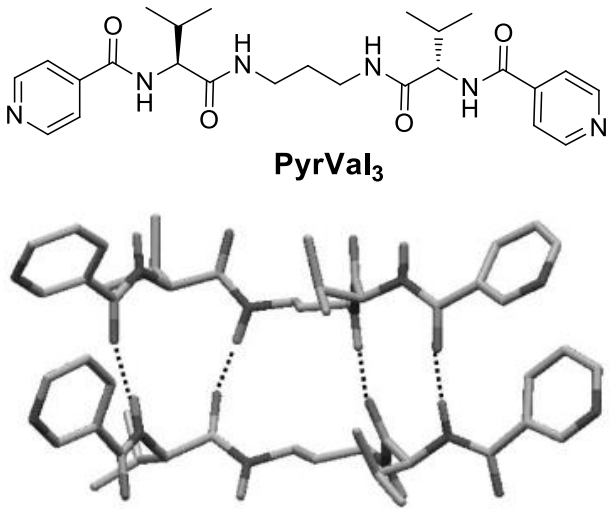

Figure 8. Structure of pyridine functionalized bolaamphiphilic gelators and corresponding energy minimized model (MACROMODEL 7.0, AMBER).[34]

These gels were further coordinated to Pd by post-diffusion of palladium salts and applied as catalysts in the oxidation of benzyl alcohol. Although a modest catalytic activity has been observed

(50% conversion in 48h), it was interesting to observe that the pre-assembly of the gelator was a critical factor for achieving stable Pd(II) complexes.

Another example of molecular multitopic systems was presented by Liu and coworkers, who reported the gelation, in the presence of Cu(II), of a hydrogel known to self-assemble into helical nanotubes, obtaining a chiral catalyst active for the Diels-Alder reaction between cyclopentadiene and an aza-chalcone.[35] It was shown that the resultant Cu(II)-gel nanotubes were able to accelerate the reaction and enhance its stereoselectivity. The alignment of the Cu(II) catalytic centres on the surface of the chiral nanotube provide a stereochemically favoured environment for the Diels-Alder reaction, giving the desired products in high enantiomeric excess.

Finally in the field of organometallic gelators, it is important to highlight the contribution of Dötz et al., who reported the use of a Palladium-CNC pincer biscarbene as an air stable organometallic molecular gelator able to catalyse C-C bond formation reactions in gel state, such as the double Michael addition of α-cyanoacetate to methyl vinyl ketone.[36]

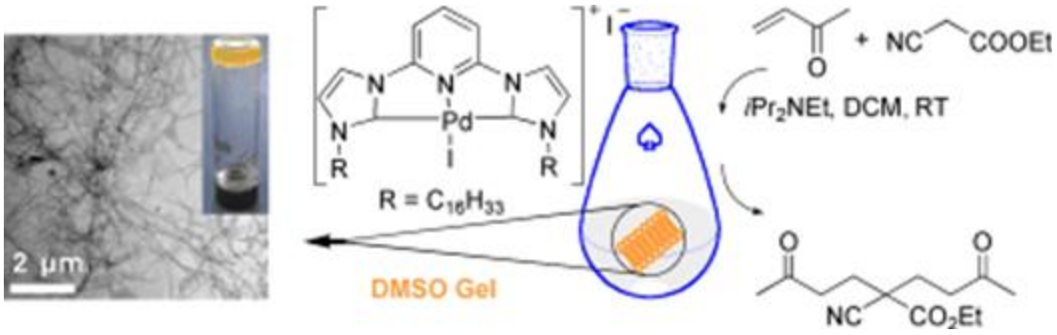

Figure 9. Macroscopic and microscopic structure of the Palladium Pincer complex and and its application as catalyst in a double Michael addition reaction.[36]

Although it has been clearly demonstrated that gels provide powerful tools for chemical catalysis, there are still some issues that need to be improved, such as:

- Taking advantage of supramolecular chirality inside the gel in order to induce enantioselective transformations
- Improve loading capacity of metallogels
- Enhancement of mechanical stability of gels
- Understanding how gels can favour certain reaction pathways
- Understand relationship between gel properties and reaction outcome
- Enhancement of specificity and strength of substrate binding and chemical reactivity of catalytically active sites.

Some of these issues are partly addressed by this thesis.

1.4. Click Chemistry

1.4.1. Definition

The molecules produced by living systems have always fascinated and inspired synthetic organic chemists. Despite significant advances in synthetic organic chemistry in the last years, the man-made materials often do not match the superb properties of nature's materials, such as proteins, sugars or DNA.[37] These nature's primary molecules are composed by simple building blocks, such as amino acids, monosaccharides and nucleotides, respectively, joined by reversible condensation processes involving carbon-heteroatom connections.[38] This strategy of making large oligomers from relatively simple building blocks may be described as nature's way of performing combinatorial chemistry with remarkable modularity and diversity.[39]

Taking a cue from nature's approach, the combination between a set of powerful, highly reliable, versatile and selective reactions that quickly generate new molecules by "clicking" small units together through heteroatom links (C-X-C), with the design of libraries of building blocks, has become the preferred strategy for the development of new compounds with desired property profiles.[40] This strategy was defined as "click chemistry", being first introduced by K. B. Sharpless in 1998. Later, in 2001 Kolb, Finn and Sharpless applied the very useful and "green" concept of a "click" reaction by describing it as a selective, high-yield reaction carried under mild water-tolerant conditions and with no by-products.[41]

According to the "click" philosophy, reactions defined as click reactions should be modular, wide in scope, robust, stereospecific, and require only benign conditions, simple workup and purification procedures, without the need of chromatographic methods.[42] Furthermore, the process should be insensitive to oxygen and water, comprise easily available starting materials and reactants and carried in no solvent, benign solvent (water) or a solvent that could be easily removed, giving a product that should be stable under physiological conditions.[43]

In this sense, click chemistry is not limited to a single kind of reaction, but rather defines a synthetic concept or framework that comprises a range of reactions having different reaction mechanisms, but common reaction trajectories.[44] Some of the reactions that fulfil the abovementioned criteria and thus, fit extremely well in the group of "click reactions" are:

- Huisgen 1,3-dipolar cycloaddition
- [4+2]-cycloaddition (Diels Alder)
- Nucleophilic substitution/ring opening reactions
- Carbonyl reactions of the non-aldol type, for example formation of ureas.

- Addition to carbon-carbon multiple bonds

The increasing interest in rapid reactions that meet the three main criteria of an ideal synthesis (efficiency, versatility and selectivity) extended the application of 'click' reactions not only to the field of drug discovery, including the development of new molecules through combinatorial chemistry, target-templated *in vitro* chemistry, proteomics and DNA research, through the use of bioconjugation reactions, but also to the field of materials science, mainly on improving the mechanical and thermo-physical properties on polymers and gels by participating in cross-linking reactions.[45,46]

1.4.2. The Huisgen 1,3-dipolar cycloaddition

Between all the reactions that achieve a "click status", the Huisgen 1,3-dipolar cycloaddition of alkynes and azides is regarded as the premier example of a 'click' reaction.[39] This reaction was first reported in 1893 by Michael, who suggested that the reaction between but-2-ynedioate and azidobenzene at 100 ºC resulted in the formation of regioisomeric triazoles.[47] However, only later in 1960 this reaction was recognized for its generality, scope and mechanism, following the studies carried by Huisgen on reactions between azoalcanes and ring-strained open olefins. The reaction was defined as [3+2] 1,3-dipolar cycloaddition, and involved the coupling between a 1,3-dipole and a multiple bond system, defined as dipolarophile, giving a five membered heterocycle (**Figure 10**).[48]

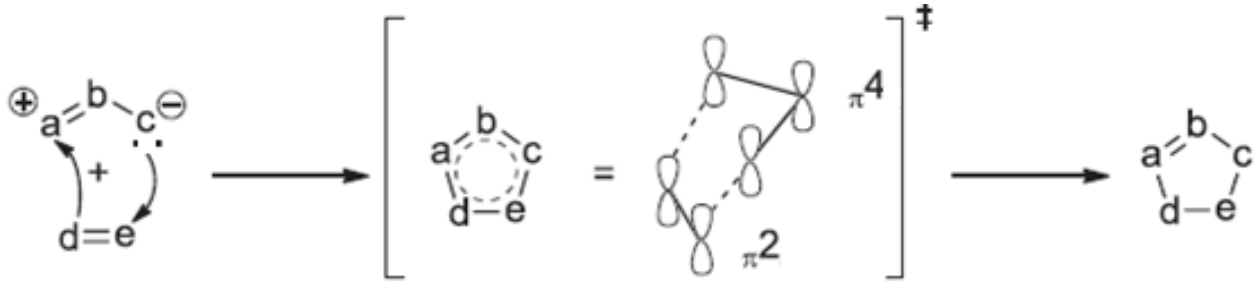

Figure 10. Schematic representation of a 1,3-dipolar cycloaddition reaction.

While the 1,3 dipole, also called ylide, bears a positive and a negative charge over three atoms and has 4π-electrons, the dipolarophile is a reactive alkene moiety containing 2π-electrons. Examples of dipolarophiles may include α,β-unsaturated aldehydes, ketones, esters, allyl alcohols, allylic halides, vinyl ethers or alkynes. The reaction proceeds through a pericyclic concerted or ionic stepwise mechanism as represented in **Figure 10**, forming a highly ordered four-centred transition state typical in concerted pericyclic reactions.[49] Due to their high activation energy (24-26 kcal/mol), these cycloadditions are often very slow even at elevated temperatures (180 ºC-120 ºC for 12h-24h), producing mixtures of 1,4- and 1,5-regioisomers.[50] Such lack of regioselectivity may

be explained by the small difference between the HOMO-LUMO energy gaps of the reactants. Due to their high proximity, the difference between the activation enthalpies to obtain the 1,4- or 1,5-regioisomer is also too small to promote a stereoselective reaction, thus resulting in a mixture of products.[51]

Despite of this lack of regioselectivity, coupled with long reaction times and harsh conditions not tolerated by certain sensitive functional groups in the substrates, the ease of synthesis of the alkyne and azide functionalities together with their kinetic stability and tolerance to a wide variety of functional groups and reaction conditions are advantageous characteristics that make this reaction particularly attractive.[39]

1.4.3. The Cu(I)-catalyzed Huisgen azide-alkyne cycloaddition (CuAAC)

As a result of this growing interest in Huisgen 1,3-dipolar cycloadditions, the groups of Medal and Sharpless, independently, discovered a copper catalysed variant of this reaction. While the former presented a copper(I)-catalysed solid-phase synthesis of 1,2,3-triazoles, using copper(I) salts as catalysts and mild reaction conditions to afford exclusively 1,4-dissubstituted 1,2,3-triazoles, the latter proposed a copper-catalysed azide-alkyne cycloaddition under solution-phase conditions, where copper (II) salts were reduced *in situ* by using ascorbic acid or sodium ascorbate in water: alcohol solvent mixture.[52,53]

The catalytic system introduced by Sharpless and Fokin has been regarded as the most efficient, since it is highly tolerant to most functional groups, including free amines, alcohols and carboxylic acids, and can be carried in aqueous reaction media with organic co-solvents such as alcohols or DMSO. Additionally, the main advantages of reducing copper(II) salts *in situ* are the broad applicability of this method and its compatibility with oxygen and water, meaning that there is no need of inert gas conditions. Furthermore, the application of this method provides very high yields, low amount or no byproducts and uncomplicated work up procedures.

On the other side, the addition of Cu(I) salts such as CuI, $CuOTf{\cdot}C_6H_6$ and $[Cu(CH_3CN)_4]PF_6$, often require the use of inert conditions together with the presence of a nitrogen base to improve product purity and yield, preventing the formation of undesired byproducts such as diacetylenes, bistriazoles or 5-hydroxytriazoles.[53]

The discovery that Cu(I) catalysis could dramatically increase the reaction rate up to 10^7 times and improve regioselectivity, affording exclusively 1,4-regioisomers have put this reaction at the centre of "click chemistry", being sometimes defined as the 'click' reaction.[39] Besides the high reaction rate, this reaction can be applicable to a wide variety of substrates with manifold functional groups, such as hydroxyl, ester, carboxylic acid, amide, sulphonamide and amine substituents.

Moreover, the catalytic process is insensitive towards the presence of air, occurring in a wide range of solvents and pH, and performing well in a broad temperature range.[54]

The Cu(I)-catalysed azide-alkyne cycloaddition (CuAAC) reaction proceeds through a stepwise catalytic pathway, which lowers the activation barrier by 11 kcal/mol in comparison with the concerted [3+2] cycloaddition of a copper acetylene complex with the corresponding azide.[53,55] The mechanistic key steps, based on computational and experimental studies, are represented in **Figure 11**.

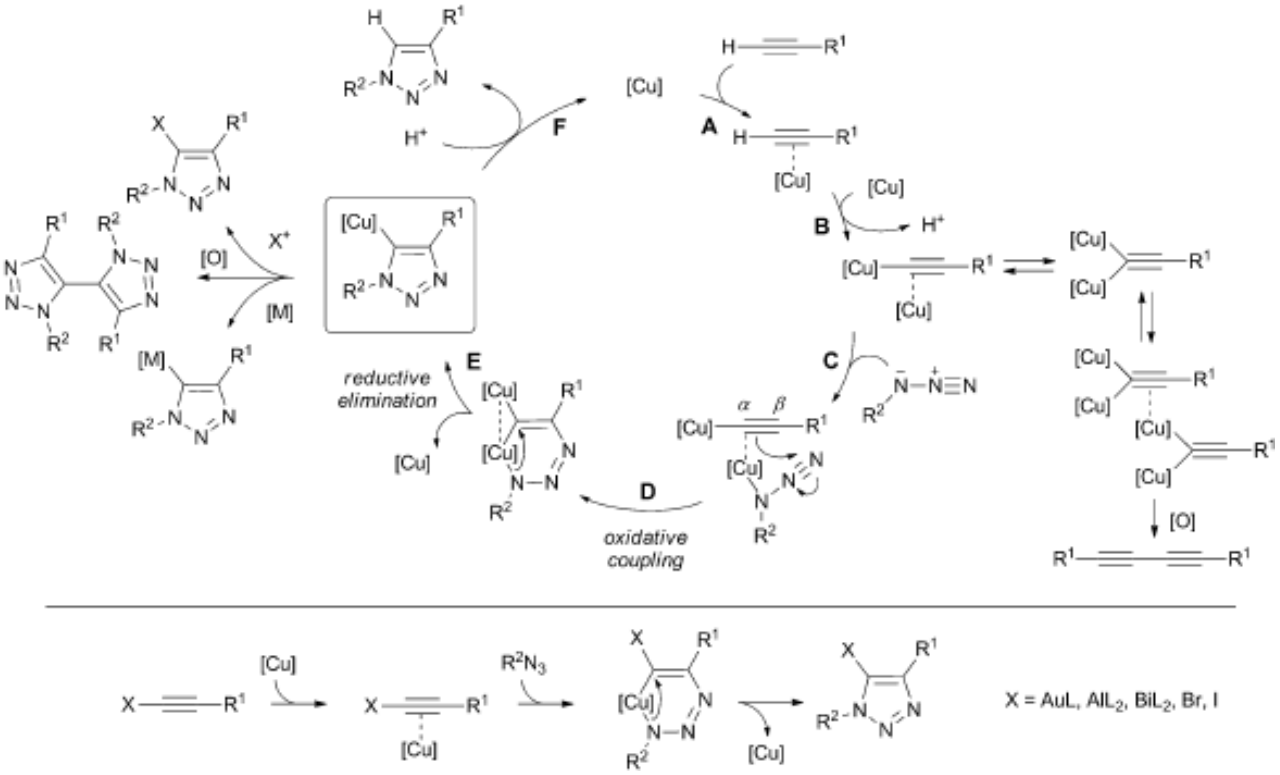

Figure 11. Proposed mechanism of the CuAAC. ([Cu] denotes a copper fragment that varies in the number of ligands and in the formal oxidation state).[57]

The reaction begins by π-coordination of Cu(I) species with the alkyne (A), causing an increase in the acidity of the terminal alkyne. This is supported by a decrease in *pKa* from 25 to 15, which makes the deprotonation in aqueous media possible without the need of adding a base. The addition of an excess of sodium ascorbate may also help on the deprotonation of the π-complexed alkyne in organic protic media, whereas in aprotic media this step is disfavoured, being sometimes necessary the addition of a base such as triethylamine, DIPEA or pyridine.[56] The coordination of an additional copper(I) to the activated alkyne (B) reduces its electron density and results in the formation of a γ-coordinated Cu(I) acetylide. This second Cu(I) remains π-coordinated at the α-carbon of the γ-bound acetylide and the coordination of the azide to this metal centre occurs by displacement of one ligand in the copper(I) coordination sphere (C). This coordination is done

preferably by the terminal nitrogen of the azide, which due to its π-donating capacity increases the electron density of the metal centre, facilitating the subsequent oxidative coupling (D).[57] Thus, it is reasonable that alkynes having electron withdrawing groups could also accelerate the reaction.[58] This characteristic may also be the key for the stereoselective formation of 1,4-regioisomers. The preference of Cu(I) to coordinate the α-carbon of acetylide directs a nucleophilic attack to the β-carbon at the terminal electrophilic nitrogen of the coordinated azide, upon oxidative coupling. As a result of this rate-limiting step, a six-membered copper-containing intermediate is formed and stabilized, according to computational methods, by geminal bimetallic coordination (D).[56,59]

However, it is still unclear whether Cu(III) is intermediately formed, or if both metal centres cooperate in the oxidation step. In the metallocycle formed by oxidative coupling, the azide is well positioned for subsequent ring contraction by a transannular association of the N(1) lone pair of electrons with the C(5)-Cu π-orbital.[55] Thus, the final step of the mechanism consists on ring contraction and Cu(I) exclusion via reductive elimination (E), affording a Cu(I)-bound triazolide in a highly exothermic process. In aqueous media, the generated triazole derivative readily undergoes protonolysis (F), releasing the triazole and allowing the Cu(I) to re-enter the catalytic cycle. Due to the involvement of a second Cu(I) centre, the reaction proceeds through a second-order rate depending on concentration of Cu(I).[56,57]

The unique catalytic ability of Cu(I) may be explained not only by the combined tendency to engage terminal alkynes in both γ and π-interactions, but also by the rapid exchange of ligands in its coordination sphere, especially in an aqueous environment.[60]

1.4.4. "Click" chemistry in the synthesis of new materials

There is an increasing demand for the construction of soft materials systems with precise control over architecture, domain size, functionality, polarity, solubility and reactivity. Much of the inspiration for constructing such complex, multifunctional materials may be founded on a combination of organic chemistry, biology and bioconjugation chemistry.[61] It is widely established that highly complex biological systems rely on a modest library of monomers linked together by few, but efficient, organic reactions.[62] A close examination of nature's favourite molecules, reveals a preference for making carbon-heteroatom bonds over carbon-carbon bonds.[63] For example, proteins are formed from amino acid building blocks joined by amide links. This carbon-heteroatom approach is in good agreement with the principles of "click" philosophy.

As mentioned along this introductory part, CuAAC has been viewed as an ideal reaction for chemical synthesis, considering its advantageous characteristics such as fast reaction rates, high

efficiency, excellent regiospecificity and bioorthogonality. The fact that alkynes and azides are not present in nature renders CuAAC reaction highly compatible with different drugs, proteins and cells. The chemoselectivity of this reaction allows its use in the modification of highly functionalized biomolecules such as polypeptides, nucleic acids or polysaccharides.[64]

As a result of these unique characteristics, the applications of CuAAC rapidly extended through a broad range of fields, including drug development (enzyme inhibitors, combinatorial screening), biochemistry (*de novo* peptide synthesis, carbohydrates, oligonucleotides), biomaterials (synthesis of hydrogels, microgels or nanogels), colloids (inorganic nanoparticles, nanocarriers) and planar surfaces (biosensors, microarrays).[65] Furthermore, the fact that this reaction proceeds in high yield, under mild conditions and in physiologic medium makes it highly attractive for bioconjugation.

Taking advantage of the ability of CuAAC for bioconjugation purposes, Barthélémi and coworkers reported the synthesis of glycosyl-nucleoside fluorinated amphiphiles (GNF) derived from the *2H,2H,3H,3H*-perfluoro-undecanoyl hydrophobic chain.[66]

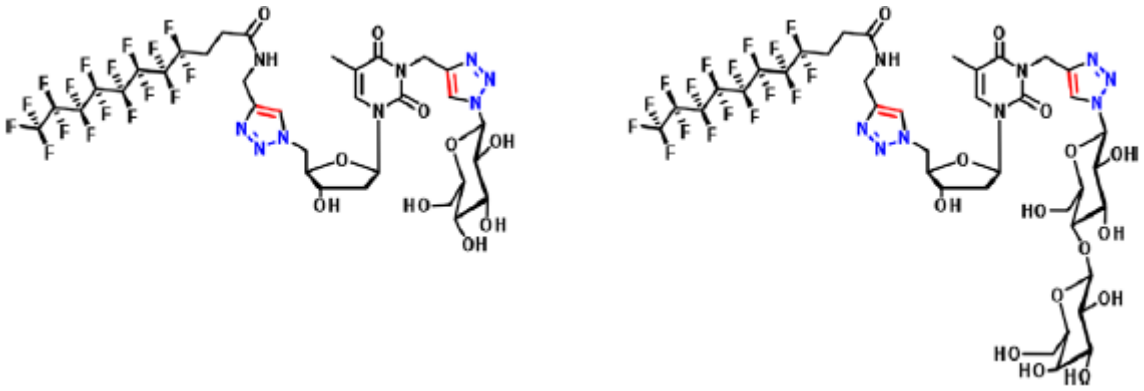

Figure 12. Structure of GNFs synthesized by double 'click' chemistry.[66]

The gels were synthesized through double ‘click’ chemistry route and spontaneously self-assembled in supramolecular structures in the presence of water or cellular medium. Cell viability studies proved the non-toxicity of these gels for human cells (Huh7). This is a clear example of bioconjugation using ‘click’ chemistry, resulting in the synthesis of a supramolecular nucleic acid derivative.

The versatility of CuAAC was well represented in a study carried by *Budin et al.*, where this reaction was used as a biomimetic coupling reaction, driving to the *de novo* self-assembly of phospholipid membranes.[67] An oleyl azide and an alkyne analogue of the lysophospholipid 1-palmitoyl-sn-glycero-3-phosphocholine were used as substrates. After the ‘click’ coupling of the precursors, bilayer assembly occurred spontaneously in water due to hydrophobic effect, resulting in the formation of large spherical and tubular vesicle structures composed by phospholipid

membranes. In another interesting study, CuAAC was applied in the stabilization and reinforcement of molecular gels. [68] In the presence of Cu(I) and an appropriate bivalent additive, gel thermostability was increased upon CuAAC-promoted cross-linking. Furthermore, the obtained gels exhibited greater T_{gel} and rigidity (*G'*) than the pure molecular gels.

In the field of organometallic chemistry, the capacity of CuAAC chemistry on generating mild coordination triazole ligands was explored for the preparation of metallosupramolecular gels containing the tridentade 2,6-bis(1,2,3-triazol-4-yl)pyridine (BTP) ligand.[69] Upon coordination of Zn(II) or Eu(III) in a ligand/metal 2:1 or 3:1 ratio, respectively, supramolecular gels exhibiting different optical properties could be obtained. Apart from this interesting feature, the metallogels exhibited multi-responsive self-healing behaviour.

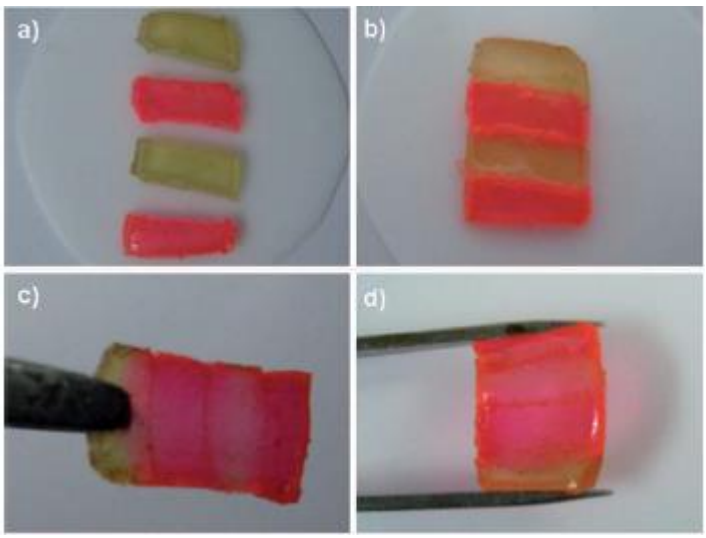

Figure 13. Photographs of a gel containing no Zn(II) and 100% Eu(III) showing the self-healing behaviour. (a) Four blocks of cut gels, two red ones were dyed with rhodamine B; (b) joined blocks by simply joining together the fresh surfaces; (c) stable self-supporting bar formed after healing for 6h at RT without any external intervention; (d) squeezing.[69]

It was postulated that the dynamic nature of metal: BTP association allowed the exchange of ligands and metal ions between two adjacent building blocks, resulting in the formation of new complexes that lead to bridges between the supramolecular network and consequent self-healing ability.

Since CuAAC has been extensively used on the synthesis of new gelators and improvement of their properties, it would be interesting to take also advantage of this reaction for the development of new catalytic gelators functionalized with 1,2,3-dissubstituted triazoles. The synthesis of these heterogeneous catalytic materials would be of high value regarding the growing applications and importance of this reaction along the several fields of chemical science. Furthermore, the possibility of developing new biocompatible and biodegradable hydrogels that could be used in the catalysis of bioconjugation 'click' reactions would be highly attractive,

regarding the reported capacity of free Cu(I) to generate reactive oxygen species from O_2 and consequent cytotoxicity in physiological environment.[70,71] All these factors constituted a special motivation for joining together ‘click’ reactions and supramolecular gels as the main focus of this research work.

1.5. References

[1] Flory P. Introductory Letter. Faraday Discussions of the Chemical Society 1974; 57: 7-18.

[2] Sangeetha NS, Maitra U. Supramolecular gels: Functions and uses. Chemical Society Reviews 2005; 34: 821-836.

[3] Huang X, Terech P, Raghavan SR, Weiss RG. Kinetics of 5α-Cholestan-3β-yl N-(2-Naphtyl)carbamate/n-alkane organogel formation and its influence on the fibrillar networks. Journal of American Chemical Society 2005; 127: 4336-4344.

[4] Estroff L, Hamilton A. Water gelation by small molecules. Chemical Society Reviews 2004; 104: 1201-1218.

[5] Terech P, Weiss RG. Low molecular mass gelators of organic liquids and the properties of their gels. Chemical Reviews 1997; 97: 3133-3159.

[6] Van Esch JH, Feringa BL. New functional materials based on self-assembling organogels: From serendipity towards design. Angewandte Chemistry Internationa Edition 2000; 39: 2263-2266.

[7] Suzuki M, Hanabusa K. Polymer organogelators that make supramolecular organogels through physical cross-linking and self-assembly. Chemical Society Reviews 2010; 39: 455-463.

[8] Smith DK. Supramolecular Gels: Building bridges. Nature Chemistry 2010; 2: 162-163.

[9] Xie P, Zhang R. Liquid crystal elastomers, networks and gels: advanced smart materials. Journal of Materials Chemistry 2005; 15: 2529-2550.

[10] Stupp SI, Palmer LC. Supramolecular chemistry and self-assembly in organic materials design. Chemistry of Materials 2014; 26: 507-518.

[11] George M, Weiss R. Molecular organogels. Soft matter comprised of low-molecular-mass organic gelators and organic liquids. Accounts of Chemical Research 2006; 31:489-497.

[12] Hirst AR, Escuder B, Miravet JF, Smith DK. High-tech applications of self-assembling supramolecular nanostructured gel-phase materials: From regenerative medicine to electronic devices. Angewandte Chemistry International Edition 2008; 47: 8002-8018.

[13] Becerril J, Burgete MI, Escuder B, Galindo F, Gavara R, Miravet JF, Luis SV, Peris G. Self-assembly of small peptidomimetic cyclophanes. Chemistry – A European Journal 2004; 20: 3979-3890.

[14] Steed JW. Supramolecular gel Chemistry: developments over the last decade. Chemical Communications 2011; 47: 1379-1383.

[15] Terech P. Metastability and sol phases: Two keys for the future of molecular gels. Langmuir 2009; 25: 8370-8372.

[16] Moffat JR, Smith DK. Metastable two-component gel – exploring the gel-crystal interface. Chemical Communications 2008; 2248-2250.

[17] Jonkheijm P, van der Schoot P, Schenning AP, Meijer EW. Probing the solvent-assisted nucleation pathway in chemical self-assembly. Science 2006; 313: 80-83.

[18] Liu XY, Sawant PD. Formation kinetics of fractal nanofiber networks in organogels. Applied Physics Letters 2001; 79: 3518-3520.

[19] Chung YM, Simmons KL, Gutowska A, Jeong B. Sol-gel transition temperature of PLGA-g-PEG aqueous solutions. Biomacromolecules 2002; 3: 511-516.

[20] Hirst AR, Coates IA, Boucheteau TR, Miravet JF, Escuder B, Castelletto V, Hamley IW, Smith DK. Low-molecular-weight gelators: Elucidating the principles of gelation based on gelator solubility and a cooperative self-assembly model. Journal of American Chemical Society 2008; 130: 9113-9121.

[21] Mark HF. Encyclopedia of Polymer Science and Technology, 3 edn., John Wiley & Sons, Inc., 2004.

[22] Brinksma J, Feringa BL, Kellogg RM, Vreeker R, van Esch J. Rheology and thermotropic properties of bis-urea-based organogels in various primary alcohols. Langmuir 2000; 16: 9249-9255.

[23] Abdallah DJ, Weiss RG. Organogels and low molecular organic gelators. Advanced Materials 2000; 12: 1237-1247.

[24] Escuder B, LLusar M, Miravet JF. Insight on the NMR study of supramolecular gels and its application to monitor molecular recognition on self-assembled fibers. Journal of Organic Chemistry 2006; 71: 7747-7752.

[25] Eelkema R, van Esch JH. Catalytic control over the formation of supramolecular materials. Organic Biomolecular Chemistry 2014; 12: 6292-6296.

[26] Díaz DD, Kühbeck D, Koopmans RJ. Stimuli-responsive gels as reaction vessels and reusable catalysts. Chemical Society Reviews 2011; 40: 427-448.

[27] Escuder B, Rodríguez-Llansola F, Miravet JF. Supramolecular gels as active media for organic reactions and catalysis. New Journal of Chemistry 2010; 34: 1044-1054.

[28] Döring A, Birnbaum W, Kuckling D. Responsive hydrogels – structurally and dimensionally optimized smart frameworkds for applications in catalysis, micro-system technology and material science. Chemical Society Reviews 2013; 42. 7391-7420.

[29] Rodríguez-Llansola F, Escuder B, Miravet JF. Remarkable increase in basicity associated with

supramolecular gelation. Organic & Biomolecular Chemistry 2009; 7: 3091-3094.

[30] Guler MO, Stupp SI. A self-assembled nanofiber catalyst for ester hydrolysis. Journal of the American Chemical Society 2007; 129: 12082-12083.

[31] Rodríguez-Llansola F, Escuder B, Miravet JF. Switchable performance of an L-proline-derived basic catalyst controlled by supramolecular gelation. Journal of American Chemical Society 2009; 131: 11478-11484.

[32] Rodríguez-Llansola F, Miravet JF, Escuder B. A supramolecular hydrogel as a reusable heterogeneous catalyst for the direct aldol reaction. Chemical Communications 2009; 7303-7305.

[33] Xing B, Choi M, Xu B. Design of coordination polymer gels as stable catalytic systems. Chemistry – A European Journal 2002; 8: 5028-5032.

[34] Miravet JF, Escuder B. Pyridine-functionalised ambidextrous gelators: towards catalytic gels. Chemical Communications 2005; 5796-5798.

[35] Jin Q, Zhang L, Cao H, Wang T, Zhu X, Jiang J, Liu M. Self-assembly oc copper(II) ion-mediated nanotube and its supramolecular chiral catalytic behaviour. Langmuir 2011; 27: 13847-13853.

[36] Tu T, Assenmacher W, Peterlik H, Weisbarth R, Nieger M, Dötz KH. An air-stable organometallic Low-molecular-mass gelator: Synthesis, aggregation, and catalytic application of palladium pincer complex. Angewandte Chemistry International Edition 2007; 46: 6368-6371.

[37] Nandivada H, Jiang X, Lahann J. Click Chemistry: Versatility and control in the hands of materials scientists. Advanced Materials 2007; 19: 2197-2208.

[38] Kolb HC, Finn MG, Sharpless KB. Click Chemistry: Diverse chemical function from a few good reactions. Angewandte Chemistry 2001; 40: 2004-2021.

[39] Moses JE, Moorhouse AD. The growing applications of click chemistry. Chemical Society Reviews 2007; 36: 1249-1262.

[40] Hou J, Liu X, Shen J, Zhao G, Wang PG. The impact of click chemistry in medicinal chemistry. Expert Opinion on Drug Discovery 2012; 7: 489-501.

[41] Liang L, Astruc D. The copper(I)-catalyzed alkyne-azide cycloaddition (CuAAC) “click” reaction and its applications. An Overview. Coordination Chemistry Reviews 2011; 255: 2933-2945.

[42] Bock VD, Hiemstra H, van Maarseveen JH. CuI-catalyzed alkyne-azide “click” cycloadditions

from a mechanistic and synthetic perspective. European Journal of Organic Chemistry 2006; 2006: 51-68.

[43] Thirumurugan P, Matosiuk D, Jozwiak K. Click chemistry for drug development and diverse chemical-biology interactions. Chemical Reviews 2013; 113: 4905-4979.

[44] Kolb HC, Sharpless K. The growing impact of click chemistry on drug discovery. Drug Discovery Today 2003; 8: 1128-1137.

[45] Tasdelen MA. Diels-Alder "click" reactions: recent applications in polymer and material science. Polymer Chemistry 2011; 2: 2133-2145.

[46] Diaz DD, Rajagopal K, Strable E, Schneider J, Finn MG. "Click" chemistry in a supramolecular environment: organogels by copper(I)-catalyzed azide-alkyne [3+2] cycloaddition. Journal of American Chemical Society 2006; 128: 6056-6057.

[47] Michael A. Ueber die Einwirkung von Diazobenzolimid auf Acetylendicarbonsäuremethylester. Journal für Praktische Chemie 1893; 48: 94-95.

[48] Huisgen R. 1,3-dipolar cycloadditions. Past and Future. Angewandte Chemistry International Edition 1963; 10: 565-598.

[49] Huisgen R. Kinetics and Mechanism of 1,3-dipolar cycloadditions. Angewandte Chemistry International Edition 1963; 2: 633-696.

[50] Zhang L., Chen X, Xue P, Sun HHY, Williams ID, Sharpless KB, Fokin VV, Jia G. Ruthenium-catalyzed cycloaddition of alkynes and organic azides. Journal of American Chemical Society 2005; 127: 15998-15999.

[51] Gothelf KV, Jørgensen KA. Asymmetric 1,3-dipolar cycloaddition reactions. Chemical Reviews 1998; 98: 863-909.

[52] Tornøe C, Christian W, Christensen C, Meldal M. Peptidotriazoles on solid phase: [1,2,3]-Triazoles by regiospecific copper(I)-catalyzed 1,3-dipolar cycloadditions of terminal alkynes to azides. Journal of Organic Chemistry 2002; 67: 3057-3064.

[53] Rostovtsev VV, Green LG, Fokin VV, Sharpless KB. A stepwise Huisgen cycloaddition process: copper(I)-catalyzed regioselective "ligation" of azides and terminal alkynes. Angewandte Chemistry International Edition 2002; 41: 2596-2599.

[54] Himo F, Lovell T, Hilgraf R, Rostovtsev VV, Noodleman L, Sharpless KB, Fokin VV. Copper(I)-catalyzed synthesis of azoles. DFT study predicts unprecedented reactivity and intermediates. Journal of American Chemical Society 2005; 127: 210-216.

[55] Bock VD, Hiemstra H, Maarseveen JH. CuI-catalyzed alkyne-azide "click" cycloadditions

from a mechanistic and synthetic perspective. European Journal of Organic Chemistry 2006; 51-68.

[56] Buckley BR, Dann SE, Heaney H. Experimental evidence for the involvement of dinuclear alkynylcopper(I) complexes in alkyne-azide chemistry. Chemistry – A European Journal 2010; 16: 6278-6284.

[57] Schulze B, Schubert US. Beyond click chemistry – Supramolecular interactions of 1,2,3-triazoles. Chemical Society Reviews 2014; 43: 2522-2571.

[58] Kislukhin AA, Hong VP, Breitenkamp KE, Finn MG. Relative performance of alkynes in copper-catalyzed azide-alkyne cycloaddition. Bioconjugate Chemistry 2013; 24: 684-689.

[59] Ahlquist M, Fokin VV. Enhanced reactivity of dinuclear copper(I) acetylides in dipolar cycloadditions. Organometallics 2007; 26: 4389-4391.

[60] Hein JE, Fokin VV. Copper-catalyzed azide-alkyne cycloaddition (CuAAC) and beyond: new reactivity of copper(I) acetylides. Chemical Society Reviews 2010; 39: 1302-1315.

[61] Iha RK, Wooley KL, Nyström AM, Burke DJ, Kade MJ, Hawker CJ. Applications of orthogonal, “click” chemistries in the synthesis of functional soft materials. Chemical Reviews 2009; 109: 6620-5686.

[62] Lutz JF. 1,3-dipolar cycloadditions of azides and alkynes: A universal ligation tool in polymer and materials science. Angewandte Chemistry International Edition 2007; 46: 1018-1025.

[63] Nwe K, Brechbiel MW. Growing applications of “click chemistry” for bioconjugation in contemporary biomedical research. Cancer Biotherapy and Radiopharmaceuticals 2009; 24: 289-302.

[64] Wong CH, Zimmerman SC. Orthogonality in organic, polymer, and supramolecular chemistry: from Merrifield to click chemistry. Chemical Communications 2013; 49: 1679-1695.

[65] Llutz JF, Zarafshani Z. Efficient construction of therapeutics, bioconjugates, biomaterials and bioactive surfaces using azide-alkyne “click” chemistry. Advanced drug delivery reviews 2008; 60: 958-970.

[66] Godeau G, Brun C, Arnion H, Staedel C, Barthélémy P. Glycosyl-nucleoside fluorinated amphiphiles as components of nanostructured hydrogels. Tetrahedron Letters 2010; 51: 1012-1015.

[67] Budin I, Devaraj NK. Membrane assembly driven by a biomimetic coupling reaction. JACS 2012; 134: 751-753.

[68] Diaz DD, Rajagopal K, Strable E, Schneider J, Finn MG. “Click” chemistry in a

supramolecular environment: stabilization of organogels by copper(I)-catalyzed azide-alkyne [3+2] cycloaddition. Journal of the American Chemical Society 2006; 128: 6056-6057.

[69] Yuan J, Fang X, Zhang L, Hong G, Lin Y, Zheng Q, Xu Y, Ruan Y, Weng W, Xia H, Chen G. Multi-responsive self-healing metallo-supramolecular gels based on “click” ligand. Journal of Materials Chemistry 2012; 22: 11515-11522.

[70] Li Y, Trush MA, Yager JD. DNA damage caused by reactive oxygen species originating from a copper-dependent oxidation of the 2-hydroxy catechol of estradiol. Carcinogenesis 1994; 15: 1421-1427.

[71] Thorne PS, Kim JS, Adamcakova-Dodd A. Copper nanoparticles generate reactive oxygen species (ROS) after air delivery to alveolar type-II cells *in vitro*. European Respiratory Journal 2011; 38 (Suppl 55).

Chapter 2

Aims of the thesis

The growing use of Cu(I) azide-alkyne cycloaddition (CuAAC) on the synthesis of novel materials leads to a general environmental concern, regarding the inherent toxicity of copper(I). The excessive use of copper sources in the catalysis of the CuAAC usually result in a significant amount of toxic, coloured and expensive copper complexes in the end products. Thus, increasing environmental concerns about waste disposal led to more environmentally friendly metal-free click strategies, such as the coupling of azides with activated alkynes or strained cyclooctines.[1,2]

Although this catalytic reaction achieve similar performances to the copper(I) catalysed variant, the synthesis of this kind of compounds is difficult and not generally applicable. Furthermore, it has been reported that very hydrophobic and reactive cyclooctynes lead to pharmacokinetic problems in mice, and are able to embark in unwanted side reactions with endogenous nucleophiles such as thiols.[3] Last but not least, this strain-promoted 'click' catalysis often result in a mixture of regioisomeric products, which may limit its application.[4]

Thus, the use of heterogeneous catalysts capable of coordinating copper(I) has been regarded as a valuable alternative to minimize the toxic effects of the metal, overcoming the several drawbacks of the strain-promoted azide-alkyne cycloaddition. As mentioned in the introductory part of this thesis, supramolecular gels have been regarded as efficient heterogeneous catalysts due to the formation of extended catalytic networks that provide a high proximity between the catalytic sites. Although their ability as heterogeneous organocatalysts has been widely proven, reports on the use of these materials as metallocatalysts are scarce. [5]

Coupling these two subjects together, this thesis aims the design, synthesis and characterization of molecular gels that could be applied as heterogeneous catalysts for the copper(I) catalysed Huisgen 1,3-dipolar cycloaddition. Peptide amphiphilic and bolaamphiphilic gelators will be synthesized applying 'click' methods, using CuAAC as a tool for the synthesis of the desired catalysts. By applying CuAAC synthetic methodology, compounds having a triazole moiety in its composition could be obtained. This triazole fragment would provide the gelators with coordination ability to copper(I), enabling their application as catalysts in their own synthesis. Thus, the study of self-replication ability of the gelators is also another subject of interest in this thesis.

---

[1] Agard NJ, Prescher JA, Bertozzi CR. A strain-promoted [3+2] azide-alkyne cycloaddition for covalent modification of biomolecules in living systems. Journal of American Chemical Society 2004; 126: 15046-15047.
[2] Lutz JF. Copper-free azide-alkyne cycloadditions: New insights and perspectives. Angewandte Chemistry International Edition 2008; 47: 2182-2184.
[3] Chang PV, Prescher JA, Sketten EM, Baskin JM, Miller IA, Agard NJ, Lo A, Bertozzi CR. Copper-free click chemistry in living animals. Proceedings of the Natural Academy of Sciences U.S.A. 2010; 107: 1821-1826.
[4] Kido N, Brechbiel MW. Growing applications of "click chemistry" for bioconjugation in contemporary biomedical research. Cancer Biotherapy and Radiopharmaceuticals 2009; 24: 289-302.
[5] Escuder B, Miravet JF. in *Functional molecular gels*, Vol 1 (Eds:. Miravet J, Escuder B), Royal Society of Chemistry, Cambridge, 2014, pp. 117-153.

Another important goal of this doctoral thesis is to investigate the influence of the metal on the final properties of the gels. The gels will be characterized regarding their physico-chemical, structural and morphological properties in the presence and absence of the metal, with special attention being directed to the influence of copper(I) on their self-assembly. The copper loading capacity is also regarded as an important parameter, seeking the use of this gels as 'green' heterogeneous catalysts. Finally, the catalytic activity of the metallogels will be evaluated towards the 'model' click reaction between benzylazide and phenylalkyne.

This thesis also aims to test the versatility of the synthesized gelators by applying them as reaction vessels for the catalysis of multicomponent reaction systems, in an approach to more efficient, greener and time-saving catalytic processes. Regarding the considerable importance of 'click' and aldol reactions in the fields of drug discovery and materials science, the construction of a "one-pot" system for these reactions that could be catalysed by a tandem heterogeneous catalyst would be of high value for the straightforward synthesis of new 'clicked' aldol compounds.

Finally, CuAAC reaction will also be applied on the synthesis of functional fluorescent gelators in the presence of a multicomponent catalytic gel network. The main objective is to get deeper insights on the self-assembly process of the gel product, following the formation of the correspondent fluorescent fibres by confocal fluorescent microspectroscopy. This study would allow a better understanding of the role of the hybrid organic-inorganic gel network on the catalysis of 'click' reactions in heterogeneous systems, opening new routes for the synthesis of new multicomponent functional materials.

Chapter 3

Catalytic and self-replication behaviour of gelators functionalized with triazole fragments

Two different families of low molecular weight gelators derived from L-valine bearing phenyltriazole or benzyltriazole fragments were synthesized. The influence of the substituent group on the physico-chemical properties of the gels was investigated. The catalytic performance of the triazole functionalized gels in the Huisgen 1,3-dipolar cycloaddition of alkynes and azides was also evaluated.

3.1. Introduction

The discovery that Cu(I) catalysts could dramatically increase the reaction rate up to 10^7 times and improve regioselectivity, affording exclusively 1,4-regioisomers, has raised the importance of this reaction, enabling unique applications in synthesis, medicinal chemistry and materials science.[1]

The most common catalysts used in azide-alkyne cycloadditions are copper(II)/copper(I) salts, such as $CuSO_4$ in the presence of the reducing agent sodium ascorbate, CuI, CuBr, Cu(OAc), or copper(I) complexes like $[Cu(MeCN)_4]PF_6$ or $[Cu(MeCN)_4]OTf$.[2] Although these catalysts often provide mild reaction conditions, the thermodynamic instability of Cu(I), which usually results in easy oxidation to Cu(II) and/or to disproportion to Cu(0) and Cu(I), potentiated the research of copper ligands able to stabilize and modulate the catalytic activity of the Cu(I) centre.[3]

Recent investigations suggest that the complexes of polytriazole ligands coordinated to Cu(I) have the ability to catalyse the same reaction from where they are derived.[4] The mild coordination ability of the triazole functionality allow the stabilization of Cu(I) oxidation state and avoids the occurrence of disproportion reactions.[5] Examples of efficient polytriazole ligands include the tris[(1-benzyl-1H-1,2,3-triazol-4-yl)methyl]amine (TBTA) or its analogue bearing bulky tert-butyl groups, 2-[4-{(bis[(1-tert-butyl-1H-1,2,3-triazol-4-yl)methyl]amino)methyl}-1H-1,2,3-triazol-1-yl]ethyl hydrogen sulfate (BTTES), described as the one of the most efficient ligands for the copper catalysed azide-alkyne cycloaddition (CuAAC) reported so far.[6] TBTA has also been investigated as a heterogeneous catalyst for CuAAC after being anchored onto a NovaSyn® TG amino resin.[4]

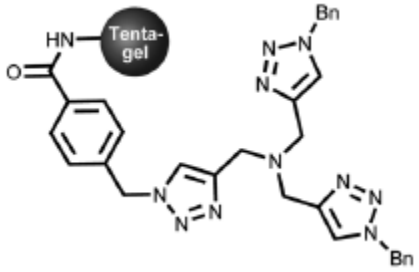

Figure 14. Polymeric solid support anchoring TBTA for the immobilization of Cu(I) in heterogeneous CuAAC.[4]

In the concept of green 'click' chemistry, heterogeneous catalysts take advantage over homogeneous catalysts, since the isolation and recycling of the catalytic system is facilitated, encouraging the synthesis in large scale. Polymer solid supports containing Amberlist®,[7,8] silica-supported Cu(I) catalysts,[9,10] metal organic frameworks (MOF)[11] or copper on charcoal (Cu/C)[12] are other examples tested in heterogeneous CuAAC.[5,13] Despite in some cases near quantitative yields were obtained within 12h at rt for Huisgen's cycloadditions between several azides and alkynes, problems associated with metal leaching, poor metal loading capacity or bad catalytic performance in certain solvents make these heterogeneous catalytic systems not universally applicable. An

example of success in the field of polymer-supported catalysts for 'click' reaction was achieved by Pericàs and co-workers, who reported the synthesis of a tris(triazolyl)methanol ligand immobilized onto a Merrifield resin.[14] The catalytic activity was tested in the model 'click' reaction between benzylazide and phenylalkyne, revealing that it could be repeatedly used in 1:1 MeOH-water, achieving quantitative conversions in just 4h of reaction, although some copper(I) leaching occurs after five consecutive catalytic cycles. Such tris(triazolyl)methanol-Cu(I) complex had previously been reported as an efficient homogeneous catalyst for the Huisgen 1,3-dipolar cycloaddition.[15]

Although a wide range of organic and inorganic solid catalytic supports have been investigated, the application of supramolecular gels as heterogeneous catalytic media for the Huisgen 1,3-dipolar cycloaddition of alkynes and azides is rare. In the field of 'click' reactions, Liu and co-workers have reported a hydrogelator which self-assembled into helical nanotubes in the presence of Cu(II), leading to a chiral catalyst active for a Diels-Alder reaction, while Gao and co-workers reported the application of chiral binaphthylbispyridine-based copper(I) metallogels as catalysts for the Huisgen 1,3-dipolar cycloaddition.[16,17]

Herein, we report the design, synthesis and catalytic performance of low molecular weight gelators derived from amino acid *L*-valine, functionalized with triazole fragments as a supramolecular mimic of the multivalent features of covalent polytriazole ligands such as TBTA. Two different families of bolaamphiphilic gelators exhibiting the same *L*-valine derived central core functionalized with a phenyltriazole (**PhTzVal$_n$**) or a benzyltriazole (**BzTzAVal$_n$**) have been synthesized.

Apart from the autocatalytic activity of gelators **PhTzVal$_n$**, the influence of the catalytic fragment on the properties of both gelator families and their catalytic performance to the model 'click' reaction have also been investigated.

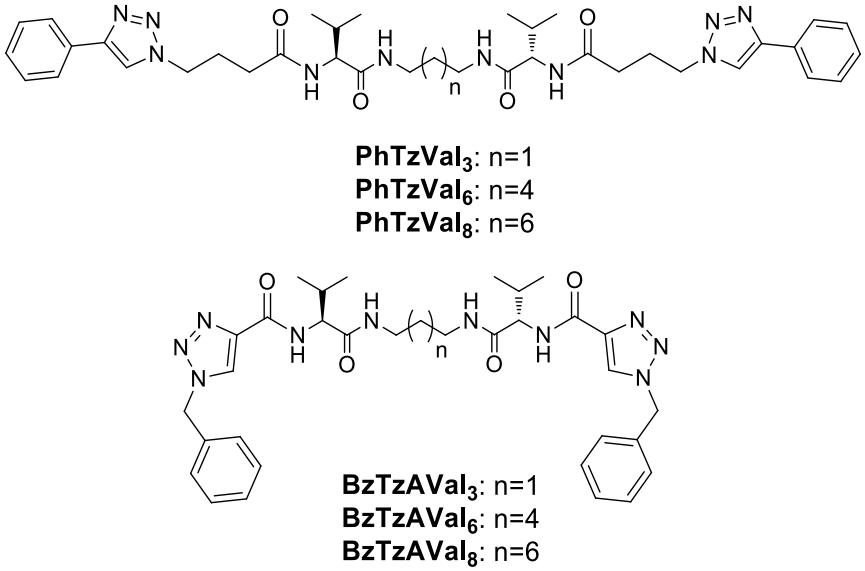

Figure 15. Structure of **PhTzVal$_n$** and **BzTzAVal$_n$** families of gelators studied in this chapter.

3.2. Results and Discussion

3.2.1. Compounds bearing a phenyltriazole catalytic fragment (PhTzVal$_n$)

3.2.1.1. Design and synthesis

The bolaamphiphilic gelators synthesized in this project are composed by a *L*-valine derived central core, as represented in **Figure 16**.

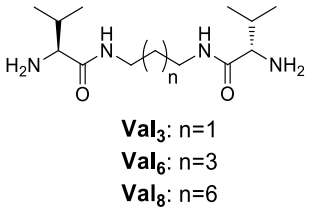

Figure 16. Structure of the central core present in the bolaamphiphilic gelators.

This central fragment was obtained through a "one-pot" reaction between the carboxybenzyl (Cbz) protected *L*-valine amino acid and the desired alkylidenediamine using ethyl chloroformate as activation agent and triethylamine as a base (**Figure 17**).

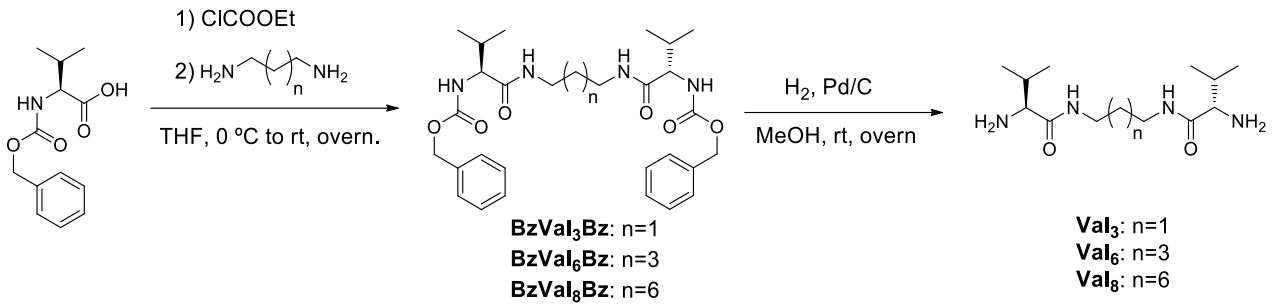

Figure 17. Synthetic scheme for the synthesis of *L*-valine derived central core.

In the first step of this reaction, the deprotonated carboxylic acid of the Cbz-*L*-valine attacks the carbonyl group of the ethyl chloroformate, guiding to the formation of a carboxylic anhydride as intermediary.

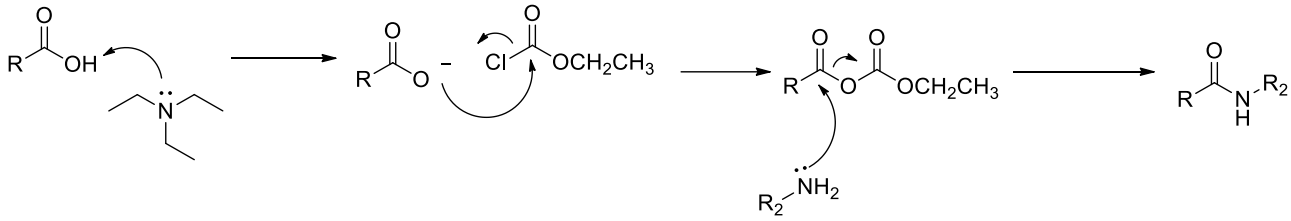

Figure 18. Mechanism of formation of the intermediary carboxylic anhydride.

The reaction proceeds with the attack of the primary amine nucleophile to the carbonyl group of the intermediary carboxylic anhydride, resulting in the formation of a Cbz-protected *L*-valine alkylidenediamide.

The elimination of the carboxybenzyl group by hydrogenolysis using 15% Pd/C as catalyst yields the deprotected amine.

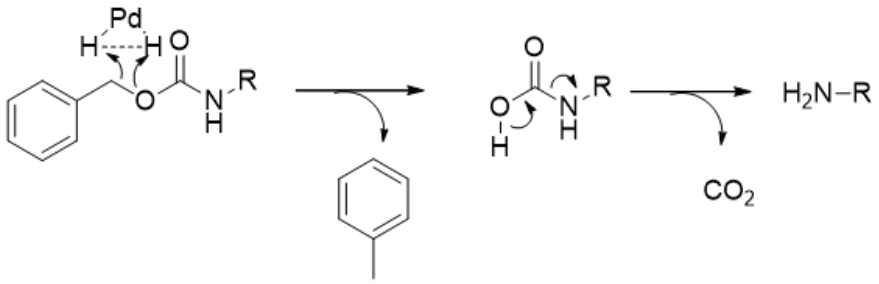

Figure 19. Mechanism of elimination of the carbobenzybenzoyl protecting group.

Once the central core has been synthesized, it was reacted by simple peptide coupling with the activated ester of bromobutyric acid, obtaining the correspondent bromide derivative.

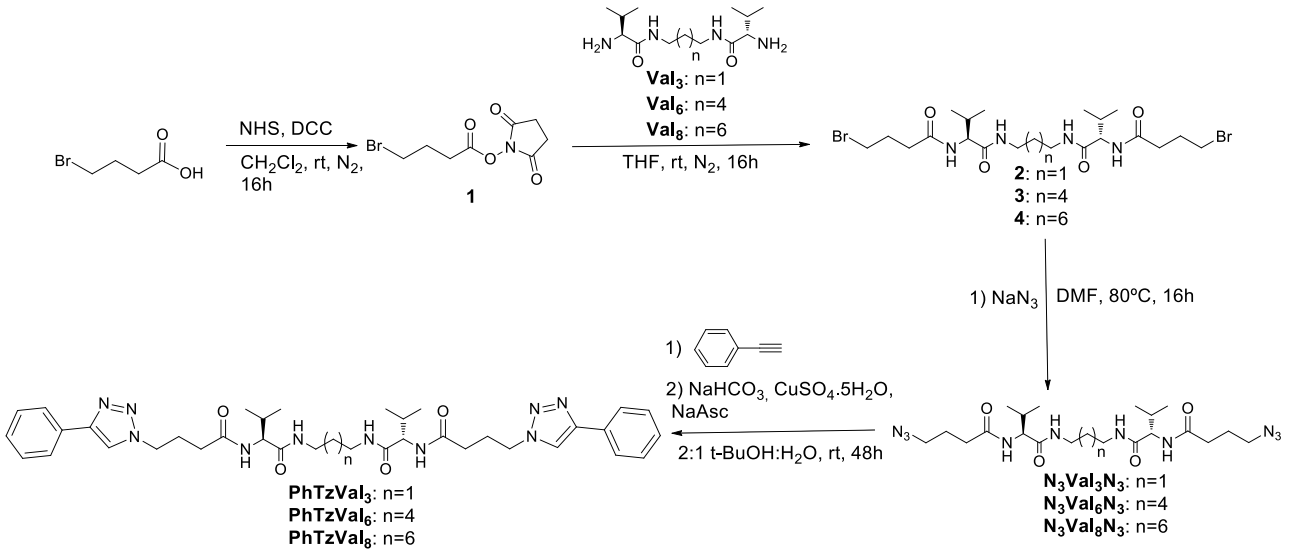

Figure 20. Scheme for the synthesis of **PhTzVal$_n$** gelators.

The bromobutyric acid was activated using dicyclohexylcarbodiimde and *N*-hydroxysuccinimide (DCC/NHS). The first step of this reaction consists on the attack of the carboxylic acid to the central atom of DCC, resulting in the formation of an *O*-acylisourea intermediate, which offers similar reactivity to the corresponding carboxylic acid anhydride. The consequent attack of the *N*-hydroxysuccinimide to the enhanced electrophilic carboxylate group leads to the formation of an ester and a stable dicyclohexylurea (DCU), which precipitates from the solution and thus, can be easily separated by filtration. The final step consisted on the attack of the activated ester by the nucleophilic primary amine, obtaining the corresponding amide product (**Figure 21**).

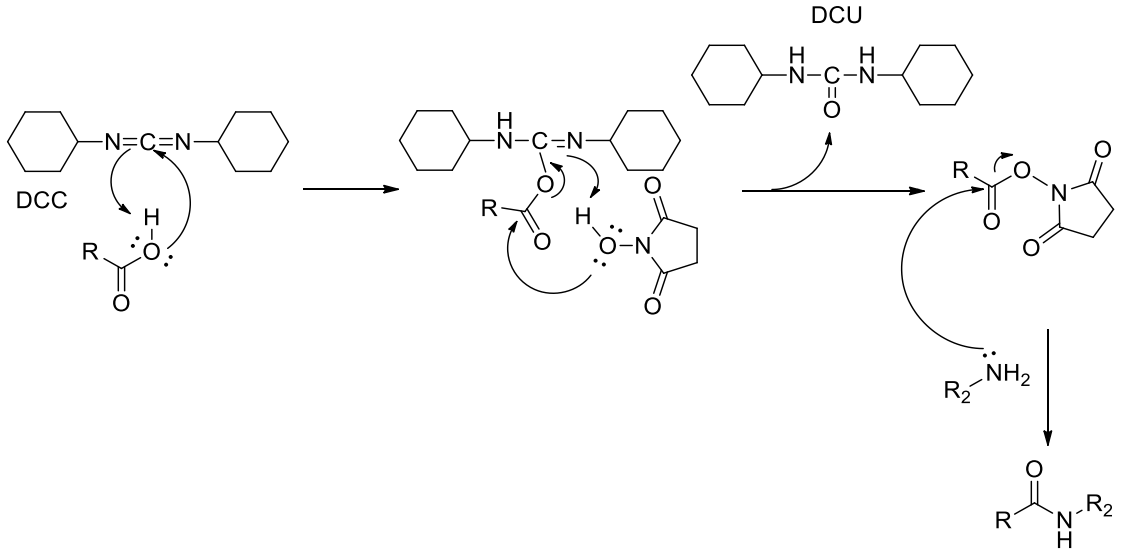

Figure 21. Mechanism of peptide coupling using DCC/NHS.

Using the activated bromobutyric acid, this final step resulted in the formation of a mixture of products substituted with a bromine and/or a carboxylic group. This probably occurs due to the high electronegativity of Br, which is also considered a good leaving group. Thus, the bromide intermediary **BrVal$_n$Br** obtained from the peptide coupling reactions was not isolated, and the resultant mixture was immediately reacted with NaN_3, obtaining the correspondent bisazide derivatives (**N$_3$Val$_n$N$_3$**) by a typical bimolecular nucleophilic substitution (S_N2) reaction. In the S_N2 reaction, the departure of the living group occurs simultaneously with the attack by the nucleophile (**Figure 22**).

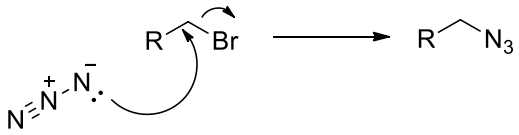

Figure 22. S_N2 reaction mechanism.

The final step of the synthesis consisted in a Huisgen 1,3-dipolar cycloaddition with commercially available phenylacetylene, yielding the **PhTzVal$_n$** family of gelators. This reaction occurs between a dipolarophile and a 1,3-dipolar compound, leading to the formation of five membered heterocycles.

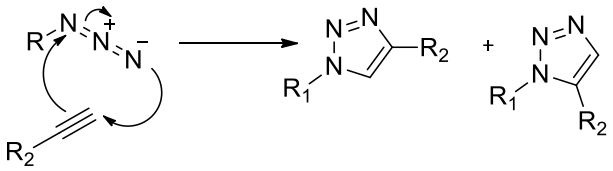

Figure 23. Mechanism of uncatalyzed Huisgen 1,3-dipolar cycloaddition.

The 2π electrons of the dipolarophile and the 4π electrons from the dipolar compound participate in the reaction, guiding to a [3+2] cycloaddition. As the two possible HOMO-LUMO interactions are closely related in terms of energy, the reaction leads to a mixture of an approximately 1:1 mixture of regioisomers. However, the presence of copper(I) as catalyst provides some regioselectivity for the reaction, favouring the formation of 1,4-disubstituted regioisomers.

The structures of the two families of gelators (**PhTzVal$_n$** and the corresponding bisazide derivatives **N$_3$Val$_n$N$_3$**) obtained by this synthetic route are represented in **Figure 24**.

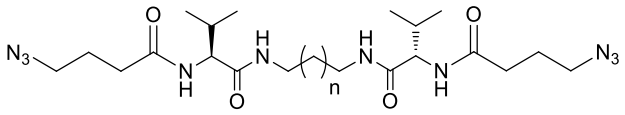

$N_3Val_3N_3$: n=1
$N_3Val_6N_3$: n=4
$N_3Val_8N_3$: n=6

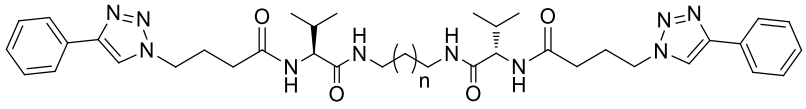

$PhTzVal_3$: n=1
$PhTzVal_6$: n=4
$PhTzVal_8$: n=6

Figure 24. Structure of the intermediate **$N_3Val_nN_3$** and final **$PhTzVal_n$** gelators.

The synthesized bolaamphiphilic gelators exhibit a central apolar carbon chain as a spacer between the *L*-valine fragments, and pending polar azide (**$N_3Val_nN_3$**) or triazole (**$PhTzVal_n$**) fragments. The four amide bonds present in their structure could contribute for gelation by building intermolecular hydrogen bonds.

3.2.1.2. Viscoelastic and Thermotropic Properties

The gelation ability of the family of compounds **$PhTzVal_n$** was tested in variety of solvents with different polarity, ranging from toluene to methanol (**Table 1**). The triazolyl functionalized compounds **$PhTzVal_n$** were able to form self-sustainable gels in several solvents (organogels), including water and/or water-alcohol mixture (hydrogels). Between the investigated compounds, the one with the longest carbon chain length **$PhTzVal_8$** showed the best gelation ability, returning a gel in all the tested solvents (**Table 1**). The good gelation ability of these compounds arises from the amphiphilic character of the molecules, composed by an apolar moiety which comprises a middle carbon chain, and a more polar moiety comprising the presence of amides and the ending triazole fragment.

Table 1. Gelation experiments of compounds **PhTzVal$_n$**[a].

Solvent	PhTzVal$_3$	Aspect	PhTzVal$_6$	Aspect	PhTzVal$_8$	Aspect
Toluene	PP	-	PP	-	G	transparent
Dichloromethane	G	transparent	PP	-	G	translucent
Ethanol	G	transparent	G	translucent	G	translucent
H_2O	SP	-	I	-	G	transparent
H_2O:t-BuOH (1:1)	G	transparent	G	translucent	G	translucent
2-propanol	G	transparent	SP	White	G	translucent
Methanol	G	transparent	G	translucent	G	translucent
Acetonitrile	G	transparent	G	translucent	G	translucent

[a] I: Insoluble, G: Gel, SP: Swollen precipitate, PP: Precipitate, *c* = 8 mg/mL.

Similar gelation experiments were carried in the presence of copper(I). The formation of metallogels **Cu(I)-PhTzVal$_n$** was successfully achieved by heating the copper salt Cu[(MeCN)$_4$]PF$_6$ together with the **PhTzVal$_n$** gelators in a 1:2 molar ratio until complete dissolution, followed by sonication. The **PhTzVal$_n$** gelators self-assembled in the presence of the metal, resulting in the formation of a coordination compound resembling most probably to the Cu(I)-TBTA described in literature,[5] where the triazole fragment coordinates the central copper(I) atom in a tetrahedral geometry.[18]

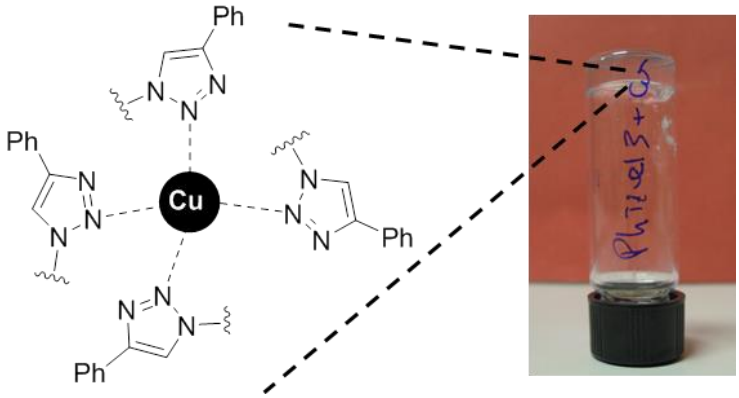

Figure 25. Scheme of the Cu(I) coordination to the gel network (A) and macroscopic aspect of the metallogel Cu(I)-**PhTzVal$_3$** in 1:1 H_2O:*t*-BuOH. The presence of dinuclear Cu(I) species cannot be discarded**.**

All the compounds belonging to the **PhTzVal$_n$** family were able to form gels with and without the presence of copper in the selected solvents, meaning that metal coordination was not the essential driving force for the self-assembly of the compounds.

Amongst the parameters that could describe a specific gel, sol-to-gel and gel-to-sol transitions are relatively easy to identify by using visual inspection techniques, such as dropping ball technique, bubble motion or the inverted test tube method. The last method was applied to

determine the minimum gelation concentration (m.g.c.) of the **PhTzVal$_n$** gels and corresponding metallogels in three different solvents, including 1:1 H_2O:*t*-BuOH, EtOH and MeOH.

Table 2. Minimum gel concentration of the **PhTzVal$_n$** native gelators and of the correspondent metallogels.

	Concentration (mM)/Solvent					
	H_2O:*t*-BuOH		**EtOH**		**MeOH**	
Gelator	**Native**	**Metallogel**	**Native**	**Metallogel**	**Native**	**Metallogel**
PhTzVal$_3$	4.1	5.2	4.4	4.4	4.7	4.9
PhTzVal$_6$	2.7	3.4	6.0	4.5	4.9	3.9
PhTzVal$_8$	2.9	2.9	6.9	5.5	7.4	6.5

The lowest minimum gelation concentrations were obtained for the native gels (without metal) in 1:1 H_2O:*t*-BuOH, meaning that these compounds have a higher tendency to form gels in mixture of polar/apolar protic solvents, which is well in accordance with the amphiphilic nature of their structure. The lower minimum gelation concentration observed for the gelators with longer carbon chain length **PhTzVal$_6$** and **PhTzVal$_8$** in H_2O:*t*-BuOH also supports this statement. In more polar solvents such as EtOH and MeOH, the minimum gelation concentration of such compounds considerably increases, in contrast with the one determined for the most polar gelator **PhTzVal$_3$**.

Regarding the metallogels, the presence of copper caused a decrease in the minimum gelation concentration (m.g.c.) of the gelators **PhTzVal$_6$** and **PhTzVal$_8$** in EtOH and MeOH, meaning that it could positively contribute for the gelation of these compounds (**Table 2**). However, in the solvent media H_2O:*t*-BuOH, the opposite effect is observed for the gels **PhTzVal$_3$** and **PhTzVal$_6$**, while in the gel **PhTzVal$_8$** the minimum gelation concentration is maintained. Such behavior suggests that the metal influences the self-assembly process of the gelators, creating a more polar environment that facilitates the formation of the gels in polar organic solvents in respect to the less polar mixture H_2O:*t*-BuOH.

The thermoreversibility of gels formed by the standard heating-cooling method allows the identification of characteristic temperatures regarding the assembly and disassembly processes. In sol-to-gel and gel-to-sol transitions, the temperature at which the gel is formed (T_{gel}) and the one at which the gel loses its structural integrity (T_{sol}) may also be identified by simple visual inspection techniques. The thermotropic characterization of the gels **PhTzVal$_n$** and the corresponding metallogels was achieved by the determination of the T_{sol}.

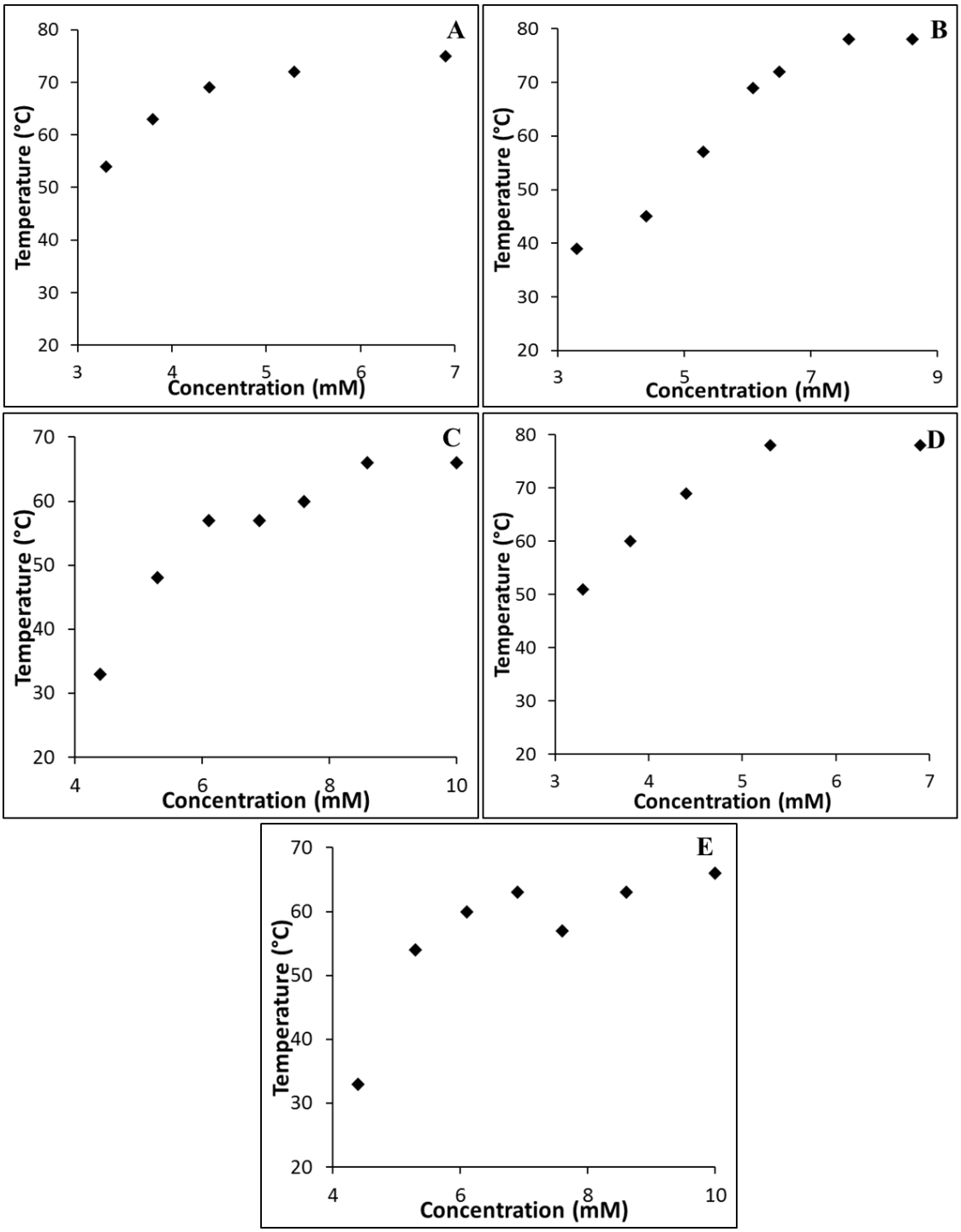

Figure 26. T_{sol} of the gels **PhTzVal$_3$** (A), **PhTzVal$_6$** (B), **PhTzVal$_8$** (C) and of the metallogels **Cu(I)-PhTzVal$_3$** (D) **and Cu(I)-PhTzVal$_8$** (E), determined using EtOH as solvent medium.

By looking at **Figure 26A-C**, it can be concluded that the gel **PhTzVal$_3$** exhibit the highest T_{sol} values, suggesting that it is able to form the strongest gels in EtOH. For example, at a concentration of 4.4 a 5.3 mM, this gel exhibits a T_{sol} of 69 ºC and 72 ºC, respectively, which is considerably higher than the one exhibited by the gels **PhTzVal$_6$** (45 ºC and 57 ºC, respectively) and **PhTzVal$_8$** (33 ºC and 48 ºC, respectively) under similar concentrations. This suggests that for

EtOH, as the carbon chain length of the gelator molecule increases, the gels become more fragile and more difficult to form. Such hypothesis is also confirmed by the higher m.g.c. registered for the gels with longer carbon chain **PhTzVal$_6$** and **PhTzVal$_8$** in this specific solvent (**Table 2**). It is important to highlight that the gels prepared for this experiment were aged for 1 h, while the ones used in the determination of the minimum gel concentration have been aged just for 20 minutes. This different aging time may explain the formation of gels below the m.g.c. values determined in **Table 2**.

The effect of the presence of copper in the thermotropic properties of the gels **PhTzVal$_3$** and **PhTzVal$_8$** was also evaluated (**Figure 26D-E**). In both cases, it was observed that the coordination with copper resulted in the formation of gels with slightly higher T_{sol}, suggesting that the metal reinforced the structure of the gel probably by inducing crosslinking within the gel network. While in the metallogel **Cu(I)-PhTzVal$_3$** this effect was better observed for higher gel concentrations such as 5.3 mM and 6.9 mM, where the T_{sol} increased from 72 ºC and 75 ºC, respectively, to 78 ºC (boiling point of the ethanol) in the metallogel **Cu(I)-PhTzVal$_8$** this effect was observed in the whole range of concentrations tested. This accentuated reinforcement effect observed in the gels **Cu(I)-PhTzVal$_8$** is well in accordance with their lower m.g.c. values, if compared with the ones found for the native gels (**Table 2**). For the gels **PhTzVal$_3$**, this parameter remained constant independently on the presence of the metal.

The addition of copper provided these compounds with thixotropic ability, being able of recovering the gels once they are broken.

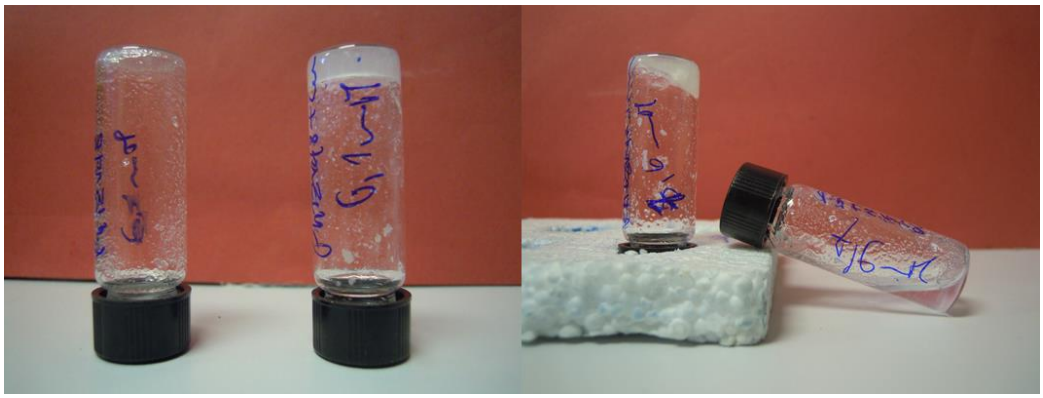

Figure 27. Macroscopic aspect of the **PhTzVal$_8$** gels of the corresponding metallogels at concentrations of 6.1 mM and 7.6 mM, 24h after their disintegration in the T_{sol} determination experiment.

After finishing the experiment for the T_{sol} determination, the disintegrated gels were left at room temperature. On the next day, it could be observed that the disrupted gels present on the vials containing copper(I) have been recovered, acquiring their initial gel form. This phenomenon was common to all the **Cu(I)-PhTzVal$_n$** gels and for all the concentrations, supporting the hypothesis that the copper(I) may form cross-linking metal bridges between the several gelator molecules or aggregates during the self-assembly process. After breaking the recovered gels with a spatula and subsequent aging for one day, the gels were able to regenerate, creating a network capable of entrapping all the solvent. Such repeatable self-healing ability could potentiate the use of these metallogels in tissue regeneration.

3.2.1.3. Structural and Morphologic Characterization

To assess if the metal-ligand interaction influenced the final structural arrangement of the hybrid metal-organic gel networks, wide angle X-ray diffraction (WAXD) was performed on the native and hybrid metallogels (**Figure 28**). The diffractograms revealed that the native gelator **PhTzVal$_3$** exhibits a totally amorphous pattern, while the ones having longer carbon chain self-assembled in a more ordered structure, with low-angle peaks at 21.8 Å (**PhTzVal$_6$**) and 26.4 Å (**PhTzVal$_6$**) assignable to the length of partially extended molecules, as described before for related analogues.[19]

However, in the presence of the metal, sharp diffraction peaks appeared together with the broad signals of gelators that can be assigned to a periodic disposition of copper atoms coordinated to the network.

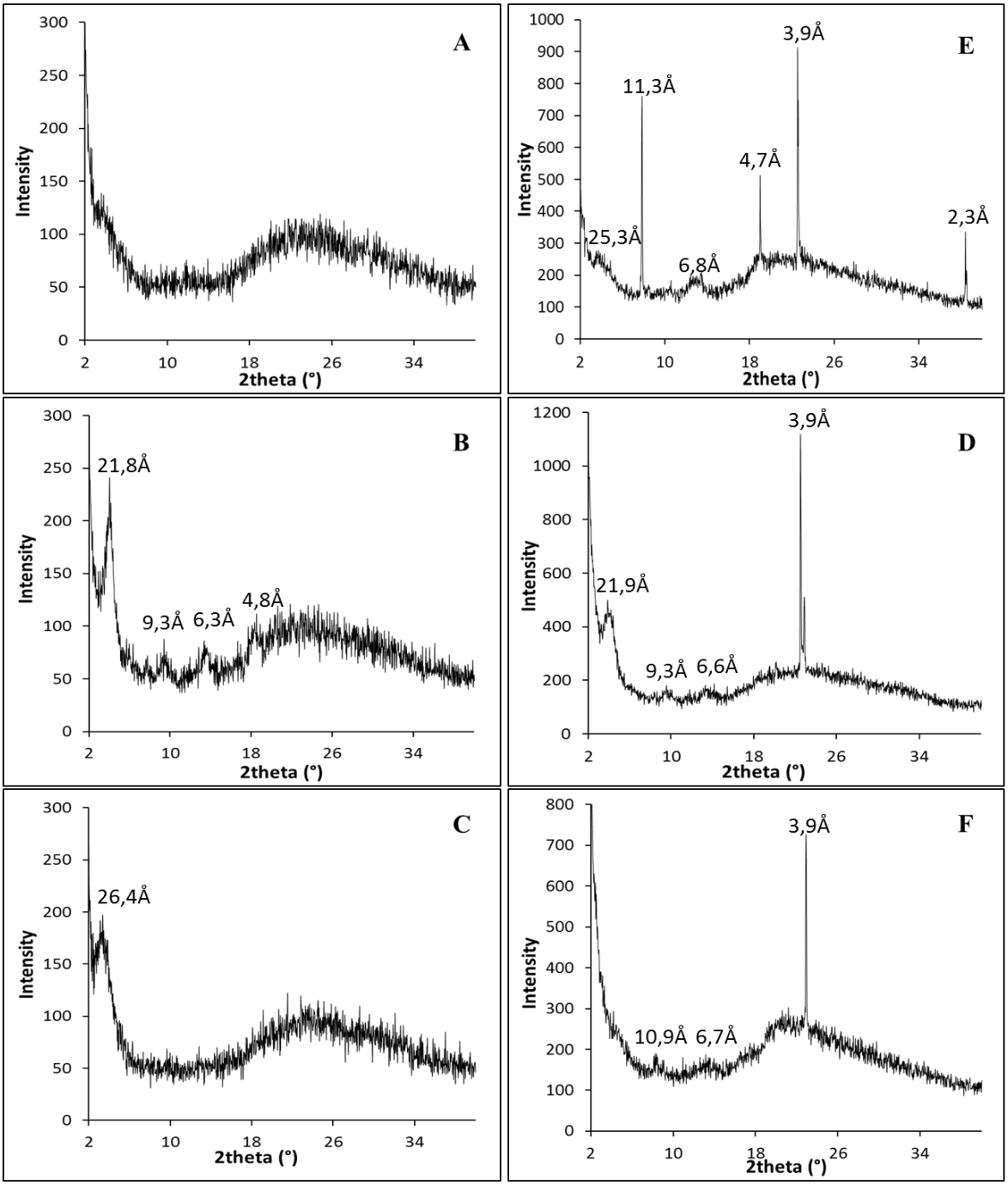

Figure 28. XRD analysis of gels **PhTzVal$_3$** (A), **PhTzVal$_6$** (B), **PhTzVal$_8$** (C), and of **Cu(I)-PhTzVal$_3$** (D), **Cu(I)-PhTzVal$_6$** (E), **Cu(I)-PhTzVal$_8$** (F) metallogels.

It should be mentioned that these peaks do not correspond to free copper salt $Cu[(MeCN)_4]PF_6$, for whom a periodicity of 1:1/2 between the first two peaks could be observed in the obtained diffractogram (**Figure 29**).

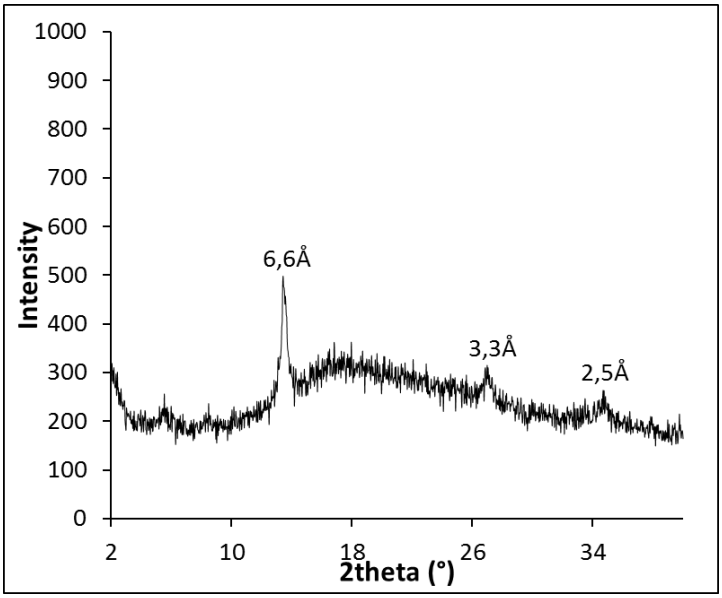

Figure 29. Diffractogram of the copper salt $[Cu(MeCN)_4]PF_6$.

The influence of the metal on the self-assembly of the gelator molecules was more pronounced in the shorter carbon chain length gelator **PhTzVal$_3$** (**Figure 28D**), resulting in the formation of a metallogel with a more crystalline structure. Although the presence of the metal is not the main driving force for gelation of the compounds belonging to the **PhTzVal$_n$** family, as observed for other metallogels reported in literature,[17,20,21,22,23,24] it seems that the metal-ligand interactions have some influence on the self-assembly process of these gelators. It has already been reported that metal-ligand interactions could influence the gelation, resulting in multifunctional metallogels with new interesting properties that could not be achieved in organogels, such as optical, catalytic or magnetic properties.[25,26,27]

The influence of the copper and of the carbon chain length on the mechanical properties of the gels was evaluated by rheology (**Figure 30**). This science refers to the response of materials to an applied stress, giving information on their capacity to store energy or to dissipate it as heat. Two components can be extracted from rheological analysis, one related with energy storage *G'* and another referring to energy dissipation (*G"*). When *G'* > *G"* means that the material presents a viscoelastic behaviour and is able to store energy, recovering its original shape upon an applied stress. On the other hand, if *G'* < *G"*, the material loses its viscoelastic properties and behaves as a viscous material. The measurement of the storage modulus *G'* and loss modulus *G"* were performed as a function of the oscillatory frequencies. For all the samples, it was observed that *G'* was almost constant and about one order of magnitude larger than *G"* over all the frequency range, highlighting the strong consistency of the gels. This suggests that the gels present a static network that is not easy to break, being classified as hard gels. Furthermore, the typical frequency sweep

curves obtained for the native gels in EtOH suggest that the strength of the gel decreases as the middle carbon chain length increases, which is consistent with the results provided by the m.g.c. and T_{sol} experiments for the native gels.

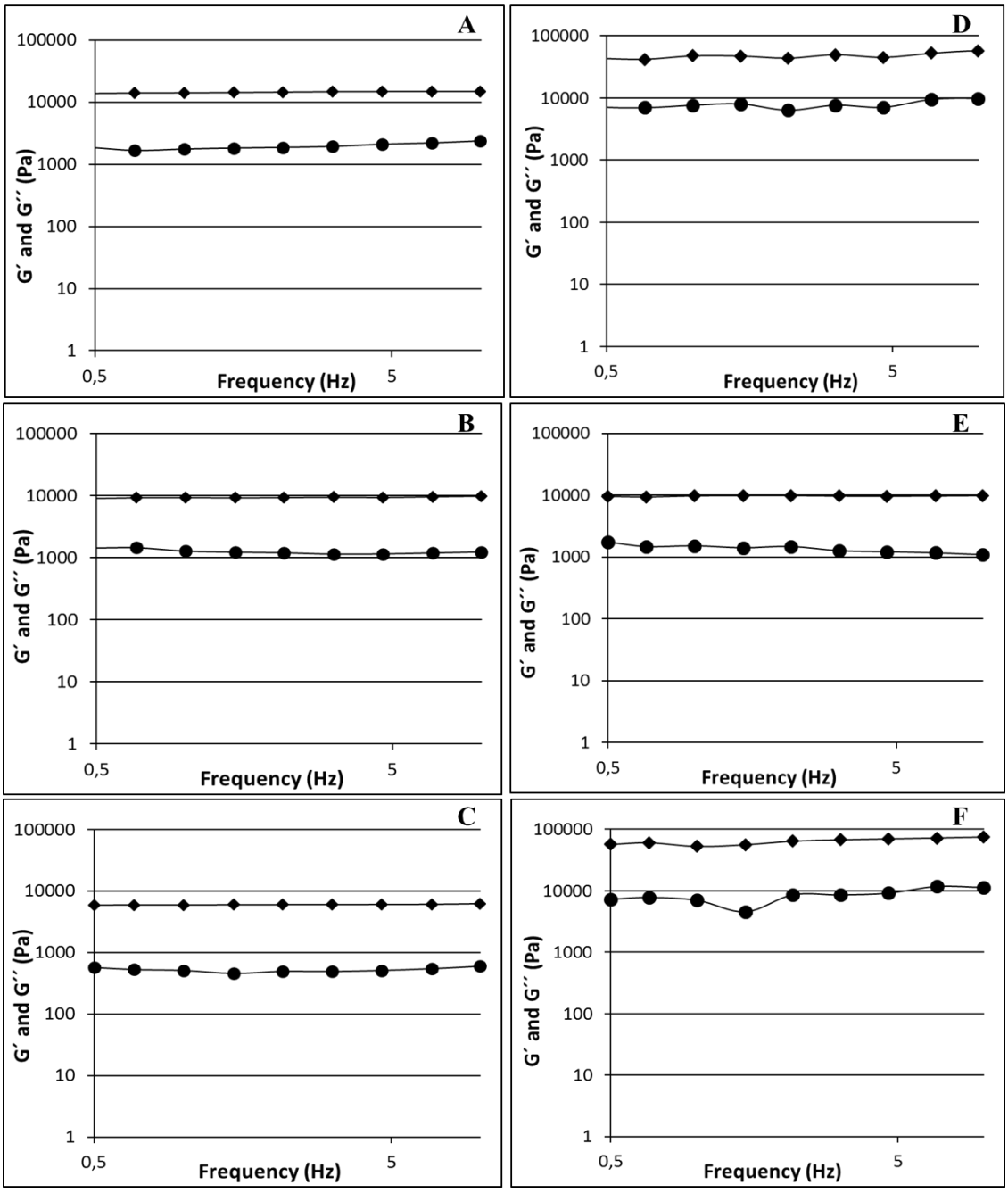

Figure 30. Typical sweep frequency curves with *G'* (◆) and *G''* (●) of the gels **PhTzVal$_3$** (A), **PhTzVal$_6$** (B), **PhTzVal$_8$** (C) and the corresponding metalogels **Cu(I)-PhTzVal$_3$** (D), **Cu(I)-PhTzVal$_6$** (E) and **Cu(I)-PhTzVal$_8$** (F). The gels were formed using EtOH as solvent medium.

Similarly to what has been observed for the native gels, in the presence of the metal, G' was also one order of magnitude higher than *G''* along all the frequency range.The analysis of the frequency sweep curves obtained for the metallogels allowed to conclude that the presence of the metal

increases the strength of the gel, being this effect more pronounced in the metallogel **Cu(I)-PhTzVal$_8$**.

The viscoelastic behaviour of the gels and the corresponding metallogels was investigated by stress-sweep tests (**Figure 31**). In this experiment, the samples are subjected to oscillating stress, and their response measured in terms of elastic storage *G'* and loss moduli *G"*. The native gels exhibit large linear viscoelastic regions where *G*' and *G*" remains constant until an oscillatory stress 250 Pa is applied, beyond which both the elastic moduli and the loss moduli starts to decrease abruptly. Here it is also evident that the gels become more viscoelastic with the increase of the carbon spacer length and that *G'* continues to be one order of magnitude higher than *G"*, highlighting the high viscoelasticity of the static gel network. For the metallogels, a similar relationship between *G*' and *G"* has been observed, with the former being constantly higher than the later, independently of the applied stress. However, in the metallogels this behaviour is maintained to higher oscillatory stress values than in the native gels, exhibiting 4-5 fold greater resistance to stress. For example, the metallogels **Cu(I)-PhTzVal$_3$** and **Cu(I)-PhTzVal$_8$** exhibit a constant *G'* and *G"* until oscillatory stress values of 1000 and 1260 Pa, whereas the correspondent native gels were not able to resist to oscillating stress higher than 250 Pa. This fact highlights the reinforcement of the gel network by the metal, which is in accordance with the increase in T_{gel} observed in the metallogels. Furthermore, the viscoelasticity of the metallogels were always higher than the one of the native gels, except for the gel **Cu(I)-PhTzVal$_6$**, whose viscoelasticity seem to be similar to its metal free analogue gel.

For both native and metallogels **Cu(I)-PhTzVal$_3$** and **Cu(I)-PhTzVal$_8$**, it is also peculiar to observe that when they are submitted to high oscillating stress, (> 1000 Pa), an abrupt decrease of *G'* and *G"* is observed, corresponding to their deformation. The strong viscoelasticity together with the hard nature of these metallogels could explain their thixotropic behaviour.

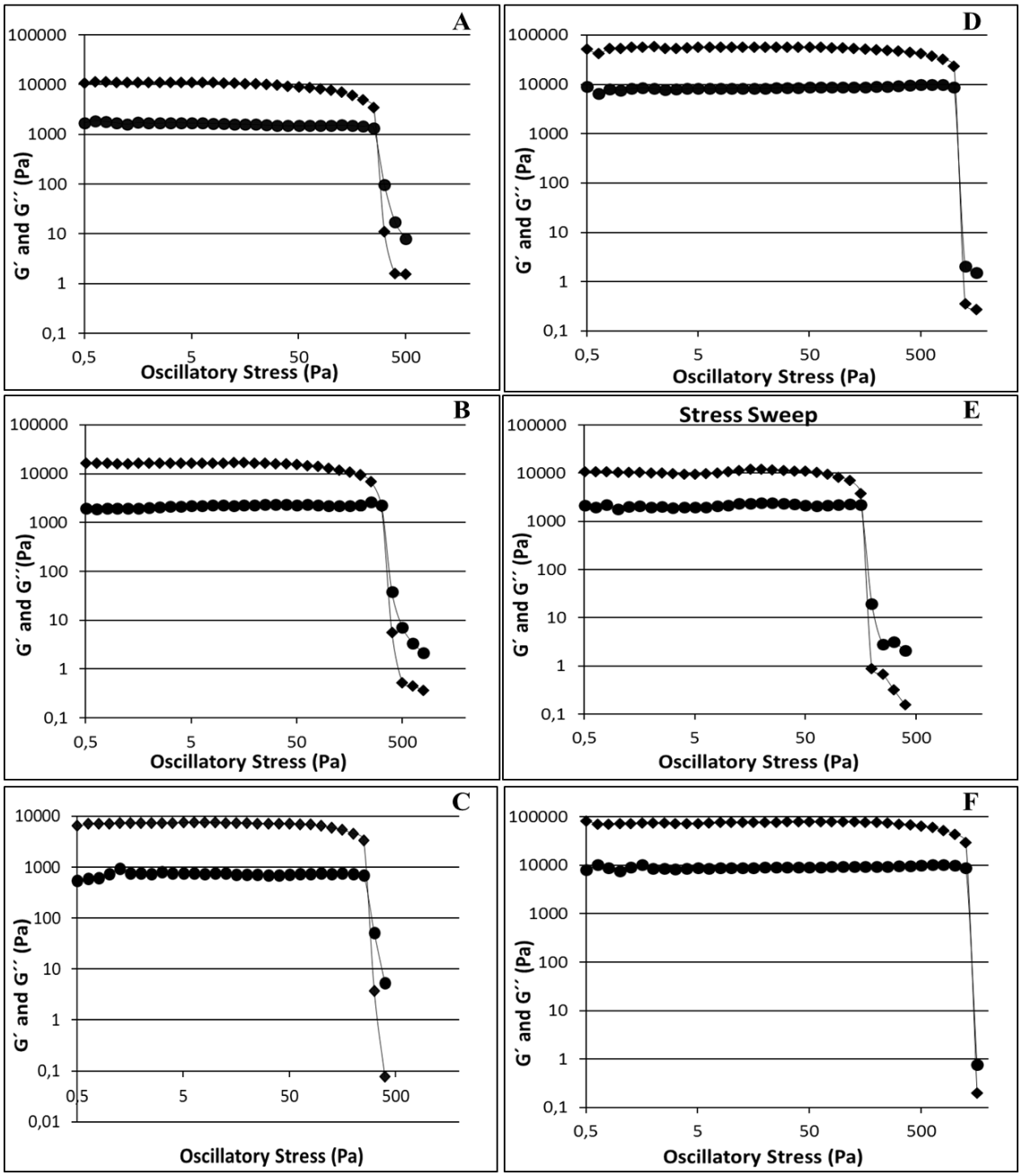

Figure 31. Typical stress-sweep curves with *G'* (◆) and *G''* (●) of the gels **PhTzVal$_3$** (A), **PhTzVal$_6$** (B), **PhTzVal$_8$** (C) and the corresponding metalogels **Cu(I)-PhTzVal$_3$** (D), **Cu(I)-PhTzVal$_6$** (E) and **Cu(I)-PhTzVal$_8$** (F). The gels were formed using EtOH as solvent medium.

The native gels and the corresponding metallogels were also studied by circular dichroism (CD) spectroscopy in order to have some insight on the chirality of the resultant self-assembled materials (**Figure 32**). All the gels exhibited a positive or negative dichroism signal, evidencing that the chiral information present at molecule scale was transferred into gel-phase assemblies. The spectra of the native gels having a longer carbon chain length **PhTzVal$_6$** and **PhTzVal$_8$** are characterized by the presence of an intense negative band at 207 and 197 nm, respectively,

suggesting similar supramolecular arrangement. The gel with the smallest carbon chain length **PhTzVal$_3$** seems to self-assemble in a different conformation, exhibiting two negative bands at 224 and 207 nm together with a positive lobe at 190 nm, which is characteristic of a helical type conformation.[28]

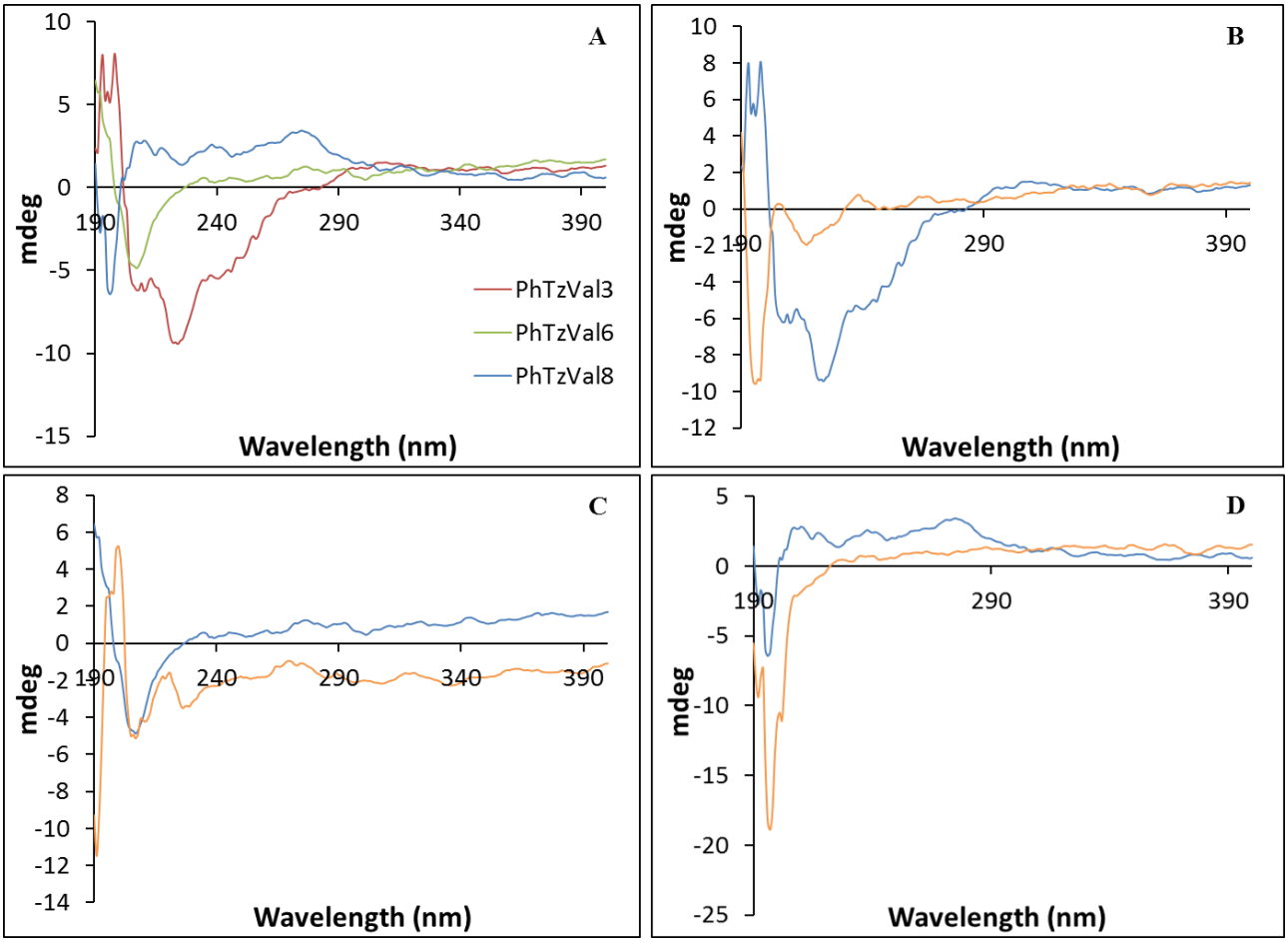

Figure 32. Circular dichroism spectroscopy of the gels: A) CD spectra corresponding to native gels. B-D) Comparison between native gels (blue) and metallogels (orange) **PhTzVal$_3$**, **PhTzVal$_6$** and **PhTzVal$_8$**, respectively.

Such kind of helical arrangement has been also observed on *L*-valine derived bolaamphiphilic gelators functionalized with proline fragments and having a three carbon spacer.[29] These results suggest that gelator with smallest carbon chain self-assembles in a different supramolecular packaging structure in comparison with the ones with largest carbon chain, which is in accordance with the WAXD studies on the native gelators. This different supramolecular organization is derived by the preferred formation of hydrogen bonds between different hydrogen donor and hydrogen acceptor atoms on two consecutive column packed molecules, leading to different energetically stable molecular packaging models depending on the odd/even carbon spacer length (**Figure 33**).[30] Furthermore, the appearance of a negative band followed by a positive band in the CD spectrum of **PhTzVal$_3$** may suggest that the molecule aggregates in an anticlockwise orientation of the

chromophores (M)-chirality.[31]

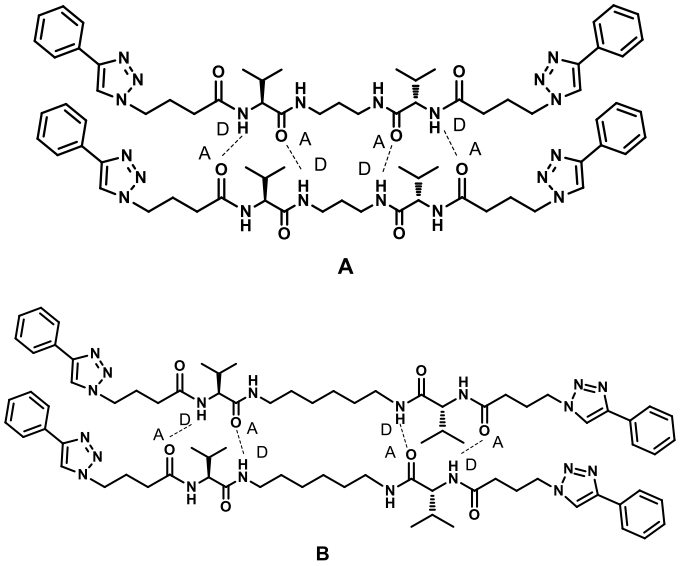

Figure 33. Models suggested for the packing of compounds **PhTzVal$_3$** (A) and **PhTzVal$_6$** (B). A: Acceptor; D: Donor.

The presence of the metal did not have a significant influence on the supramolecular aggregation of the gels, except for the **PhTzVal$_3$** gel, where a blue-shift of the band at 224 nm to 217 nm followed by a decrease in intensity was observed. Furthermore, a change in the signal of the positive band at 195 nm has also been observed. This suggests that the copper influences the supramolecular packing of the gelator, probably by interfering in the intramolecular or intermolecular interactions during the self-assembly process, providing a different conformational orientation. In the metallogel **Cu(I)-PhTzVal$_6$**, it seems that the addition of copper(I) induced an helical-type arrangement suggested by the appearance of a positive band around 195 nm. This copper-induced helical type arrangement may be on the source of the worse mechanical properties evidenced by the corresponding metallogel, when compared with the mechanical performance of **Cu(I)-PhTzVal$_3$** and **Cu(I)-PhTzVal$_8$**.

The obtained metallogels were also analysed by TEM, revealing some differences in the morphology of the fibres depending on the carbon chain length. For this experiment, the gels were prepared in MeOH and analysed without staining. While in the gel having the shortest carbon chain length, it was possible to observe a highly crosslinked network of fibres having 10-12 nm width (**Figure 34A**), the metallogels with six carbon chain length presented smaller fibres, which may also reflect its worse mechanical performance (**Figure 34B**).

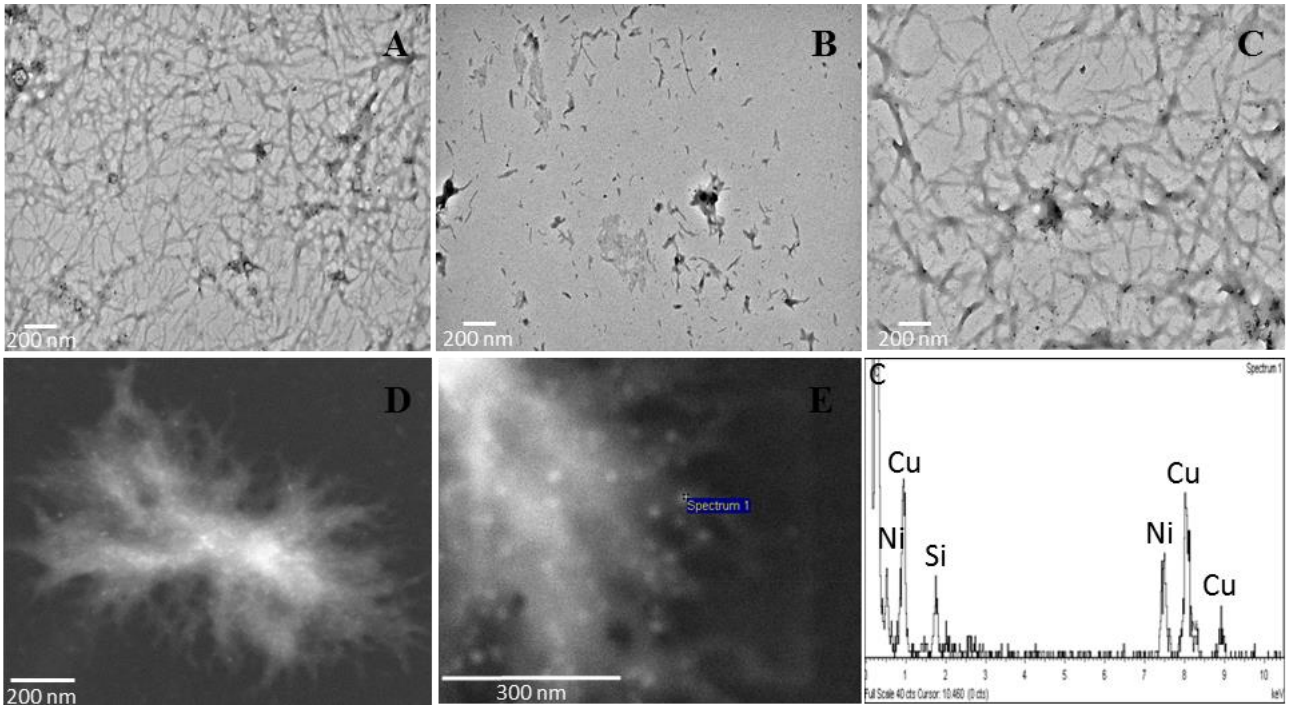

Figure 34. TEM analysis of metallogels **Cu(I)-PhTzVal$_3$** (A), **Cu(I)-PhTzVal$_6$** (B), **Cu(I)-PhTzVal$_8$** (C). STEM analysis of metallogels formed by compound **PhTzVal$_6$** (D, E) and the correspondent EDS elemental analysis (F). Magnifications are 12000x (A-C), 80000x (E), 100000x (D).

The presence of copper on the gel network allowed the characterization of these structures using scanning transmission electron microscopy (STEM) and without staining. The analysis was performed on the **PhTzVal$_6$** sample previously prepared for TEM analysis. The white contrast of the fibers (**Figure 34D-E**) constitutes an evidence of the successful formation of a hybrid organic-inorganic network. Energy-dispersive X-ray spectroscopy (EDS) analysis performed on the fibres revealed the presence of Cu together with C and O, confirming the successful coordination of the copper to the gel (**Figure 34F**).

3.2.1.4. Autocatalytic behaviour of PhTzVal$_n$ gels

As gelators **PhTzVal$_n$** are synthesized through a click reaction it may be proposed to use **Cu(I)-PhTzVal$_n$** metallogels as catalysts for the ligand synthesis starting from the azide precursors (autocatalysis) (**Figure 35**). As observed for the **PhTzVal$_n$** family, the bis-azide precursors **N$_3$Val$_n$N$_3$** also form gels in methanol, both in the presence and absence of copper. The obtained **N$_3$Val$_n$N$_3$** gels were transparent and colourless but acquired a green colour when formed in the presence of the copper salt $[Cu(MeCN)_4]PF_6$.

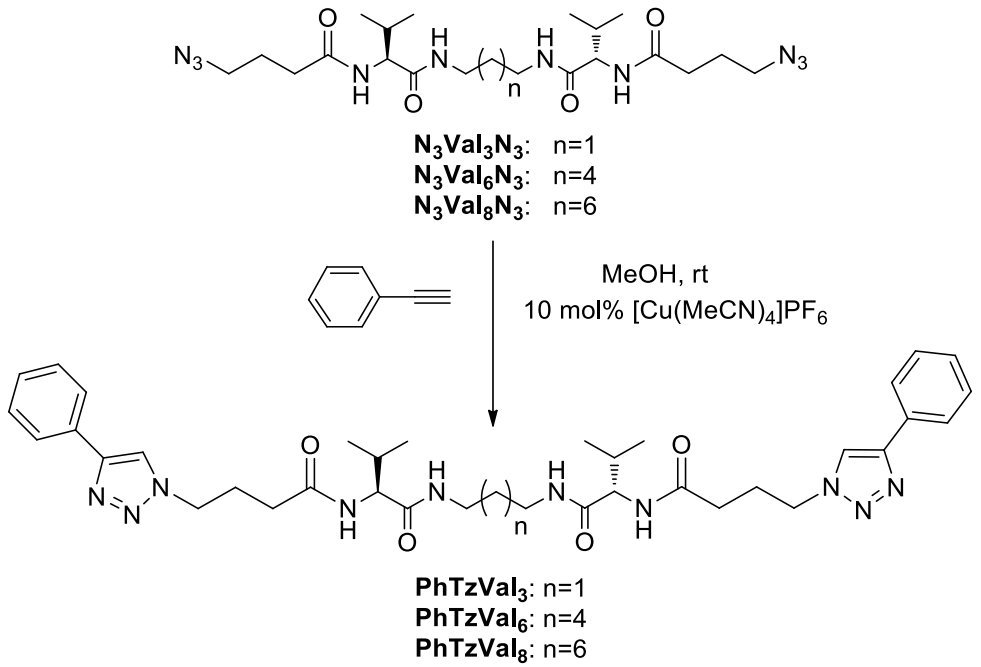

Figure 35. Huisgen's 1,3-dipolar cycloaddition guiding to the formation of the **PhTzVal$_n$** catalysts.

For the study of the autocatalytic ability of the metallogels **Cu(I)-PhTzVal$_n$**, the reactant **N$_3$Val$_n$N$_3$**, the gelator **PhTzVal$_n$** and the copper salt $[Cu(MeCN)_4]PF_6$, in a molar ratio 10:1:1, were gelled together in a 4 mL screw-capped vial containing methanol as solvent, following by the addition of phenylacetylene on the top of the two-component gel. In these autocatalytic reactions, a little excess of copper salt was used attending to the possibility that some of the **N$_3$Val$_n$N$_3$** gel could also participate in copper coordination. The aim of the autocatalysis experiment was to evaluate if there was an increase in the rate of the reaction due to the continuous production of catalyst. As observed in **Figure 36**, all the metallogels exhibited autocatalytic activity, being capable of catalysing their own synthesis.

In the absence of an initial amount of **Cu(I)-PhTzVal$_n$** metallogel an induction time with low or null conversion is observed, corresponding to the lapse required to obtain a minimum amount of active coordinated copper by slow catalysis of uncoordinated $[Cu(MeCN)_4]PF_6$. This effect is particularly evident in **Figure 36A**.

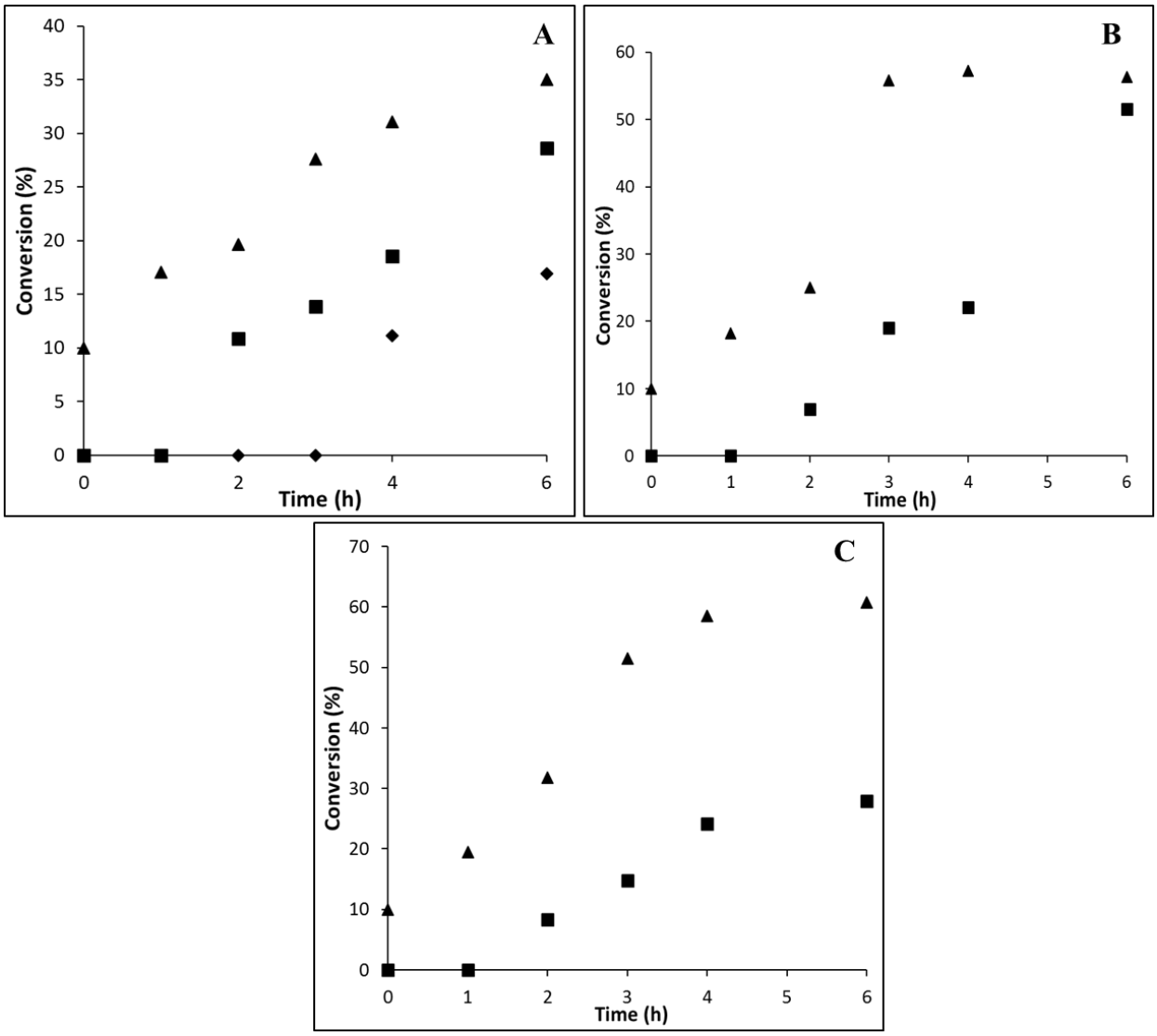

Figure 36. Kinetics of the Huisgen's 1,3-dipolar cycloaddition between $\mathbf{N_3Val_nN_3}$ and phenylacetylene in the presence of 5 mol% $[Cu(MeCN)_4]PF_6$ (♦), 10 mol% $[Cu(MeCN)_4]PF_6$ (■) and in the presence of 10 mol% metallogels (▲) **Cu(I)-PhTzVal$_3$** (A), **Cu(I)-PhTzVal$_6$** (B) and **Cu(I)-PhTzVal$_8$** (C), during the first 6 h of reaction.

It is remarkable to mention that both reactant $\mathbf{N_3Val_nN_3}$ and catalyst **Cu(I)-PhTzVal$_n$** are in the gel phase. Therefore, it could be proposed that initially the reaction could take place in those azide groups at the vicinity of the Cu-Triazole (Tz) catalytic sites. However, as the reaction continues the number of azide groups near catalytic centres would decrease and we could expect a decrease in the catalytic activity with time. Nevertheless, all the gel catalysts drive the reaction until completion, being the time required for achieving a quantitative conversion 48h for the gelator **PhTzVal$_3$** and 14h for the gelators with longer carbon chain **PhTzVal$_6$** and **PhTzVal$_8$**.

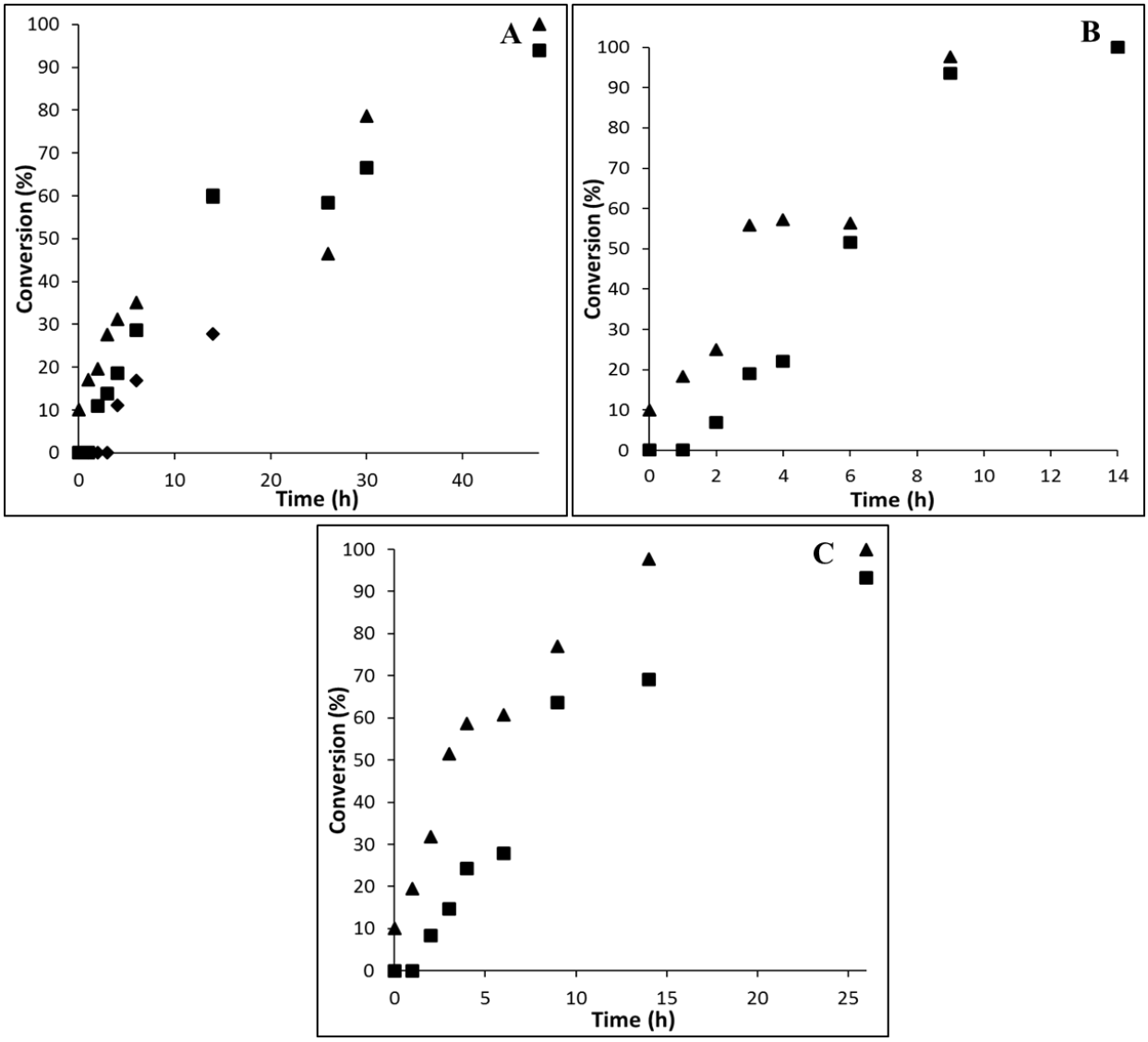

Figure 37. Kinetics of the Huisgen's 1,3-dipolar cycloaddition between $\mathbf{N_3Val_nN_3}$ and Phenylacetylene in the presence of 5 mol% $[Cu(MeCN)4]PF_6$ (♦), 10 mol% $[Cu(MeCN)4]PF_6$ (■) and in the presence of 10 mol% metallogels **Cu(I)-PhTzVal$_3$** (A), **Cu(I)-PhTzVal$_6$** (B) and **Cu(I)-PhTzVal$_8$** (C), during 48h (A), 14h (B) and 25h (C).

These results are not surprising taking into consideration the well-known dynamic behaviour of molecular gels that involves a reversible disassembly-reassembly process, as well as the reported lability of Tz-Cu complexes which could allow the translocation of copper(I) ions all over the fibrillar network.[32,5] These dynamic processes would be responsible for the re-location of reactive $\mathbf{N_3Val_nN_3}$ components close to the catalytic centres and/or the translocation of metal ions towards **PhTzVal$_n$** molecules close to the azide analogues. This dynamic behaviour of ligands and metal ions along a gel phase has been already reported in BTP based gels with repeating self-healing ability.[33]

A brief comparison between the results obtained in **Figure 36** suggest a positive influence of the carbon chain length on the catalytic performance of the metallogelators, with the gels **PhTzVal$_6$**

and **PhTzVal$_8$** exhibiting a higher catalytic activity than the corresponding analogue with a 3 carbon chain, **PhTzVal$_3$**. Any direct relationship between the observed catalytic activity and the amount of copper coordinated to the **PhTzVal$_n$** gels or to the initial **PhTzVal$_n$/N$_3$Val$_n$N$_3$** two-component gel mixtures was completely discarded, as the amount of copper coordinated to them was found to be >99% in all cases, determined by ICP-MS. Furthermore, the formation of the **Cu(I)-PhTzVal$_8$** complex was successfully confirmed by mass spectrometry, where a peak corresponding to the mass of the gelator coordinating copper in a 2:1 ratio has been observed ($[M+H]^+$=831.4097).

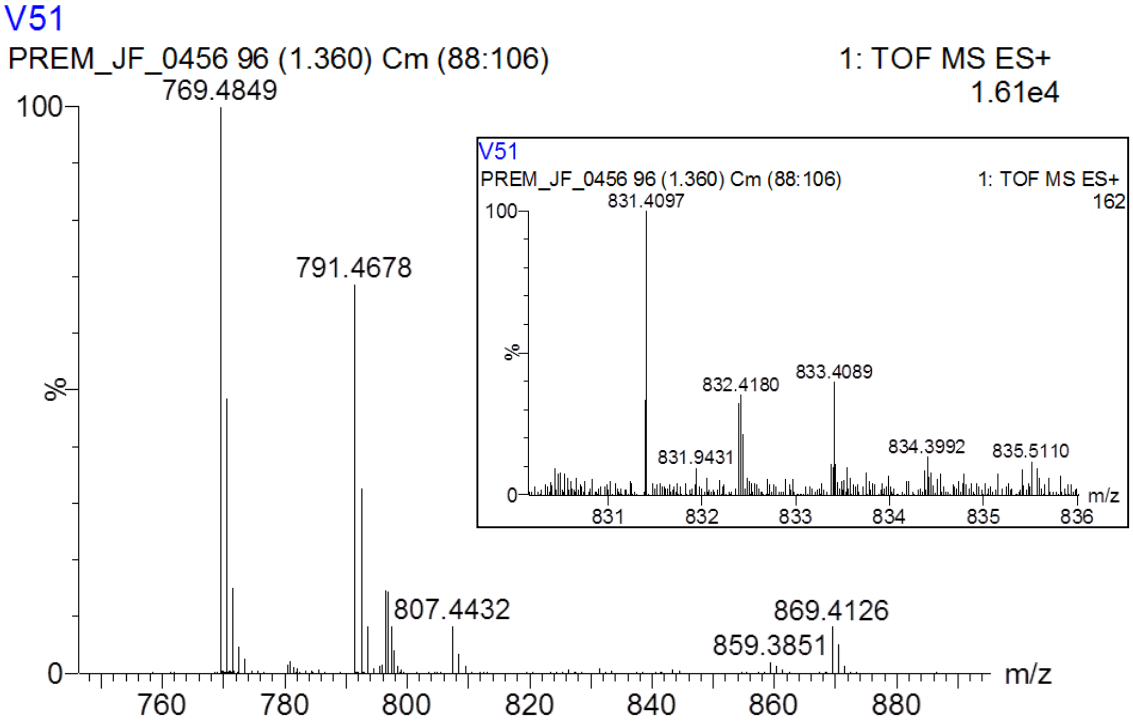

Figure 38. Mass spectra of the **Cu(I)-PhTzVal$_8$** metallogel. The inset represents an amplification of the zone m/z= 830-836.

To better understand if the difference observed in the catalytic performance of these materials is related with a different supramolecular arrangement of the gel network, the mixtures were analysed by WAXD at different stages of the reaction. For comparative issues, the bisazide metallogels **Cu(I)-N$_3$Val$_n$N$_3$** were also investigated (**Figure 39**).

The obtained diffractograms suggest that the initial mixtures having a lower periodicity (low short-range order) have a better catalytic performance. These characteristics are readily observed in the initial hybrid mixtures **Cu(I)-PhTzVal$_6$-N$_3$Val$_6$N$_3$** (**Figure 39F**) and **Cu(I)-PhTzVal$_8$-N$_3$Val$_8$N$_3$** (**Figure 39J**), resulting in a higher catalytic ability of these compounds.

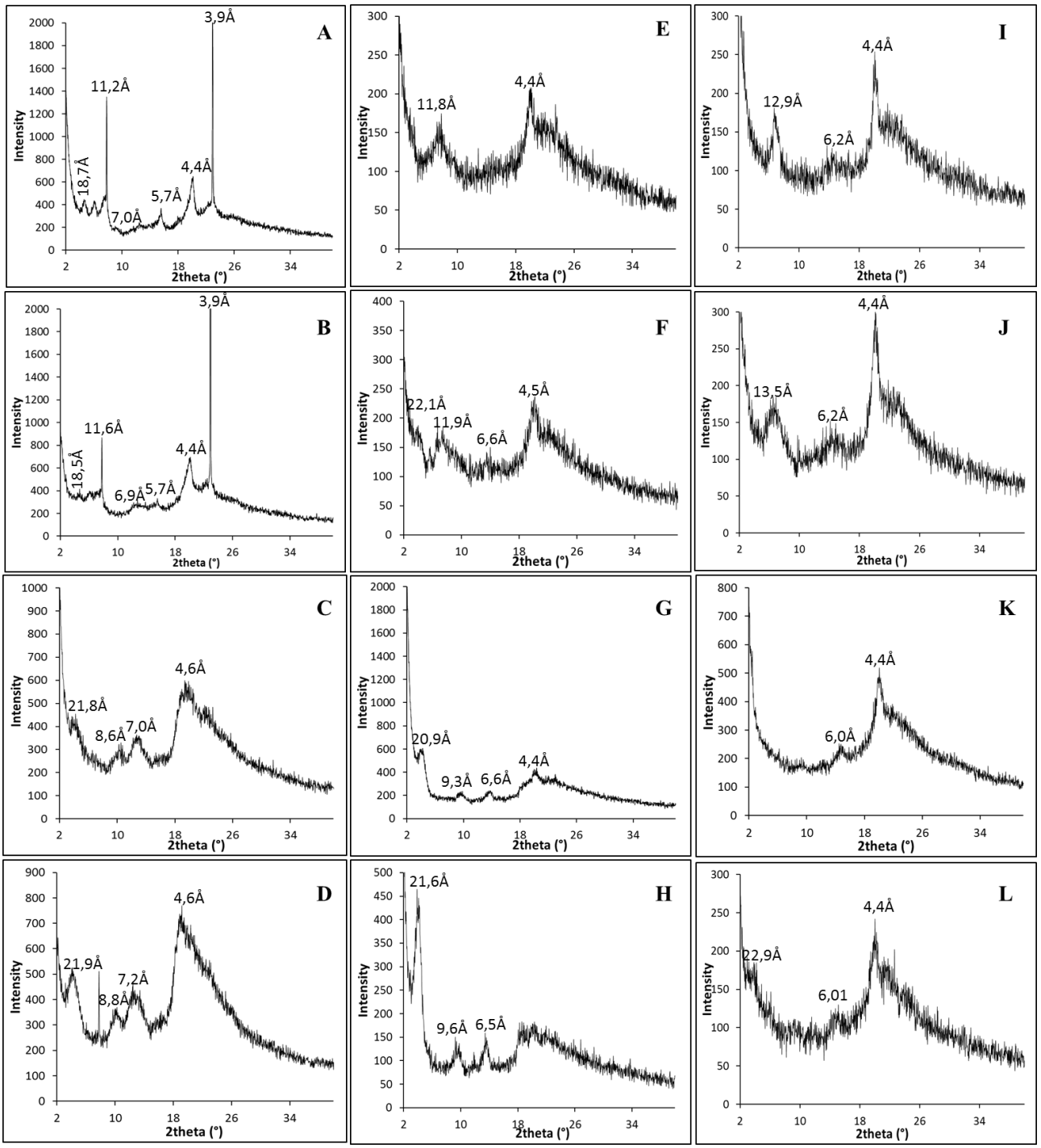

Figure 39. WAXD performed to the metallogels **Cu(I)-N$_3$Val$_3$N$_3$** (A), **Cu(I)-N$_3$Val$_6$N$_3$** (E), **Cu(I)-N$_3$Val$_8$N$_3$** (I) and to the multicomponent metallogels **Cu(I)-PhTzVal$_3$-N$_3$Val$_3$N$_3$** (B-D), **Cu(I)-PhTzVal$_6$-N$_3$Val$_6$N$_3$** (F-H) and **Cu(I)-PhTzVal$_8$-N$_3$Val$_8$N$_3$** (J-L) mixtures after 0 (B, F, J), 4 (G, K), 20 (C, H, L) and 48h (D) reaction.

These results are quite reasonable, if we consider that a higher interplanar distance between the several gelator layers facilitates the formation of the phenyltriazole fragment at the end of the reactant **N$_3$Val$_n$N$_3$** layers, due to a lower steric hindrance. The expansion of the structure resultant from the formation of the final product is well observed in the multicomponent gel **Cu(I)-PhTzVal$_3$-N$_3$Val$_3$N$_3$** after 20h (**Figure 39C**) and 48h reaction (**Figure 39D**) and for **Cu(I)-**

PhTzVal$_8$-N$_3$Val$_8$N$_3$ after 20h reaction (**Figure 39L**). In the multicomponent gel **Cu(I)-PhTzVal$_6$-N$_3$Val$_6$N$_3$**, this expansion was observed in a less extent, due to the high similarity between the supramolecular arrangement of the initial mixture (**Figure 39F**) and the one of final product (**Figure 39H**), although the peak around 21Å becomes more intense and defined along the reaction time (**Figure 39G-H**).

The lower catalytic activity from the gelator **Cu(I)-PhTzVal$_3$** may also be related with a possible coordination of Cu(I) to **N$_3$Val$_3$N$_3$**. The most intense peak present in the diffractogram of **Cu(I)-N$_3$Val$_3$N$_3$** appears at 3.9Å (**Figure 39A**), which is well in accordance with the one belonging to the metallogels **Cu(I)-PhTzVal$_n$** (**Figure 28D-F**). On the other hand, this peak is absent in the diffractograms corresponding to **Cu(I)-N$_3$Val$_6$N$_3$** and **Cu(I)-N$_3$Val$_8$N$_3$** (**Figure 39B-C**). It is well known from literature that the gelators having a central spacer with 3 carbons self-assembles in a different way in comparison with the bolaamphiphilic gelators having a higher spacer, which might have contributed for the different diffractograms observed in the different **Cu(I)-N$_3$Val$_n$N$_3$** metallogels.[30] This particular self-assembly behaviour may cause additional competition for the coordination of the copper when the gelators **PhTzVal$_3$** and **N$_3$Val$_3$N$_3$** are heated together with the copper salt, causing a depletion in the catalytic performance of **Cu(I)-PhTzVal$_3$**.

In all the difractograms, it is also important to highlight the appearance of a peak around 4.5Å, that according to previously reported xerogels, can be ascribed to the periodicity in the direction of the hydrogen bonding array, thus suggesting a self-assembly of the gelator molecules in a vertical direction (Z axis) both in the azides and in the final product.[34]

WAXD analysis performed on the hybrid multi-component metallogel mixtures at 50% conversion (**Figure 39C**, **Figure 39G**, **Figure 39K**) revealed the structural rearrangement of the system may lead to a slowdown of the reaction, achieving a kind of *plateau* at this stage (**Figure 36**). By looking at **Figure 39C**, **Figure 39G** and **Figure 39K**, it is observed that at this point of the reaction, the structure of the hybrid multi-component gel mixtures resembles more the one of the final product (**Figure 39D**, **Figure 39H** and **Figure 39L**), although 50% of reactant is still present. This structural rearrangement acts as an inflection point on the catalytic activity of these compounds, since after this *plateau*, the kinetics increases again towards the completion of the reaction (**Figure 37**).

The morphology of the hybrid multi-component organic-inorganic gels was also analysed at different stages of the reaction by TEM. For this experiment, the gels were prepared in MeOH and analysed without staining.

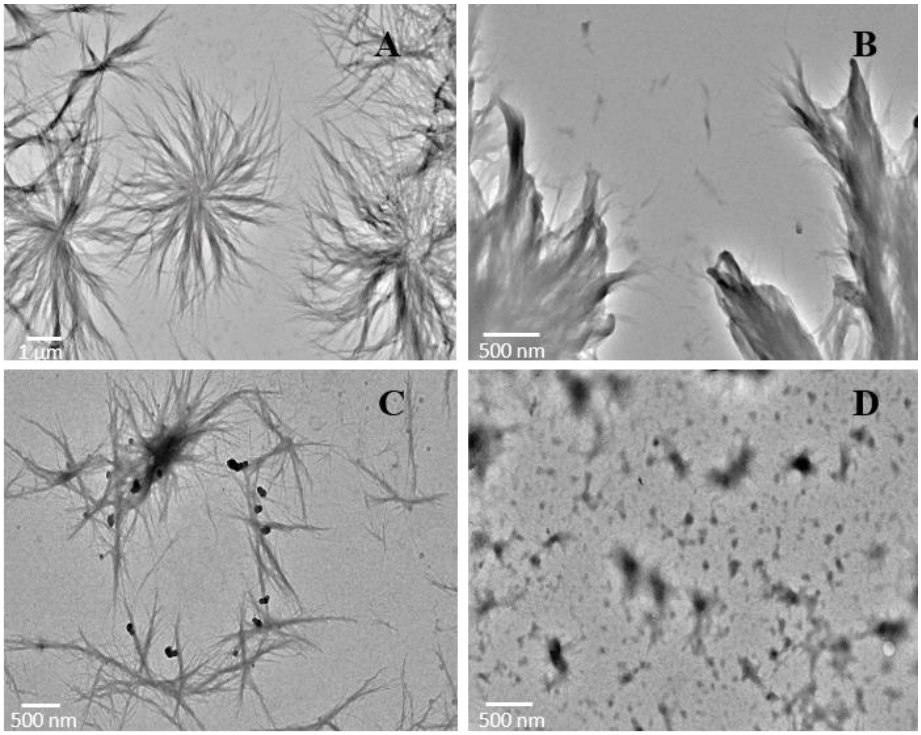

Figure 40. TEM analysis of **Cu(I)-$N_3Val_6N_3$** (A), **Cu(I)-PhTzVal_6-$N_3Val_6N_3$** (B), **Cu(I)-PhTzVal_6-$N_3Val_6N_3$** after 4h reaction (C) and **Cu(I)-PhTzVal_6-$N_3Va_{l6}N_3$** after 20h reaction (D).

Figure 40A shows that the gel network of **Cu(I)-$N_3Val_6N_3$** is composed by long and thin fibres exhibiting a flower-like morphology. The presence of these fibres, together with some smaller fibres belonging to the catalyst was observed in **Figure 40B** and **Figure 40C**. On **Figure 40C**, corresponding to 4 h reaction, it could be also observed some dark nucleus that probably belong to the final product, considering their high similarity with the fibres present at the end of the reaction (**Figure 40D**), which in turn have a similar morphology to the fibres represented in **Figure 34B**, belonging to the pure metallogel.

3.2.2. Compounds functionalized with benzyltriazole group (BzTzAVal$_n$)

3.2.2.1. Design and Synthesis

These kind of gelators present in their structure a benzyltriazole group as catalytic fragment, coupled directly to the central core by an amide bond.

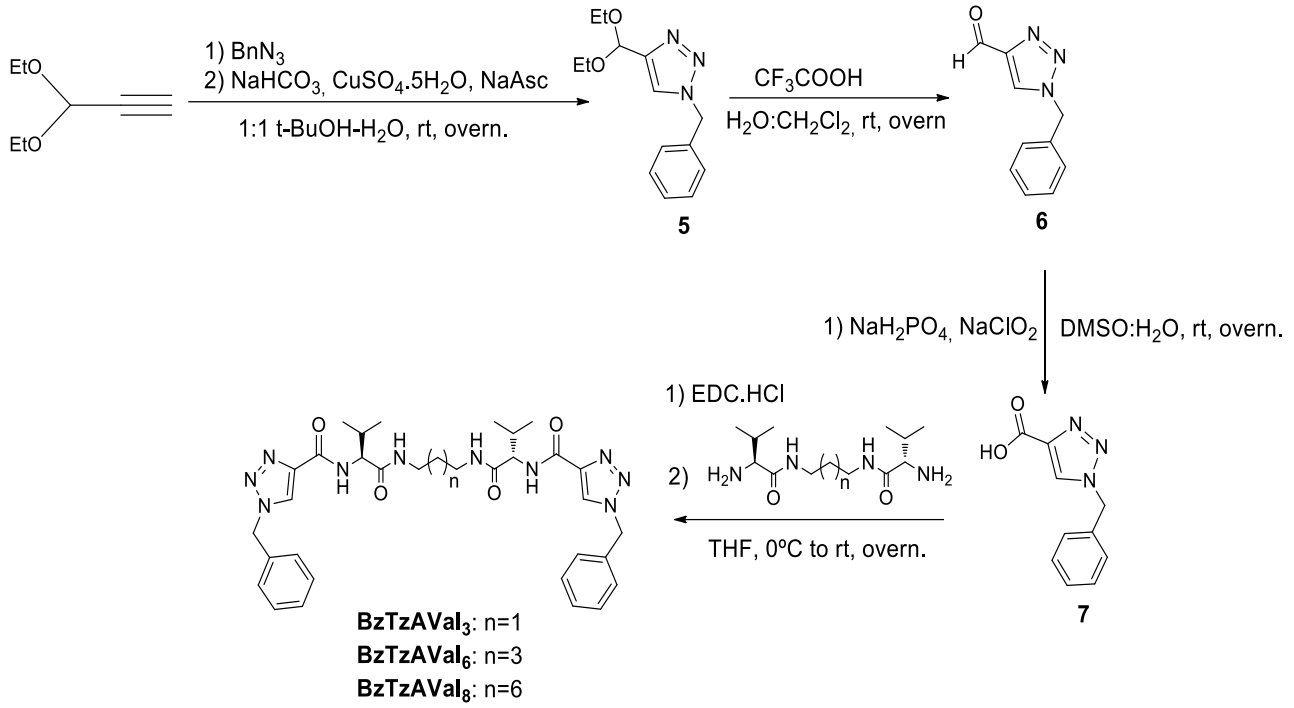

Figure 41. Scheme for the synthesis of **BzTzAVal$_n$** family of gelators

The synthesis of the benzyltriazole fragment has been performed as reported in literature.[4] The first step included a copper(I) catalysed azide-alkyne cycloaddition between the benzylazide and the diethylpropargylacetal. The acetal group is then hydrolysed to aldehyde in the presence of trifluoroacetic acid.

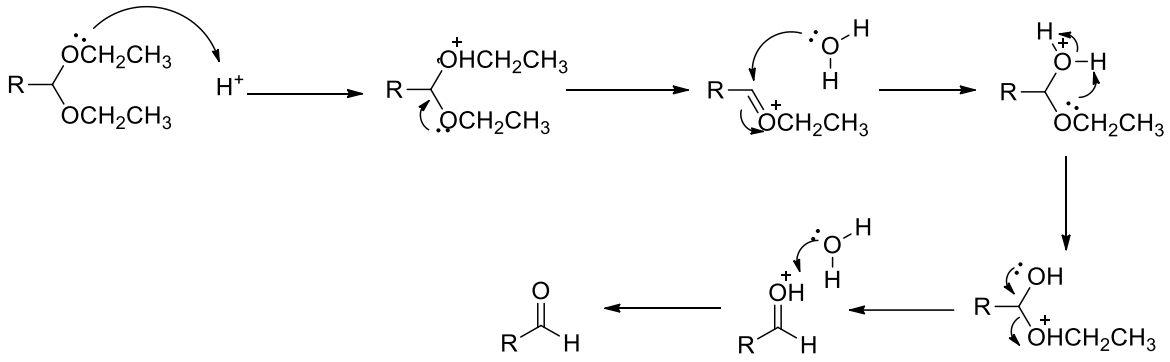

Figure 42. Mechanism of acetal hydrolysis.

The obtained aldehyde was then oxidized to carboxylic acid through a Pinnick-Lindgren oxidation, in the presence of $NaClO_2$ and NaH_2PO_4.[35]

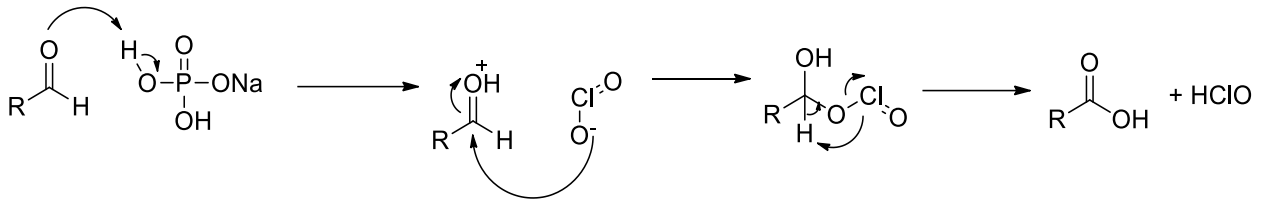

Figure 43. Mechanism of Pinnick-Lindgren oxidation.

In this reaction, the byproduct hypochlorous acid (HOCl) is highly reactive and can consume the chlorite ions needed for the oxidation reaction. Furthermore, it can easily react with double bonds of the organic substrate. As a result, DMSO was used as a radical scavenger to avoid the occurrence of these undesirable side reactions.

The synthesis of the *L*-valine benzyltriazolyl (**BzTzAVal$_n$**) family of compounds was achieved by simple peptide coupling between the central core synthesized in **section 3.2.1.1** and the carboxylic acid of the benzyltriazole, using EDC·HCl as coupling agent (**Figure 41**). The reaction proceeds through the formation of the *O*-acylurea intermediate, which is then attacked by the primary amine to obtain the desired amide product and a water-soluble urea hydrochloride salt.

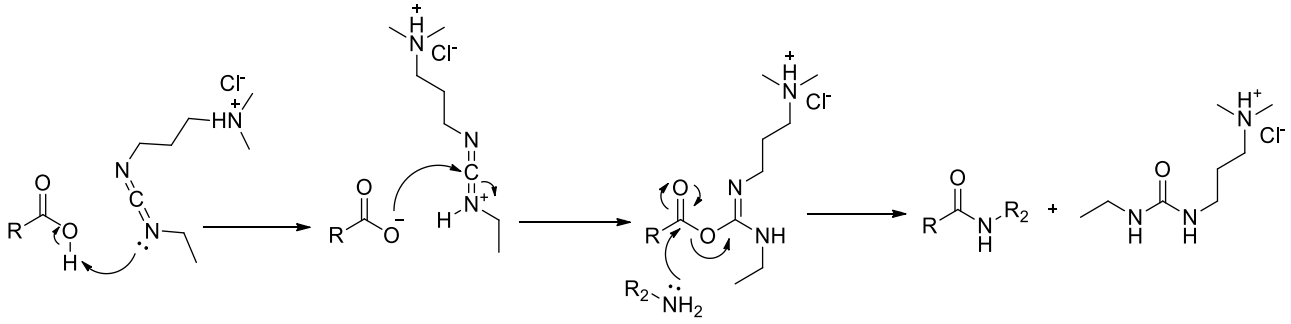

Figure 44. EDC·HCl coupling mechanism**.**

In analogy with the **PhTzVal$_n$** family of gelators, bolaamphiphilic **BzTzVal$_n$** compounds bearing 3, 6 and 8 carbon spacer have been synthesized.

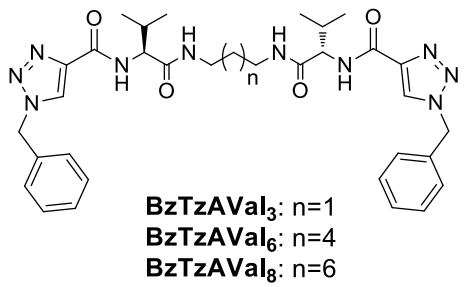

Figure 45. Structure of the family of gelators **BzTzAVal$_n$**.

3.2.2.2. Viscoelastic and Thermotropic Properties

The gelation performance of the family of compounds **BzTzAVal$_n$** was tested in a variety of solvents with different polarity, ranging from toluene to methanol (**Table 3**). Similarly to what has been observed to the **PhTzVal$_n$** family of compounds, the gel exhibiting the longer carbon chain length **BzTzAVal$_8$** showed the best gelation ability, although its gelation performance was not as good as than the one of the analogue gelator **PhTzVal$_8$**.

Table 3. Gelation experiments of compounds BzTzVal$_n$[a].

Solvent	BzTzAVal$_3$	Aspect	BzTzAVal$_6$	Aspect	BzTzAVal$_8$	Aspect
Toluene	SP	white	SP	white	I	-
Dichloromethane	S	-	PP	-	G	translucent
Ethanol	PP	-	G	opaque	G	opaque
H_2O	PP	-	I	-	I	-
H_2O:t-BuOH (1:1)	PP	-	SP	white	SP	white
THF	G	translucent	SP	white	G	translucent
Methanol	PP	-	SP	white	G	opaque
Acetonitrile	G	translucent	PP	-	SP	white

[a] I: Insoluble, S: Soluble, G: Gel, SP: Swollen precipitate, PP: Precipitate c = 8 mg/mL.

Although none of the native gelators from the family **BzTzAVal$_n$** was able to form consistent gels in the solvent mixture 1:1 H_2O:*t*-BuOH, the addition of the copper salt $[Cu(MeCN)_4]PF_6$ in a ligand:Cu 2:1 molar ratio provided the gelation of the compound **BzTzAVal$_3$**, resulting in the formation of the metallogel **Cu(I)-BzTzAVal$_3$**. However, this was an isolated case of metal-promoted gelation for the compound **BzTzAVal$_3$** and in the solvent system 1:1 H_2O:*t*-BuOH. Any attempt of adding copper to **BzTzAVal$_3$** in other solvent media or to the remaining gelators **BzTzAVal$_6$** and **BzTzAVal$_8$** in order to induce their metal-driven gelation was unsuccessful.

Due to the absence of a common solvent that promote the gelation of the three compounds from the **BzTzAVal$_n$** family, the minimum gel concentration (m.g.c.) was determined for the gelators **BzTzAVal$_3$** and **BzTzAVal$_8$** using the solvents 1:1 H_2O:*t*-BuOH and EtOH, respectively, and further compared with the corresponding m.g.c. obtained for the analogue compounds **PhTzVal$_3$** and **PhTzVal$_8$**. The gelator **BzTzAVal$_6$** was not considered due to its poor gelation ability.

Table 4. Minimum gelation concentrations of the native gelators and of the metallogels from families **BzTzAVal$_n$** and **PhTzVal$_n$**.

	Concentration (mM)/Solvent			
	H_2O:*t*-BuOH		EtOH	
Gelator	**Native**	**Metallogel**	**Native**	**Metallogel**
BzTzAVal$_3$	-	7.8	-	-
BzTzAVal$_8$	-	-	8.0	8.0
PhTzVal$_3$	4.1	5.2	4.4	4.4
PhTzVal$_8$	2.9	2.9	6.9	5.5

The results from **Table 4** show that the compounds **BzTzAVal$_3$** and **BzTzAVal$_8$** present a relatively similar minimum gel concentration, although in different solvents. However, the higher m.g.c. of these gelators compared to the one determined for analogue gelators belonging to the family **PhTzVal$_n$** suggest a decreased gelation ability from the formers in respect to the laters. These results highlight the importance of the alkyl chain present in the **PhTzVal$_n$** family of compounds in the design of efficient gelators, arising from the peptide coupling of the central core with the bromobutyric acid. Thus, it may be suggested that the reason for the poorer gelation ability of the compounds from **BzTzAVal$_n$** family may be related with the presence of the voluminous benzyltriazole next to the amide, which can interfere with the intermolecular hydrogen bond formation and consequent self-assembly of the gelator.

The characteristic temperature corresponding to gel-to-sol transition was determined for the compound **BzTzAVal$_8$** and compared with the one observed for the gelator **PhTzVal$_8$**, previously determined in **Section 3.2.1.2** using EtOH as solvent media. For the gelator having the lowest carbon chain length, **BzTzAVal$_3$**, such comparison could not be done due to its inability to form gels in ethanol.

As observed in the graphics from **Figure 46**, the T_{sol} of the compounds **PhTzVal$_8$** and **BzTzAVal$_8$** are very similar, except for the concentration of 7.6 mM where these temperatures are 57 ºC and 33 ºC, respectively. This high discrepancy was quite expected since the minimum gelation concentration of **BzTzAVal$_8$** is considerably higher than the one determined for the gel **PhTzVal$_8$** (**Table 4**).

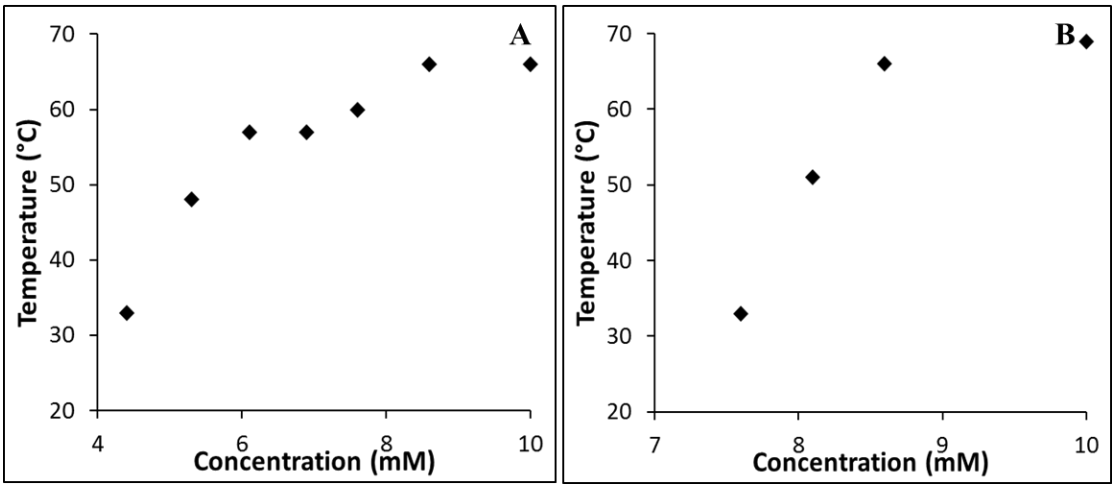

Figure 46. T_{sol} of the gels **PhTzVal$_8$** (A) and **BzTzAVal$_8$** (B). EtOH was used as solvent medium.

It is important to highlight that the mismatch between the m.g.c. registered in **Table 4** and the concentrations used for determination of T_{sol} might arise from different aging times of the gels, from 20 minutes in the m.g.c. experiments to 1 h in the T_{sol} assays. However, it can be observed that the T_{sol} of the gel **BzTzAVal$_8$** shows an accentuated increase for small changes in concentration. By changing the concentration in just 1 mM, from 7.6 to 8.6 mM, the T_{sol} of the gel **BzTzAVal$_8$** increases by two fold, from 33 ºC to 66 ºC, whereas the T_{sol} corresponding to the gel **PhTzVal$_8$** increases from 57 ºC to 60 ºC for the same concentrations. Although it is true that such concentrations are well far away from the minimum gelation concentration determined for the gel **PhTzVal$_8$**, meaning that the obtained gel is so consistent that the change in T_{sol} is not significant, if the two first concentrations are compared (4.4 and 5.3 mM), whose T_{sol} are 33 ºC and 48 ºC, respectively, it is also possible to conclude that the change in T_{sol} of **PhTzVal$_8$** is not as clear as than the one observed for the **BzTzAVal$_8$**.

3.2.2.3. Structural and Morphologic Characterization

The structural arrangement of the native gel **BzTzAVal$_8$** and of the corresponding metallogel, formed in EtOH, was evaluated by WAXD. As done for the determination of the minimum gel concentration, in the case of the gel **Cu(I)-BzTzAVal$_3$** the structural characterization was performed in the gel formed using 1:1 H_2O:*t*-BuOH as solvent media.

As observed in **Figure 47A**, the molecules of the native gelator **BzTzAVal$_8$** self-assemble in a structure exhibiting some periodicity, although a wide peak characteristic of amorphous objects is also observed around 2θ= 25º. However, in this case, the addition of the metal appears to have no influence on the aggregation of the gel **Cu(I)-BzTzAVal$_8$** considering the high similarity between the diffractograms represented in **Figure 47A-B**. On the other hand, the molecules of **BzTzAVal$_3$**

seem to pack in a more ordered structure in the presence of the metal than the ones of the metallogel **Cu(I)-BzTzAVal$_8$**, providing some long-range order to the metallogel **Cu(I)-BzTzAVal$_3$**. Such ordered arrangement from the metallogel having the smaller middle carbon chain has already been observed for the gel **Cu(I)-PhTzVal$_3$** and is probably related with their characteristic different packing.

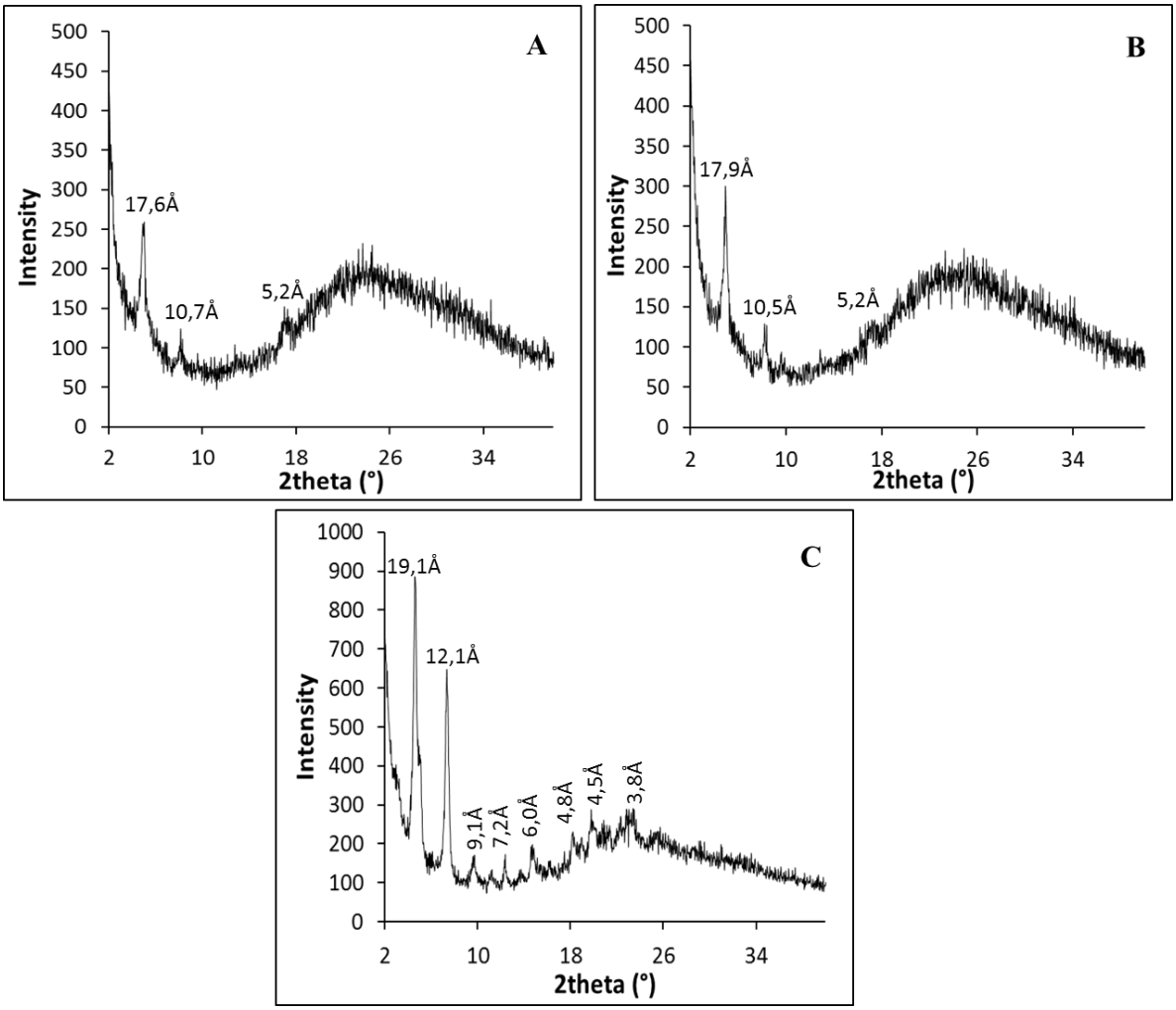

Figure 47. WAXD analysis of gels **BzTzAVal$_8$** (A), **Cu(I)-BzTzAVal$_8$** (B) and **Cu(I)-BzTzAVal$_3$** (C).

However, in the specific case of the compound **Cu(I)-BzTzAVal$_3$**, it is also expected some influence in the self-assembly process arising from the presence of the Cu(I), since the metal acts as the main driving force to promote the gelation of this compound in the 1:1 H_2O:*t*-BuOH mixture. Thus, it is possible that the crosslinking induced by the coordination of the benzyltriazole fragment from the several **BzTzAVal$_3$** to the metal centre favours the formation of a more ordered network, resulting in a crystalline-like structure (**Figure 47C**).

In an attempt to retrieve additional information on the supramolecular structural organization of these benzyltriazole functionalized gelators, the resulting gels were analysed by CD spectroscopy.

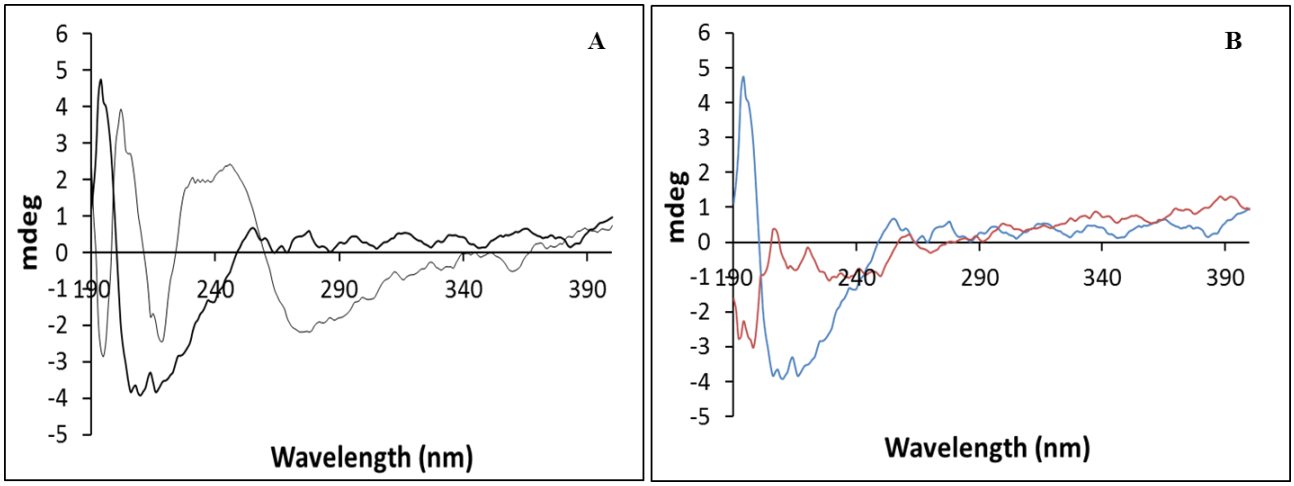

Figure 48. Circular Dichroism spectroscopy of gels **BzTzAVal$_8$** (A), **Cu(I)-BzTzAVal$_8$** (A-B) and **Cu(I)-BzTzAVal$_3$** (C). A: **BzTzAVal$_8$** (grey), **Cu(I)-BzTzAVal$_8$** (black). B: **Cu(I)-BzTzAVal$_3$** (red) and **Cu(I)-BzTzAVal$_8$** (blue).

The native gel **BzTzAVal$_8$** exhibit three negative bands at 279 nm, 219 nm and 194 nm, together with two positive bands at 202 and 247 nm (**Figure 48A**). The addition of copper to the gelator **BzTzAVal$_8$** simplifies the spectrum into two negative bands at 216 and 210 nm and a positive band 190 nm, suggesting an helical arrangement (**Figure 48A**).[28] The presence of alternate negative and positive bands arise from the chiral conformation of the self-assembled gel network, which is less evident on the gelator **Cu(I)-BzTzAVal$_3$**, considering the absence of bands in its dichroism spectrum (**Figure 48B**).

The results obtained by CD spectroscopy are in good agreement with the TEM images of the benzyltriazole functionalized gelators. In the gelator with the largest carbon chain **BzTzAVal$_8$**, it is well observed the presence of fibres with helical morphology (**Figure 49A-B**), which is in accordance with the sequence of negative and positive bands found on the corresponding CD spectrum (**Figure 48A grey**).

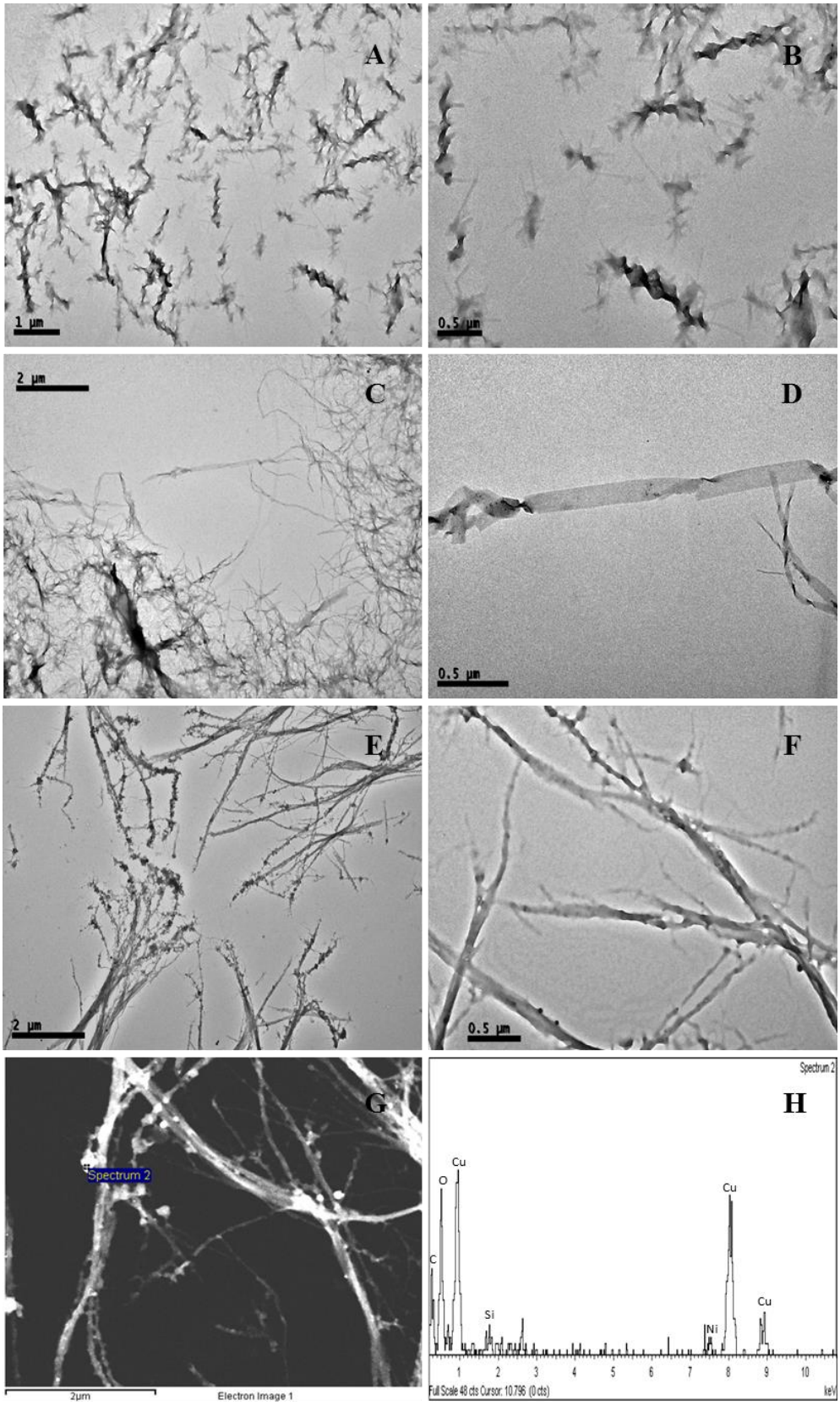

Figure 49. TEM pictures of the gelator **BzTzAVal$_8$** (A-B), corresponding metallogel **Cu(I)-BzTzAVal$_8$** (C-D), and metallogel **Cu(I)-BzTzAVal$_3$** (E-F). STEM picture of **Cu(I)-BzTzAVal$_3$** (G) and corresponding EDS spectrum (H).Magnifications are 2500x (A), 2000x (C-E) and 8000x (B, D, F) and 40000x (G).

The introduction of the copper lead to the formation of flat fibres with less ellipcity (**Figure 49C-D**), which explains the simplification of the CD spectrum (**Figure 48A black**). Regarding the metallogel **Cu(I)-BzTzAVal$_3$**, flat fibres with 60 nm width have been detected by TEM (**Figure 49E-F**). The presence of Cu nanoparticles is well observed along the fibres both by TEM and STEM-EDS analysis (**Figure 49E-H**).

3.2.3. Non-aggregating compounds

3.2.3.1. Design and Synthesis

One of the major advantages of the catalytic gels is the capacity of bringing together their catalytic fragments upon self-assembly, providing a better access of the substrate to the catalytic site and consequent higher catalytic activity.[36] To evaluate the catalytic activity of **PhTzVal$_n$** and **BzTzVal$_n$** in the gel phase, a non-aggregating molecule containing a benzyltriazole fragment has been synthesized.

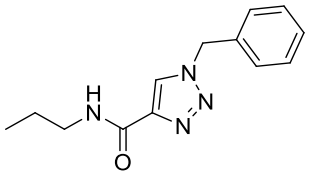

BzTzAPropyl

Figure 50. Structure of the non-aggregating analogue **BzTzAPropyl**.

The molecule **BzTzAPropyl** was synthesized by simple peptide coupling between the propylamine and the carboxylic acid of the benzyltriazole, using EDC·HCl as coupling agent.

3.3. Catalysis of model 'click' reaction

The fact that some of the synthesized compounds were able to form hydrogels allowed the possibility of studying their catalytic performance in H_2O:*t*-BuOH, where 'click' reactions generally occur.

Table 5. Gelation experiments of gels and blanks in H_2O:t-BuOH and in acetonitrile[a].

Compound	H_2O:*t*-BuOH	Aspect	Acetonitrile	Aspect
Cu(I)-PhTzVal$_3$	G	Transparent	G	transparent
Cu(I)-PhTzVal$_6$	G	Translucent	G	Translucent
Cu(I)-PhTzVal$_8$	G	translucent	G	Translucent
Cu(I)-BzTzAVal$_3$	G	opaque	-	-
Cu(MeCN)$_4$PF$_6$	S	-	S	-
Cu(I)-BzTzAPropyl	S	-	S	-

[a] I: Insoluble, S: Soluble, G: Gel, c = 8 mg/mL.

Additionally, this hydrogelation ability constitutes an advantage for a future application of this gelators in 'click' reactions occurring in biological environments. Thus, the catalytic activity of the metallohydrogels in the model reaction between phenylacetylene and benzylazide was investigated.

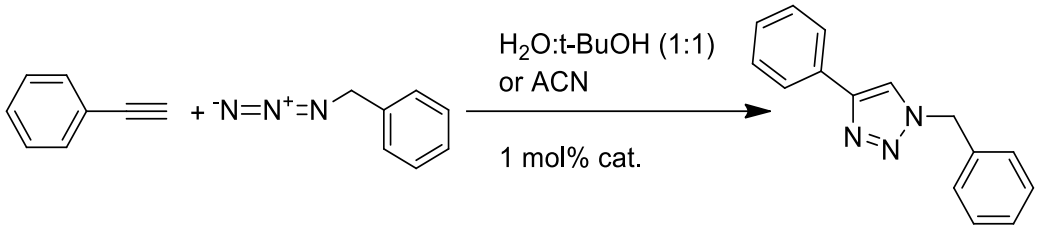

Figure 51. Huisgen's 1,3-dipolar cycloaddition between phenylacetylene and benzylazide.

The reaction was performed in a 1:1 *t*-BuOH:H_2O mixture in the presence of the metallogel catalyst (1 mol%), in air and at room temperature, for periods between 3 to 15h. The obtained results are summarized in **Table 6**. With the goal of increasing the solubility of the $[Cu(MeCN)_4]PF_6$ in the blank experiments, avoiding possible catalysis by formation of copper aggregates, the model reaction represented in **Figure 51** was also carried in acetonitrile for a period of 5h (**Table 6**).

The results suggest some catalytic activity by the metallogels **Cu(I)-PhTzVal$_n$** and **Cu(I)-BzTzAVal$_3$** in the first 3h of reaction. The metallogel **Cu(I)-BzTzAVal$_3$** seems to exhibit the highest catalytic activity in this short time period, achieving a 25% higher conversion comparing with the blanks (**Table 6E-F**). However, at longer reaction periods, this catalytic activity seems to decrease, as the conversions approach the ones of the blank assays. The catalytic performance of the gelators **Cu(I)-PhTzVal$_n$** in the first 3 hours is relatively lower in comparison with the one of **Cu(I)-BzTzAVal$_3$**, exhibiting only 10% higher conversions than the blanks for a similar period of time (**Table 6A-C**).

Independently on the presence of a heterogeneous or homogeneous copper(I) catalyst, the reaction seems to stop after 8h, reaching *plateau* around 50-70% conversion which is maintained after 15h reaction. Problems associated with the use of copper(I), such as thermodynamic instability of Cu(I), which may oxidise to Cu(II) or disproportion to Cu(0) and Cu(I), possible aggregation of the Cu(I)-acetylides formed during the catalytic cycle providing a resting state for the catalyst or formation of polynuclear Cu(I) aggregates are conditions that may contribute for the entanglement of the catalytic cycle, preventing the reaction to proceed until complete conversion.[37]

Table 6. Study of the catalytic activity of the gelators and the blanks in 1:1 H_2O:*t*-BuOH and acetonitrile.

Solvent		1:1 *t*-BuOH:H_2O				Acetonitrile
Entry	**Catalyst**	**Conversion at 3h (%)[a]**	**Conversion at 6h (%)[a]**	**Conversion at 8h (%)[a]**	**Conversion at 15h (%)[a]**	**Conversion at 5h (%)**
A	**Cu(I)-PhTzVal$_3$**	21	44	63	-	18
B	**Cu(I)-PhTzVal$_6$**	24	56	62	59	27
C	**Cu(I)-PhTzVal$_8$**	19	43	53	64	24
D	**Cu(I)-BzTzAVal$_3$**	38	60	68	-	25
E	**Cu(MeCN)$_4$PF$_6$**	13	41	54	67	11
F	**Cu(I)-BzTzAPropyl**	9	53	66	72	10

[a] Typical procedure: Catalytic experiments were performed at room temperature without stirring, using 500 µL of 1:1 H_2O:*t*-BuOH as solvent medium. The reactants in stoichiometric proportion (0.21 mmol) were mixed and added directly at the top of the metallogel catalyst (1 mol%) composed by the gelator (4.2 x 10^{-3} mmol) and the copper salt $[Cu(MeCN)_4]PF_6$ (0.80 mg; 2.1x10^{-3} mmol). In the case of the blank experiments, the copper-triazole complex was composed by **BzTzAPropyl** (2.05 mg; 8.4 x 10^{-3} mmol) and $[Cu(MeCN)_4]PF_6$ (0.80 mg; 2.1x10^{-3} mmol). At the end of the experiment, the products were directly extracted with 700 µL $CDCl_3$. The organic phase was dried over anhydrous $MgSO_4$ and the conversion determined by ^{1}H-NMR.

For longer reaction times (6h, 8h and 15h reaction), in the presence of the non-aggregating compound **Cu(I)-BzTzAPropyl** (**Table 6F**), the reaction seems to follow a similar trend to the one carried in the presence of the metallogels **Cu(I)-PhTzVal$_n$**, **Cu(I)-BzTzAVal$_3$** or even in the presence of the copper salt $[Cu(MeCN)_4]PF_6$, suggesting that neither the presence of the triazole fragment nor the presence of a gel are having a positive influence on the conversion, which is not in accordance to the theories reported in literature. A considerable high mismatch between these results and the ones reported in literature has been observed, where conversions did not exceed 4% in 72h for the reaction carried out in the presence of $[Cu(MeCN)_4]PF_6$.[4,5]

This could suggest the occurrence of catalysis by the formation of copper aggregates in our experiments, arising from a possible limited solubility of the salt $[Cu(MeCN)_4]PF_6$ in the 1:1 *t*-BuOH:H_2O mixture. To confirm this hypothesis, the reaction was also carried in acetonitrile, where the $[Cu(MeCN)_4]PF_6$ is highly soluble regarding the presence of acetonitrile ligands in the structure of the copper complex.

The conversions obtained for the model 'click' reaction carried in acetonitrile in the presence of the several compounds (**Table 6**) are very similar between each other, allowing to conclude that catalysis by the bolaamphiphilic metallogels is poor, giving only 10% to 17% higher conversion in respect to the blank assays (**Table 6E-F**).

To better understand if the low catalytic activity of the gelators is related with a deficient

coordination of the copper(I), the amount of metal coordinated by each gelator was determined by ICP-MS (**Table 7**).

Table 7. Amount of copper(I) coordinated by the gelators.

Compound	% Cu coordinated
Cu(I)-PhTzVal$_3$	99.5
Cu(I)-PhTzVal$_6$	99.5
Cu(I)-PhTzVal$_8$	99.3
Cu(I)-BzTzAVal$_3$	62.4

It is important to highlight the remarkable copper loading of the gelators belonging to the **PhTzVal$_n$** family, coordinating >99% of copper initially present in solution. In contrast, the compound **Cu(I)-BzTzAVal$_3$** was able to coordinate 63% of copper(I), an amount that could be just the needed to achieve the formation of the gel, since in this particular case the metal is the main driving force for the gelation of this compound in the 1:1 *t*-BuOH:H_2O mixture. Although the gelator **Cu(I)-BzTzAVal$_3$** exhibited a lower copper loading efficiency, there was no significant differences in the conversions achieved for the catalysis of the model 'click' reaction in comparison with the gelators **PhTzVal$_n$**. However, some copper(I) leaching might occur during the catalytic process, resulting in a moderated catalytic performance of these gelators.

3.4. Conclusion

L-valine derived low molecular weight gelators functionalized with triazole units were successfully synthesized. The gelators were able to coordinate copper, building hybrid organic-inorganic gels capable of catalysing the Huisgen 1,3-dipolar cycloaddition of alkynes and azides. An interesting catalytic performance was particularly observed for the gels from **PhTzVal$_n$** family, which were able to catalyse their own synthesis in a self-replication catalytic process.

The gelators synthesized in this Chapter exhibited catalytic activity during the first 3 hours for the model 'click' reaction, allowing their use as heterogeneous catalysts. Except for the gelator **BzTzAVal$_3$** which exhibited metal-driven self-assembly in H_2O:*t*-BuOH, all the other compounds were able to gelate without the presence of the metal. This particular characteristic could allow the loading of metal ions with affinity to triazole ligands (Fe, Mn, Ru, Rh, Pd) without singnificantly disturbing their gelation ability.[38]

Furthermore, the formation of the metallogel in water or water: alcohol mixtures, together with their high copper(I) loading capacity allow the application of these gelators as potential

heterogeneous catalysts for ‘click’ reactions occurring in biological media. The fact that these gelators are derived from aminoacids constitutes an additional advantage on the use of these compounds as catalytic systems for bioconjugation ‘click’ reactions, regarding their biodegrability and biocompability. Although the catalytic performance os these gelators is relatively similar to the one of the $[Cu(MeCN)_4]PF_6$, their use in bioconjugation ‘click’ reactions may be still preferred considering the inherent cytotoxicity of Cu(I) salts against cellular medium.

3.5. References

[1] Hou J, Liu X, Shen J, Zhao G, Wang PG. The impact of click chemistry in medicinal chemistry. Expert Opinion in Drug Discovery 2012; 7: 489-501.

[2] Berg R, Straub BF. Advancements in the mechanistic understanding of the copper-catalyzed azide-alkyne cycloaddition. Beilstein Journal of Organic Chemistry 2013; 9: 2715-2750.

[3] Hein JE, Fokin VV. Copper-catalyzed azide-alkyne cycloaddition (CuAAC) and beyond: new reactivity of copper(I) acetylides. Chemical Society Reviews 2010; 39: 1302-1315.

[4] Chan TR, Fokin VV. Polymer-supported copper(I) catalysts for the experimentally simplified azide-alkyne cycloaddition. QSAR & Combinatorial Science 2007; 26: 1274-1279.

[5] Chan TR, Hilgraf R, Sharpless KB, Fokin VV. Polytriazoles as copper(I)-stabilizing ligands in catalysis. Organic Letters 2004; 6: 2853-2855.

[6] Bevilacqua V, King M, Chaumontet M, Nothisen M, Gabillet S, Buisson D, Puente C, Wagner A, Taran F. Copper-chelating azides for efficient click conjugation reactions in complex media. Angewandte Chemistry International Edition 2014; 53: 5872-5876.

[7] Girard C, Önen E, Aufort M, Beauvière S, Samson E, Herscovici J. Reusable polymer-supported catalyst for the [3+2] Huisgen cycloaddition in automation protocols. Organic Letters 2006; 8: 1689-1692.

[8] Jlalia I, Beauvineau C, Beauvière S, Önen E, Aufort M, Beauvineau A, Khaba E, Herscovici J, Meganem F, Girard C. Automated synthesis of 96 product-sized library of triazole derivatives using a solid-phase supported copper catalyst. Molecules 2010; 15: 3087-3120.

[9] Li P, Wang L, Zhang Y. SiO_2-NHC-Cu(I): an efficient and reusable catalyst for [3+2] cycloaddition of organic azides and terminal alkynes under solvent-free reaction conditions at room temperature. Tetrahedron 2008; 64: 10825-10830.

[10] Shamin T, Paul S. Silica functionalized Cu(I) as a green and recyclable heterogeneous catalyst for the Huisgen 1,3-dipolar cycloaddition in water at room temperature. Catalysis Letters 2010; 136: 260-265.

[11] Luz I, i Xamena FL, Corma A. Bridging homogeneous and heterogeneous catalysts with MOFs: “Click” reactions with Cu-MOF catalysts. Journal of Catalysis 2010; 276: 134-140.

[12] Lipshutz BH, Taft BR. Heterogeneous copper-in-charcoal-catalyzed click chemistry. Angewandte Chemistry International Edition 2006; 45: 8235-8238.

[13] Dervaux B, Du Prez FE. Heterogeneous azide-alkyne click chemistry: towads metal-free end products. Chemical Science 2012; 3: 959-966.

[14] Ozkal E, Özçubukçu S, Jimeno C, Pericàs MA. Covalently immobilized tris(triazolyl)methanol-Cu(I) complexes: highly active and recyclable catalysis for CuAAC reactions. Catalysis Science and Technology 2012; 2: 195-200.

[15] Özçubukçu S, Ozkal E, Jimeno C, Pericàs MA. A highly active catalyst for Huisgen 1,3-dipolar cycloadditions based on tris(triazolyl)methanol-Cu(I) structure. Organic Letters 2009; 20: 4680-4683.

[16] Jin Q, Zhang L, Cao H, Wang T, Zhu X, Jiang J, Liu M. Self-assembly of copper(II) ion-mediated nanotube and is supramolecular chiral catalytic behaviour. Lagmuir 2011; 27: 13847-13853.

[17] He Y, Bian Z, Kang C, Cheng Y, Gao L. Chiral binaphtlylbisbipyridine-based copper(I) coordination polymer gels as supramolecular catalysts. Chemical Communications 2010; 46: 3532-3534.

[18] Díez-González S. Well-defined copper(I) complexes for click azide-alkyne cycloaddition reactions: one click beyond. Catalysis Science & Technology 2011; 1: 166-178.

[19] Escuder B, Martí S, Miravet JF. Organgel formation by coaggregation of adaptable amidocarbamates and their tetraamide analogues. Langmuir 2005; 21: 6776-6787.

[20] Jin Q, Zhang L, Cao H, Wang T, Zhu X, Jiang J, Liu M. Self-assembly of copper(II) ion-mediated nanotube and its supramolecular chiral catalytic behaviour. Langmuir 2011; 27: 13847-13853.

[21] Bunzen J, Bruhn T, Bringmnn G, Lützen A. Synthesis and helicate formation of a new family of BINOL-based bis(pyridine) ligands. Journal of the American Chemical Society 2009; 131: 3621-3630.

[22] Lam ST, Yam VWW. Synthesis, characterization and photophysical study of alkynylrhenium(I) tricarbonyl diamine complexes and their metal-ion coordination-assisted metallogelation properties. Chemistry – A European Journal 2010; 16: 11588-11593.

[23] Shen JS, Mao GJ, Zhou YH, Jiang YB, Zhang HW. A ligand-chirality controlled supramolecular hydrogel. Dalton Transactions 2010; 39: 7054-7058.

[24] Joshi SA, Kulkarni ND. A new trinuclear Cu(II) complex for inositol as a hydrogelator. Chemical Communications 2009; 17: 2341-2343.

[25] Tam AYY, Yam VWW, Recent advances in metallogels. Chemical Society Reviews 2013; 42: 1540-1567.

[26] Piepenbrock MOM, Lloyd GO, Clarke N, Steed JW. Metal-and anion-binding supramolecular

gels. Chemical Society Reviews 2013; 42: 1540-1567.

[27] Steed JW. Anion-tuned supramolecular gels: A natural evolution from urea supramolecular chemistry. Chemical Society Reviews 2010; 39: 3686-3699.

[28] Han S, Lim Y. Covalent capture of α-helical peptides in polymer hydrogel network for polyacrylamide gel stabilization by electrophoresis. Journal of Polymer Science, Part A: Polymer Chemistry 2014; 52: 596-599.

[29] Rodríguez-Llansola F, Miravet JF, Escuder B. Supramolecular gel formation and self-correction induced by aggregation-driven conformational changes. Chemical Communications 2009; 209-211.

[30] Tsekova DS, Sáez JA, Escuder B, Miravet JF. Solvent-free construction of self-assembled 1D nanostructures from low-molecular-weight organogelators: sublimation vs gelation. Soft Matter 2009; 5: 3727-3735.

[31] Murata K, Aoki M, Suzuki T, Harada T, Kawabata H, Komori T, Ohseto F, Ueda K, Shinkai S. Thermal and light control of sol-gel phase transition in cholesterol-based organic gels. Novel helical aggregation modes as detected by circular dichroism and electron microscopic observation. Journal of the American Chemical Society 1994; 116: 6664-6676.

[32] Bock VD, Hiemstra H, van Maarseveen JH. Cu^{I}-catalyzed alkyne-azide 'click' cycloadditions from a mechanistic and synthetic perspective. European Journal of Organic Chemistry 2006; 2006: 51-68.

[33] Yuan J, Fang X, Zhang L, Hong G, Lin Y, Zheng Q, Xu Y, Ruan Y, Weng W, Xia H, Chen G. Multi-responsive self-healing metallo-supramolecular gels based on "click" ligand. Journal of Materials Chemistry 2012; 22: 11515-11522.

[34] Escuder B, Miravet JF, Sáez JA. Molecular recognition through divalente interactions with a self-assembled network of a supramolecular organogel. Organic & Biomolecular Chemistry 2008; 6: 4378-4383.

[35] Giri AG, Mondal MA, Puranik VG, Ramana CV. Effect of allylic substituents on ring closing metathesis: the total synthesis of stagonolide B and 4-*epi*-stagonolide B. Organic & Biomolecular Chemistry 2010; 8: 398-406.

[36] Escuder B, Rodríguez-Llansola F, Miravet JF. Supramolecular gels as active media for organic reactions and catalysis. New Journal of Chemistry 2010; 34: 1044-1054.

[37] Schulze B, Schubert US. Beyond click chemistry – Supramolecular interactions of 1,2,3-triazoles. Chemical Society Reviews 2014; 43: 2522-2571.

[38] Huang D, Zhao P, Astruc D. Catalysis by 1,2,3-triazole- and related transition metal complexes. Coordination Chemistry Reviews 2014; 272: 145-165.

3.6. Supporting Info

3.6.1. Compounds Bearing a PhenylTriazolyl fragment

3.6.1.1. General Gelation Procedures

3.6.1.1.1. Gels $\mathbf{PhTzVal_n}$

The $\mathbf{PhTzVal_n}$ gelator was heated in a 4 mL screw-capped vial in the presence of 500 µL of solvent, until complete dissolution (~1 min). The resultant hot solution was then sonicated for 40 seconds, resulting in a gel which was subsequently allowed to stabilize for 20 minutes at room temperature. The formation of a gel was confirmed by the inversion tube test, where the resultant solid-like soft material did not flow upon inversion of the flask. The formation of the metallogels was achieved by heating together the gelator and the copper salt $[Cu(MeCN)_4]PF_6$ in a 2:1 molar ratio.

3.6.1.1.2. Two-component gels $\mathbf{PhTzVal_n/N_3Val_nN_3}$

For the formation of the two component metallogels, $\mathbf{N_3Val_nN_3}$ ($2.7x10^{-2}$ mmol) was heated together with the catalyst composed by the gelator $\mathbf{PhTzVal_n}$ ($2.7x10^{-3}$ mmol) and the copper salt $[Cu(MeCN)_4]PF_6$ ($2.7x10^{-3}$ mmol) in MeOH (300 µL) until complete dissolution. The resultant hot solution was then sonicated for 20 seconds, forming a gel which was subsequently allowed to age for 20 minutes at room temperature. Yellow translucent materials that retained the solvent upon inversion of the vial were obtained.

3.6.1.2. Rheology

The gels $\mathbf{PhTzVal_n}$ and the corresponding metallogels were prepared in 8 mL screw-capped vials at concentration of 8.6 mM and using EtOH as a solvent. The samples were then aged overnight and analysed by rheology on a AR 1000-N rheometer, using an aluminium plate FTC (25 nm diameter). The gap distance was fixed at 1 mm. A homogeneous layer of gel was placed between two plates. Frequency and stress sweep steps were performed at 25 ºC. Viscoelastic properties were studied under oscillatory experiments. For this purpose, the experimental conditions to achieve a linear viscoelastic regime (LVR) were determined by running a stress sweep step (oscillatory stress 0.5 to the flow point, at a frequency of 1 Hz) and a frequency sweep step (0.5-100 Hz at 1 Pa). The storage and loss modulus independence with frequency and oscillatory stress applied defined the

linear viscoelastic regime. Three replicates of each sample were done to assure the accuracy of the results.

3.6.1.3. Autocatalytic experiments

Catalytic experiments were performed at room temperature and without stirring. Phenylacetylene (8.2 mg; 8.9 µL; 3 eq) dissolved in MeOH (158 µL) was added on the top of the two-component catalytic metallogel (10 mol%), and the resultant mixture allowed to react for 1 to 48h. The reaction was stopped by adding 35 wt% H_2O_2 (20 µL) to promote the oxidation and consequent precipitation of copper. The resultant mixture was dried under nitrogen flow. For the blank assays, the reactant was added on the top of the gel **$N_3Val_nN_3$** formed in the presence of $[Cu(MeCN)_4]PF_6$ (10 mol%), and allowed to react in similar conditions. The conversion was determined by ^{1}H-NMR in d_6-DMSO.

3.6.1.4. Synthesis and Characterization

For structural reasons, the synthesis of the *L*-valine central core (**Val_n**) was first described (**Figure 52**). All reagents, starting materials and solvents (p.a. grade) were purchased from commercial suppliers and used as received without further purification.

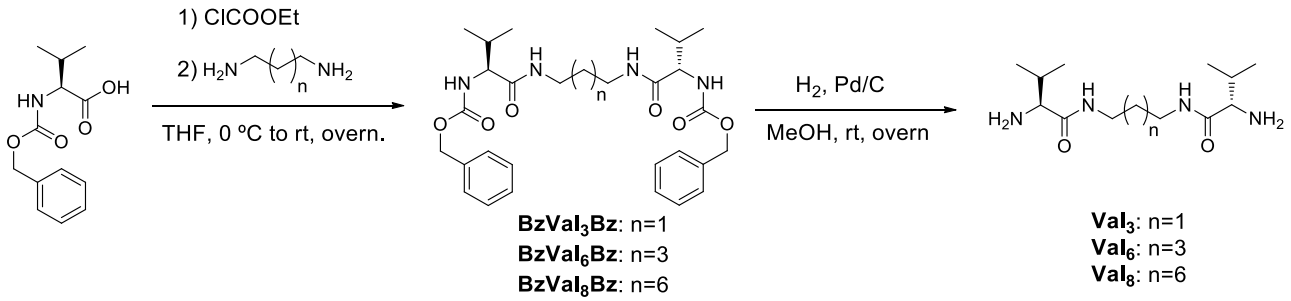

Figure 52. Scheme for the synthesis of the central *L*-valine core.

3.6.1.5. General Procedure for the synthesis of compounds $BzVal_nBz$

A solution of trimethylamine (31.84 mmol) in THF (20 mL) was added dropwise to a solution of N-CBz-*L*-Valine (31.84 mmol) in THF (180 mL) under N_2. To this mixture, ice cooled chloroformate (31.84 mmol) was added at 0-5 ºC and the pasty reaction allowed to stir for 30 min in an ice bath. To this mixture, a solution of 1,3-diamino-propane (15.16 mmol) in THF (20 mL) was added

dropwise for 20 min and the system maintained at 0 ºC for 1h, being then allowed to react at room temperature for 16h. The resultant solid was filtered and washed sequentially with a cold solution of 1M NaOH (10 mL), water (25 mL) and cold methanol (10 mL). The obtained white solid was allowed to dry at 60 ºC in vacuum overnight.

Compound **BzVal$_3$Bz** was obtained as a white solid (6.14 g; 75%). Characterization: ^{1}H NMR (300 MHz, d$_6$-DMSO): δ (ppm) 7.88 (br s, CON<u>H</u>CH$_2$ + CON<u>H</u>CH, 2H), 7.35-7.19 (m, Ph-H, 5H), 7.20 (d, *J* = 8.8 Hz, Benzyl-N<u>H</u>, 2H), 5.01 (s, Ph-C<u>H</u>$_2$, 2H), 3.76 (t, *J* = 7.9 Hz, -CONHC<u>H</u>, 1H), 3.09-2.99 (m, -CONHC<u>H</u>$_2$, 2H), 1.95-1.89 (m, -C<u>H</u>(CH$_3$)$_2$, 1H), 1.53-1.49 (m, -CH$_2$C<u>H</u>$_2$, 2H), 0.83 (d, *J* = 6.7 Hz, CH(C<u>H</u>$_3$)$_2$, 6H).

Compound **BzVal$_6$Bz** was obtained as a white solid (6.5 g; 70%)**.** Characterization: ^{1}H NMR (300 MHz, d$_6$-DMSO): δ (ppm) 7.83 (br s, CONHCH$_2$ + CONHCH, 2H), 7.34-7.29 (m, Ph-H, 5H), 7.15 (d, *J* = 8.73 Hz, Benzyl-NH, 2H), 5.01 (s, Ph-CH$_2$, 2H), 3.77 (t, *J* = 7.9 Hz -CONHCH, 1H), 3.05-2.94 (m, -CONHCH$_2$, 2H), 1.93-1.87 (m, -CH(CH$_3$)$_2$, 1H), 1.35 (br s, -CH$_2$CH$_2$CH$_2$, 2H), 1.22 (br s, -CH$_2$CH$_2$CH$_2$, 2H), 0.82 (d, *J* = 6.6 Hz, CH(CH$_3$)$_2$, 6H).

Compound **BzVal$_8$Bz** was obtained as a white solid (8 g; 77%)**.** Characterization: ^{1}H NMR (300 MHz, d$_6$-DMSO): δ (ppm) 7.82 (br s, CONHCH$_2$ + CONHCH, 2H), 7.33-7.27 (m, Ph-H, 5H), 7.15 (d, *J* = 8.8 Hz, Benzyl-NH, 2H), 5.01 (s, Ph-CH$_2$, 2H), 3.76 (t, -CONHCH, 1H), 3.06-2.95 (m, -CONHCH$_2$, 2H), 1.93-1.87 (m, -CH(CH$_3$)$_2$, 1H), 1.36 (br s, -CH$_2$CH$_2$CH$_2$CH$_2$, 2H), 1.21 (br s, -CH$_2$CH$_2$CH$_2$CH$_2$, 4H), 0.82 (d, *J* = 6.8 Hz, CH(CH$_3$)$_2$, 6H).

3.6.1.6. **General Procedure for the synthesis of compounds Val$_n$**

Palladium catalyst (30 wt% Pd/C) was suspended in MeOH (150 mL) and stirred at room temperature for 10 min. Then, **BzVal$_n$Bz** (5 mmol) was added and the reaction mixture allowed to stir under H$_2$ (g) for 16h. The black reaction mixture was filtered over celite and the filtrate concentrated at the rotavapor. The resultant product was dried at room temperature under vacuum.

Val$_3$ was obtained as a colourless liquid (1.3 g; 98%). Characterization: ^{1}H NMR (300 MHz, d$_6$-DMSO): δ (ppm) 7.88 (br s, -CON<u>H</u>CH$_2$, 1H), 3.06 (dd, *J* = 13.0, 6.6 Hz, -CONHC<u>H</u>$_2$, 2H), 2.89 (d, *J* = 5.1 Hz, NH$_2$C<u>H</u>, 1H), 1.88-1.78 (m, -C<u>H</u>(CH$_3$)$_2$, 1H), 1.51-1.47 (m, -CH$_2$C<u>H</u>$_2$, 2H), 0.81 (dd, *J* = 24.2, 6.8 Hz, CH(C<u>H</u>$_3$)$_2$, 6H).

Val$_6$ was obtained as a white solid (1.5 g ; 95%). Characterization: ^{1}H NMR (300 MHz, d$_6$-DMSO): δ (ppm) 7.74 (br s, -CON<u>H</u>CH$_2$, 1H), 3.07-2.97 (m, -CONHC<u>H</u>$_2$, 2H), 2.87 (d, *J* = 5.2 Hz, NH$_2$C<u>H</u>,

1H), 1.86-1.76 (m, -C<u>H</u>$(CH_3)_2$, 1H), 1.39-1.35 (m, -$CH_2C\underline{H_2}CH_2$, 2H), 1.23 (br s, -$CH_2CH_2C\underline{H_2}$, 2H), 0.80 (dd, *J* = 22.9, 6.8 Hz, $CH(C\underline{H_3})_2$, 6H).

Val$_8$ was obtained as a white solid (1.6 g; 91%). Characterization: ^{1}H NMR (300 MHz, d_6-DMSO): δ (ppm) 7.78 (br s, -CON<u>H</u>CH_2, 1H), 3.12-3.02 (m, -CONHC<u>H</u>$_2$, 2H), 2.92 (d, *J* = 5.2 Hz, $NH_2C\underline{H}$, 1H), 1.89-1.81 (m, -C<u>H</u>$(CH_3)_2$, 1H), 1.44-1.40 (m, -$CH_2C\underline{H_2}CH_2CH_2$, 2H) 1.28 (br s, -$CH_2CH_2C\underline{H_2}C\underline{H_2}$, 4H), 0.85 (dd, *J* = 23.4, 6.8 Hz, $CH(C\underline{H_3})_2$, 6H).

Once the central *L*-valine core has been obtained, we proceeded to the synthesis of the gelators **PhTzVal$_n$**. The synthetic pathway for obtaining the family of compounds **PhTzVal$_n$** is represented on **Figure 53**.

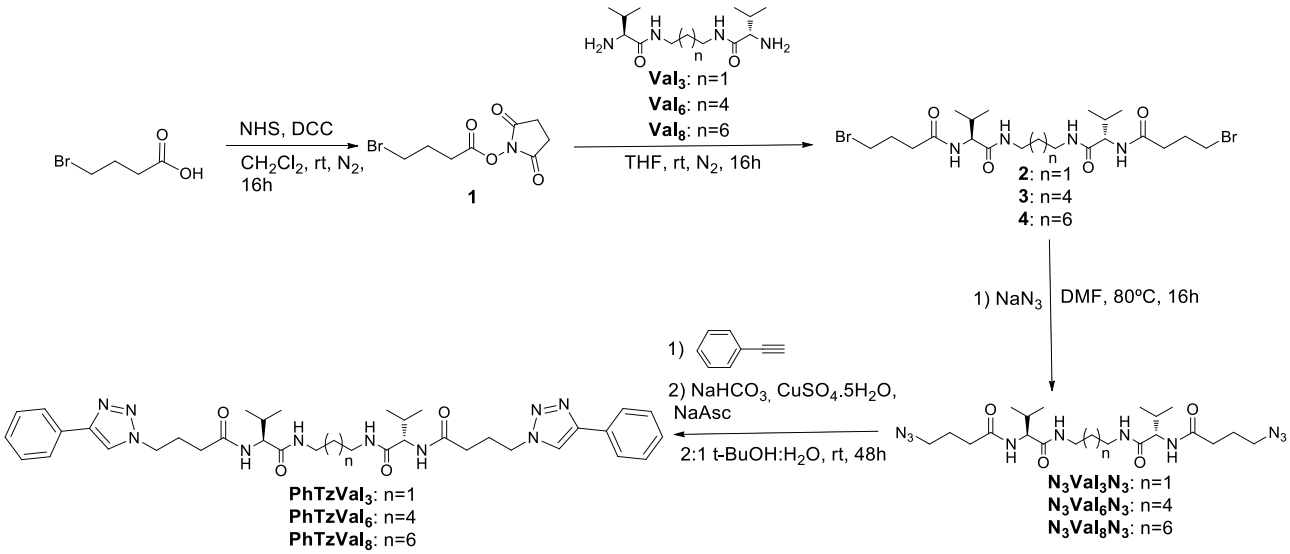

Figure 53. Scheme for the synthesis of **PhtzVal$_n$** gelators.

3.6.1.7. Synthesis of compound 1

A solution of *N,N*-dicyclohexylcarbodiimide (6.240 g, 30.24 mmol) in anhydrous CH_2Cl_2 (15 mL) was added dropwise to a suspension of bromobutyric acid (5 g, 29.94 mmol) and N-hydroxysuccinimide (3.446 g, 29.94 mmol) in CH_2Cl_2 (30 mL) under N_2 at 0ºC. After stirring overnight at rt, the white precipitate was filtered and the resultant solution concentrated to half and put into the freezer (-20 ºC) overnight. The remaining dicyclohexylurea was filtered again and the resultant solution evaporated, giving a pale brown solid (4.060 g, 70%). Characterization: ^{1}H NMR (300 MHz, d_6-DMSO): δ (ppm) 3.59 (t, *J* = 6.8 Hz, $BrC\underline{H_2}CH_2$-, 2H), 2.85-2.81 (m,

C<u>H</u>$_2$CONCOC<u>H</u>$_2$C<u>H</u>$_2$-, 6H), 2.15 (q, *J* = 6.8 Hz, BrCH$_2$C<u>H</u>$_2$-, 2H). ^{13}C (75 MHz, d$_6$-DMSO): δ (ppm) 169.00, 167.75, 31.48, 29.48, 27.45, 25.57.

3.6.1.8. General Procedure for the synthesis of compounds 2-4

A solution of **1** (3.67 mmol) in THF (15 mL) was added dropwise to a solution of **Val$_n$** (8.08 mmol) in THF (10 mL) under N_2 at rt. After stirring for 2h, the resultant precipitate was filtered, washed with 0.1M NaOH (10 mL) and water (20 mL), and dried under vacuum, affording **5-7** as a white solids. The compounds were directly used in the next step without further purification.

3.6.1.9. General Procedure for the synthesis of compounds N$_3$Val$_n$N$_3$

A solution of compound **2-4** (1.508 mmol) in DMF (10 mL) was added to a suspension of NaN_3 (15.08 mmol) in DMF (10 mL) and heated under N_2 to 80 ºC overnight. After cooling to rt, the crude was poured into cold water and the resultant precipitate filtered, washed with water (10 mL) and dried under vacuum.

Compound **N$_3$Val$_3$N$_3$** was obtained as a bright brown solid (0.425 g; 57%). Characterization: ^{1}H NMR (300 MHz, d$_6$-DMSO): δ (ppm) 7.87 (m, -CON<u>H</u>CH + -CON<u>H</u>CH$_2$, 2H), 4.05 (**t**, *J* = 7.9 Hz, -CONHC<u>H</u>, 1H), 3.27 (m, N$_3$C<u>H</u>$_2$CH$_2$CH$_2$-, 2H), 3.10 (m, -CONHC<u>H</u>$_2$, 2H), 2.23 (m, N$_3$CH$_2$C<u>H</u>$_2$CH$_2$-, 2H), 1.92 (m, -C<u>H</u>(CH$_3$)$_2$, 1H), 1.73 (m, N$_3$CH$_2$C<u>H</u>$_2$CH$_2$-, 2H), 1.50 (m, -CH$_2$C<u>H</u>$_2$, 2H), 0.82 (d, *J* = 6.7 Hz, -CH(C<u>H</u>$_3$)$_2$, 6H). ^{13}C (75 MHz, d$_6$-DMSO): δ (ppm) 171.81, 171.42, 58.40, 50.77, 36.65, 32.46, 30.71, 29.55, 25.04, 19.64, 18.09. ESI-MS (m/z) = 495.3152 [M+H]$^+$; $C_{21}H_{38}N_{10}O_4$. Calculated for $C_{21}H_{38}N_{10}O_4$: 491.3156

Compounds **N$_3$Val$_6$N$_3$** (0.502 g, 62%) was obtained as a pale brown solid. Characterization: ^{1}H NMR (300 MHz, d$_6$-DMSO): δ (ppm) 7.87 (m, -CON<u>H</u>CH + -CON<u>H</u>CH$_2$, 2H), 4.05 (t, *J* = 7.9 Hz, -CONHC<u>H</u>, 1H), 3.30 (m, N$_3$C<u>H</u>$_2$CH$_2$CH$_2$-, 2H), 3.04 (m, -CONHC<u>H</u>$_2$, 2H), 2.23 (m, N$_3$CH$_2$C<u>H</u>$_2$CH$_2$-, 2H), 1.90 (m, C<u>H</u>(CH$_3$)$_2$, 1H), 1.73 (m, N$_3$CH$_2$C<u>H</u>$_2$CH$_2$-, 2H), 1.35 (m, -CH$_2$C<u>H</u>$_2$CH$_2$, 2H), 1.23 (br s, -CH$_2$CH$_2$C<u>H</u>$_2$, 2H), 0.82 (d, *J* = 6.7 Hz, -CH(C<u>H</u>$_3$)$_2$, 6H). ^{13}C (75 MHz, d$_6$-DMSO): δ (ppm) 171.71, 171.25, 58.31, 50.77, 38.71, 32.48, 30.81, 29.42, 26.42, 25.08, 19.64, 18.71. ESI-MS (m/z) = 537.3625 [M+H]$^+$; $C_{24}H_{44}N_{10}O_4$. Calculated for $C_{24}H_{44}N_{10}O_4$: 537.3622

Compound **N$_3$Val$_8$N$_3$** was synthesized as a pale brown solid (0.656 g; 77%). Characterization: ^{1}H NMR (300 MHz, d$_6$-DMSO): δ (ppm) 7.84 (m, -CON<u>H</u>CH + -CON<u>H</u>CH$_2$, 2H), 4.06 (**t**, *J* = 7.9 -

CONHC<u>H</u>, 1H), 3.30 (m, $N_3C\underline{H_2}CH_2CH_2$-, 2H), 3.10-2.93 (m, -CONHC$\underline{H_2}$, 2H), 2.23 (m, $N_3CH_2C\underline{H_2}CH_2$-, 2H), 1.90 (m, -C$\underline{H}(CH_3)_2$, 1H), 1.74 (m, $N_3CH_2C\underline{H_2}CH_2$-, 2H), 1.36 (m, -$CH_2C\underline{H_2}CH_2CH_2$, 2H), 1.22 (br s, -$CH_2CH_2C\underline{H_2}$, 2H), 0.81 (d, J = 6.7 Hz, -CH($C\underline{H_3}$)$_2$, 6H). ^{13}C (75 MHz, d_6-DMSO): δ (ppm) 171.70, 171.23, 58.30, 50.77, 38.78, 32.48, 30.81, 29.42, 29.07, 26.70, 25.08, 19.64, 18.70. ESI-MS (m/z) = 565.3939 $[M+H]^+$; $C_{26}H_{48}N_{10}O_4$. Calculated for $C_{26}H_{48}N_{10}O_4$: 565.3938.

3.6.1.10. General Procedure for the synthesis of compounds PhTzVal$_n$

Phenylacetylene (2.12 mmol) was added to a suspension of **N_3Val$_n$$N_3$** (0.71 mmol) in mixture of 2:1 *t*-BuOH:H_2O (15 mL), followed by the addition of sodium hydrogenocarbonate (0.226 mmol), $CuSO_4.5H_2O$ (0.106 mmol, 5 mol%) and sodium ascorbate (0.425 mmol; 20 mol%). After stirring at room temperature for 48h, *t*-BuOH was evaporated and treated with 1M HCl (10 mL). The resultant precipitate was filtered under vacuum and washed with water (3x10 mL) and diethylether (1x10 mL). The product was filtered through silica (90:10 $CHCl_3$:MeOH) to remove possible coordinated copper.

Compound **PhTzVal$_3$** was obtained as a pale yellow solid (0.346 g; 70%). Characterization: ^{1}H NMR (300 MHz, d_6-DMSO): δ (ppm) 8.55 (s, triazole-<u>H</u>, 1H), 7.86 (m, Ph-<u>H</u> + -CON<u>H</u>CH + CON<u>H</u>CH_2, 4H), 7.43 (t, J = 7.4 Hz, Ph-<u>H</u>, 2H), 7.31 (t, J = 7.4 Hz, Ph-<u>H</u>, 1H), 4.38 (t, J = 6.6 Hz, Triazole-C$\underline{H_2}CH_2CH_2$-, 2H), 4.06 (t, J = 7.8 Hz, -CONHC<u>H</u>, 1H), 3.4 (m, -CONHC$\underline{H_2}$, 2H), 2.21 (m, Triazole-$CH_2CH_2C\underline{H_2}$-, 2H), 2.07 (m, Triazole-$CH_2C\underline{H_2}CH_2$-, 2H), 1.91 (m, C<u>H</u>C$(CH_3)_2$, 1H), 1.51 (m, -$CH_2C\underline{H_2}$, 1H), 0.81 (d, J = 6.4 Hz, -CH($C\underline{H_3}$)$_2$, 6H). ^{13}C (75 MHz, d_6-DMSO): δ (ppm) 171.64, 171.43, 146.77, 131.31, 129.30, 128.22, 125.57, 121.79, 58.44, 49.57, 36.69, 32.31, 29.58, 26.35, 19.66, 18.68. ESI-MS (m/z) = 721.3912 $[M+Na]^+$; $C_{37}H_{50}N_{10}O_4$. Calculated for $C_{37}H_{50}N_{10}O_4$: 721.3914

Compound **PhTzVal$_6$** was isolated as a pale yellow solid (0.315 g; 60%). Characterization: ^{1}H NMR (300 MHz, d_6-DMSO): δ (ppm) 8.55 (s, triazole-<u>H</u>, 1H), 7.81 (m, Ph-<u>H</u> + -CON<u>H</u>CH + CON<u>H</u>CH_2, 4H), 7.43 (t, J = 7.4 Hz, Ph-<u>H</u>, 2H), 7.31 (t, J = 7.4 Hz, Ph-<u>H</u>, 1H), 4.38 (t, J = 6.4 Hz, Triazole-C$\underline{H_2}CH_2CH_2$-, 2H), 4.08 (t, J = 7.6 Hz, -CONHC<u>H</u>, 1H), 3.02 (m, -CONHC$\underline{H_2}$, 2H), 2.21 (m, Triazole-$CH_2CH_2C\underline{H_2}$-, 2H), 2.10-2.05 (m, Triazole-$CH_2C\underline{H_2}CH_2$-, 2H), 1.90 (m, C<u>H</u>C$(CH_3)_2$, 1H), 1.35 (m, -$CH_2C\underline{H_2}CH_2$, 2H), 1.22 (br s, -$CH_2CH_2C\underline{H_2}$, 2H) 0.81 (d, J = 6.3 Hz, -CH($C\underline{H_3}$)$_2$, 6H). ^{13}C (75 MHz, d_6-DMSO): δ (ppm) 171.59, 171.21, 146.85, 131.48, 129.17, 128.10, 125.69,

121.61, 58.57, 49.62, 35.89, 32.19, 30.76, 29.40, 26.46, 26.34, 19.59, 18.60. ESI-MS (m/z) = 763.4390 $[M+Na]^+$; $C_{40}H_{56}N_{10}O_4$. Calculated for $C_{40}H_{56}N_{10}O_4$: 763.4348

Compound **PhTzVal$_8$** was synthesized a pale yellow solid (0.317 g; 58%). Characterization: ^{1}H NMR (300 MHz, d_6-DMSO): δ (ppm) 8.55 (s, triazole-H, 1H), 7.81 (m, Ph-H + -CONHCH + CONHCH$_2$, 4H), 7.43 (t, *J* = 7.3 Hz, Ph-H, 2H), 7.31 (t, *J* = 7.3 Hz, Ph-H, 1H), 4.38 (t, *J* = 5.7 Hz, Triazole-CH$_2$CH$_2$CH$_2$-, 2H), 4.09 (t, *J* = 7.7 Hz, -CONHCH, 1H), 3.02 (m, -CONHCH$_2$, 2H), 2.21-2.19 (m, Triazole-CH$_2$CH$_2$CH$_2$-, 2H), 2.08 (m, Triazole-CH$_2$CH$_2$CH$_2$-, 2H), 1.91 (m, CHC(CH$_3$)$_2$, 1H), 1.35 (m, -CH$_2$CH$_2$CH$_2$CH$_2$, 2H), 1.20 (br s, -CH$_2$CH$_2$CH$_2$CH$_2$, 4H) 0.81 (d, *J* = 6.3 Hz, -CH(CH$_3$)$_2$, 6H). ^{13}C (75 MHz, d_6-DMSO): δ (ppm) 171.56, 171.24, 146.77, 131.31, 129.29, 128.21, 125.57, 121.77, 58.34, 49.55, 32.19, 29.40, 29.06, 26.70, 26.39, 19.64, 18.66. ESI-MS (m/z) = 791.4702 $[M+Na]^+$; $C_{42}H_{60}N_{10}O_4$. Calculated for $C_{42}H_{60}N_{10}O_4$: 791.4697

3.6.2. Compounds bearing a benzyltriazolyl fragment

3.6.2.1. Gelation Procedures

The gelator **BzTzAVal$_n$** was heated in a 4 mL screw-capped vial in the presence of 500 µL of solvent, until complete dissolution (~1 min). The resultant hot solution was then sonicated for 1 min, resulting in the formation of a gel which was allowed to stabilize for 20 minutes at room temperature. For the formation of the metallogels, the gelator was heated together with the copper salt $[Cu(MeCN)_4]PF_6$ in a 2:1 molar ratio, following a similar gelation procedure as the pure gel.

3.6.2.2. Synthesis and Characterization

The synthetic pathway for obtaining the family of compounds **BzTzAVal$_n$** is represented on **Figure 54**. All reagents, starting materials and solvents (p.a. grade) were purchased from commercial suppliers and used as received without further purification.

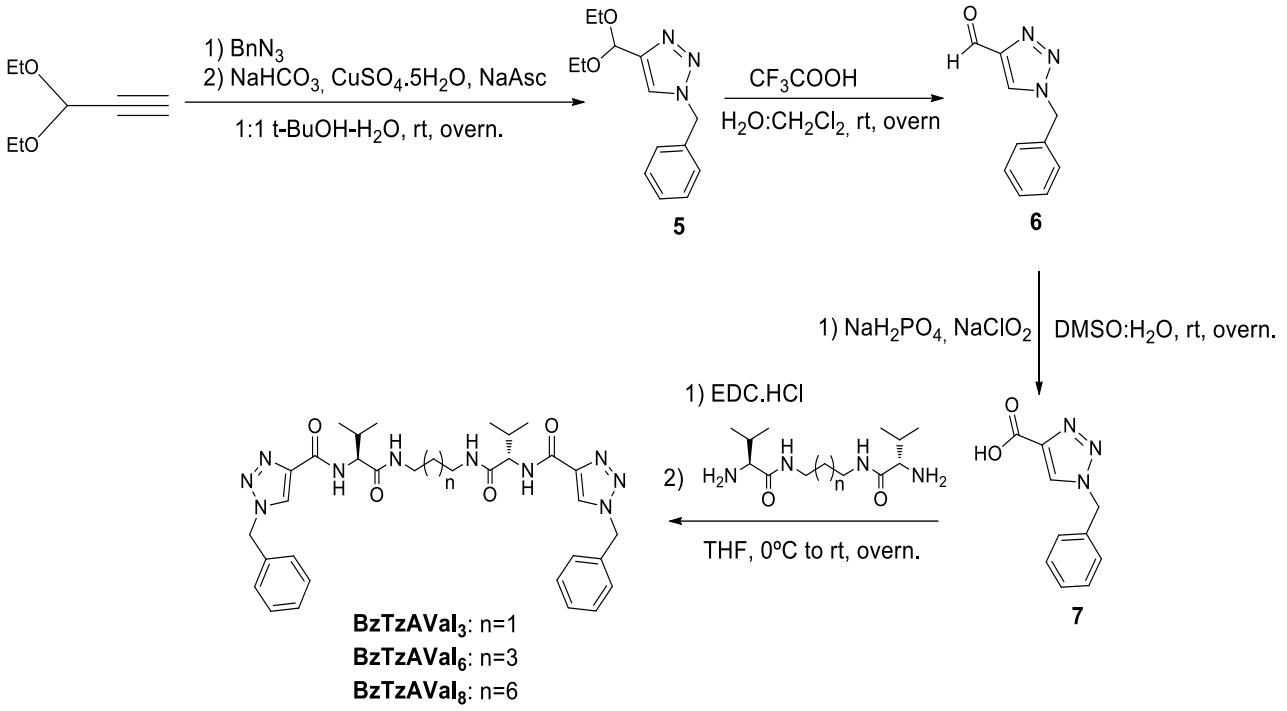

Figure 54. Scheme for the synthesis of **BzTzAVal$_n$** gelators.

3.6.2.2.1. Synthesis of Compound 5

Compound **5** was synthesized according to a procedure reported in literature, with small modifications.[4] Briefly, diethylpropargylacetal (3 g; 23.41 mmol; 3.36 mL) and benzylazide (3.58 g; 29.92 mmol; 3.37 mL) were dissolved in a 1:1 mixture of *t*-BuOH/H_2O (4 mL). To this solution, sodium bicarbonate (0.301 g; 3.58 mmol), copper(II) sulphate pentahydrate (0.29 g; 1.17 mmol; 5 mol%) and sodium ascorbate (0.93 g; 4.68 mmol) were added, and the resultant mixture stirred at room temperature overnight. After completion of the reaction (TLC Hex/EtOAc 1:1), ethyl acetate (15 mL) was added and the organic phase washed with saturated NaHCO3 (3 x 10 mL) and brine (2 x 10 mL). The organic extractions were dried over anhydrous MgSO4 and the solvents removed in vacuum. The obtained crude mixture was purified by column chromatography (60:40 Hex:AcOEt), giving a white crystalline powder (4.29 g; 70%). Characterization: ^{1}H NMR (300 MHz, $CDCl_3$): δ (ppm) 7.49 (s, triazole-H, 1H), 7.36-7.29 (m, Ph-H, 5H), 5.69 (s, Ph-CH_2-, 2H), 7.91 (s, Triazole-CH, 1H), 3.66-3.56 (m, -CH(CH_2CH$_3$)$_2$, 4H), 1.21 (t, *J* = 7.1 Hz, -CH(CH$_2$CH_3)$_2$, 6H).

3.6.2.2.2. Synthesis of Compound 6

To a solution of **5** (3 g; 11.39 mmol) in CH_2Cl_2 (2 mL), water (1 mL) was added, followed by TFA (0.037 g; 9.68 mmol; 0.74 mL), and the reaction mixture stirred vigorously for 6h at room temperature. EtOAc (10 mL) was added and the organic phase washed with a saturated solution of

NaHCO3 (3 x 10 mL) and brine (2 x 10 mL). The organic extracts were dried over anhydrous $MgSO_4$ and the solvents removed in vacuum, giving a white solid (1.82 g; 78%). Characterization: ^{1}H NMR (300 MHz, $CDCl_3$): δ (ppm) 10.11 (s, Triazole-C<u>H</u>O, 1H), 7.98 (s, Triazole-<u>H</u>, 1H), 7.41-7.29 (m, Ph-H, 5H), 5.58 (s, Ph-C<u>H$_2$</u>-, 2H).

3.6.2.2.3. Synthesis of compound 7

To a solution of **8** (1.7 g; 8.28 mmol) in DMSO (10 mL), a 3M solution of $NaH_2PO_4.2H_2O$ (1.94 g; 12.43 mmol) in water was added. A solution of 0.4M $NaClO_2$ was added dropwise at 0 ºC and under stirring, and the resultant mixture allowed to react for 16h at room temperature. The resultant mixture was quenched in brine (10 mL) and stirred for 10 min. The obtained precipitate was filtered under vacuum and washed with water (3 x 10 mL), giving a white solid (1.28 g; 70%). Characterization: ^{1}H NMR (300 MHz, d_6-DMSO): δ (ppm) 13.01 (br s, Triazole-COO<u>H</u>, 1H), 8.75 (s, Triazole-<u>H</u>, 1H), 7.38-7.33 (m, Ph-<u>H</u>, 5H), 5.64 (s, Ph-C<u>H$_2$</u>-, 2H).

3.6.2.2.4. General Procedure for the synthesis of BzTzAVal$_n$ gelators

A solution of **8** (0.92 mmol) in THF (5 mL) was added dropwise to a clear solution of the *L*-valine diamine (1.93mmol, 2.1eq) and EDC.HCl (1.93 mmol, 2.1eq) in THF (10 mL) under N_2 at 0°C, and the resulting mixture allowed to react overnight at rt. After concentration of the mixture on the rotavapor, 1M NaOH (10 mL) was added and the resulting precipitate filtered under vacuum and washed with water (3x15 mL). The resultant solid was dried at 60 ºC under vacuum. giving a white solid.

Compound **BzTzAVal$_3$** was obtained as a white solid (0.27 g; 45%). Characterization: ^{1}H NMR (300 MHz, d_6-DMSO): δ (ppm) 8.68 (s, triazole-<u>H</u>, 1H), 8.12 (t, *J* = 5.4 Hz, -CON<u>H</u>CH$_2$, 1H), 7.91 (d, *J* = 9.0 Hz, Triazole-CON<u>H</u>, 1H), 7.35 (s, Ph-H, 5H), 5.64 (s, Ph-C<u>H$_2$</u>-, 4H), 4.29 (**t**, -CONHC<u>H</u>, 1H) 3.11-3.02 (m, -CONHC<u>H$_2$</u>, 2H), 2.06-2.01 (m, -C<u>H</u>(CH$_3$)$_2$, 2H), 1.57-1.52 (m, -CH$_2$C<u>H$_2$</u>, 2H), 0.85 (t, *J* = 6.1 Hz, -CH(C<u>H$_3$</u>)$_2$, 6H). ^{13}C NMR (75 MHz, d_6-DMSO) δ 170.84, 159.56, 142.89, 136.03, 129.25, 128.73, 128.77, 127.09, 57.98, 53.62, 36.89, 31.41, 29.44, 19.65, 18.68. ESI-MS (m/z) = 643.3757 $[M+H]^+$; $C_{36}H_{48}N_{10}O_4$. Calculated for $C_{33}H_{42}N_{10}O_4$: 643.3469.

Compound **BzTzAVal$_6$** was obtained as a white solid (0.26 g; η=40%). Characterization: ^{1}H NMR 300 MHz, d_6-DMSO): δ (ppm) 8.68 (s, triazole-<u>H</u>, 1H), 8.10 (br s, -CON<u>H</u>CH$_2$, 1H), 7.91 (d, *J* = 9.1 Hz, Triazole-CON<u>H</u>, 1H), 7.35 (s, Ph-H, 5H), 5.64 (s, Ph-C<u>H$_2$</u>-, 4H), 4.28 (t, *J* = 8.7 Hz, -CONHC<u>H</u>, 1H) 3.08-2.99 (m, -CONHC<u>H$_2$</u>, 2H), 2.08-2.00 (m, -C<u>H</u>(CH$_3$)$_2$, 2H), 1.39-1.35 (m, -

$CH_2C\underline{H_2}CH_2$, 2H), 1.23 (br s, $-CH_2CH_2C\underline{H_2}$, 2H), 0.87 (dd, *J* = 13.7, 7.6 Hz, $-CH(C\underline{H_3})_2$, 6H). ^{13}C NMR (75 MHz, d_6-DMSO) δ 170.68, 159.62, 143.09, 135.92, 129.19, 128.68, 128.44, 126.85, 58.07, 53.77, 39.04, 29.33, 26.71, 19.57, 18.52. ESI-MS (m/z) = 707.3768 $[M+Na]^+$; $C_{36}H_{48}N_{10}O_4$. Calculated for $C_{42}H_{48}N_{10}O_4$: 707.3758.

The final product **BzTzAVal$_8$** was obtained as a white solid (0.40; 60%). Characterization: ^1H NMR (300 MHz, d_6-DMSO): δ (ppm) 8.68 (s, triazole-H, 1H), 8.07 (br s, $-CONHCH_2$, 1H), 7.89 (d, *J* = 8.9 Hz, Triazole-CONH, 1H), 7.35 (s, Ph-H, 5H), 5.64 (s, Ph-$C\underline{H_2}$-, 4H), 4.28 (t, *J* = 7.7 Hz, -CONHCH, 1H) 3.08-2.99 (m, -CONHC$\underline{H_2}$, 2H), 2.05-1.98 (m, -C$\underline{H}(CH_3)_2$, 2H), 1.39-1.35 (m, $-CH_2C\underline{H_2}CH_2CH_2$, 2H), 1.20 (br s, $-CH_2CH_2C\underline{H_2}C\underline{H_2}$, 4H), 0.85 (t, *J* = 6.3 Hz, $-CH(C\underline{H_3})_2$, 6H). ^{13}C NMR (75 MHz, d_6-DMSO) δ 170.72, 159.55, 142.89, 136.00, 129.25, 128.74, 128.46, 127.06, 57.99, 53.63, 38.85, 31.46, 29.30, 26.42, 19.62, 18.65. ESI-MS (m/z) = 713.4252 $[M+H]^+$; $C_{38}H_{52}N_{10}O_4$. Calculated for $C_{38}H_{52}N_{10}O_4$: 713.4251.

3.6.2.2.5. Synthesis of non-aggregating compound BzTzAPropyl

A solution of propiolamine (0.091 mL) in anhydrous CH_2Cl_2 (2 mL) was added dropwise to a suspension of **7** (0.25 g; 1.22 mmol) and EDC.HCl (0.23g; 1.22 mmol) under N_2 at 0 ºC, and the resulting mixture allowed to react for 16h under N_2 at room temperature. After addition of CH_2Cl_2 (20 mL), the organic phase was washed with 1M NaOH (2 x 10 mL) and brine (2 x 10 mL). The organic extracts were then dried over anhydrous $MgSO_4$, filtered and evaporated in the rotavapor, giving a white fluffy solid (0.11 g; 41%). Characterization: ^1H NMR (300 MHz, $CDCl_3$): δ (ppm) 8.68 (s, triazole-H, 1H), 7.96 (s, $-CONHCH_2$, 1H), 7.35 (s, Ph-H, 5H), 7.16 (br s, *J* = 8.9 Hz, Triazole-CONH, 1H), 5.55 (s, Ph-$C\underline{H_2}$-, 4H), 3.41 (d, *J* = 6.7 Hz, -CONHC$\underline{H_2}$, 2H) 1.64 (dd, *J* = 14.4 Hz, *J* = 7.1 Hz $-CH_2C\underline{H_2}$, 2H), 0.99 (t, *J* = 7.1 Hz $-CH_2CH_2C\underline{H_3}$, 3H). ^{13}C NMR (75 MHz, $CDCl_3$) δ 159.44, 143.81, 133.77, 129.37, 129.08, 128.23, 125.07, 54.52, 40.82, 22.87, 11.36. ESI-MS (m/z) = 245.1400 $[M+H]^+$; $C_{13}H_{16}N_4O$. Calculated for $C_{13}H_{16}N_4O$: 245.1402

3.6.3. General Procedure catalytic experiments model 'click' reaction

Catalytic experiments were performed at room temperature without stirring. All the reactions were performed for periods of 3h, 6h, 8h and 15h using 500 µL of 1:1 H_2O-*t*BuOH, or acetonitrile, as solvent media. Briefly, the reactants in stoichiometric proportion (0.21 mmol) were mixed and added directly at the top of the metallogel catalyst (1 mol%), composed by the gelator and the copper salt $[Cu(MeCN)_4]PF_6$ in a 2:1 or 4:1 molar ratio, depending on the number of triazole fragments present in the molecule. At the end of the experiment, the products were directly

extracted with 700 µL $CDCl_3$. The organic phase was dried over anhydrous $MgSO_4$ and the conversion determined by ^{1}H-NMR.

3.6.4. General characterization methods

3.6.4.1. Minimum gel concentration

For retrieving the minimum gel concentration, the native gels, or the correspondent metallogels, were formed in 4 mL screw-capped vials in concentrations ranging from 8 mg/mL to 2.5 mg/mL, using 500 µL of the desired solvent. Each gel was formed following the gelation procedure described for the corresponding family of compounds and allowed to age for 20 minutes. The minimum concentration at which the gel withstands gravity upon inversion of the vial was considered as the minimum gelation concentration (m.g.c.).

3.6.4.2. Temperature of gel-to-sol transition

The pure gels, or the correspondent metallogels, were formed in 4 mL screw-capped vials in concentrations ranging from 3.3 to 10 mM, using 400 µL of EtOH. Each gel was formed following the gelation procedure described for the corresponding family of compounds and allowed to age for 1 hour. The vials were then heated using a thermostat (Radleys) from 30 ºC to a maximum of 78 ºC (boiling temperature of the EtOH), allowing to stabilize every 3 ºC for 10 minutes. The temperature at which the gel disintegrate upon inversion of the vial was defined as the T_{sol}.

3.6.4.3. Quantification of Coordinated copper

After the formation of the catalytic metallogel, 100 µL of surrounding solution were collected with a 1 mL syringe and filtered through a 0.22 µm filter. The filter was washed with a solution of 5% HNO_3 (2x1 mL) in Milli-Q water to remove remaining uncoordinated copper. A 25 mL solution of the sample in 5% HNO_3 was prepared and the concentration of copper(I) determined by inductively coupled plasma-mass spectrometry (ICP-MS) using a Varian 710-ES.

3.6.4.4. Wide-angle X-ray Diffraction

The obtained gels/metallogels were dried on air or by lyophilization (Telstar LyoQuest), depending on the nature of the gel (organogel or hydrogel), and the resultant powder resuspended in hexane. The suspension was applied into the glass sample holder and the solvent allowed to evaporate. The resultant powdered sample was analysed by X-ray diffraction (XRD) at room temperature using a Bruker D4 Endeavor X-ray powder diffractometer with Cu-K_α radiation. Data were collected for 2θ

values between 2º and 40º with a step size of 0.03º and a time step of 10 s.

3.6.4.5. Transmission Electron Microscopy

A small portion of the gel/metallogel was placed on a nickel grid coated with carbon and allowed to dry on air. Images were recorded in a JEOL 2100 microscope without using any stain.

3.6.4.6. Circular Dichroism

Circular Dichroism spectra were carried out in pressed pellets composed by 1 (%m/m) lyophilized gel:KBr on a Jasco J-810 spectropolarimeter.

3.6.4.7. Nuclear Magnetic Resonance

^{1}H and ^{13}C NMR spectra measurements were recorded in a Varian Mercury 300 MHz spectrometer at 30 ℃.

Chapter 4

Tandem ‘click’-aldol Catalytic System: Towards “organo-click” reactions

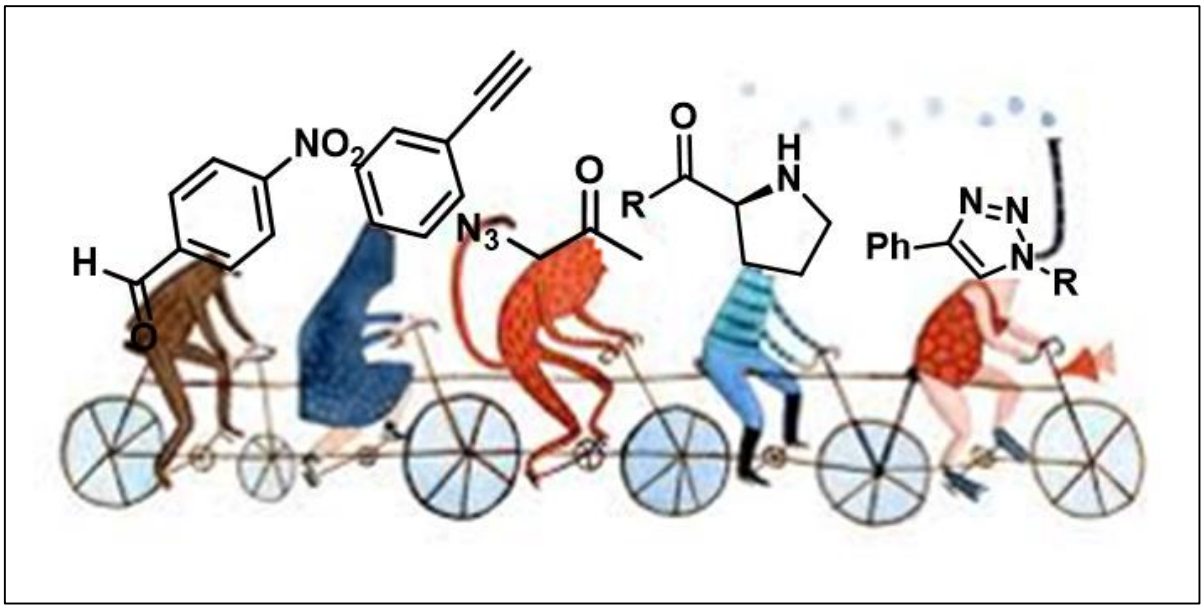

A new tandem system comprising a ‘click’ and an aldol addition reaction is presented. The performance of the gel towards the catalysis of intermediate ‘click’ and aldol addition reactions, as well as in the global three-component reaction has been investigated. Finally, a possible catalytic mechanistic pathway has been proposed.

4.1. Introduction

The term systems chemistry was first applied by von Kiedrowski to describe the chemical origins of biological organization.[1] In the field of chemistry, research in complex systems has been intimately linked with systems biology, especially in understanding how the function of a biological system is related to the interactions between the several molecular components. Thus, complex systems comprise the study of all variables simultaneously, including topics such as multicomponent reactions, replicating networks or self-assembling systems.[2]

Nature, particularly biological systems, have always been a focus of inspiration for chemists, not only due to the vast diversity that the living organisms are able to create, but also to the extraordinary synthetic strategies developed. Enzymes, the catalysts used by living systems, are a clear example of nature efficiency. These organisms are responsible to perform diverse chemical transformations with high selectivity and specifity, being able to produce structurally complicated compounds through multienzimatic cascade reactions.[3] By contrast, in classical synthetic chemistry, individual transformations are conducted as stepwise processes, punctuated by the purification and isolation of intermediates at each stage of the sequence. Thus, in an attempt to mimic different aspects of synthetic strategies that operate in biological systems, chemists have been challenged to design artificial systems that simulate the multienzimatic ability of performing multistep reactions.[4]

As a result of a growing interest in mimicking nature processes, much attention has been directed to "one-pot" processes involving multiple catalytic transformations followed by a single work up.[5] "One-pot" tandem reactions, where multiple catalysts and reagents combined in a single reaction vessel undergo in a sequence of precisely staged catalytic steps have become highly attractive.[6] Depending on the number of catalytic species or whether there is intervention in the reaction system, tandem catalysis can be subcategorized in three different categories: orthogonal, auto-tandem or assisted tandem catalysis (**Figure 55**).[7]

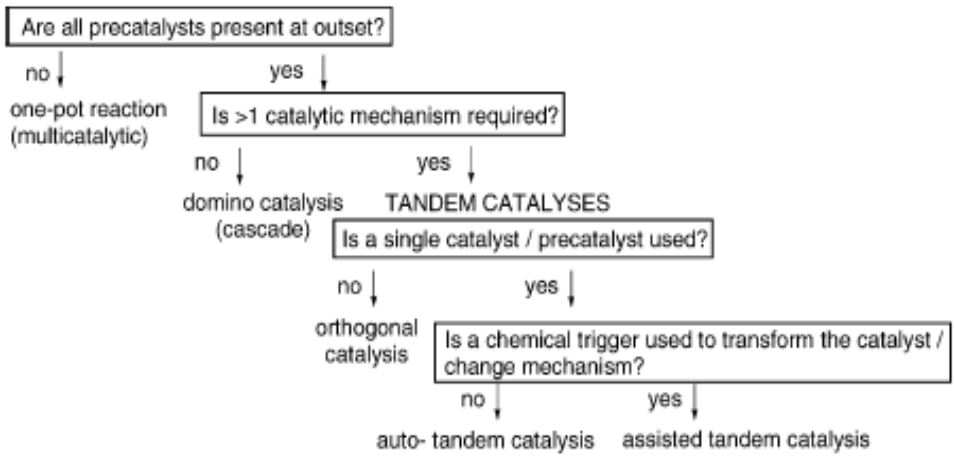

Figure 55. Flowchart for classification of one-pot processes involving sequential elaboration of an organic substrate via multiple catalytic transformations.[7]

As observed in the scheme represented in **Figure 55**, orthogonal tandem catalysis can be defined as a "one-pot" reaction in which sequential catalytic processes occur through two or more functionally distinct, and preferably non-interfering catalytic cycles.[6] In this process, all the catalysts, or precatalysts, as well as all the reactants, are present from the outset of the reaction.[8] During the mechanistic pathway, catalyst A transforms substrate A to an intermediate B, which is subsequently converted to product P by catalyst B (**Figure 56**).

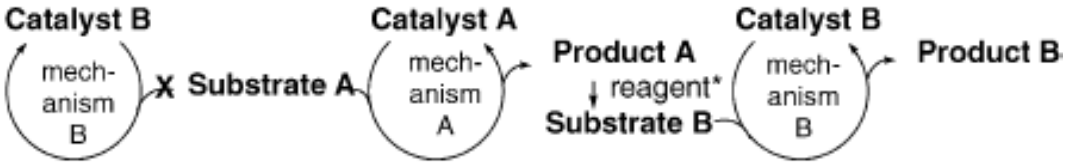

Figure 56. Schematic illustration of orthogonal catalysis (*Additional reagent, if required, must be present from the outset of the reaction).[7]

However, if only one catalyst is present in the reaction system, tandem catalysis may be defined as auto-tandem or assisted tandem catalysis. Auto-tandem catalysis involve two or more mechanistically distinct catalysis promoted by a single catalyst precursor, where both cycles occur spontaneously by cooperative interaction of several species (catalyst, substrate, additional reagents if required) present from the outset of the reaction. As represented in **Figure 57**, catalyst A converts substrate A into the product A, which in turn acts as a substrate for a second type of catalytic transformation mediated by catalyst A.

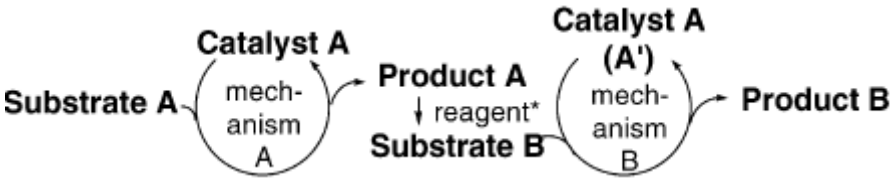

Figure 57. Schematic illustration of auto-tandem catalysis (*Additional reagent, if required, must be present from the outset of the reaction).[7]

Finally, in assisted tandem catalysis, deliberate intervention in the system is involved to switch between one catalytic site and another.[6] Such intervention usually consists on the addition of a further reagent to trigger a change in mechanism. During this type of catalytic process, catalyst A assists the conversion of substrate A into product A before being transformed (often by direct manipulation of the active site) into catalyst B, which then acts on the product of the original catalytic site. In contrast to the previously described techniques, two catalytic processes cannot occur simultaneously, since the two catalysts do not coexist (**Figure 58**).

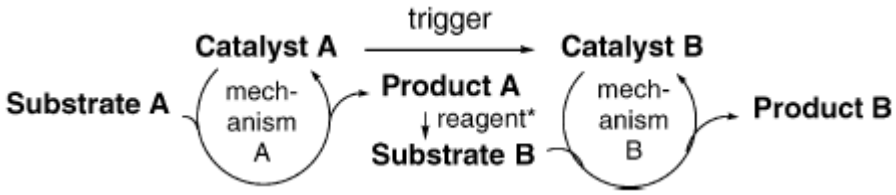

Figure 58. Schematic illustration of assisted-tandem catalysis (*Additional reagent may or may not be required).[7]

From the synthetic chemists' point of view, ideal reaction strategies for the preparation of structurally complex substances should involve sequences in which stereocontrolled formation of multiple carbon-carbon bonds occur in a single step starting from simple and readily available materials.[9] In this field, aldol addition reactions are among the transformations that have greatly simplified the construction of asymmetric C-C bonds, being particularly important both in complex molecule synthesis and in the preparation of optically active small molecule building blocks.[10]

The reaction typically includes a carbonyl pro-nucleophile, which is an enolizable aldehyde, ketone or carboxylic acid derivative, and a carbonyl electrophile, usually an aldehyde and rarely a ketone. It commonly proceeds through the formation of an intermediate enolate, which requires some activation energy to undergo addition to electrophilic reaction component, often guiding to the formation of a product containing one or two adjacent stereocenters.[11]

Earlier methods to achieve efficient asymmetric induction were based on the addition of stoichiometric quantities of chiral reagents.[12] However, since the pioneering finding by Barbas and his co-workers that *L*-proline could act as a catalyst in intermolecular direct aldol reaction, several

catalysts bearing *L*-proline moieties have been developed.[13] In this field, an important research has been done by *Rodríguez-Llansola et al.*, who designed and developed new supramolecular gelators functionalized with *L*-proline fragments that could be applied as heterogeneous catalysts for aldol addition reactions.[14] A clear example of an efficient supramolecular catalyst is the amphiphilic hydrogel **ProValDoc**, which successfully catalysed the direct aldol reaction between the cyclohexanone and 4-nitrobenzaldehyde with high enantioselectivity (**Figure 59**).[15] It has been proposed that the catalytic mechanism proceeds via enamine formation, but hydrophobic interactions also played an important role both on the self-assembly of the gelator and on the approach of the reactants to the catalytic centre.[16]

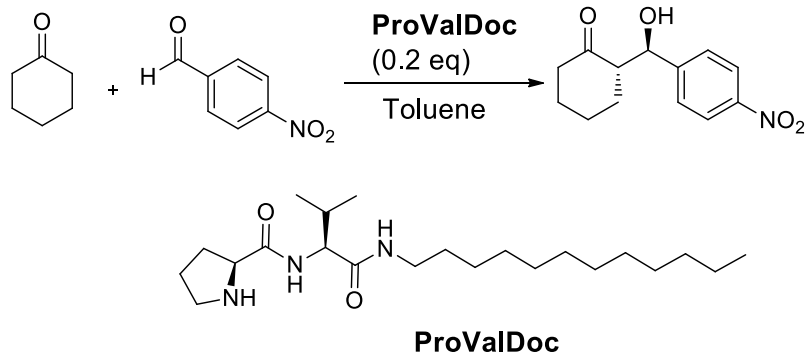

Figure 59. Direct aldol reaction between cyclohexanone and 4-nitrobenzaldehyde in the presence of the organocatalytic hydrogel **ProValDoc**.

Several tandem or multicomponent systems comprising combinations of aldol reactions with other important transformations, such as aldol-allylation,[17] 1,4-addition-aldol,[18,19] Michael-aldol[20] or amination-aldol[21] have been investigated for the synthesis of natural products or respective building blocks. On the other hand, in the field of 'click' chemistry such systems are not common. Particularly for CuAAC reaction, very few examples of multicomponent systems are found in literature, being the "one-pot" synthesis of 1,4-disubstituted 1,2,3-triazoles starting from α-bromoketone one of the most practical and useful, since terminal acetylene reacts with the in-situ generated azide, providing a safer synthetic procedure.[22,23] A clear example of a tandem 'click' reaction is the tandem enantioselective biocatalytic epoxide ring opening and [3+2] azide-alkyne cycloaddition, which occurs in the presence of halohydrin dehalogenase and the traditional catalytic mixture copper(II) sulphate/sodium ascorbate.[24] However, very little work has been done on matching together in a "one-pot" system aldol and 'click' reactions, which are nowadays highly important in the field of pharmaceutical and materials industries.[25,26]

Having this in mind, our investigation was focused on joining these two reactions in an orthogonal tandem catalytic 'click'/aldol system. In a green and sustainable chemistry perspective, water was used as the preferred solvent to carry out the multicomponent reaction. Taking advantage of the work done in this thesis, as well as of the research carried in our group, **Cu(I)-PhTzVal$_3$** and **ProValDoc** were selected as the most suitable catalysts for the construction of the tandem catalytic system. The catalytic performance of both **ProValDoc** and **Cu(I)-PhTzVal$_3$** was evaluated alone and in the two-component gel system.

4.2. Results and Discussion

4.2.1. Design and Synthesis of the gelators

In this project, a bolaamphiphilic gelator and an amphiphilic gelator were tested as suitable heterogeneous catalysts for the design of the tandem 'click'/aldol system. The bolaamphiphilic compound is composed by a central diaminopropane core linked to a *L*-valine fragment in both sides and functionalized with a phenyltriazole moiety separated by a four carbon alkyl chain (**Figure 60**). The gelator has in its structure four amide bonds that together with the aromatic rings could contribute for the self-assembly process. The design and synthesis of the **PhTzVal$_3$** gelator has been already described in **Chapter 3**. Briefly, the *L*-valine derivative central core was attached to the activated ester of the bromobutyric acid by simple peptide coupling, followed by a nucleophilic substitution of the halide with an azide and consequent coupling with the commercially available phenylacetylene through a copper(I) catalysed Huisgen 1,3-diplolar cycloaddition.

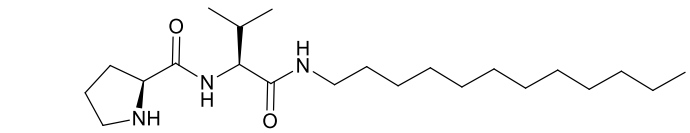

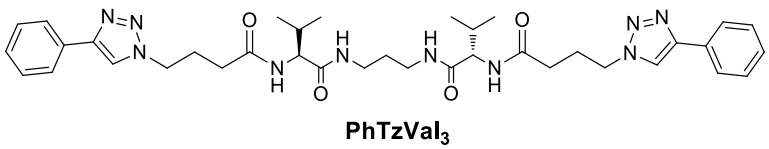

Figure 60. Structure of the gelators **ProValDoc** and **PhTzVal$_3$**.

The **ProValDoc** hydrogelator is structurally composed by a *L*-valine amino acid functionalized with a proline moiety and coupled to a long hydrophobic carbon tail, which could act as the main gelation motif. The gelator was synthesized by simple peptide coupling of the *L*-valine with dodecylamine, followed by reaction with the *L*-proline applying similar methodology.

4.2.2. Viscoelastic, Structural and Morphological Properties

Both gelators **ProValDoc** and **Cu(I)-PhTzVal$_3$** were able to aggregate in water at concentrations of 2 mM and 5.7 mM, respectively, producing a swollen precipitate that can flow along the solution. Typical thermotropic and viscoelastic properties such as gel-to-sol transitions or minimum gelation concentration have not been investigated since it was impossible to obtain a strong gel that did not flow upon inversion of the test tube. Thus, characterization of the gelators was focused on their structural and morphological properties.

As observed for the organogels of **PhTzVal$_n$** family in **Chapter 3**, the gelator **PhTzVal$_3$** was able to aggregate with and without the presence of the copper. In this Chapter, CuBr was used as the copper source, as the copper complex $[Cu(MeCN)_4]PF_6$ is more appropriate to organic solvents. The common procedure for the gelation of the compounds consisted on heating the gelator until complete dissolution, followed by sonication of 20 seconds for the gelator **PhTzVal$_3$**, and one hour for the gelator **ProValDoc**.

A first attempt to build the two-component gel **Cu(I)-PhTzVal$_3$/ ProValDoc** for the tandem catalytic system consisted on heating both gelators together and in the presence of the copper salt CuBr. However, the solution rapidly acquired a blue/green colour and the total dissolution of the gelators could not be reached. It seems that in some way both compounds were competing for the coordination of the copper salt. Thus, the formation of the two-component metallogel was achieved by the addition of **ProValDoc** aggregates to the vial containing the **Cu(I)-PhTzVal$_3$** metalloaggregates. In this case, it is possible that both gels can compete for coordination of Cu(I) considering the known liability of Cu(I)-Tz complexes.

In an attempt to investigate if there was a co-aggregation or just an orthogonal assemble phenomenon, the two-component gel **Cu(I)-PhTzVal$_3$/ ProValDoc**, as well as their pure components were analysed by wide-angle X-ray diffraction (WAXD) (**Figure 61**).

The hydrogel **ProValDoc** self-assembles in an organized and crystalline structural arrangement. This gelator presents a structure showing a high periodicity that is specially evidenced between $2\theta = 18^\circ$ to $2\theta = 25^\circ$, where the lattice plans are periodically distributed with a constant distance of 0.2 Å between them. The hydrophobic interactions responsible for the aggregation of this gelator contribute to the formation of a highly organized closely packed structure, where the proline groups are oriented outside and the hydrophobic tail to the middle, resembling a surfactant

system.[16] It has been already published that this gelator can generate several polymorphs presenting different self-assembly and distinct catalytic activity for the direct aldol addition between the 4-nitrobenzaldehyde and the cyclohexanone.[27] In this case, WAXD results suggest that polymorph A has been obtained (**Figure 61A**), which based on literature, is the one exhibiting the best catalytic activity.[27]

The gelator **PhTzVal$_3$** aggregates in a semi-amorphous structure both in the presence and absence of the copper salt CuBr (**Figure 61B-C**). It is peculiar to see that in the presence of copper, it seems that the gelator acquires a more unorganized structure regarding the sharp peaks obtained in the corresponding diffractogram (**Figure 61C**).

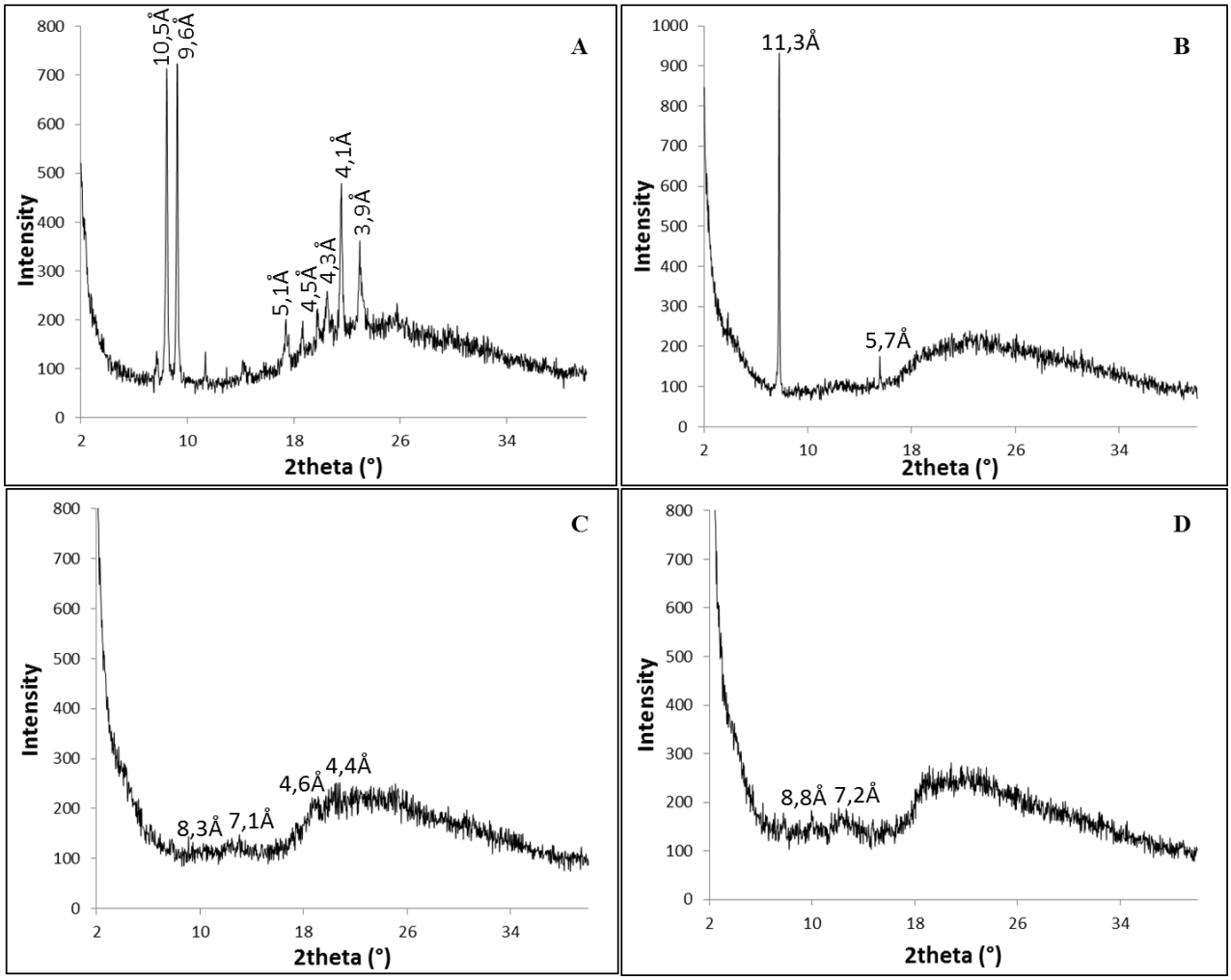

Figure 61. Diffractograms obtained for the hydrogels **ProValDoc** (A), **PhTzVal$_3$** (B), **Cu(I)-PhTzVal$_3$** (C) and **Cu(I)-PhTzVal$_3$/ProValDoc** (D).

The diffractogram corresponding to the two-component metallogel **Cu(I)-PhTzVal$_3$/ProValDoc** present a high similarity with the one obtained for the metallogel **Cu(I)-PhTzVal$_3$** alone, which may be indicative of orthogonal self-assembly rather than a co-assembly

process. The difference between both is that in self-sorting systems, the molecules aggregate independently and the different assemblies are orthogonal to each other, maintaining the structural arrangement of the pure initial components, while in co-assembled mixtures, the molecules may randomly or specifically aggregate, forming a gel with a totally different structural arrangement and fibre morphology when compared with the initial pure gelators.[28,29] However, it is curious to see that the structural arrangement of the two component-gel **Cu(I)-PhTzVal$_3$/ProValDoc** contains only structural information from one of the pure components, as no lattice peaks corresponding to the structure of pure **ProValDoc** could be observed (**Figure 61D**).

To further confirm the presence of an orthogonally self-assembled network, the morphology of the fibres obtained for the two-component hydrogel **Cu(I)-PhTzVal$_3$/ProValDoc** were analysed by TEM and compared with the ones belonging to the pure gels.

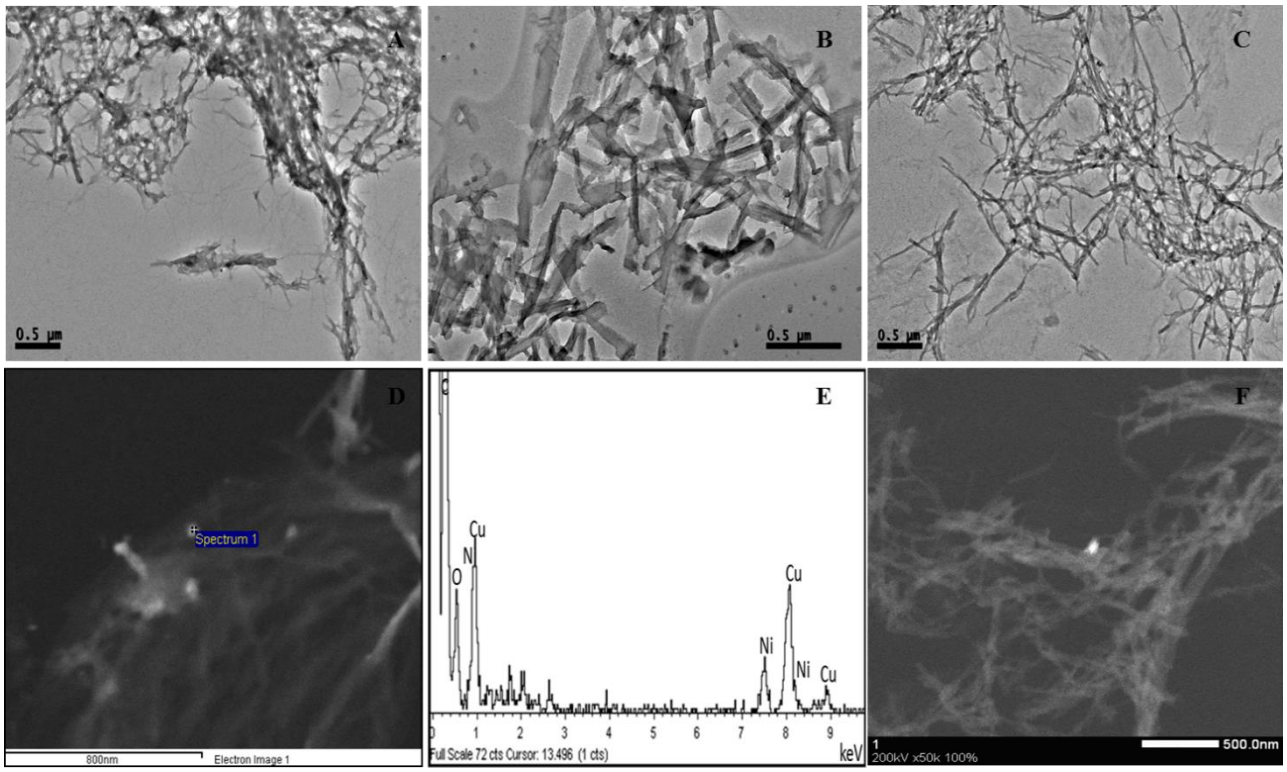

Figure 62. TEM pictures of the metallogels **Cu(I)-PhTzVal$_3$/ProValDoc** (A), **ProValDoc** (B), **Cu(I)-PhTzVal$_3$** (C) and STEM pictures of the **Cu(I)-PhTzVal$_3$/ProValDoc** (D), **Cu(I)-PhTzVal$_3$** (F). EDS spectrum taken from the STEM picture of **Cu(I)-PhTzVal$_3$/ProValDoc** (E). Magnifications are 8000x (A-C) and 50000x (F).

The obtained pictures revealed that both the gel **Cu(I)-PhTzVal$_3$** and the two-component gel **Cu(I)-PhTzVal$_3$/ProValDoc** exhibit a highly crosslinked network of long and thin fibres with high similarity. This similarity is also evidenced in the STEM pictures, which could be acquired without staining due to the presence of the metal along the fibre network. The white contrast supports the

wide distribution of copper(I) through the network of the samples **Cu(I)-PhTzVal$_3$** and **Cu(I)-PhTzVal$_3$/ProValDoc**. The presence of copper was further confirmed by EDS analysis, where only carbon, oxygen, copper and nickel were detected, this last one arising from the sample grid. The absence of a 1:1 Cu:Br ratio in the EDS spectrum confirms the successful coordination of the metal to the phenyltriazole aggregates, resulting in the formation of an extended organometallic network.

The fibres exhibited by the **ProValDoc** aggregates appears to be larger in width (**Figure 62B**) than the ones observed for the **Cu(I)-PhTzVal$_3$** and **Cu(I)-PhTzVal$_3$/ProValDoc**. However, looking at the TEM pictures, it is difficult to evaluate whether the fibers of the gelator **ProValDoc** are present in the two-component gel **Cu(I)-PhTzVal$_3$/ProValDoc**, although the majority of fibers in the mixed gel appear to be thin and more comparable to the metalloaggregates of **Cu(I)-PhTzVal$_3$**.

The results obtained by XRD and TEM analysis may suggest that the structure of the **ProValDoc** could have been disrupted in some way due to the presence of the metallogel **Cu(I)-PhTzVal$_3$**, probably due to possible interference of copper that could be present in solution, which could be probably coordinated by the nitrogen of the proline fragment. To confirm this hypothesis, the amount of copper coordinated by the metallogels **Cu(I)-PhTzVal$_3$** and **Cu(I)-PhTzVal$_3$/ProValDoc** was determined by ICP-MS. For this experiment, the attempt to form a gel of **Cu(I)-ProValDoc** was unsuccessful, resulting always in a blue greenish solution. Thus, this sample was not considered for ICP-MS analysis.

Table 8. Amount of copper coordinated by the gelators **Cu(I)-PhTzVal$_3$** and by the two-component gel **Cu(I)-PhTzVal$_3$/ProValDoc**[a]

Compound	% Cu coordinated
Cu(I)-PhTzVal$_3$	70.6
Cu(I)-PhTzVal$_3$/ProValDoc	78.7

[a] **ProValDoc** and **Cu(I)-PhTzVal$_3$** gels were formed in water, at concentrations of 2 mM and 5.7 mM, respectively.

The amount of copper coordinated by the two-component metalloaggregates **Cu(I)-PhTzVal$_3$/ProValDoc** is around 8% higher than the one determined for the pure metalloaggregates **Cu(I)-PhTzVal$_3$**. These results may suggest that **ProValDoc** is also capable of coordinating some copper, although it appears that some oxidation occurs as suggested by the blue greenish colour of the solution. **ProValDoc** is known to self-assemble in an intercalated bilayer structure supported not only by the van der Waals and hydrophobic interactions of the closely packed alkyl chains, but also by H-bonding between the nitrogen from the proline and the oxygen from the amide of two consecutive molecules, as represented in **Figure 63**.[16] However, besides supporting the self-

assembled structure of **ProValDoc** through H-bonding, the nitrogen and the oxygen also constitute preferential sites for metal coordination.

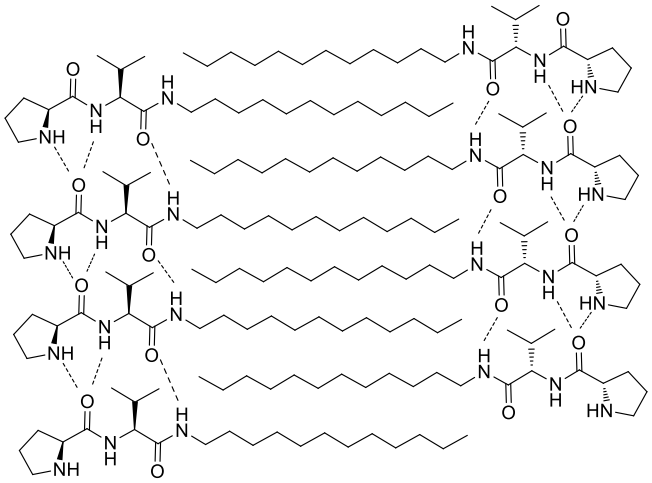

Figure 63. Proposed packing structure of **ProValDoc** hydrogels.

Thus, in the presence of CuBr, the heteroatoms might coordinate copper, being then unavailable to participate in the self-assembly process of the gelator. This might be the main cause for the unsuccessful gelation of **ProValDoc** in the presence of CuBr. Furthermore, it was observed that the initially brownish **Cu(I)-PhTzVal$_3$** metalloaggregates turned blue upon addition of **ProValDoc** aggregates, suggesting some interference of the copper(I) with the **ProValDoc** gelator (**Figure 64**).

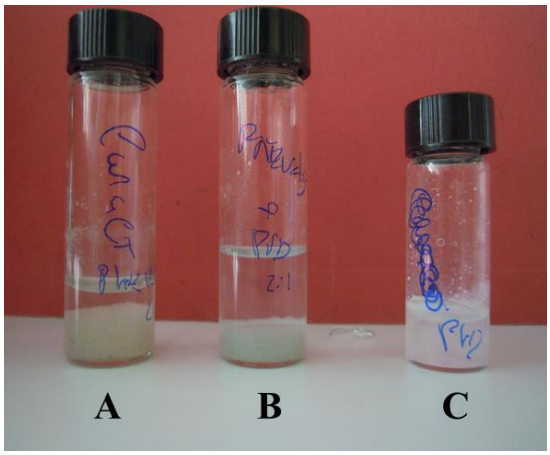

Figure 64. Macroscopic aspect of the metalloaggregates **Cu(I)-PhTzVal$_3$** (A), **Cu(I)-PhTzVal$_3$/ProValDoc** (B) and of the **ProValDoc** (C) aggregates.

The disruption of the aggregates network of **ProValDoc** in the presence of CuBr would explain the absence of diffraction signals of **ProValDoc** in the two-component gel **Cu(I)-PhTzVal$_3$/ProValDoc**.

4.2.3. Tandem Catalytic System

The design of the multicomponent catalytic system requires the presence of, at least, one specimen that could undergo both a 'click' as well as an aldol addition reaction. The synthesis of this reactant (**N_3Cet**) was achieved by simple reaction of the chloroacetone with sodium azide, as reported elsewhere.[30] The compounds chosen to complete the tandem system were the commercially available phenylacetylene and *p*-nitrobenzaldehyde (**Figure 65**).

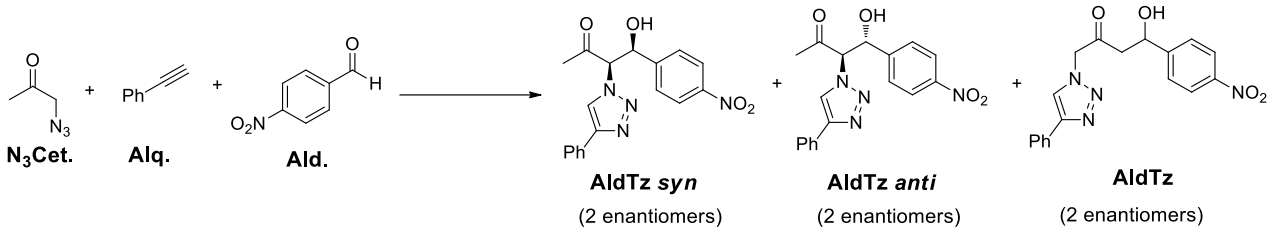

Figure 65. Structures of reactants and possible products involved in the tandem 'click'-aldolic system.

As usual in aldol addition reactions, two possible diastereoisomers can be obtained as main reaction products, such as **AldTz *syn*** and **AldTz *anti***, together with the correspondent enantiomers. Considering the stronger acidity of the α-hydrogen positioned between the azide and carbonyl group, the formation of the compound **AldTz,** arising from a possible addition on the methyl group of the reactant **N_3Cet**, would not be expected. This complex reaction system can be divided in two stepwise 'click' and aldol addition reactions, as represented in **Figure 66**.

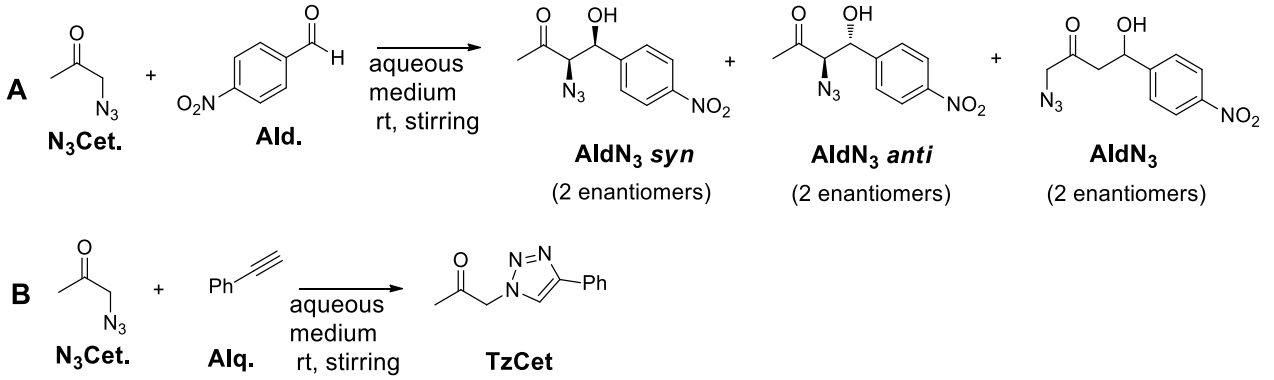

Figure 66. Click (A) and aldolic (B) reactions guiding to the formation of the possible intermediates **TzCet** and **$AldN_3$**.

Once again, given the stronger acidity of the proton positioned between the carbonyl and the azide group of the reactant **N_3Cet**, the product **$AldN_3$** would not be obtained. Experiments performed on these reactions confirmed the absence of NMR signals corresponding to this product (**Figure 67**).

4.2.3.1. Study of the reaction conditions

The intermediate reactions (**Figure 66**) were first checked separately using phosphate buffer (PB) pH 7.4 or distilled water at pH 6.3 as solvent media. The reactions were performed by stirring the reactants in 1 mL (**Figure 66A**) or 2 mL of solvent (**Figure 66B**) at room temperature and without the presence of catalyst (**Table 9**). The liquid reactant **N_3Cet** was used as solvent media for the *p*-nitrobenzaldehyde, and the resultant solution transferred into the reaction vessel.

Table 9. Conversions found for the intermediate reactions in 0.1 M phosphate buffer (pH= 7.4) and distilled water (pH= 6.3).

Entry	Solvent	Reaction	Conversion at 1 d (%)[a]	Products (ratio syn:anti)	Conversion at 3 d (%)[a]	Products	Conversion at 5 d (%)[a]	Products (ratio *syn:anti*)
1A	PB	A	60	69:31	-	n.d.[b]	96	62:38
1B		B	0	-	0	-	0	-
2A	H_2O	A	15	n.d.[b]	11	50:50	27	68:32
2B		B	0	-	0	-	0	-

[a] Typical procedure: Reaction A: The reactant *p*-nitrobenzaldehyde (0.86 mg, $5.7x10^{-3}$ mmol) was dissolved in the N_3Cet (5.6 mg; $5.7x10^{-2}$ mmol) and transferred to a 8 mL screw-capped vial containing 1 mL solvent medium. The resultant mixture stirred for a maximum period of 5 days at room temperature. At the end of the experiment, the products were directly extracted with $CDCl_3$ (3x 330 µL). The organic phase was dried over anhydrous $MgSO_4$ and the conversion determined by ^{1}H-NMR. Reaction B: A similar procedure was followed for this reaction, using as reactants phenylacetylene (5.82 mg; $5.7x10^{-2}$ mmol) and **N_3Cet** (5.6 mg; $5.7x10^{-2}$ mmol). [b] not detected in the ^{1}H-NMR spectra.

Although no final product arising from the 'click' reaction has been obtained, the conversions registered for the aldol addition reaction carried in PB buffer were surprisingly high. The reaction carried in buffer achieved a conversion of 96% (**Table 9, entry 1A**), much higher than the 27% obtained when carried in water for a similar period of time (**Table 9, entry 2A**), although the ratio *syn:anti* was practically similar. A typical spectra of the reaction carried in the presence of PB is represented in **Figure 67**. It was possible to identify the peaks corresponding to the two diastereoisomers **AldN_3** ***syn*** and **AldN_3** ***anti***, which present considerably different coupling constants (*J*). The *J* determined for **AldN_3** ***anti*** is in well accordance with the one found in literature.[30]

Figure 67. Typical spectrum of the reaction between **N_3Cet** and *p*-nitrobenzaldehyde.

The high conversion for the reaction carried in PB could suggest the occurrence of catalysis that could derive from the presence of the phosphate anion. The reaction was also carried at different PB concentrations for 24h to evaluate if there was a trend depending on the concentration of buffer (**Table 10**).

Table 10. Aldol addition between **N_3Cet** and *p*-nitrobenzaldehyde carried at different concentrations of PB buffer at pH=7.4.

Entry	Concentration (M)	Conversion at 1 d (%)[a]	Products (ratio *syn:anti*)
1	0.01	68	66:34
2	0.1	68	68:32
3	1	77	66:34

[a] Typical procedure: The reactant *p*-nitrobenzaldehyde (0.86 mg, $5.7x10^{-3}$ mmol) was dissolved in the N_3Cet (5.6 mg; $5.7x10^{-2}$ mmol) and transferred to a 8 mL screw-capped vial containing 1 mL solvent medium. The resultant mixture stirred for a period of 1 day at room temperature. At the end of the experiment, the products were directly extracted with $CDCl_3$ (3x 330 µL). The organic phase was dried over anhydrous $MgSO_4$ and the conversion determined by ^{1}H-NMR.

The relatively similar conversions obtained upon increase of buffer concentration discarded a possible catalytic activity of the phosphate anion. However, to further confirm this hypothesis, the same reaction was also carried in buffers having different functional groups, such as the 4-(2-

hydroxyethyl)-1-piperazineethanesulfonic acid (HEPES) or the 2-Amino-2-hydroxymethyl-propane-1,3-diol (TRIS). As the buffers PB and HEPES present a similar tetrahedral geometry of the corresponding anionic functional group, the buffer TRIS was also tested for comparison (**Figure 68**).

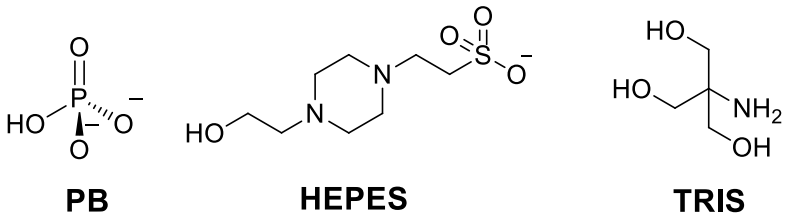

Figure 68. Structure of the buffers tested as solvent media in the aldol addition reaction at pH 7.4.

Similarly to what was done in the previous experiments, the reaction was carried out in 1 mL of 0.1M buffer pH= 7.4 and at room temperature with stirring for 24h (**Table 11**).

The results show that abnormally high conversions were also observed if HEPES or TRIS were used as solvent media in the aldol addition between **N_3Cet** and *p*-nitrobenzaldehyde. Apart from the similar conversions achieved using the different buffers, the similar ratio between the **AldN_3** ***syn*** and **AldN_3** ***anti*** suggest that the reaction occurs by a similar mechanism independently of the buffer.

Table 11. Conversions registered for aldol addition between **N_3Cet** and *p*-nitrobenzaldehyde carried in different 0.1 M buffers (pH=7.4).

Entry	Buffer	Conversion at 24h (%)[a]	Products (ratio *syn:anti*)
1	PB	60	69:31
2	HEPES	56	66:34
3	TRIS	76	67:33

[a] Typical procedure: The reactant *p*-nitrobenzaldehyde (0.86 mg, $5.7x10^{-3}$ mmol) was dissolved in the **N_3Cet** (5.6 mg; $5.7x10^{-2}$ mmol) and transferred to a 8 mL screw-capped vial containing 1 mL solvent medium. The resultant mixture stirred for a period of 1 day at room temperature with stirring. At the end of the experiment, the products were directly extracted with $CDCl_3$ (3x 330 µL). The organic phase was dried over anhydrous $MgSO_4$ and the conversion determined by ^{1}H-NMR.

Thus, it can be purposed that the pH of the solvent (pH= 7.4) may probably be the main driving force for the occurrence of the reaction. If the pH of the medium is higher than the *pKa* of the **N_3Cet**, the compound will be easily deprotonated, guiding to the formation of the corresponding products. Furthermore, the lower conversion (15%) achieved by this same reaction when carried in

distilled water (pH= 6.3) for 24h also support this hypothesis (**Table 9, entry 2A**). Considering this finding, distilled water was selected as the best solvent to investigate the catalytic activity of the gelators in the absence of background catalysis.

4.2.3.2. Catalysis in the intermediate aldol addition and 'click' reaction

The intermediate aldol addition and 'click' reactions (**Figure 66**) were tested in the presence of the catalytic gelators **ProValDoc** and **Cu(I)-PhTzVal$_3$** and using distilled water as preferred reaction medium. For the formation of the former metallogelator, the compound $[Cu(MeCN)_4]PF_6$ was also tested initially as a possible copper source. The obtained results evidence the good catalytic activity of the gelators (**Table 12, entries 1, 3 and 4**), achieving considerably higher conversions than the corresponding blanks carried out in water (**Table 12, entries 2 and 6**).

Table 12. Conversions achieved by the intermediate aldol addition and 'click' reactions in the presence of different catalysts.

Entry	Reaction	Catalyst (%mol)	Copper salt	Conversion at 1 d (%)[a]	AldN$_3$ (ratio *syn:anti*)	Conversion at 3 d (%)[a]	AldN$_3$ (ratio *syn:anti*)	Conversion at 5 d (%)[a]	AldN$_3$ (ratio *syn:anti*)
1	A	**ProValDoc** (15)	-	13	52:48	50	55:45	57	57:43
2	A	-	-	15	n.d.[b]	11	50:50	27	68:32
3	B	**Cu(I)-PhTzVal$_3$** (5)	CuBr	-	-	75	-	-	-
4	B	**Cu(I)-PhTzVal$_3$** (5)	$[Cu(MeCN)_4]PF_6$	-	-	50	-	-	-
5	B	CuBr (5)	-	-	-	40	-	-	-
6	B	-	-	-	-	0	-	-	-

[a] Typical procedure: Reaction A: The reactant *p*-nitrobenzaldehyde (0.86 mg, $5.7x10^{-3}$ mmol) was dissolved in the **N$_3$Cet** (5.6 mg; $5.7x10^{-2}$ mmol) and transferred to a 4 mL screw-capped vial containing 450 µL of solvent medium and 15 mol% of catalytic gelator **ProValDoc** (0.33 mg; $8.5x10^{-4}$ mmol). The resultant mixture stirred for a maximum period of 5 days at room temperature. At the end of the experiment, the products were directly extracted with $CDCl_3$ (3x 330 µL). The organic phase was dried over anhydrous $MgSO_4$ and the conversion determined by ^{1}H-NMR. Reaction B: A similar procedure was followed for this reaction, using as reactants phenylacetylene (5.82 mg; $5.7x10^{-2}$ mmol), **N$_3$Cet** (5.6 mg; $5.7x10^{-2}$ mmol) and 5 mol% of the desired catalyst in a 8 mL screw-capped vial. [b] not detected in the ^{1}H-NMR spectra.

The catalysis of aldol additions in the presence of the gelator **ProValDoc** has been already reported.[14,15,16] In the presence of the *L*-proline functionalized gel, the reaction follows a similar

mechanistic pathway involving the formation of an enamine intermediate, which is well in accordance to what has been reported in literature for *L*-proline catalysed aldol additions.[31] The catalytic mechanism proceeds via enamine formation between *L*-proline and the corresponding donor substrate. The formation of the enamine occurs following the formation of an iminium ion intermediate, leading to the ketone enamine that serves as C-nucleophile in the carbon-carbon forming step (**Figure 69**). The enamine attacks the carbonyl group of the aldehyde acceptor with high enantiofacial selectivity, imposed by a highly organized tricyclic hydrogen bonded framework. The nucleophilic attack of a water molecule and cleavage of the proline from the aldol substrate complete the mechanism[31,32]

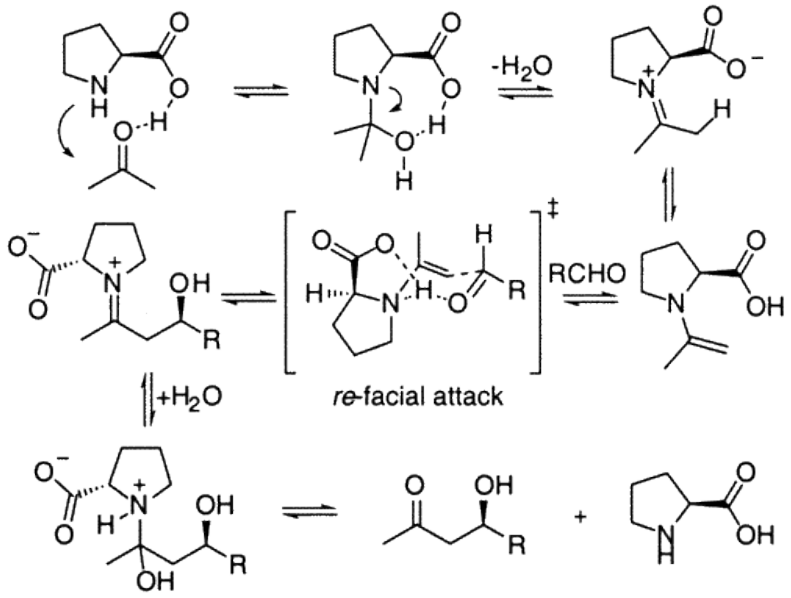

Figure 69. Proposed mechanistic pathway for the catalysis of aldol additions in the presence *L*-proline.[31,32]

Regarding the 'click' reaction, the metallogel **Cu(I)-PhTzVal$_3$** formed in the presence of CuBr exhibited higher catalytic activity than the one gelated using the copper complex [Cu(MeCN)$_4$]PF$_6$ as the copper source. While in the first case 75% conversion was registered after 3 days reaction, in the former the observed conversion was only 50% (**Table 12, entries 3-4**). This might be due to the better solubility of the copper salt CuBr in water in comparison with the one of the [Cu(MeCN)$_4$]PF$_6$, which is more appropriate for reactions occurring in organic media.[33] Nevertheless, independently on the salt used as copper source, the conversions achieved in the presence of the metalloaggregates **Cu(I)-PhTzVal$_3$ (Table 12, entries 3-4)** for the 'click' reaction were always higher than the one observed for the blank reaction carried out only in the presence of the copper salt CuBr (**Table 12, entry 5**), suggesting some catalytic activity derived from the presence of the gelator.

Once the intermediates **AldN$_3$** or **TzCet** are obtained from the reactions represented in **Figure 66**, the final product can be reached by an additional 'click' or aldol addition reaction respectively, depending on the competitivity of the system and consequently, on the major product obtained in the first set of intermediate reactions. The reactions leading to the synthesis of the final aldol-'click' products are represented in **Figure 70**.

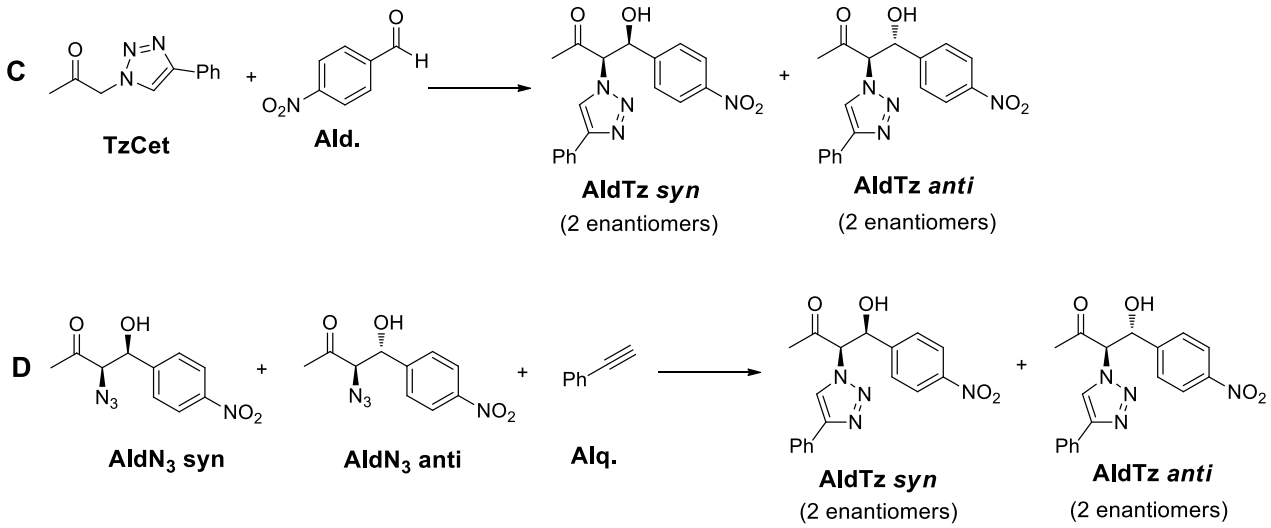

Figure 70. Aldol addition (C) and 'click' (D) reactions guiding to the formation of the final products **AldTz *syn*** and **AldTz *anti***.

The catalytic activity of the gels **ProValDoc** and **Cu(I)-PhTzVal$_3$** was mainly investigated for the aldol addition represented in **Figure 70C**, using CuBr as copper source. For these experiments, the compound **TzCet** was synthesized in large scale through a Huisgen 1,3-dipolar cycloaddition between the **N$_3$Cet** and the commercially available phenylacetylene, in the presence of the catalytic system $CuSO_4$/sodium ascorbate. The catalytic reactions were carried out at room temperature and with stirring for a maximum period of 4 days. In all the experiments, 10 equivalents of **TzCet** was used to displace the equilibrium in the direction of the products, considering the known reversibility of the aldol addition reaction.[34] As both **TzCet** and *p*-nitrobenzaldehyde were highly insoluble in water, the **TzCet** was first dissolved in 50 µL DMSO and the resultant yellow solution used to solubilize the *p*-nitrobenzaldehyde. The conversions achieved were determined by ^{1}H-NMR (**Table 13**).

Surprisingly, higher conversions were achieved in the presence of the **Cu(I)-PhTzVal$_3$** metalloaggregates. A conversion of 23% was observed when the gelator **Cu(I)-PhTzVal$_3$** was used as catalyst, while in the presence of the catalytic gel **ProValDoc**, commonly used in the catalysis of aldol reactions, only 12% conversion was achieved (**Table 13**, **entries 1-2)**. Indeed, the conversion

achieved in the presence of the gelator **ProValDoc** is similar to the one observed in the presence of CuBr. The reason for such low conversions may arise from the very low solubility of the reactants **TzCet** and *p*-nitrobenzaldehyde, which precipitates when transferred into water.

Table 13. Conversions achieved by the intermediate aldol addition between **TzCet** and *p*-nitrobenzaldehyde in the presence of the gel catalysts and CuBr**.**

Entry	Catalyst (10 mol%)	Conversion at 2 d (%)[a]	Conversion at 4 d (%)[a]
1	**ProValDoc**	-	12
2	**Cu(I)-PhTzVal$_3$**	30	23
3	CuBr	-	11.5

[a] Typical procedure: Reaction A: The reactants **TzCet** (11.5 mg; $5.7x10^{-2}$ mmol) and *p*-nitrobenzaldehyde (0.86 mg, $5.7x10^{-3}$ mmol) were solubilized in 50 µL DMSO. The resultant yellow solution was then transferred to a 8 mL screw-capped vial (4 mL for the reaction with **ProValDoc**) containing the solvent medium and 10 mol% of the desired catalyst. The resultant mixture was stirred for a maximum period of 4 days at room temperature. At the end of the experiment, the products were directly extracted with $CDCl_3$ (3x 330 µL). The organic phase was dried over anhydrous $MgSO_4$ and the conversion determined by ^{1}H-NMR.

However, it is relatively surprising to see that the catalytic activity of the metallogel **Cu(I)-PhTzVal$_3$** was twice than the one observed for the proline-based gelator **ProValDoc**. A typical spectra ^{1}H-NMR spectra of this reaction could be observed in **Figure 71**, where characteristic signals corresponding to the final product **AldTz** could be identified. The coupling constant found for the proton positioned in the carbon bearing the triazole fragment in the final product (J= 3.2 Hz) is well in accordance with the one determined for the same proton of the corresponding intermediate **AldN$_3$** ***syn*** (**Figure 67**), confirming that the main product obtained from this reaction is the **AldTz** ***syn***. The absence of the **AldTz** ***anti*** could be related with some instability of this diastereoisomer.

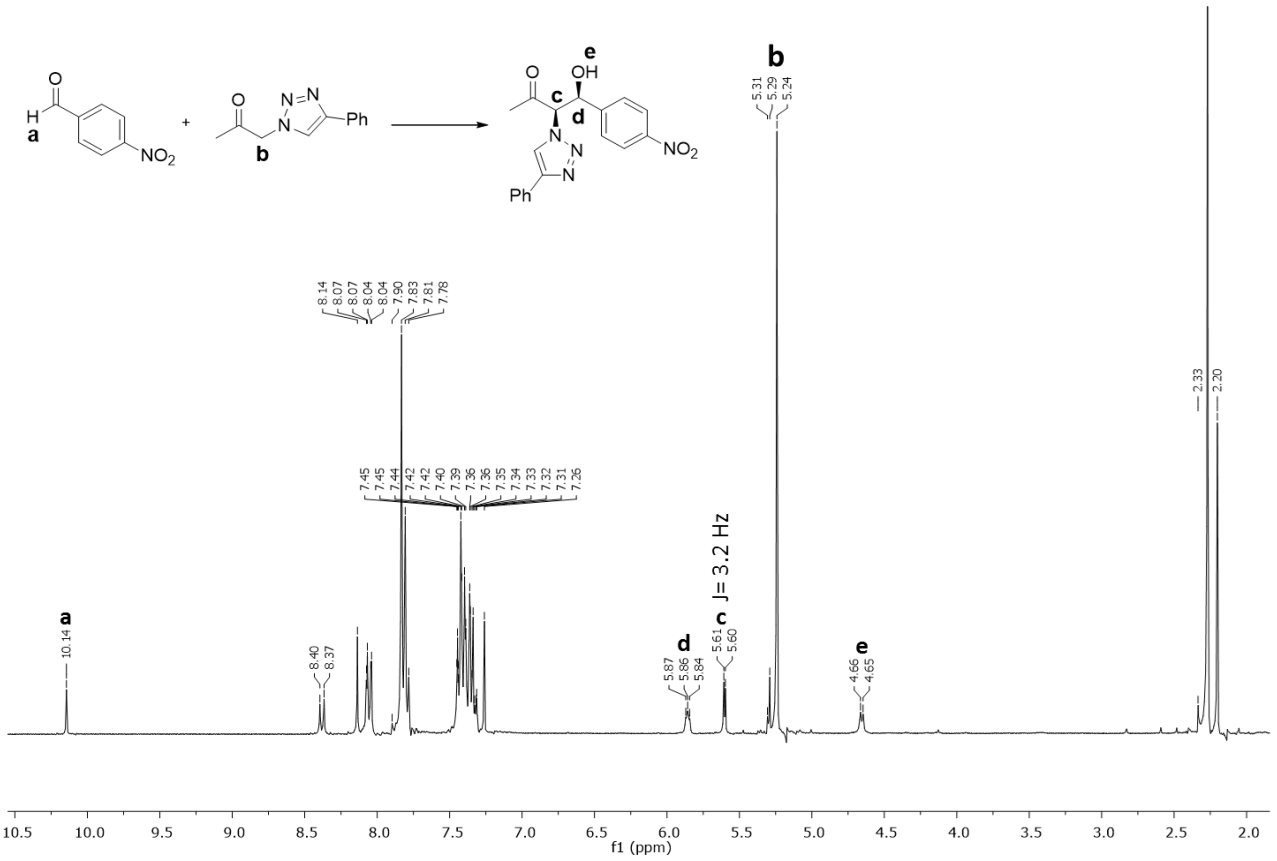

Figure 71. Typical ^{1}H-NMR spectrum of reaction between **TzCet** and *p*-nitrobenzaldehyde.

4.2.3.3. The click-aldol tandem catalytic system

After a detailed investigation of the intermediate 'click' and aldol addition reactions, the catalytic ability of the gelators was evaluated in the three-component system (**Figure 72**). The reactions were all carried in distilled water at room temperature and with stirring, for periods of 1 to 5 days. Also here, excess of **N$_3$Cet** (10 eq) was used in order to avoid the occurrence of possible retro-aldol reactions. A similar molar ratio of the commercially available phenylacetylene was also used to assure the formation of the intermediates in excess.

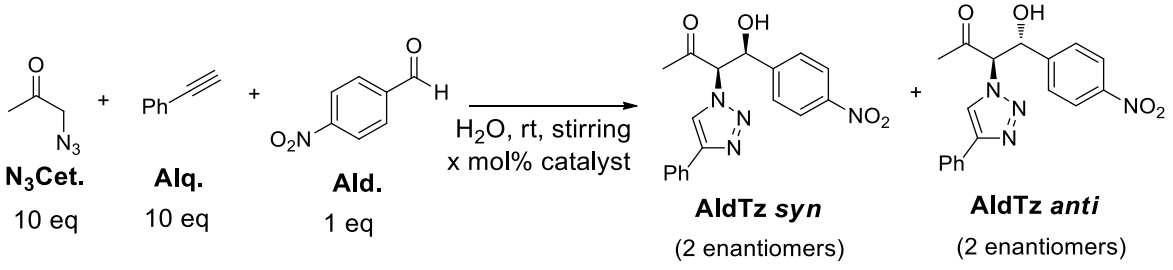

Figure 72. Structures of reactants and products involved in the tandem system.

The catalysts tested in the three-component reaction system included the **ProValDoc**, the **Cu(I)-PhTzVal$_3$** or the two-component gel **Cu(I)-PhTzVal$_3$/ProValDoc**. For the blank assays, the same reaction was carried in the presence of CuBr or only in water. The conversions achieved were determined by ^{1}H-NMR (**Table 14**).

Table 14. Conversions achieved by the three-component system with (or without) catalyst.

		Conversions after 4 days (%)[a]/Products			
Entry	**Catalyst (10mol%)**	**AldN$_3$**	**ratio *syn:anti***	**AldTz *syn***	**TzCet**
1	**Cu(I)-PhTzVal$_3$**	< 5	n.d.[b]	30	95
2	**PhTzVal$_3$**	0	-	0	0
3	**Cu(I)-PhTzVal$_3$/ProValDoc**	17	n.d.[b]	28	97
4	**ProValDoc**	66	66:34	0	0
5	CuBr	0	-	0	96
6	-	0	-	0	0

[a] The reactant *p*-nitrobenzaldehyde (0.86 mg, 5.7x10^{-3} mmol) was dissolved in **N$_3$Cet** (5.6 mg; 5.7x10^{-2} mmol) and the resultant mixture transferred to a 8 mL screw-capped vial containing 2 mL of water and, if desired, 10 mol% of catalyst. Phenylacetylene (5.82 mg; 5.7x10^{-2} mmol) was subsequently added and the mixture allowed to react at room temperature and under stirring for 4 days. At the end of the experiment, the products were directly extracted with $CDCl_3$ (3x 330 µL). The organic phase was dried over anhydrous $MgSO_4$ and the conversion determined by ^{1}H-NMR. The conversion for **TzCet** was calculated based on the phenylacetylene, while for **AldN$_3$** and **AldTz** it was determined considering the *p*-nitrobenzaldehyde as limiting reagent. [b] Not detected in the ^{1}H-NMR spectra

The obtained results highlight the good catalytic performance of the metallogel **Cu(I)-PhTzVal$_3$** for both 'click' and aldol addition reactions, although in the former only 30% conversion has been achieved (**Table 14, entry 1**). This conversion was relatively similar to the one obtained when using the two-component metallogel **Cu(I)-PhTzVal$_3$/ProValDoc** as catalyst (**Table 14, entry 3**), but considerably higher than the one obtained in the presence of pure **PhTzVal$_3$** or **ProValDoc** aggregates, where no final aldol product has been detected (**Table 14, entries 2 and 4**). Furthermore, the 'click' reaction has been successfully catalysed by the two-component metallogel **Cu(I)-PhTzVal$_3$/ProValDoc**, giving 97% of the intermediate product **TzCet** (**Table 14, entry 3**), which is relatively similar to the conversion obtained in the presence of pure **Cu(I)-PhTzVal$_3$** (**Table 14, entry 1**). This might suggest that the presence of the **ProValDoc** in the two-component metallogel **Cu(I)-PhTzVal$_3$/ProValDoc** does not have a negative influence on the catalytic activity of the metallogel **Cu(I)-PhTzVal$_3$** towards the 'click' or aldol addition reactions, although it is

clear the absence of a synergistic effect arising from the mixture of both gels. This suggests that the multicomponent reaction is being catalysed by a single catalyst, meaning that an auto-tandem catalytic process might be occurring instead of an orthogonal tandem catalysis.

Supporting this, it can be observed that the catalytic performance of the **ProValDoc** hydrogel towards the aldol addition reaction is significantly affected in the two-component gel **Cu(I)-PhTzVal$_3$/ProValDoc**, guiding to 17% conversion to the **AldN$_3$**, which is significantly lower comparing with the 66% conversion achieved by the pure **ProValDoc** gel (**Table 14, entries 3-4**). This might be due to the disruption of the macromolecular gel network belonging to the hydrogel **ProValDoc** in the presence of copper, as suggested by the data obtained from XRD (**Figure 61**) and TEM (**Figure 62**) analysis. Despite of this, some microaggregates of **ProValDoc** with catalytic activity might still exist in solution, giving **AldN$_3$** in 17%.

The multicomponent reaction was also carried in the presence of CuBr, achieving 96% conversion for the 'click' reaction, but no aldol product has been obtained. Another blank experiment consisted on performing the multicomponent reaction in the presence of distilled water and without catalysts, but as expected, neither **TzCet** nor **AldTz** have been obtained.

As the use of the two-component metallogel **Cu(I)-PhTzVal$_3$/ProValDoc** did not result in increased catalytic activity, the attention was focused on understanding the interesting catalytic behaviour of the metalloaggregates **Cu(I)-PhTzVal$_3$** towards the three-component system. For that purpose the catalytic performance was followed for periods ranging between 8h to 4 days, and the conversions achieved were determined by ^{1}H-NMR. Looking at the results obtained in **Table 15**, it can be observed that 61% of conversion was achieved just after 2 days of reaction using 10 mol% of **Cu(I)-PhTzVal$_3$** as catalyst (**Table 15, entry 3**). It is also curious to observe that the conversions achieved for the **AldTz** and the **TzCet** were relatively similar between each other during the first two days (**Table 15, entries 1-2**), suggesting that the formed **TzCet** was immediately reacting with the *p*-nitrobenzaldehyde available in the reaction medium. However, it appears that there is an accentuated increase in the kinetics of the 'click' reaction towards its completion after 2 days of reaction, coinciding with the highest conversion achieved for the **AldTz**. The lower conversions achieved after 3 and 4 days of reaction, 31% and 35%, respectively, might be caused by a possible reversion of the aldol addition due to the scarce solubility of the intermediate **TzCet**, or due to some instability of the final reaction product (**Table 15, entries 4-5**).

Table 15. Conversions achieved by the three-component system in the presence of **Cu(I)-PhTzVal$_3$**.

			Conversions(%)/Products			
Entry	**Time of reaction**	**Proportion of reactants (Ald:N$_3$Cet:Alq)**	**AldN$_3$**	**ratio *syn:anti***	**AldTz *syn***	**TzCet**
1	**8h**	1:10:10	< 5	-	20	13
2	**1 d**	1:10:10	< 5	-	26	19
3	**2 d**	1:10:10	< 5	-	61	95
4	**3 d**	1:10:10	< 5	-	31	97
5	**4 d**	1:10:10	< 5	-	35	98
6	**4 d**	1:20:10	55	n.d.[b]	28	98

[a] The reactant *p*-nitrobenzaldehyde (0.86 mg, 5.7x10^{-3} mmol) was dissolved in the desired amount of **N$_3$Cet** and the resultant mixture transferred to a 8 mL screw-capped vial containing 2 mL of water and 10 mol% of **Cu(I)-PhTzVal$_3$** catalyst, composed by the gelator **PhTzVal$_3$** (8 mg; 11.4x10^{-3} mmol) and the copper salt CuBr (0.82 mg; 5.7x10^{-3} mmol). Phenylacetylene (5.82 mg; 5.7x10^{-2} mmol) was subsequently added and the mixture allowed to react at room temperature and under stirring for 4 days. At the end of the experiment, the products were directly extracted with $CDCl_3$ (3x 330 µL). The organic phase was dried over anhydrous $MgSO_4$ and the conversion determined by ^{1}H-NMR. The conversion for **TzCet** was calculated based on the phenylacetylene, while for **AldN$_3$** and **AldTz** it was determined considering the *p*-nitrobenzaldehyde as limiting reagent. [b] not detected in the ^{1}H-NMR spectra.

The **AldTz** can also be obtained if 20 eq excess of **N$_3$Cet** is used in the three component reaction system, in the presence of 10 mol% **Cu(I)-PhTzVal$_3$** (**Table 15, entry 6**). Although the final product was formed in a relatively low amount (**28%**), the conversion achieved for the intermediate product **AldN$_3$** (55%) was considerably higher in comparison with the one obtained for the reactions carried in the presence of 10 equivalents of **N$_3$Cet**, where the conversion didn't reach the 5% (**Table 15, entries 1-5**). Thus, it can be suggested that the presence of a high excess of **N$_3$Cet** displaces the equilibrium of the aldol addition between the **N$_3$Cet** and the *p*-nitrobenzaldehyde to the products, resulting in the formation of a higher amount of **AldN$_3$**. Further 'click' coupling of the intermediate products **AldN$_3$** with the commercially available phenylacetylene guides to the formation of the final product **AldTz** in good yield.

This behaviour suggest that the three-component reaction system is able to follow two different pathways depending on the competition between reagents and on the initial reaction conditions (**Figure 73**). When initial equimolar amounts of **N$_3$Cet** and phenylacetylene are present, the three-component system follows **pathway A**, where the 'click' reaction between the **N$_3$Cet** and the phenylacetylene is kinetically favoured guiding to the formation of the intermediate **TzCet**. This

intermediate product can further undergo in an aldol addition to achieve the formation of the final products.

However, in the presence of 20 eq. **N_3Cet**, the equilibrium of the aldol addition between the **N_3Cet** and the *p*-nitrobenzaldehyde is displaced and the reaction can proceed through **pathway B**, favouring the formation of the **AldN_3.** This intermediate product subsequently undergo through a 'click' reaction with the phenylacetylene to achieve the final products.

The similar conversion achieved for the final product (35%) both pathways after 4 days reaction suggest that the **pathway A** do not favour the formation of a higher amount of final product **AldTz *syn*** in comparison with **pathway B**. Nevertheless, independently on the reaction pathway followed during the multicomponent reaction system, it is clear that the gelator **Cu(I)-PhTzVal$_3$** acts as a good tandem catalyst for both the aldol and 'click' reactions occurring in this three-component system. The 55% conversion achieved in this aldol addition reaction between **N_3Cet** and *p*-nitrobenzaldehyde together with the 98% conversion obtained for the 'click' reaction between **N_3Cet** and the phenylacetylene, using 20 eq **N_3Cet**, supports the good catalytic activity of the metallogel **Cu(I)-PhTzVal$_3$** for both reactions (**Table 15**, **entry 6**).

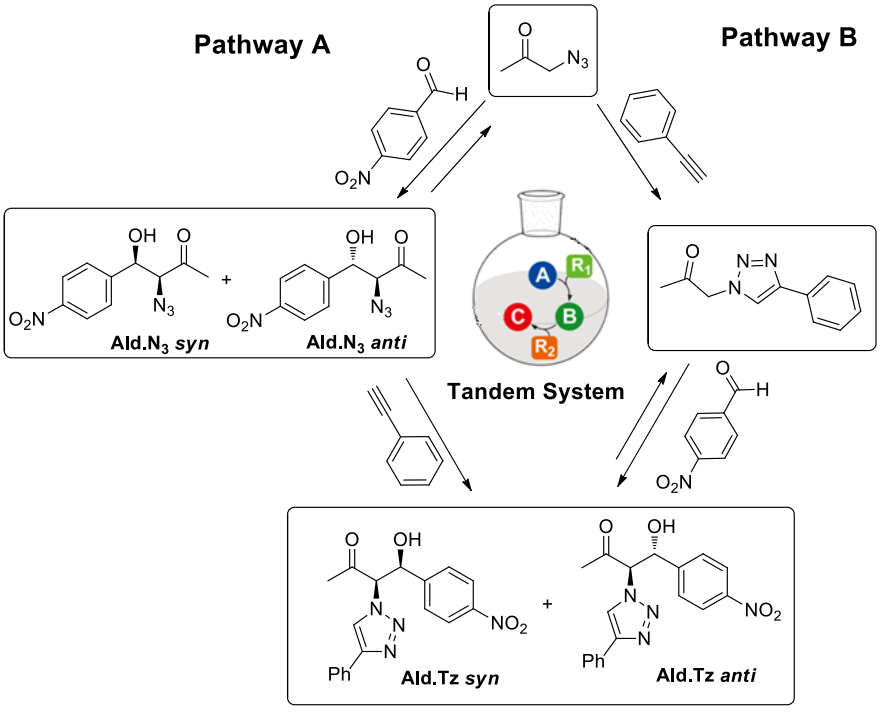

Figure 73. Possible 'click'-aldol reaction pathways in the three-component system.

To confirm the formation of the final product **AldTz**, the three-component reaction was performed in higher scale in the presence of 10 mol% **Cu(I)-PhTzVal$_3$** (**Table 15**, **entry 3**), and the resultant crude mixture purified through column chromatography using silica flash. However, the ^{1}H-NMR spectrum of the resultant fractions exhibited a mixture of peaks characteristic of product degradation, which was probably caused by the acidity of silica. This instability of the product **AldTz** ***syn*** may support the low yields obtained after 4 days reaction. Thus, the same reaction was mounted again in similar conditions and the crude mixture purified by column chromatography using alumina type II as stationary phase. Also in this case, the resultant ^{1}H-NMR spectrum was not completely pure, but some peaks of pure product could be detected together with characteristic degradation peaks. The presence of the **AldTz** was further confirmed by high-resolution mass-spectrometry, giving a hydrogenated adduct at m/z= 353.1249 (calculated 353.1250).

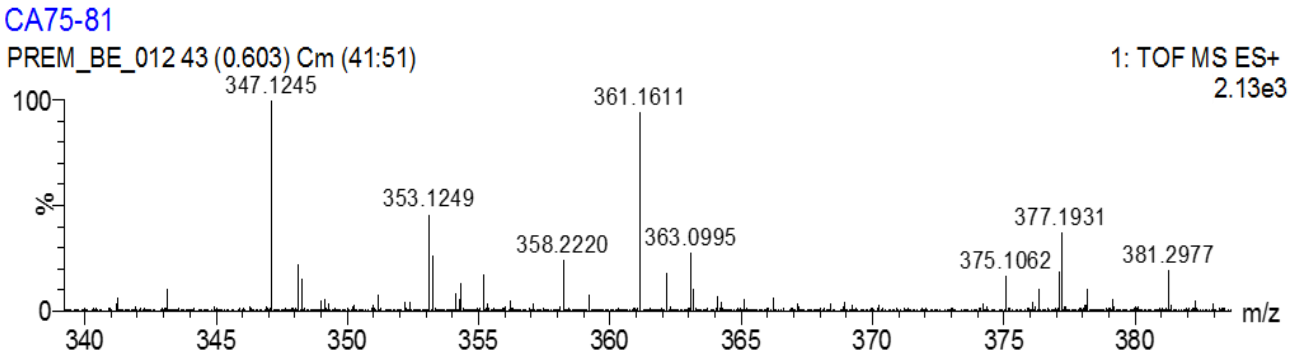

Figure 74. High-resolution mass spectrometry of one of the fractions from column chromatography of the three component reaction carried for 2 days in the presence of 10 mol% **Cu(I)-PhTzVal$_3$**. Alumina type II was used as stationary phase.

The selectivity of the catalytic system was evaluated by chiral HPLC, suggesting that there is no enantiomeric excess, since both **AldTz** ***syn*** enantiomers (t= 12.2 min and 17.7 min) are formed in an equimolar ratio in the presence of the catalytic metallogel **Cu(I)-PhTzVal$_3$**. The remaining peaks were attributed to reactants and intermediate reaction products.

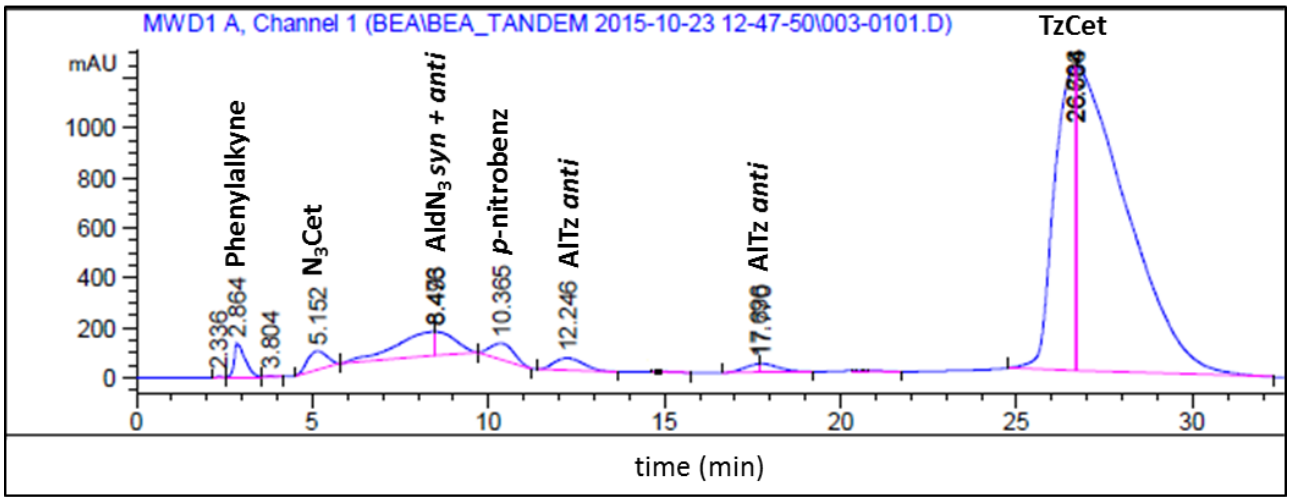

Figure 75. HPLC chromatogram of the three-component reaction carried for 2 days in the presence of 10 mol% **Cu(I)-PhTzVal$_3$**.

The mechanistic pathway by which the metallogel **Cu(I)-PhTzVal$_3$** is able to catalyse this tandem three-component reaction may be similar to the one followed by type II (fuculose-1-phosphate) aldolase, where the substrate is activated by the presence of the Zn^{2+} coordinated to a histidine fragment.[35] The type II aldolases use dihydroxyacetone phosphate (DHAP) as the substrate to produce 2-keto-3,4-dihydroxy adducts.

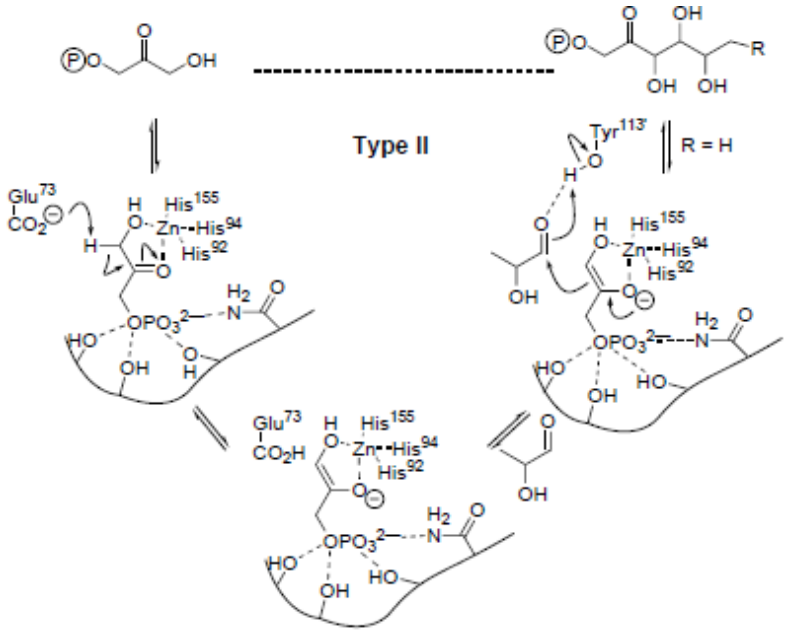

Figure 76. Type II zinc enolate aldolase mechanism carried by fuculose-1-phosphate aldolase.[35]

It has been reported that in this reaction, the Zn^{2+} polarizes the carbonyl group of the substrate by coordination, facilitating the removal of the α-hydrogen by the glutamate residue. Additionally, a tyrosine residue from the adjoining subunit also assists in the activation of the incoming aldehyde

by donating a proton to stabilize the developing charge. This hydrogen bond is responsible for the asymmetric induction at C-4, while the shielding of the *Si* face of the DHAP enediolate by protein assures the correct stereochemistry of the resultant C-3 product.[36]

In our specific case, the mild coordination ability of the triazole ligand to copper(I) may allow the coordination of the carbonyl group from the substrate of the aldol addition reaction, leading to the formation of a tetrahedral complex. Depending on the predominant reaction pathway, an azido or a triazole group of the substrate may also coordinate to the metal center (**Figure 77**).

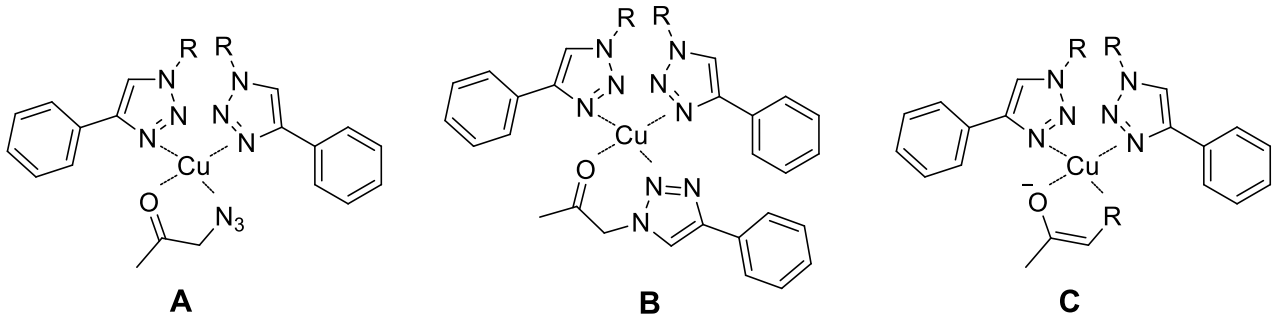

Figure 77. Proposed complexes formed between Cu(I) coordinated to the triazole fragments of the metallogel and the substrate.

Similarly to type II aldolases, this coordination of the substrate to the metal centre could polarize the carbonyl group, increasing the acidity of the α-methylene hydrogen. In addition, a possible increase in the basicity of the assembly-water interface arising from the gelation of **Cu(I)-PhTzVal$_3$** may also collaborate in the removal of the acidic α-hydrogen proton from the substrate and consequent attack on the carbonyl group from the *p*-nitrobenzaldehyde (**Figure 78**). Once **AldTz** is formed, the mild coordination ability of the triazole moiety would allow the detachment of the final product from the molecular gel, making it available to participate in a new catalytic cycle. It is important to remind that by using only CuBr as catalyst (10 mol%), no aldol product has been observed in the three component reaction (**Table 14**, **entry 5**). This result reinforces the important role of the metallogel on the catalysis of this aldol addition reaction, suggesting that an aggregation effect may also be determinant for this catalytic activity. Furthermore, it cannot be discarded an increase in the basicity of the assembly-water interface due to the coordination of water molecules to the metal centre, as reported for copper complexes containing hetero-substituted cyclens.[37]

The increase in the basicity of the assembly-water interface upon supramolecular aggregation has already been reported for bolaamphiphilic gels functionalized with *L*-proline fragment.[38] Such supramolecular induced enhancement of basicity was postulated to be caused by the close proximity of the pyrrolidinic residues on the surface of the gel fibres, which is thought to

favour the cooperative assistance of several basic groups on the deprotonation of the substrate and consequent formation of the intermediate enolate.[14]

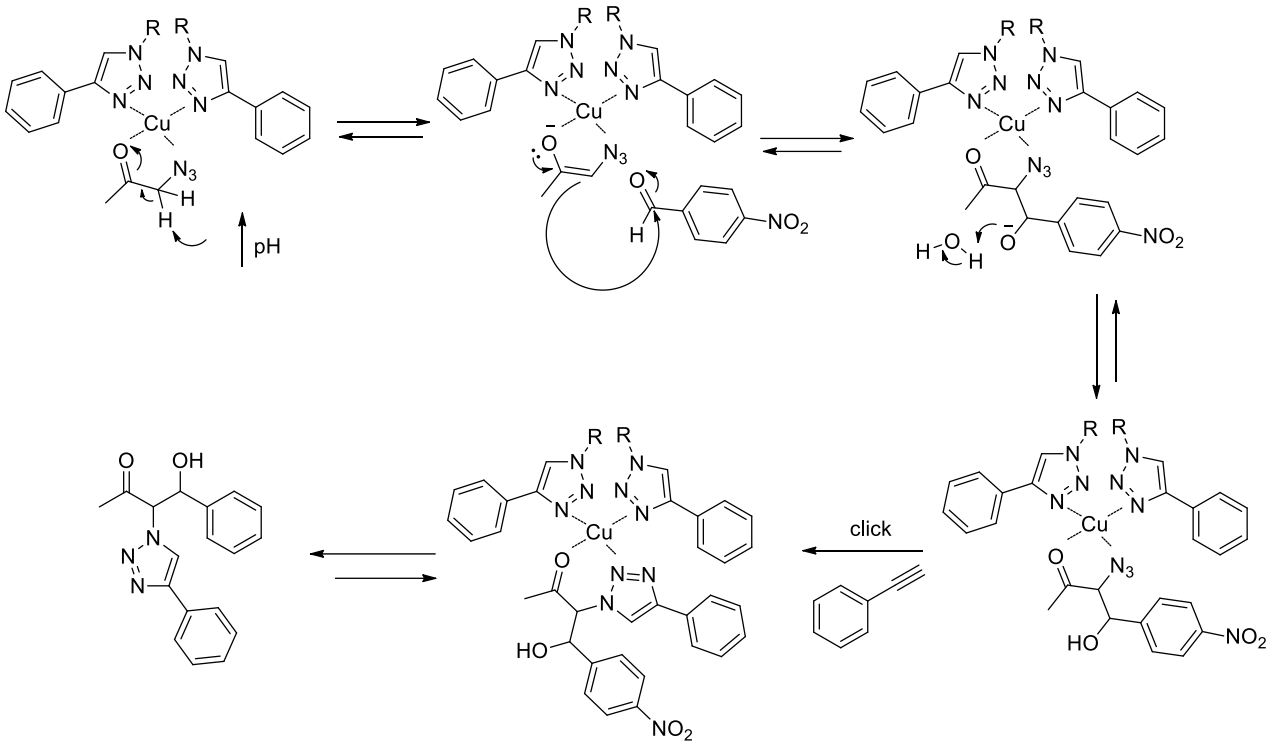

Figure 78. Proposed catalytic mechanism for the aldol reaction in the presence of the gel catalyst **Cu(I)-PhTzVal$_3$**. The represented catalytic mechanism is illustrative of reactions following pathway A.

In the case of this three-component system, a small increase in the basicity of the assembly-water interface provided by the proximity of triazole sites in the hydrogel fibres could easily promote catalysis of the multicomponent reaction, considering the acidic nature of the α-hydrogen of **N$_3$Cet**. The acidic environment of this proton arises not only from its position between a carbonyl and an azide group, but also from the polarization of the carbonyl group upon coordination of the substrate to the copper(I) centre. This hypothesis is in accordance with the increased kinetics of the reaction when performed in different buffers at pH= 7.4 (**Table 11**).

4.3. Conclusion

The design and synthesis of a gelator that could be used in the catalysis of a multicomponent 'click'-aldol reaction system was successfully achieved. The three-component reaction was performed in the presence of metallogel **Cu(I)-PhTzVal$_3$** (10 mol%), achieving around 65% conversion in only 2 days. The fact that both intermediates **AldN$_3$** and **TzCet** could be obtained in

high yields when 20 eq **N_3Cet** is present at the outset of the multicomponent reaction highlights the good catalytic activity of the metallogel **Cu(I)-PhTzVal$_3$** for both reactions.

It has been proposed that the catalysis of the aldol addition in the presence of the metallogel **Cu(I)-PhTzVal$_3$** follows a type II aldolase mechanistic pathway, where the coordination of the substrate to the metal centre results in the polarization of the carbonyl group and consequent increase in the acidity of the α-hydrogen, whose the removal might be assisted by an increase in the basicity of the medium provided by the supramolecular gelation of the catalyst.

This unexpected biomimetic catalytic activity shown by the metallogel **Cu(I)-PhTzVal$_3$** may contribute to the application of triazole functionalized compounds on the catalysis of aldol-type reactions, as well as on the tandem catalysis of similar 'click'-aldol multicomponent systems. Furthermore, the amino acid derived nature of this tandem metallo-hydrogel catalyst confers it with additional biocompatibility and biodegradability, allowing its use in similar tandem reactions occurring in a biological environment.

4.4. References

[1] Stankiewicz J, Eckardt LH. Chembiogenesis 2005 and Systems Chemistry Workshop. Angewandte Chemistry International Edition 2006; 45: 342-344.

[2] Ludlow RF, Otto S. Systems Chemistry. Chemical Society Review 2008; 37: 101-108.

[3] Ricca E, Brucher B, Schrittwieser JH. Multi-enzymatic cascade reactions: Overview and Perspectives. Advanced Synthesis & catalysis 2011; 353: 2239-2262.

[4] Climent MJ, Corma A, Iborra S, Sabater MJ. Heterogeneous catalysts for tandem reactions. ACS Catalysis 2014; 4; 870-891.

[5] Robert C, Thomas CM. Tandem catalysis: a new approach to polymers. Chemical Society Reviews 2013; 42: 9392-9402.

[6] Lohr TL, Marks TJ. Orthogonal tandem catalysis. Nature Chemistry 2015; 7: 477-482.

[7] Fogg DE, Santos EN. Tandem catalysis: a taxonomy and illustrative review. Coordination Chemistry Reviews 2004; 248: 2365-2379.

[8] Wasilke JC, Stephen SJ, Baker RT, Bazan GC. Concurrent tandem catalysis. Chemical Reviews 2005; 105: 1001-1020.

[9] Ramarchary DB, Barbas CF. Towards organo-click chemistry: development of organocatalytic multicomponent reactions through combinations of aldol, Wittig, Knoevenagel, Michael, Diels-Aler and Huisgen cycloaddition reactions. Chemistry - A European Journal 2004; 10: 5323-5331.

[10] Nelson SG. Catalyzed enantioselective aldol additions of latent enolate equivalents. Tetrahedron: Asymmetry 1998; 9: 357-389.

[11] Tang Z, Jiang F, Cui X, Gong LZ, Mi AQ, Jiang YZ, Wu YD. Enantioselective direct aldol reactions catalyzed by L-prolinamide derivatives. PNAS 2004; 101: 5755-5760.

[12] Palomo C, Oiarbide M, García JM. Current progress in the asymmetric aldol addition reaction. Chemical Society Reviews 2004; 33: 65-75.

[13] List B, Lerner RA, Barbas CF. Proline-catalyzed direct asymmetric aldol reactions. Journal of American Chemical Society 2000; 122: 2395-2396.

[14] Rodríguez-Llansola F, Escuder B, Miravet JF. Switchable performance of an L-proline-derived basic catalyst controlled by supramolecular gelation. Journal of American Chemical Society 2009; 131: 11478-11484.

[15] Rodríguez-Llansola F, Miravet JF, Escuder B. A supramolecular hydrogel as a reusable heterogeneous catalyst for the direct aldol reaction. Chemical Communications 2009; 7303-7305.

[16] Berdugo C, Miravet JF, Escuder B. Substrate selective catalytic molecular hydrogels: the role of the hydrophobic effect. Chemical Communications 2013; 49: 10608-10610.

[17] Wang X, Meng Q, Perl NR, Xu Y, Leighton JL. Tandem aldol-allylation and aldol-aldol reactions with ketone-derived enolsilanes: Highly diastereoselective single-step synthesis of complex teriary carbinols. Journal of American Chemical Society 2005; 127: 12806-12807.

[18] Arnold LA, Naasz R, Minnaard AJ, Feringa BL. Catalytic enantioselective synthesis of (-)-Prostaglandin E_1 methyl ester based on a tandem 1,4-addition-aldol reaction. Journal of Organic Chemistry 2002; 67: 7244-7254.

[19] Feringa BL, Pineschi M, Arnold LA, Imbos R, de Vries AH. Highly enantioselective catalytic conjugate addition and tandem-conjugate addition-aldol reactions of organizing reagents. Angewandte Chemistry International Edition English 1997; 36: 2620-2623.

[20] Bui T, Barbas CF. A proline-catalyzed asymmetric Robinson annulation reaction. Tetrahedron Letters 2000; 41: 6951-6954.

[21] Vhowdari NS, Ramachary DB, Barbas CF. Organocatalytic asymmetric assembly reactions: One-pot synthesis of functionalized β-amino alcohols from aldehydes, ketones and azidocarboxylates. Organic Letters 2003; 5: 1685-1688.

[22] Odlo K, Høydahl EA, Hansen TV. One-pot synthesis of 1,4-disubstituted 1,2,3-triazoles from terminal acetylenes and in situ generated azides. Tetrahedron Letters 2007; 48: 2097-2099.

[23] Appukkuttan P, Dehaen W, Fokin VV, van der Eycken E. A microwave-assisted click chemistry synthesis of 1,4-disubstituted 1,2,3-triazoles via a copper(I)-catalyzed three-component reaction. Organic Letters 2004; 6: 4223-4225.

[24] Campbell-Verduyn LS, Szymanski W, Postema CP, Dierckx RA, Elsinga PH, Janssen DB, Feringa BL. One pot 'click' reactions: tandem enantioselective biocatalytic epoxide ring opening and [3+2] azide alkyne cycloaddition. Chemical Communications 2010; 46: 898-900.

[25] Binder WH, Sachsenhofer R. 'Click' Chemistry in polymer and material science: an update. Macromolecular rapid communications 2008; 29: 952-981.

[26] Mlynarski J, Paadowska J. Catalytic asymmetric aldol reactions in aqueous media. Chemical Society Reviews 2008; 37: 1502-1511.

[27] Díaz-Oltra S, Berdugo C, Miravet J, Escuder B. Study of the effect of polymorphism on the self-assembly and catalytic performance of an L-proline based molecular hydrogelator. New Journal oof Chemistry 2015, 39: 3785-3791

[28] Colquhoun C, Draper ER, Eden EGB, Cattoz BN, Morris KL, Chen L, McDonald TO, Terry AE, Griffiths PC, Serpell LC, Adams DJ. The effect of self-sorting and co-assembly on the mechanical properties of low molecular weight hydrogels. Nanoscale 2014; 6: 13719-13725.

[29] Kumar DK, Steed JW. Supramolecular gel phase crystallization: orthogonal self-assembly under non-equilibrium conditions. Chemical Society Reviews 2014; 43: 2080-2088.

[30] Martinez-Castañeda A, Kedziora K, Lavandera I, Rodríguez-Solla H, Concellón C, del Amo V. Highly enantioselective synthesis of α-azido-β-hydroxy methyl ketones catalysed by a cooperative proline-guanidinium salt system. Chemical Communications 2014; 50: 2598-2600.

[31] Sakthivel K, Notz W, Bui T, Barbas CF. Amino acid catalyzed direct asymmetric aldol reactions : A bioorganic approach to catalytic asymmetric carbon-carbon bond-forming reactions. Journal of the American Chemical Society 2001; 123: 5260-5267.

[32] List B, Lerner RA, Barbas CF. Proline-catalyzed direct asymmetric aldol reactions. Journal of American Chemical Society 2000; 122: 2395-2396.

[33] Meldal M, Tornøe CW. Cu-catalyzed azide-alkyne cycloaddition. Chemical Reviews 2008; 108: 2952-3015

[34] Trost BM, Brindle CS. The direct catalytic asymmetric aldol reaction. Chemical Society Reviews 2010; 39: 1600-1632.

[35] Machajewski TD, Wong CH. The catalytic asymmetric aldol reaction. Angewandte Chemistry International Edition 2000; 39: 1352-1374.

[36] Fessner WD, Schneider A, Held H, Sinerius G, Walter C, Hixon M, Schloss JV. The mechanism of class II, metal-dependent aldolases. Angewandte Chemistry International Edition English 1996; 35: 2219-2221.

[39] Zhang X, Liu X, Philips DL, Zhao C. Mechanistic insights into the factors that influence DNA nuclease activity of mononuclear facial copper complexes containing hetero-substituted cyclens. ACS Catalysis 2016; 6: 248-257.

[38] Rodríguez-Llansola F, Escuder B, Miravet JF. Remarkable increase in basicity associated with supramolecular gelation. Organic & Biomolecular Chemistry 2009; 7: 3091-3094.

4.5. Supporting Information

4.5.1. General Gelation Procedures

4.5.1.1. Hydrogel PhTzVal$_3$

The gelator **PhTzVal$_3$** (8 mg; 11.4x10^{-3} mmol) was heated in a 8 mL screw-capped vial at a temperature of 340 ºC for 5 minutes, in the presence of 2 mL of water. The resultant hot solution was then sonicated for 20 seconds, forming a swollen precipitate, which was subsequently allowed to age for 20 minutes at room temperature. The formation of the metallogels was achieved by heating together the gelator and the copper salt CuBr in a 2:1 molar ratio.

4.5.1.2. Hydrogel ProValDoc

The gelator **ProValDoc** (0.33 mg; 8.5x10^{-4} mmol) was heated in a 4 mL screw-capped vial containing 450 µL of water until complete dissolution. The resultant hot solution was subsequently sonicated for 1h, forming aggregates which were then allowed to age for 20 minutes at room temperature.

4.5.1.3. Two-component gel PhTzVal$_3$/ProValDoc

For the formation of the two-component gels, the **ProValDoc** gel was added to the **PhTzVal$_3$** gel/metallogel and the mixture allowed to age for 20 minutes.

4.5.2. Catalytic experiments

4.5.2.1. General procedure for intermediate two-component aldol/'click' reactions

The reactant *p*-nitrobenzaldehyde (0.86 mg, 5.7x10^{-3} mmol), or phenylacetylene (5.82 mg; 5.7x10^{-2} mmol), for aldol addition and 'click' intermediate reactions, respectively, was dissolved in the **N$_3$Cet** (5.6 mg; 5.7x10^{-2} mmol) and transferred to a 8 mL screw-capped vial containing the solvent medium and, when needed, the desired catalyst. In the case where the reactant **TzCet** was used for the intermediate aldol addition, it was dissolved in 50 µL DMSO together with the *p*-nitrobenzaldehyde, prior to their addition to the reaction medium. The resultant mixture was stirred at room temperature for the desired period of time. At the end of the experiment, the products were

directly extracted with $CDCl_3$ (3x 330 µL). The organic phase was dried over anhydrous $MgSO_4$ and the conversion determined by ^{1}H-NMR.

4.5.2.2. General Procedure for the catalysis of the three-component system

The reactant *p*-nitrobenzaldehyde (0.86 mg, $5.7x10^{-3}$ mmol) was dissolved in **N_3Cet** (5.6 mg; $5.7x10^{-2}$ mmol), and the resultant mixture added in the 8 mL screw-capped vial containing 2 mL of distilled H_2O and, when needed, 10 mol% of catalyst. Phenylacetylene (5.82 mg; $5.7x10^{-2}$ mmol) was subsequently added and the mixture allowed to react at room temperature and under stirring for an adequate period of time. At the end of the experiment, the products were directly extracted with $CDCl_3$ (3x 330 µL). The organic phase was dried over anhydrous $MgSO_4$ and the conversion determined by ^{1}H-NMR.

4.5.3. General Characterization Methods

4.5.3.1. High-Performance Liquid Chromatography

Enantiomeric excess was determined by HPLC (Agilent Technologies) using a Chiralpack IA column, λ= 254 nm, Ethanol/Hexane (v/v: 15/85), flow rate = 1.5 mL/min.

4.5.3.2. Quantification of coordinated copper

After the formation of the catalytic metallogel, 100 µL of surrounding solution were collected with a 1 mL syringe and filtered through a 0.22 µm filter. The filter was washed with a solution of 5% HNO_3 (2x1 mL) in Milli-Q water to remove remaining uncoordinated copper. A 25 mL solution of the sample in 5% HNO_3 was prepared and the concentration of copper(I) determined by inductively coupled plasma-mass spectrometry (ICP-MS) using a Varian 710-ES.

4.5.3.3. Wide-angle X-ray Diffraction

The obtained gels/metallogels were dried on air or by lyophilization (Telstar LyoQuest), depending on the nature of the gel (organogel or hydrogel), and the resultant powder resuspended in hexane. The suspension was applied into the glass sample holder and the solvent allowed to evaporate. The

resultant powdered sample was analysed by X-ray diffraction (XRD) at room temperature using a Bruker D4 Endeavor X-ray powder diffractometer with Cu-K_α radiation. Data were collected for 2θ values between 2 and 40º with a step size of 0.03º and a time step of 10 s.

4.5.3.4. Transmission Electron Microscopy

A small portion of the gel/metallogel was placed on a nickel grid coated with carbon and allowed to dry on air. Images were recorded in a JEOL 2100 microscope without using any stain.

4.5.3.5. Nuclear Magnetic Resonance

^{1}H and ^{13}C NMR spectra measurements were recorded in a Varian Mercury 300 MHz spectrometer at 30 ℃.

4.5.4. Synthesis and Characterization

All reagents, starting materials and solvents (p.a. grade) were purchased from commercial suppliers and used as received without further purification.

4.5.4.1. Synthesis of PhTzVal$_3$

This compound was synthesized as described in **Section 3.6.1.4**.

4.5.4.2. Synthesis of ProValDoc

The synthesis of this compound has been previously described.[15]

4.5.4.3. Synthesis of N_3Cet

The N_3Cet was synthesized by following a procedure previously described.[30] Briefly, sodium azide (2.6 g; 40 mmol) was poured into a solution of chloroacetone (1.85 g; 1.6 mL, 20 mmol) in dry acetone (50 mL) at room temperature and under N_2. The heterogeneous reaction mixture was vigorously stirred at room temperature for 24h, before it was filtered and the filtrate washed with

acetone. The mother liquors were concentrated on the rotavapor and the resulting oil diluted with Et_2O (50 mL) and washed with distilled water (2 x 15 mL). The organic layer was dried over anhydrous MgSO4, and the solvent and volatiles removed in vacuum, affording an orange oily product (1.478 g; 75%). Characterization: ^{1}H NMR (300 MHz, $CDCl_3$): δ (ppm) 3.95 (s, $N_3C\underline{H}_2$, 2H), 2.20 (s, $C\underline{H}_3CO$, 3H).

4.5.4.4. Synthesis of TzCet

Acetoazide (0.2 g; 2.03 mmol; 0.181 mL) and phenylacetylene (0.228 g; 2.23 mmol; 0.245 mL) were dissolved in 1:1 t-BuOH:H_2O (4 mL). To this solution, $CuSO_4.5H_2O$ (0.050 g; 0.203 mmol) and sodium ascorbate (0.161 g; 0.812 mmol) were added, and the mixture stirred for 16h at room temperature. EtOAc (20 mL) was added to the crude product and the organic phase washed with a saturated solution of $NaHCO_3$ (3 x 5 mL) and brine (3 x 5 mL). The organic extracts were dried over anhydrous $MgSO_4$ and the solvents removed on the rotavapor to give a pale yellow solid (0.31 g; 76%). Characterization: ^{1}H NMR (300 MHz, $CDCl_3$): δ (ppm) 7.82 (m, triazole-$\underline{H}$ + Ph-$\underline{H}$, 3H), 7.35 (m, Ph-$\underline{H}$ +, 3H), 5.23 (s, -COC$\underline{H}_2$, 2H), 2.26 (s, C$\underline{H}_3$CO-, 3H). ^{13}C (75 MHz, $CDCl_3$): δ (ppm) 199.03, 148.29, 130.29, 128.83, 125.80, 120.95, 58.53, 27.21. ESI-MS (m/z) = 202.0981 $[M+H]^+$; $C_{11}H_{11}N_3O$. Calculated for $C_{11}H_{11}N_3O$: 202.0980.

Chapter 5

Following the formation of a fluorescent blue/cyano emitting two-component gel by fluorescence confocal microscopy

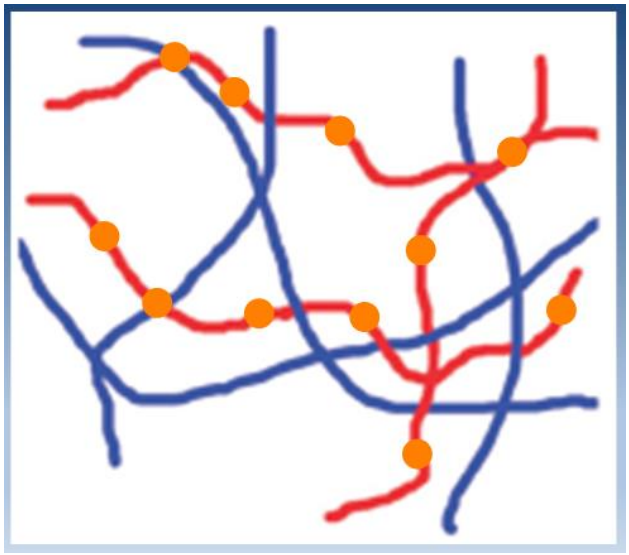

A new multicomponent hybrid organic-inorganic fluorescent gel material was obtained through a 'click' reaction between a two-component gel, composed by a fluorescent gelator capable of coordinating copper(I) and an alkyne gelator, and a non-fluorescent azidocoumarine. The evolution of the reaction system was investigated by fluorescent confocal microspectroscopy.

(work done during a secondment at the University of Bordeaux, France under the supervision of Prof. A. Del Guerzo)

5.1. Introduction

Fluorescent self-assembled organogels are interesting supramolecular soft materials with polymer-like structures, and have received particular attention due to their fascinating properties and promising practical applications in several fields ranging from drug delivery and biomimetic systems to optoelectronics, including enhanced charge transport, light harvesting, fluorescence and sensing.[1,2,3,4]

The mechanism of fluorescence can be described as the process where an atom or molecule is excited by the absorption of a photon, and de-excited by emitting another photon. This mechanism is commonly represented by the Jablonski diagram.[5]

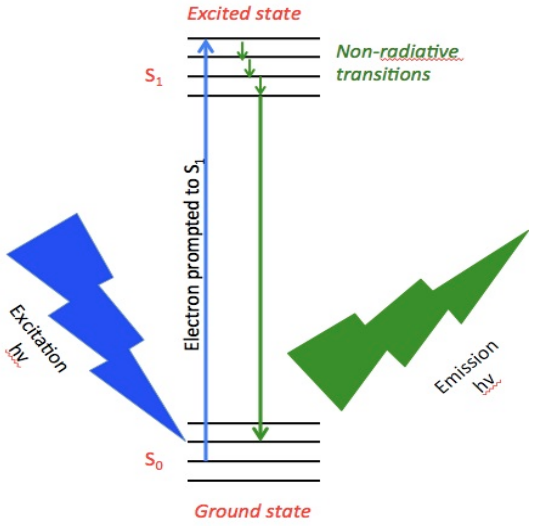

Figure 79. Jablonski diagram of the process of fluorescence.

As observed in the diagram, the excitation of a fluorophore leads to a transition to a higher electronic state ($S_0 \rightarrow S_1$). Its subsequent relaxation from the first excited singlet state to the ground singlet state ($S_1 \rightarrow S_0$) results in the emission of another photon. The fluorophore can also release its energy by a non-radiative decay, in which the excitation energy is dissipated as heat to the solvent. As a consequence of thermal relaxation, the emitted photon has always a lower energy than the absorbed photon, resulting in different wavelengths. This phenomenon is called Stokes shift.[6]

Fluorescent molecules often incorporate π-conjugated molecular systems such as oligo(phenylene vinylene) (OPV), [n] acenes, perylene bisimide, phtalocyanines, phenantrolines, porphirins, azidocumarines, or others. In the case of self-assembled materials, such chromophores usually participate in the gelation process by π-π stacking interactions, although such contributions may consume the excited state energy, debilitating the light emission of self-assembled nanomaterials.[7,8]

The self-assembly of synthetic fluorescent molecules is regarded as a very suitable tool, not

only in the preparation of new photofunctional materials, but also because by tuning the supramolecular organization, the optoelectronic properties of the constituent chromophores can be remarkedly influenced. A clear example are the OPV derivatives synthesized by George and Ajayaghosh, which were able to gelate in nonpolar hydrocarbon based solvents.[9]

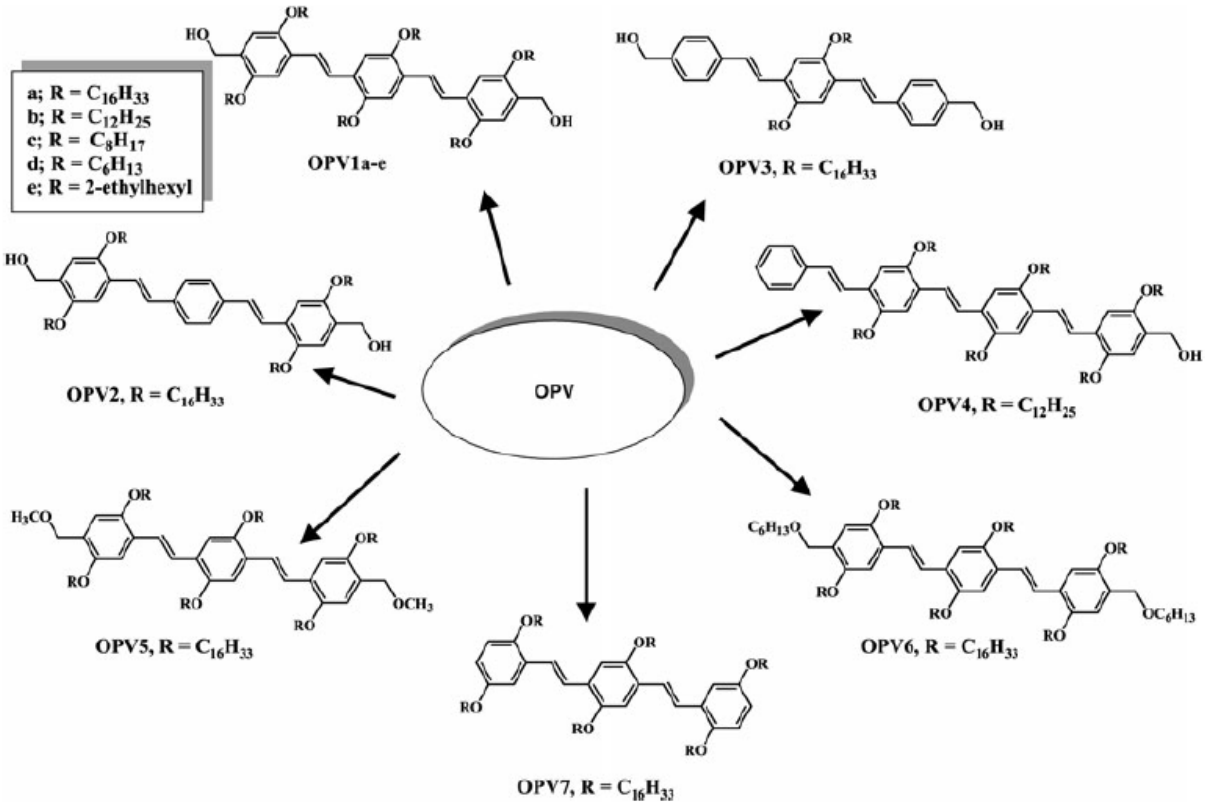

Figure 80. Library of OPV derivatives investigated by George and Ajayagosh.[9]

The compounds in solution exhibited a strong greenish-blue fluorescence, but after gelation a greenish-yellow emission was evident. It was then proven that such shifts in the absorption and emission bands were caused by the self-assembly of the OPV molecules and not by the formation of excimers. This constitutes a clear example where the strong electronic coupling between π-conjugated molecules in the fiber network induces transformations in the physico-optical properties of the chromophores.

In [n]-acene based organogels, *Del Guerzo et al* have observed the occurrence of interesting energy processes such as Förster resonance energy transfer (FRET).[10] In a further study comprising similar compounds, *Giansante et al.* discovered that by blending three [n]-acene derivatives exhibiting blue, green and orange-red emissions, an organogel that was translucent to visible light could be obtained.[11] In this study, the authors have used confocal fluorescence microspectroscopy to reveal the spectral, photophysical and anisotropic features of the individual nano-objects.

This type of technique is based on fluorescence lifetime spectroscopy, where the measurements

are directly related the lifetime of the fluorophore, defined as the average time that a chromophore remains in its excited state after absorption of a photon.[12,13] Briefly, the sample is excited with a very short pulse of light and the fluorescence intensity follows an exponential decay with a characteristic time given by the sample fluorescence lifetime.[14] The time-resolved measurements are based on the photon counting technique, which measures the arrival time of individual photons to the detector. By accumulating a large number of photons arrival times, a histogram of arrival time can be built, representing the probability density of fluorescence emission. [15]

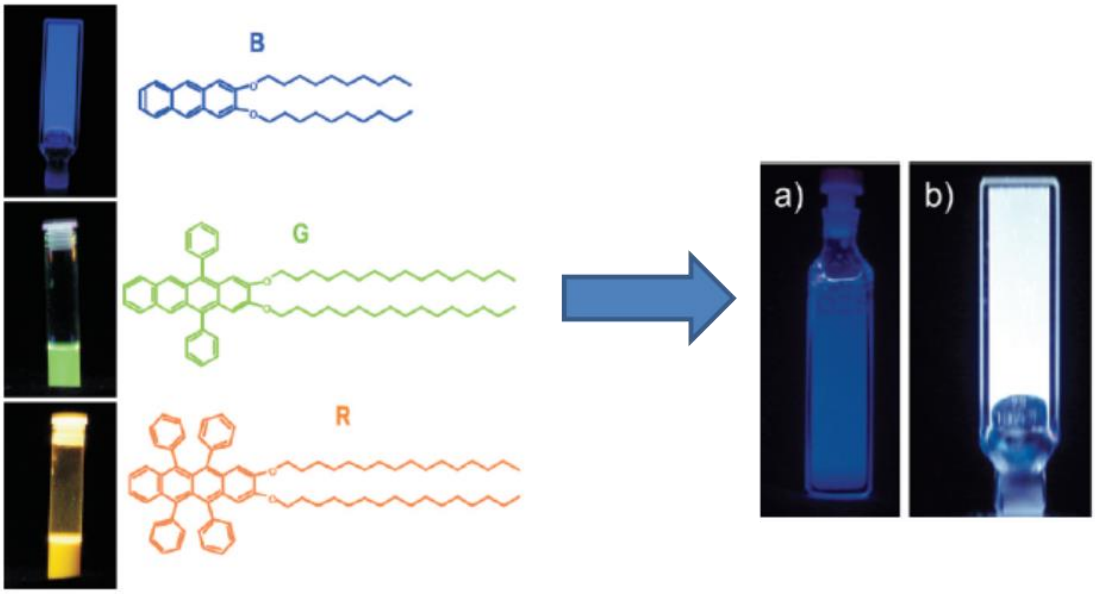

Figure 81. Pictures of a 2 mM B gel in DMSO, 10 µM G solution in THF and 10 µM R solution in THF under UV light (λ_{exc}= 365 nm) and the molecular structures. Pictures of cuvetes (a, b) with 2mM of B and 0.012 eq of G and R under UV light, λ_{exc}= 365 nm: (a) THF solution, (B) DMSO organogel.[11]

By using time-resolved fluorescence lifetime imaging microscopy they have observed that the lifetime of gel **B** in the white nanofibers was considerably shorter than the one measured for the pure gel **B**. Furthermore, they have detected that the cumulated fluorescence of **G** and **R** in the white nanofibers rose with time upon selective excitation of the gel **B**. Thus, this white light emission was the result of the partial excitation energy transfer from the anthracene derivative, which acts as light harvesting matrix, to the tetracene derivatives, which behave as energy acceptors. The same authors have completed the study by performing polarization microscopy on individual nanofibers. In this technique, molecules selectively absorb linearly polarized light when their absorption dipole is oriented parallel to the axis of the excitation beam.[16] The polarization P can vary from -1 to 1 with the angle θ of the nanofiber with respect to the orientation of the laser beam polarization. As a result, a strong variation of P with the angle θ (P> 0) is linked with a preferential orientation of the molecules in the nanofiber. In the situations where P= 0, there is an

overall depolarization and thus, no preferential orientation of the molecules.[17]

Thus, by using fluorescent polarization microscopy, *Giansante et al.* have observed a high degree of molecular order and a preferential average orientation of the gel **B** molecules in the white self-assembled nanofibers, with a similar polarization of the pure gel **B**, meaning that the orientation of the molecules was not affected in the white self-assembled nanofibers. This case is a clear example of the potential of fluorescence lifetime microscopy on the study of self-assembled systems.

Other interesting examples of functional fluorescent gels rely on azidocoumarine-based supramolecular gelators exhibiting strong fluorescent emission upon aggregation.[18] Due to the high photoluminescence efficiency, two-photon absorption and good biocompability of azidocoumarine derivatives, the fluorescent hydrogels could be used as scaffolds to image the performance of nanofibrous structures during cell culture in 2D and 3D environments.[18,19]

Inspired by these works, and being aware of the fluorescence capacity provided by the conjugated system triazole-azidocoumarine,[20] a family of fluorescent gelators functionalized with azidocoumarines were synthesized with the goal of following their self-assembly process by confocal microscopy. In a recent publication, it has been shown that it was possible to control real-time visualization of the self-assembly process by monitoring the different emission properties of the aggregates from a Pt(II) gel bearing a hydrophobic chelate and a hydrophilic triethylene gycol pendant.[21]

In this project, the formation of fluorescent aggregates would be promoted through a copper(I) catalysed Huisgen 1,3-dipolar cycloaddition between the gelator alkyne precursors and the azidocoumarine. In such a system, the azidocoumarine would be used as a pre-fluorophore (fluorescent inactive), which upon a 'click' reaction lead to the formation of triazole units with enhanced fluorescent emissions.[22] The formation of a fluorescent product would allow us to trigger not only the reaction, but also the self-assembly of the final gelator, resulting in the formation a two-component fluorescent gel.

5.2. Results and Discussion

5.2.1. Design and Synthesis

The fluorescent gelators synthesized in this chapter are functionalized with azidocoumarine fluorophores. These fragments have been widely used in bioconjugation reactions due to its small size, biocompatibility and easy synthetic procedure.[19,22] Two different azidocoumarines have been synthesized, bearing a diethylamine or a hydroxyl group as substituent (**Figure 82**).

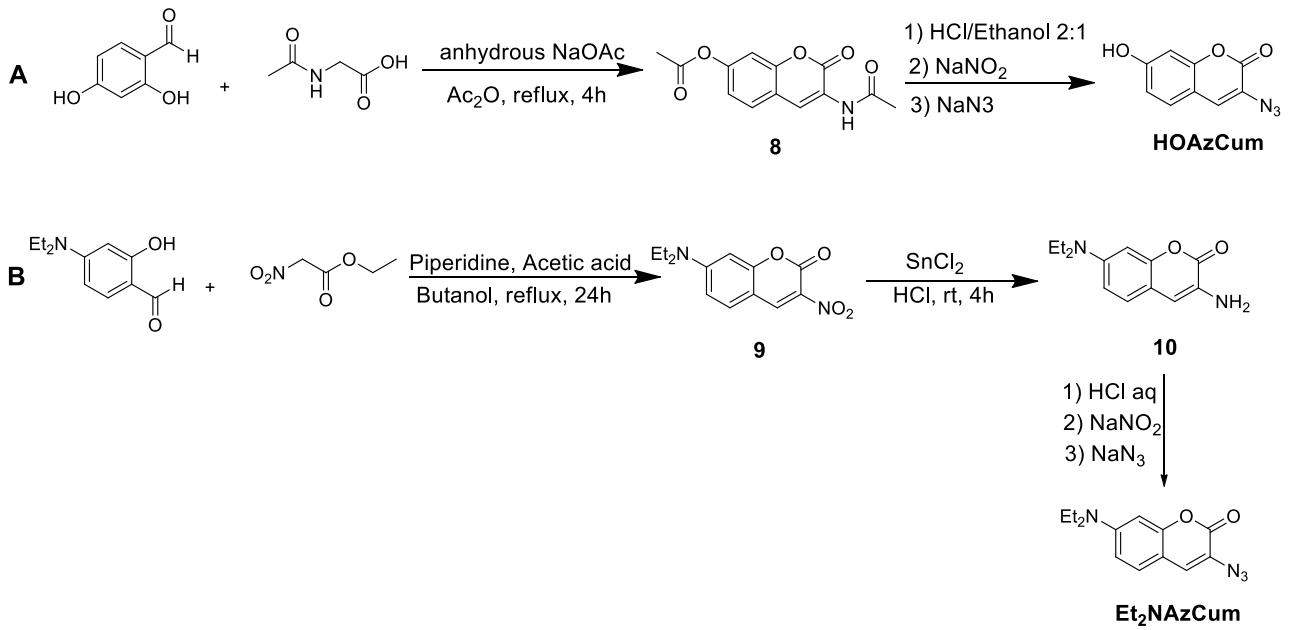

Figure 82. Scheme for the synthesis of azidocoumarine pre-fluorophores.

The synthesis of azidocoumarine represented in **Figure 82A** involved a Knoevoegel condensation between 4-diethylamino-salicylaldehyde and the ethyl nitroacetate, followed by a base-catalysed intramolecular aldol condensation of the *O*-acetyl salicylaldehyde, achieving the 3-nitro-7-diethylaminocoumarine.

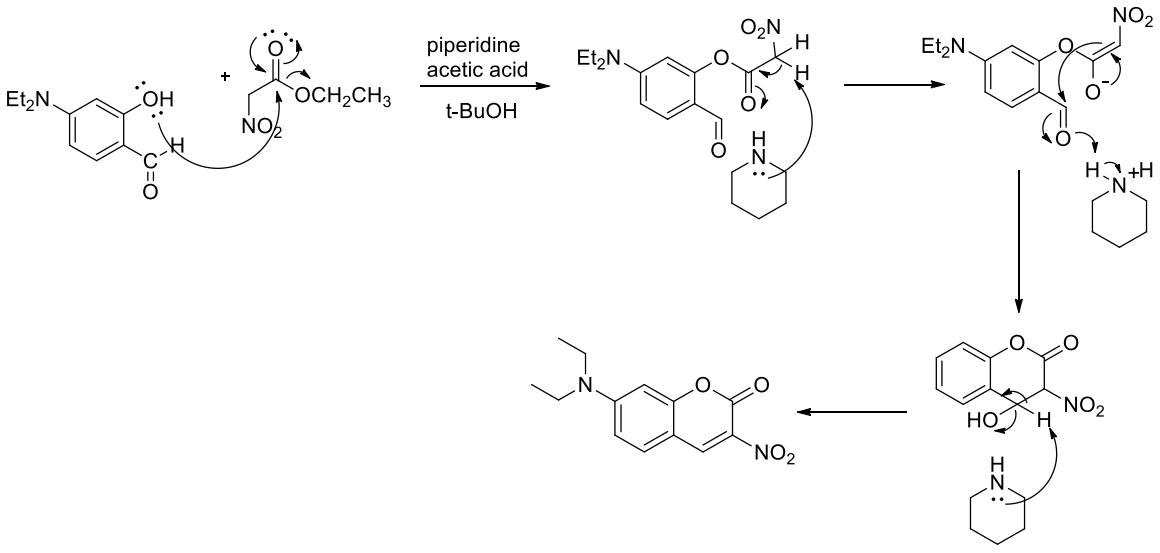

Figure 83. Mechanism for the formation of 3-nitro-7-diethylaminocoumarine.

The substituent nitro group is then reduced to primary amine in the presence of tin(II) chloride and HCl.

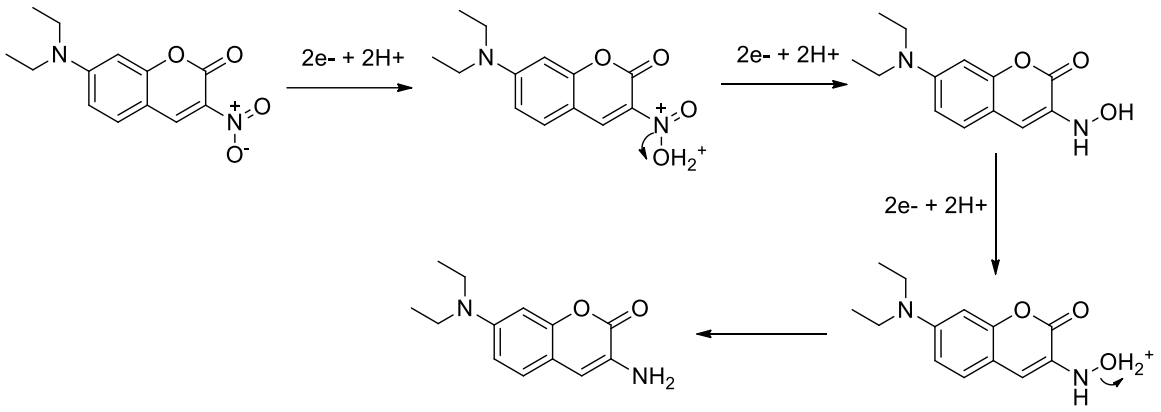

Figure 84. Mechanism for the reduction of 3-nitro-7-diethylaminocoumarine to 3-amino-diethylaminocoumarine.

The final steps consisted on the conversion of the amine group to diazonium salt by diazotization using $NaNO_2$ in HCl, followed by a nucleophilic attack of the sodium azide, as represented in **Figure 85**. This reaction had to be carried out between 0-5 ºC to avoid decomposition of the diazonium salt due to the possible loss of nitrogen.

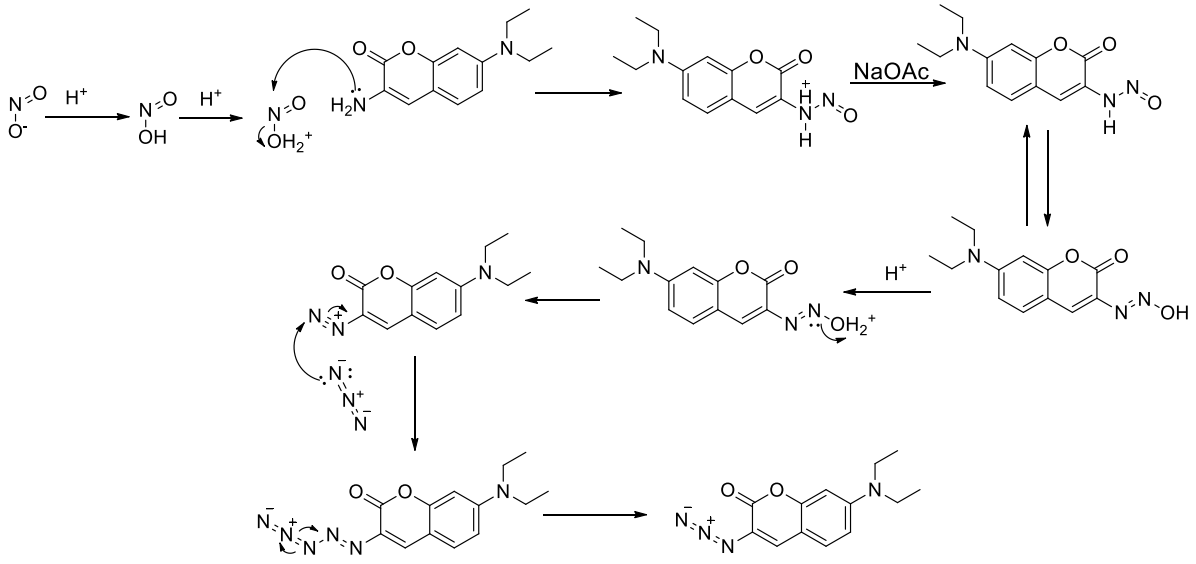

Figure 85. Mechanism of formation of 3-azido-7-diethylaminocoumarine by the intermediary diazonium salt.

The first step for synthesizing 3-azido-7-hydroxycoumarine consisted on a Perkin condensation between the acetic anhydride and the 2,4-hydroxybenzaldehyde with anhydride acetic, followed by acetylation in the presence of *N*-acetylglycine. The reaction proceeds through an acid hydrolysis (**Figure 86**) followed by typical conversion of the primary amine to the azide through the intermediary diazonium salt, in a similar mechanism as the one represented in **Figure 85**.

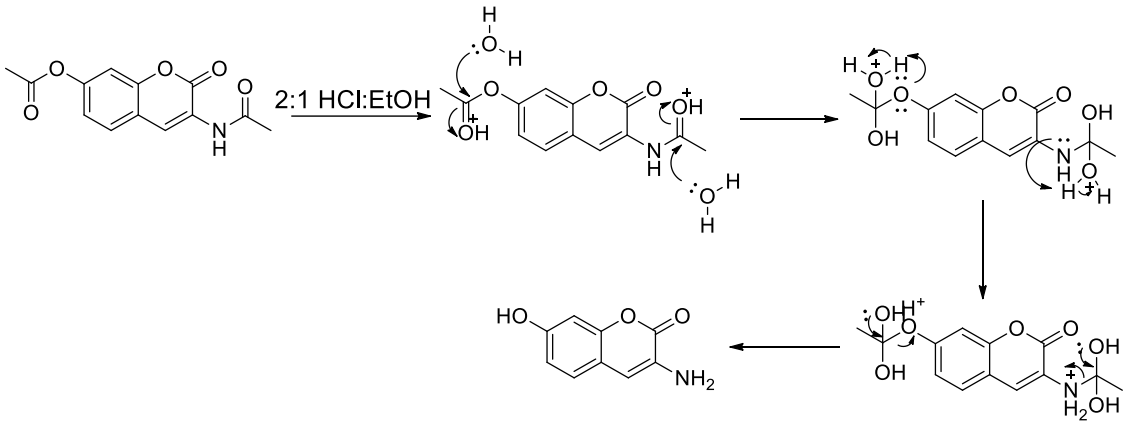

Figure 86. Mechanism of acid hydrolysis of the acetylated coumarine.

The *L*-valine azidocumarinetriazolyl (**RAzTzVal$_n$**) bolaamphiphilic family of compounds has been synthesized from peptide coupling of the pentynoic acid to compound **Val$_6$** synthesized in **Chapter 3**, using EDCI·HCl as a coupling agent, obtaining a dialkyne *L*-valine derivative. Finally, this product was coupled to the synthesized azidocoumarines through a copper(I) catalysed azide-alkyne cycloaddition, giving the final fluorescent gelators.

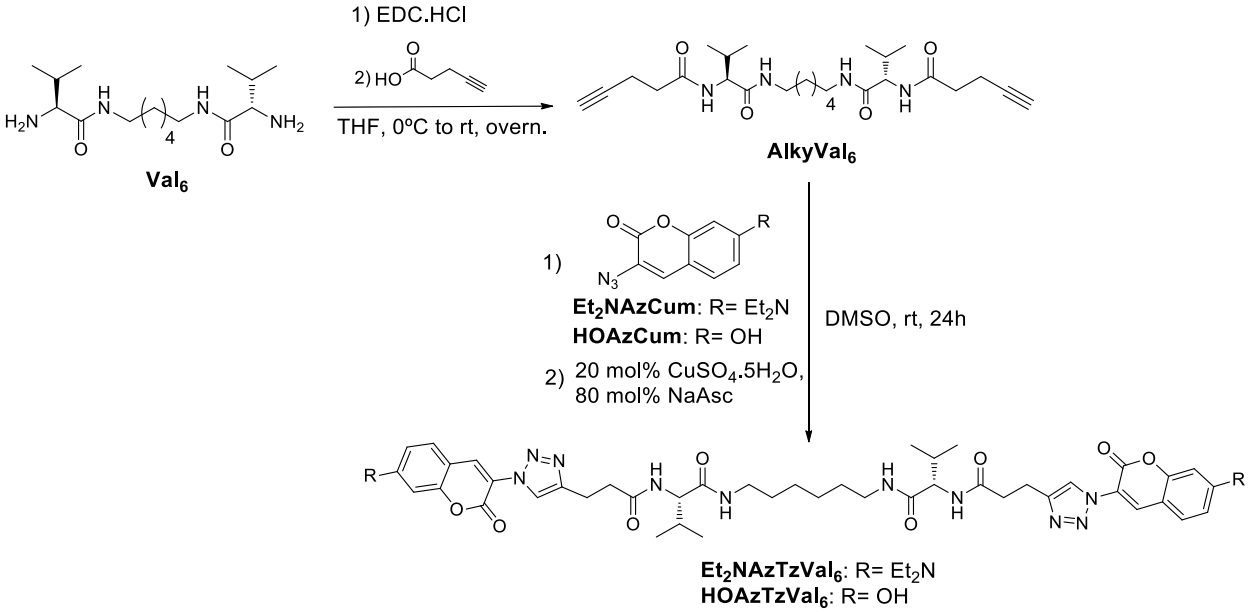

Figure 87. Structure of the bolaamphiphilic gelators **RAzTzVal$_n$**.

As reported elsewhere,[22] the azidocoumarine itself is not fluorescent but once 'clicked', the conjugation of the triazole linked to the azidocoumarine provides the resultant compounds with fluorescent properties. Based on these findings, the fluorescent compounds represented in **Figure 87** have been synthesized with the goal of following their synthesis and self-assembly process by confocal fluorescence microscopy using as catalyst one of the compounds from the family **PhTzVal$_n$**, as represented in **Figure 88**. The ability of the reactant **AlkyVal$_6$** and the catalyst **Cu(I)-**

PhTzVal$_n$ to form gels would guide to the formation of a final two-component hybrid organic-inorganic fluorescent gel network composed by the both catalytic and the fluorescent product gels. In this system, it would be expected to see the formation of the fluorescent product at the zones where the catalytic gel network intercepts the reactant gel network.

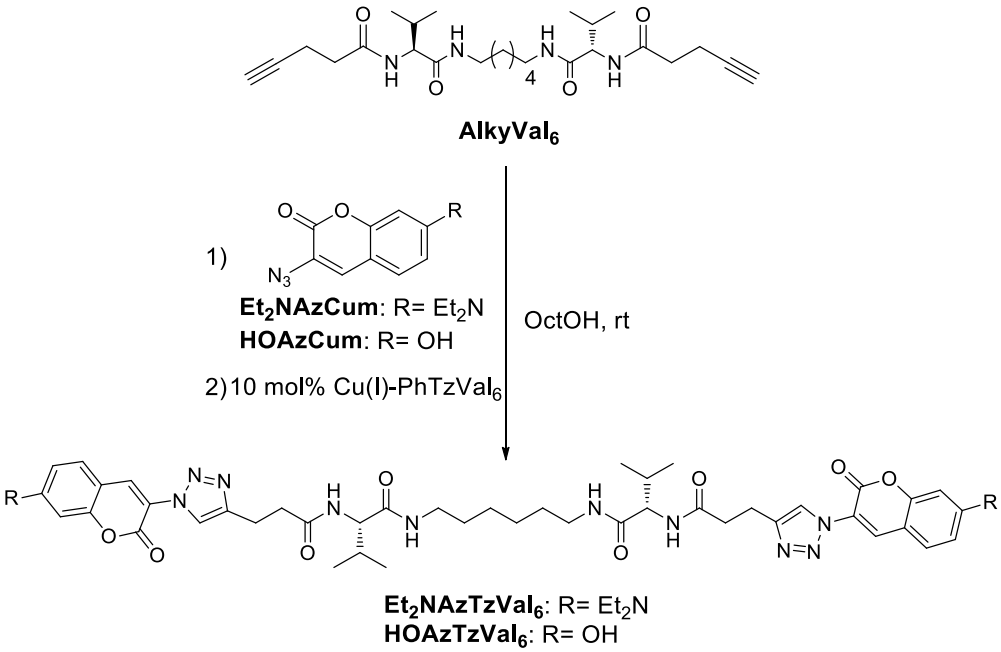

Figure 88. Reaction leading to the formation of the fluorescent bolaamphiphilic gelators **RAzTzVal$_6$**.

5.2.2. Viscoelastic properties

The ability of the fluorescent compounds **RAzTzVal$_6$**, the catalyst **PhTzVal$_6$** and the reactant **AlkyVal$_6$** to form gels was evaluated in high boiling point alcohols and in the typical solvent mixture for 'click' reactions 1:1 H_2O:*t*-BuOH (**Table 16**). The reason for selecting non-volatile solvents is related with the expected long-time exposure of the reaction system to the microscope laser during the experiments.

Table 16. Gelation experiments of compounds **RAzTzVal$_6$**, **AlkyVal$_6$** and metallocatalyst **Cu(I)-PhTzVal$_n$** [a].

Solvent	Et$_2$NAzTzVal$_6$	Aspect	HOAzTzVal$_6$	Aspect	PhTzVal$_6$	Aspect	AlkyVal$_6$	Aspect
n-BuOH	G	Transparent	G	transparent	SP	yellow	G	Transparent
H_2O:*t*-BuOH (1:1)	G	Transparent	SP	Transparent	G	Translucent	G	Transparent
t-BuOH	G	Transparent	G	transparent	G	Translucent	G	Transparent
Octanol	G	Transparent	G	Transparent	G	translucent	G	Transparent

[a] G: Gel, SP: Swollen precipitate, *c* = 8 mg/mL.

The bolaamphiphilic gelators **RAzTzVal$_6$** and **AlkyVal$_6$** demonstrated a good gelation ability in the tested solvents, resulting in the formation of transparent gels in octanol.

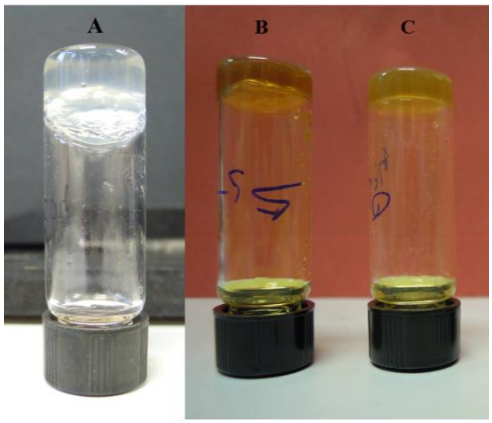

Figure 89. Macroscopic aspect of the gels **AlkyVal$_6$**, **Et$_2$NAzTzVal$_6$** and **HOAzTzVal$_6$** in octanol.

This transparent appearance of the gels is often linked to the presence of thin fibrous structures with diameters in the order of tens of nanometers in size, building a self-assembled nanostructured material. This aspect is regarded as ideal when analysing such materials by microscopy, due to the low amount of scattered light during the experiment. Similarly to the gelators **RAzTzVal$_6$**, also the catalyst **Cu(I)-PhTzVal$_6$** was able to form gels in all the tested solvents, except in n-BuOH, where suspended aggregates have been obtained. These studies allowed to select the octanol as preferred reaction medium, not only due to a common gelation ability evidenced by all the compounds involved in the reaction system for this specific solvent, but also due to its easy manipulation at room temperature.

Thus, the minimum gel concentration of the fluorescent gelators **RAzTzVal$_6$** and corresponding metallogels, as well as of the remaining reaction components **AlkyVal$_6$** and **Cu(I)-PhTzVal$_6$**, was investigated in octanol (**Table 17**). The fact that the gel **HOAzTzVal$_6$** has a higher m.g.c. than the **Et$_2$NAzTzVal$_6$** fluorescent gel suggest that the nature of the azidocoumarine substituting group has some influence on the self-assembly of the gelator. The replacement of the Et_2N group by the OH group in the terminal azidocoumarine fragment resulted in a lower gelation ability in octanol. The presence of copper(I) did not affect the gelation process, as the minimum gelation concentrations determined for the metallogels **Cu(I)-Et$_2$NAzTzVal$_6$** and **Cu(I)-HOAzTzVal$_6$** were similar to the ones of the corresponding native gels (**Table 17**).

Table 17. Minimum gelation concentrations of the reactant **AlkyVal$_6$**, the catalytic metallogel **Cu(I)-PhTzVal$_6$**, the fluorescent products **RAzTzVal$_6$** and the corresponding metallogels[a].

	Concentration (mM)	
Gelator	**Native**	**Metallogel**
Et$_2$NAzTzVal$_6$	3.4	3.4
HOAzTzVal$_6$	5.7	5.7
AlkyVal$_6$	5.6	n.d.[a]
PhTzVal$_6$	n.d.[a]	4.7

[a] Not been determined because it was not relevant for the goal of this project.

5.2.3. Structural characterization of the gels

The structural arrangement of the gels **Et$_2$NAzTzVal$_6$**, **HOAzTzVal$_6$** and of the corresponding metallogels was accessed by wide angle x-ray diffraction (WAXD).

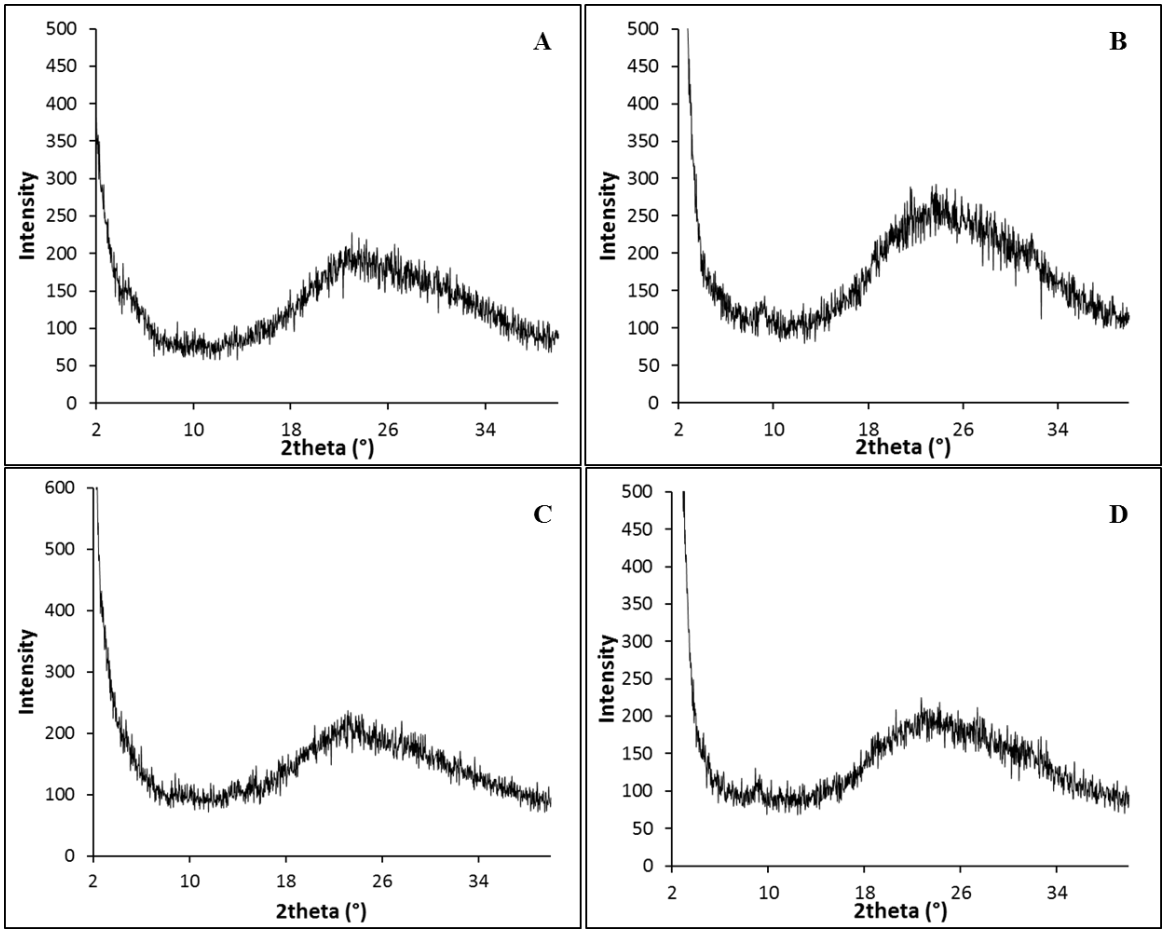

Figure 90. WAXD diffractograms of gels **Et$_2$NAzTzVal$_6$** (A), **HOAzTzVal$_6$** (B), **Cu(I)-Et$_2$NAzTzVal$_6$** (C) and **Cu(I)-HOAzTzVal$_6$**.

The diffractograms obtained in **Figure 90** suggest that the bolaamphiphilic gelators **Et$_2$NAzTzVal$_6$** and **HOAzTzVal$_6$** aggregate in a disordered and amorphous way, independently on the presence of the metal, which is in accordance with the similar m.g.c. obtained for the native gels and correspondent metallogels (**Table 17**).

5.2.4. Photophysical properties of the pure reactants and products in solution

The photophysical properties of the azidocoumarines **HOAzCum** and **Et$_2$NAzCum** and of the corresponding fluorescent products were investigated in solution. As expected, very weak or no emission has been observed for the pure azidocoumarines, although it could be detected an emission maximum at λ= 462 nm for the azidocoumarine functionalized with the diethylamino group. This low fluorescence arises from the quenching effect of the electron-rich α-nitrogen of the azido group. However, upon reaction with the gel **AlkyVal$_6$**, the obtained products exhibited a high fluorescence, with $\lambda_{em,max}$ = 427 nm (**HOAzTzVal$_6$**) and $\lambda_{em,max}$ = 485 nm (**Et$_2$NAzTzVal$_6$**). Additionally, the reactants **AlkyVal$_6$** and the catalyst **Cu(I)-PhTzVal$_6$** were completely dark, giving a noisy fluorescent spectra with remarkably low intensity.

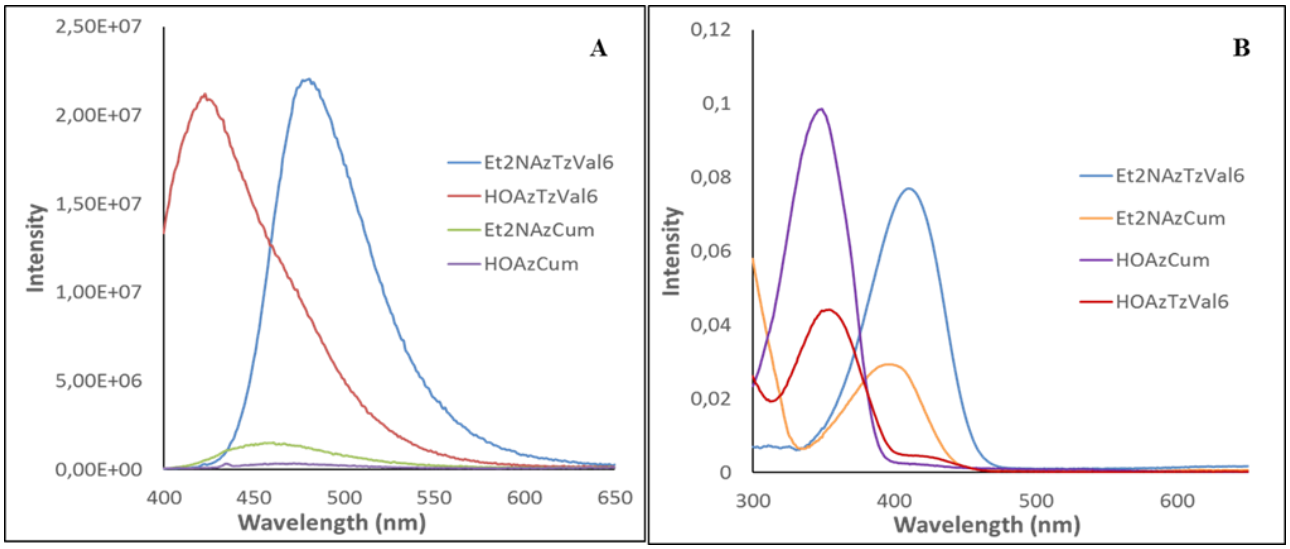

Figure 91. Emission (A) and absorption (B) spectra of the reactants **HOAzCum**, **Et$_2$NAzCum** and of the final gelators **Et$_2$NAzTzVal$_6$** (A), **HOAzTzVal$_6$** (B). For the emission spectra, compounds were excited at λ= 385 nm.

Regarding the UV-VIS spectra, a different absorption maxima has been registered depending on the substituent group of the azidocoumarine, although both the diethylamino and the hydroxyl belong to the class of electron-donating groups. While the compounds having the hydroxyl substituent exhibited a $\lambda_{abs,max}$= 355 nm, the ones having a diethylamino group in their structure present a $\lambda_{abs,max}$= 402 nm, although in the last case a red-shift to $\lambda_{abs,max}$= 414 nm has been registered for the corresponding product formed after 'click' reaction.

5.2.5. Photophysical properties of the reactants and products in gel phase by confocal fluorescent microspectroscopy

The fluorescent compounds **Et_2NAzTzVal$_6$** and **HOAzTzVal$_6$** were analysed on the confocal fluorescence microscope to investigate their emissive properties in the gel phase. Taking into account the presence of copper in the reaction system, the metallogels **Cu(I)-Et_2NAzTzVal$_6$** and **Cu(I)-HOAzTzVal$_6$** were also investigated. The polarization images were acquired together with the corresponding emission spectrum.

By analysing the images captured for the gels **Et_2NAzTzVal$_6$** and **Cu(I)-Et_2NAzTzVal$_6$**, it is possible to see that the diethylamine-substituted fluorescent compound exhibit some polarization (**Figure 92**).

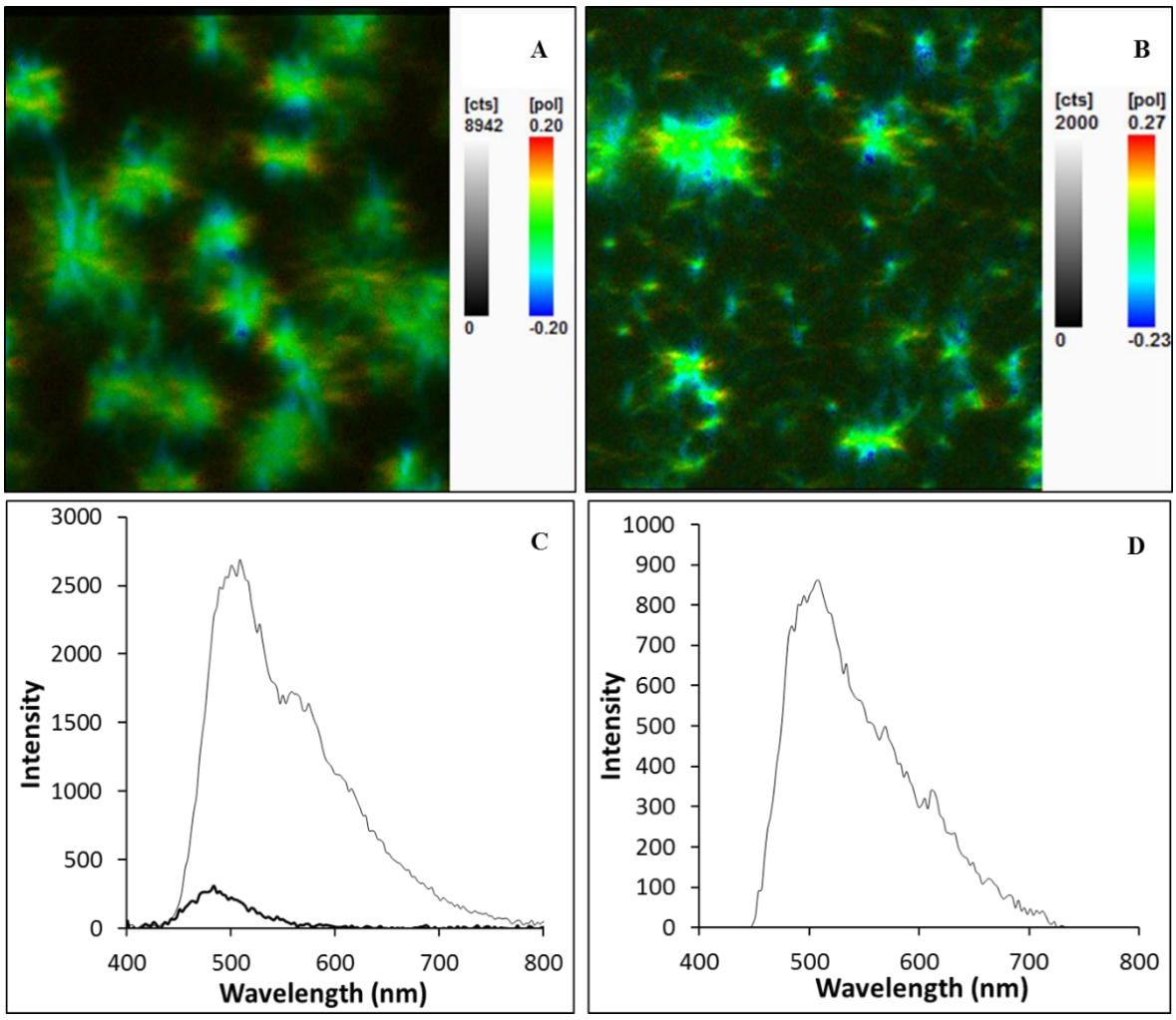

Figure 92. Fluorescent polarization confocal images (A-B) under horizontally polarized excitation (east/west, λexc= 385 nm) and spectra (C-D) performed on the gel **Et_2NAzTzVal$_6$** (A, C) and on the corresponding metallogel **Cu(I)-Et_2NAzTzVal$_6$** (B, D). Image size is 20 x 20 µm. Colour codes correspond to polarization P: from negative to positive, blue, green, yellow and red. Spectrum C was performed on the aggregates (grey) and on the background (black). Spectrum D was taken on the metallogel aggregates.

The polarization values are in the range of -0.20 ≤ P ≤ 0.15, supporting the presence of both negatively and positively polarized fibres that could arise from a possible different orientation of the gelator molecules in the fluorescent fibres in respect to the detectors. It is important to remember that in confocal fluorescence polarization imaging under linearly polarized laser excitation, the molecules selectively absorb linearly polarized light when their emission dipole is oriented parallel to the axis of the excitation beam.[11] By performing the emission spectra, it was possible to see that the both pure gel and metallogel aggregates exhibit their maximum emission at λ= 508 nm, corresponding to a cyano emission (**Figure 92C**). This value is red-shifted if compared with the maximum emission registered for the molecules of gelator in the background ($\lambda_{em,max}$= 485 nm), suggesting that the fluorescence is affected by the supramolecular self-assembly. Additionally, it can be observed that the aggregates (**Figure 92C grey**) were much more emissive than the surrounding background (**Figure 92C black**). This is quite reasonable because the self-assembly of the gelator molecules leads to the formation of an extended fluorescent network with closely-packed chromophores, and thus the measured emission may be regarded as the sum of the emission of each individual gelator molecule. Furthermore, if the fluorophores are closely packed, they can interact with each other usually by π-π stacking to form the correspondent excimers, which in turn have lower energy resulting in a red-shift of the emission spectrum.[23,24]

The presence of copper in the metallogel **Cu(I)-Et$_2$NAzTzVal$_6$** results in a quenching on the fluorescence of the gel aggregates (**Figure 92D**), although the maximum emission wavelength remains the same. The coordination to the metal centre involves the distribution of electrons between the copper and the triazole moiety, becoming less available to conjugation roles. On the other side, it is well reported that transition metals can absorb visible light by d→d transitions, decreasing the amount of incident light on the fluorophore and inducing a consequent fluorescence quenching.[25,26] Finally, the coordination of the metal did not influence the morphology of the fibres, which maintained their flower-like and thin morphology.

Similar studies were carried on the gel **HOAzTzVal$_6$** to investigate the impact of replacing the dimethylamine substituting group on the azidocoumarine by the hydroxyl group (**Figure 93**). The images acquired on the microscope suggest that the gel **HOAzTzVal$_6$** exhibit positive polarization, whereas the obtained emission spectra show a $\lambda_{max,em}$= 450 nm, resulting in a blue emission (**Figure 93C black**). Such emission seems to be slightly red-shifted in comparison with the one registered for the background, $\lambda_{em,max}$= 430 nm (**Figure 93C grey**), although this is not particularly evident on the spectrum of the metallogel **Cu(I)-HOAzTzVal$_6$**, where both the background and the aggregates exhibit their maximum emission almost at the same wavelength, λ= 430 nm (**Figure 93D**). Nevertheless, as previously denoted for the gel **Cu(I)-Et$_2$NAzTzVal$_6$**, also in

the metallogel **Cu(I)-HOAzTzVal$_6$** it is clearly observed a quenching in the fluorescence arising from the coordination of the metal to the azidocoumarine triazole fragment of the gelator.

Finally, it is important to highlight the higher emission coming from the background in comparison with the one measured for the aggregates (**Figure 93C-D**), which together with its higher m.g.c. (**Table 17**) confirms the poorer gelation ability of the compound functionalized with the hydroxyl-substituted azidocoumarine.

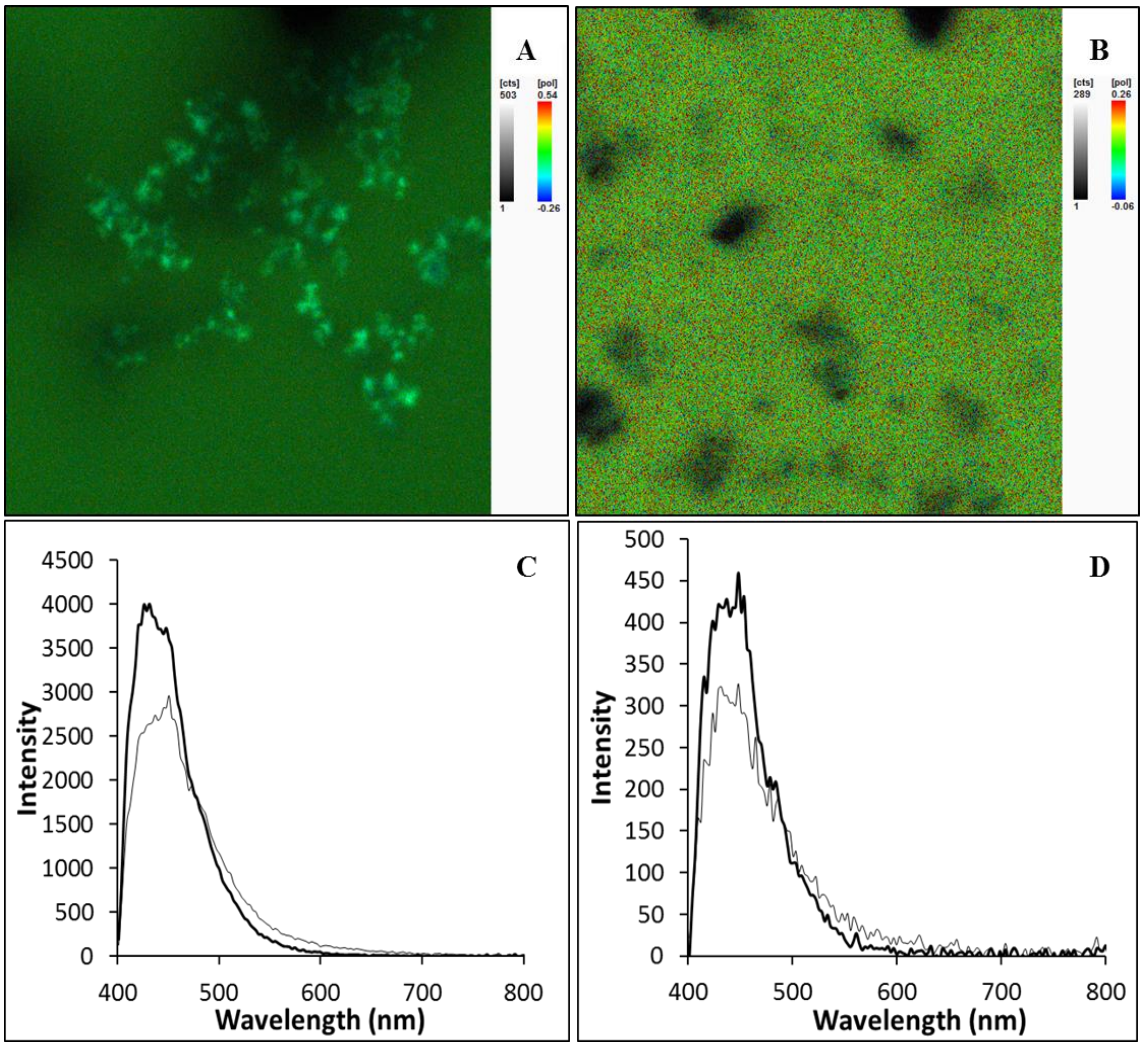

Figure 93. Fluorescent polarization confocal images (A-B) under horizontally polarized excitation (east/west, λexc= 385 nm) and spectra (C-D) performed on the gel **HOAzTzVal$_6$** (A, C) and on the corresponding metallogel **Cu(I)-HOAzTzVal$_6$** (B, D). Image size is 80 x 80 µm. Spectrum C and D were performed on the aggregates (grey) and on the background (black). Colour codes correspond to polarization P: from negative to positive, blue, green and red.

5.2.6. Investigation of the reaction system using the Cu(I)-PhTzVal$_6$ as catalyst by confocal fluorescence microspectroscopy

After studying the emission of all the intervenient compounds, a first attempt to reproduce the reaction on the microscope has been performed (**Figure 94**).

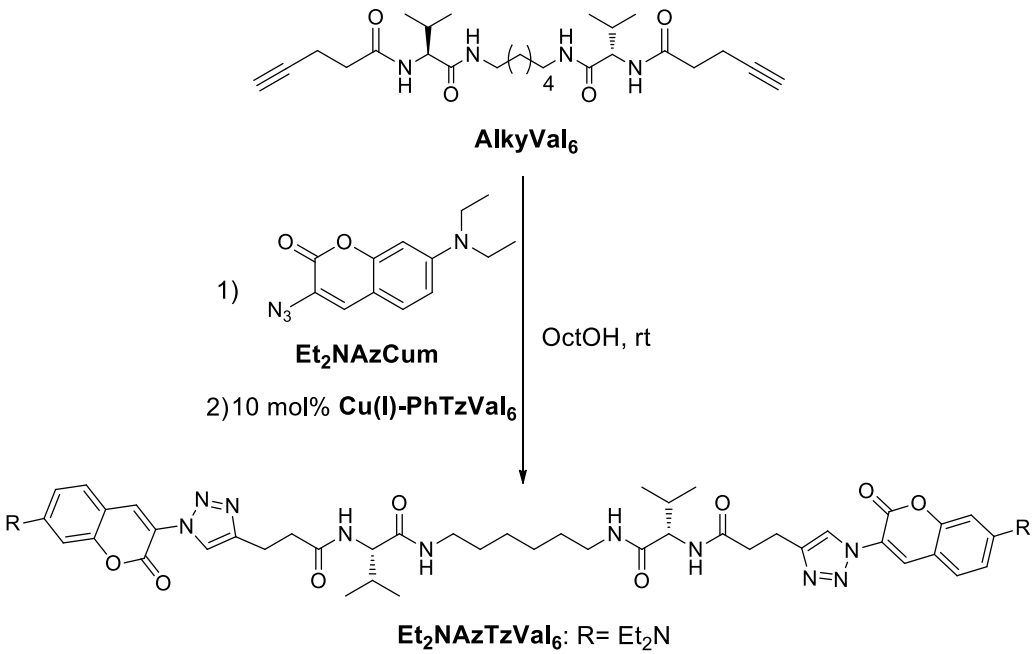

Figure 94. First reaction system studied by confocal fluorescence microspectroscopy.

For this experiment, a two-component gel composed by 10 mol% of catalytic metallogel **Cu(I)-PhTzVal$_6$** and the reactant **AlkyVal$_6$** was formed by heating-sonication method. Briefly, both gelators in the required amounts were heated in separate vials and 100 μL of the correspondent hot solutions were transferred to the sample holder, achieving the formation of a transparent gel after 2 minutes. Then, 100 μL of the reactant **Et$_2$NAzCum** was added on the top of the two-component gel and allowed to diffuse. After 16h reaction, an image of the resultant sample was acquired, as well as the correspondent emission spectra.

The obtained product exhibited the presence of cyano aggregates ($\lambda_{em,max}$= 481 nm) with a flower-like morphology (**Figure 95A**), resembling the ones observed for the pure gel **Et$_2$NAzTzVal$_6$** (**Figure 92A**). The red colour in the microscopy image means that it was acquired only with one detector, making it impossible to evaluate if the gel presented some polarization. Similarly to what was observed on the previously investigated gels, in this case it was also possible to see a blue-shift on the maximum emission of the background ($\lambda_{em,max}$= 453 nm), although the difference in intensity between the aggregates and the background emission is not so accentuated.

The spectra represented in **Figure 95B** also evidences a blue shift in both values corresponding to the maximum emission of the aggregates and the background, $\lambda_{em,max}$= 481 nm and $\lambda_{em,max}$= 453 nm respectively, in comparison with the emission registered for the aggregates and background belonging to pure **Et$_2$NAzTzVal$_6$** gel, $\lambda_{em,max}$= 508 nm and $\lambda_{em,max}$= 485 nm, respectively.

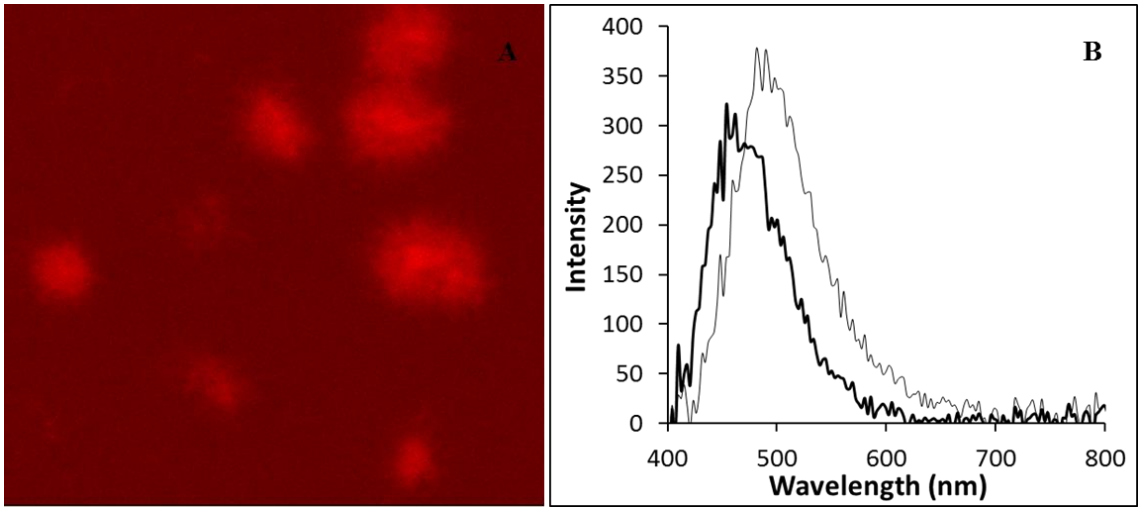

Figure 95. Fluorescent lifetime confocal image (A) and emission spectra (B) of the final gel product **Et_2NAzTzVal$_6$**. Image size is 30 x 30 µm. Spectrum B was performed on the aggregates (grey) and on the background (black).

Although the fluorescent product has been successfully obtained and analysed under the microscope, the main goal of the project was not accomplished in this first trial, since it was impossible to see in the microscope the presence of the initial two-component gel network, making it difficult to conclude if the fluorescent fibers were growing from the interception points between the **AlkyVal$_6$** and the catalytic **Cu(I)-PhTzVal$_6$** gel networks. The non-fluorescent nature of both the reactant and the catalyst makes them undetectable by confocal fluorescence microscopy.

5.2.7. Investigation of the reaction system using the Cu(I)-HOAzTzVal$_6$ as catalyst by confocal fluorescence microspectroscopy

To successfully achieve the objective of this project, it would be ideal to have a fluorescent reactant, catalyst and product emitting in different zones of the electromagnetic spectrum. Since the synthesized gelators **Et_2NAzTzVal$_6$** and **HOAzTzVal$_6$** emit in the cyano and blue zones of the spectrum, respectively, and because both were able to coordinate copper due to the presence of a triazole fragments in their structure, the dark catalytic gel **Cu(I)-PhTzVal$_6$** was replaced by the fluorescent metallogel **Cu(I)-HOAzTzVal$_6$**, in an attempt to observe the presence of an initial fluorescent catalytic network by confocal fluorescence microscopy. The reaction guiding to the formation of the fluorescent gelator **Et_2NAzTzVal$_6$** in the presence of the catalytic gel **Cu(I)-HOAzTzVal$_6$** is represented in **Figure 96**.

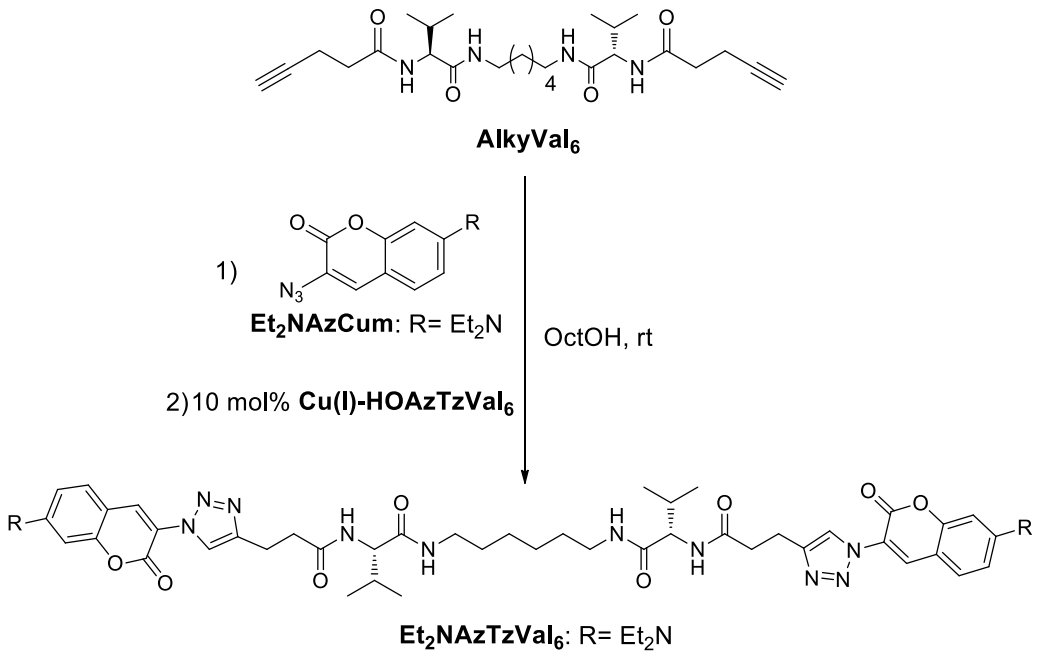

Figure 96. Reaction system for the formation of the fluorescent gel **Et₂NAzTzVal₆** in the presence of the fluorescent catalytic gel **Cu(I)-HOAzTzVal₆**.

To study the viability of this experiment, a two-component gel containing both **Et₂NAzTzVal₆** and **HOAzTzVal₆** gelators was prepared by heating them together in a 4 mL screw-capped vial until complete dissolution followed by 15 seconds sonication, resulting in the formation of a semi-viscous solution, which was then transferred to the sample holder and allowed to gel. The main goal of this experiment was to check the aspect of the two-component gel **Et₂NAzTzVal₆**/**HOAzTzVal₆** under the microscope.

The image represented in **Figure 97B** suggest that the aggregates from the two-component gel exhibit some polarization, which is in accordance to what was observed for the pure gels **Et₂NAzTzVal₆** and **HOAzTzVal₆** (**Figure 92A** and **Figure 93A**). The obtained gel network seem to exhibit an homogeneous morphology, characterized by the presence of thin and long fibres growing from a more fluorescent central nucleus, resembling the ones observed for the pure gel **Et₂NAzTzVal₆**. This homogeneous morphological aspect might suggest that both gels co-assemble, although this should be confirmed with additional XRD analysis of the mixture of gels.

All the spectra obtained for the two-component gel **Et₂NAzTzVal₆**/**HOAzTzVal₆** are composed by broad peaks exhibiting one clear shoulder around λ= 430 nm and a smooth shoulder at λ= 450 nm, which are in accordance with the characteristic emission peaks detected for **HOAzTzVal₆** background and aggregates, respectively (**Figure 93C**).

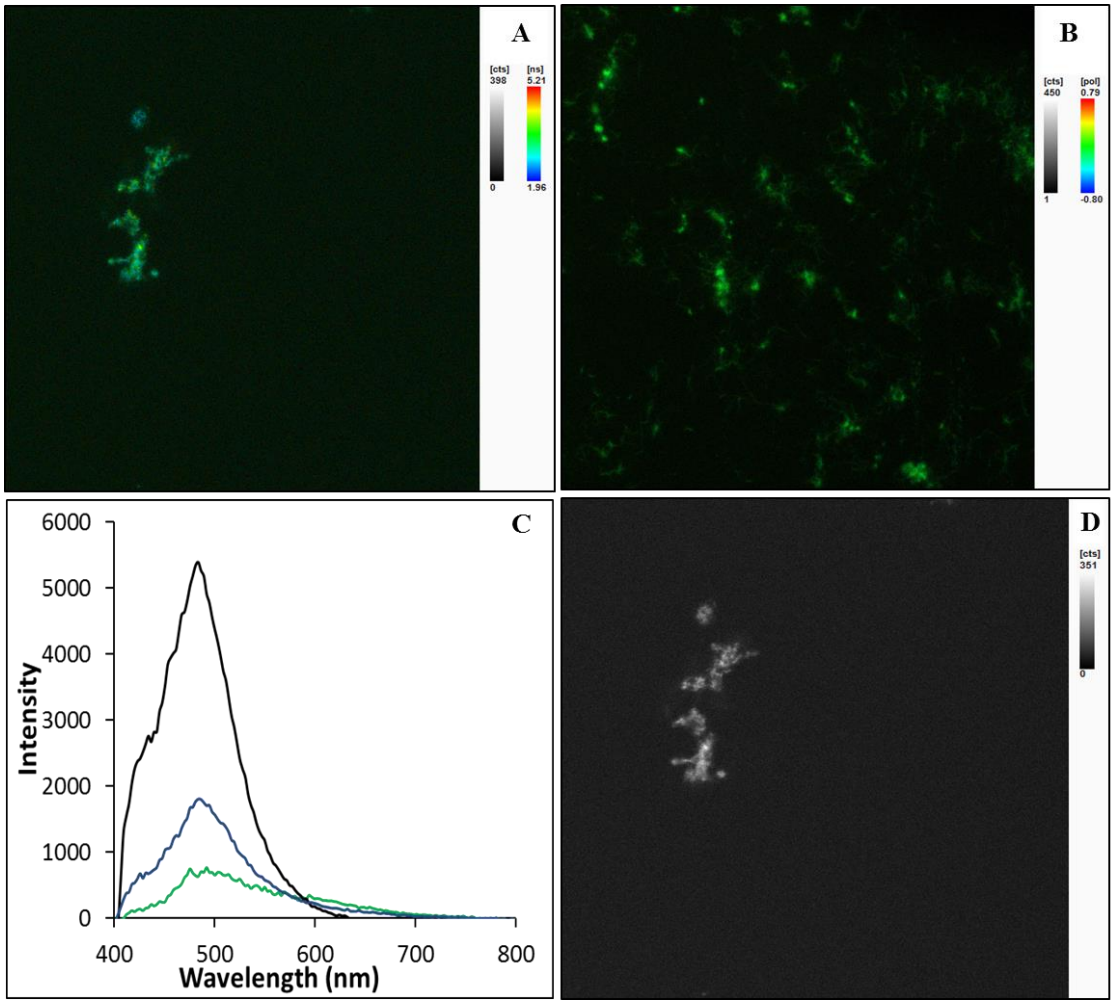

Figure 97. Fluorescent lifetime image (A), fluorescent polarization confocal image (B) under horizontally polarized excitation (east/west, λexc= 385 nm), intensity image (D), and emission spectra (C) of the two-component gel **Et$_2$NAzTzVal$_6$/HOAzTzVal$_6$**. Image size is 80 x 80 µm. Spectrum C was performed on image A on the blue aggregate at the top (blue), green aggregates at the centre (green) and on the background (black).

The maximum emission of the peaks was observed at λ = 484 nm for the background, which is in a similar range as the one registered for the background in the pure gel **Et$_2$NAzTzVal$_6$** ($\lambda_{em,max,bg}$= 485 nm), and between $\lambda_{em,max}$= 490-500 nm for the aggregates, slightly blue-shifted in comparison to the ones detected for the analogues of pure **Et$_2$NAzTzVal$_6$**, $\lambda_{em,max,agg}$= 508 nm (**Figure 92B**). Although the high emission coming from the background in these samples may bring some problems when studying the reaction system, the fact that it was possible to distinguish the presence of both the cyano and the blue gels in the two-component gel network allowed to proceed for the study of the reaction system represented in **Figure 96**.

In this experiment, the gelator **HOAzTzVal$_6$** was heated in the presence of the copper salt $[Cu(MeCN)_4]PF_6$ (2:1 gelator/copper molar ratio) at 300 ºC for 4 minutes, and put in the ultrasounds for 15 seconds. The resultant semi-viscous solution (100 µL) was rapidly taken and

transferred to a 1 mL syringe equipped with a needle on the bottom to avoid the flow of the semi-viscous solution and allow the formation of the gel inside the plastic graded tube. A semi-viscous solution of **AlkyVal$_6$** gelator obtained by a similar procedure was transferred to the top of the previously formed **Cu(I)-HOAzTzVal$_6$** metallogel. At this point, the semi-viscous solution of the gelator **AlkyVal$_6$** diffused through the previously formed catalytic gel **Cu(I)-HOAzTzVal$_6$**, resulting in the formation of a two-component metallogel **Cu(I)-HOAzTzVal$_6$/AlkyVal$_6$**. After the formation of a self-sustained gel that was able to whithstands gravity upon inversion of the syringe, 2 mL of octanol was carefully added on the top and allowed to diffuse through the mixed gel. The objective of this procedure was to wash the two-component metallogel **Cu(I)-HOAzTzVal$_6$/AlkyVal$_6$** by continuous flow, removing not only possible uncoordinated copper(I) in solution, but also non-aggregated gelator molecules which are usually responsible for a high background emission. The washed gel was then transferred to the sample holder and analysed by confocal fluorescence microspectroscopy (**Figure 98**).

The introduction of a washing step of the initial two-component metallogel **Cu(I)-HOAzTzVal$_6$/AlkyVal$_6$** by continuous flow of octanol was determinant in obtaining an image with less background emission (**Figure 98A**). Further dilution of the sample, by carefully adding 100 µL of octanol with a 1 mL syringe and without moving the sample holder, provided an image showing a clear contrast between the fluorescent **Cu(I)-HOAzTzVal$_6$/AlkyVal$_6$** aggregates and the dark background (**Figure 98B**).

The emission spectra acquired before the reaction clearly shows that the intensity of emission of the aggregates was two times more than the emission arising from the background (**Figure 98D blue**), supporting the efficiency of the washing step. In this same spectra, it could be also observed that both the background and the aggregates of the initial two-component gel **Cu(I)-HOAzTzVal$_6$/AlkyVal$_6$** emitted in the blue region, $\lambda_{em,max,bg}$= 448 nm and $\lambda_{em,max,agg}$= 431 nm, respectively (**Figure 98D blue**). As it would be expected, these maximum emission wavelengths are similar to the ones previously observed for the aggregates ($\lambda_{em,max}$= 450 nm) and background ($\lambda_{em,max}$= 431 nm) on the pure gel **Cu(I)-HOAzTzVal$_6$** (**Figure 93C**).

A solution of **Et$_2$NAzCum** (100 µL) was then carefully added on the top of the two-component gel and allowed to diffuse through it. After 16h reaction, a new image together with the corresponding spectra was acquired. It is important to highlight that during the whole process, the sample holder was not moved and all the images were acquired in similar conditions, meaning that all the pictures can be superimposed with each other.

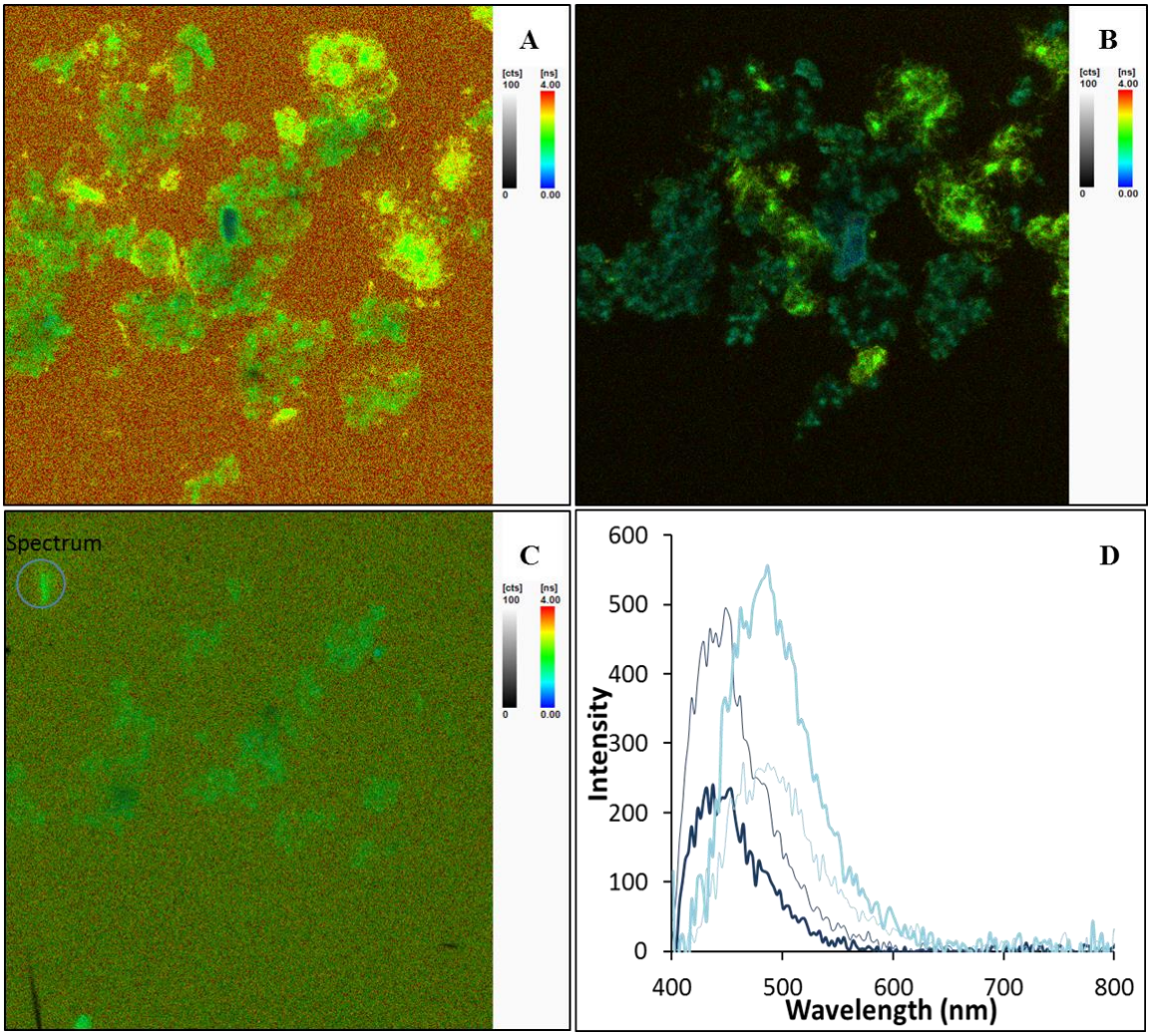

Figure 98. Fluorescent lifetime confocal images (Image size 60 x 60 µm) of the two component metallogel **Cu(I)-HOAzTzVal$_6$/AlkyVal$_6$** before reaction (A), before reaction and after dilution with 100 µL Octanol (B) and after reaction (C). Emission spectra of the **Cu(I)-HOAzTzVal$_6$/AlkyVal$_6$** before reaction (D blue) and after reaction (D cyano). The spectra were performed on the aggregates (thin line) and on the background (thick line).

The spectra acquired on the aggregate positioned on the top left corner of **Figure 98C** returned emission in the cyano region, which is in accordance with the expected spectral emission range for the fluorescent product **Et$_2$NAzTzVal$_6$**. After the reaction, the maximum emission of both the aggregates and the background shifted from blue ($\lambda_{em,max,agg}$= 448 nm and $\lambda_{em,max,bg}$= 431 nm, respectively) to cyano ($\lambda_{em,max,agg}$= 486 nm and $\lambda_{em,max,bg}$= 484 nm, respectively).

A higher magnification image of the central fibers on **Figure 98C** and the corresponding spectra were also acquired (**Figure 99**).

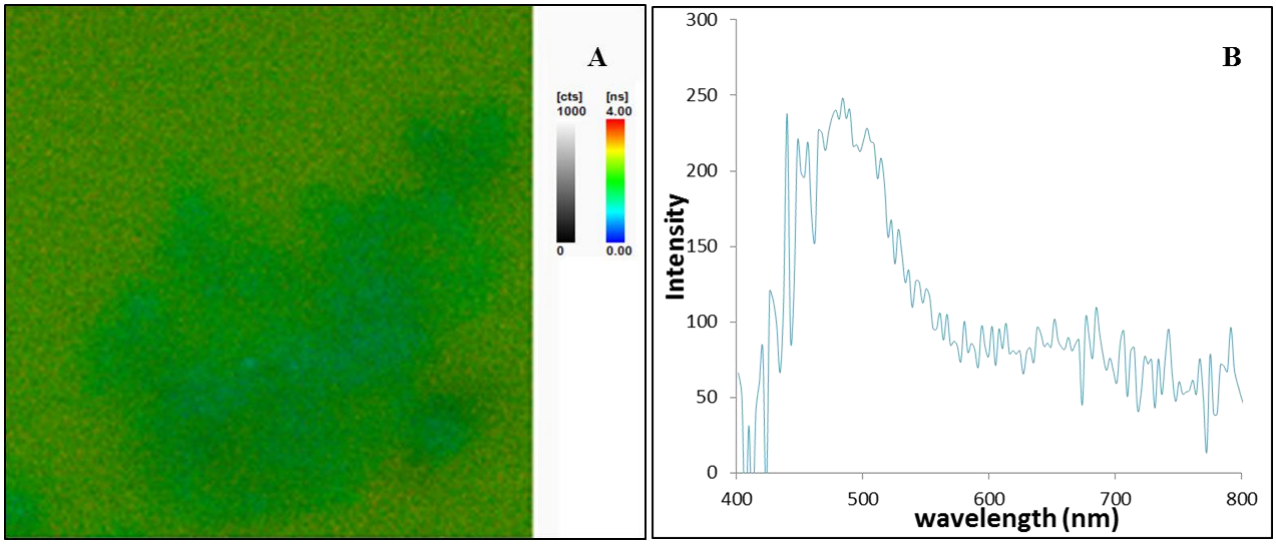

Figure 99. Fluorescent lifetime confocal images (60 x 60 µm) of fibres after reaction (A) and emission spectrum of short lifetime the aggregates (B).

The fibres exhibit a maximum emission peak at λ= 490 nm with a clear shoulder at λ=450 nm, which is in accordance with the maximum emissions observed for the aggregates in the two-component gel **Et$_2$NAzTzVal$_6$/HOAzTzVal$_6$** ($\lambda_{em,max,agg}$= 490 nm – 500 nm) and for the aggregates from the pure **HOAzTzVal$_6$** ($\lambda_{em,max,agg}$= 450 nm). The detection of fibres with characteristic emission of the catalyst and of the final product exactly in the same region where before reaction there were only fibres emitting in the blue region suggest that the final product is growing from the catalytic network. This supports that both the catalyst **HOAzTzVal$_6$** and the reactant **AlkyVal$_6$** networks are interacting with each other in the initial two-component gel **Et$_2$NAzTzVal$_6$/AlkyVal$_6$**, providing the formation of the product in the zones where the catalyst and reactant networks are present together. Although this represents a good result regarding the main objective of the project, it is not possible to observe in these images whether these two initial networks are orthogonally assembled or co-assembled (**Figure 100**), not only due to the high emission coming from the background, but also as a result of the dark emission of the reactant **AlkyVal$_6$**, making it impossible to visualize its network by confocal fluorescence microscopy. The high emission coming from the background also constituted a problem when following the self-assembly of the final product by video capture.

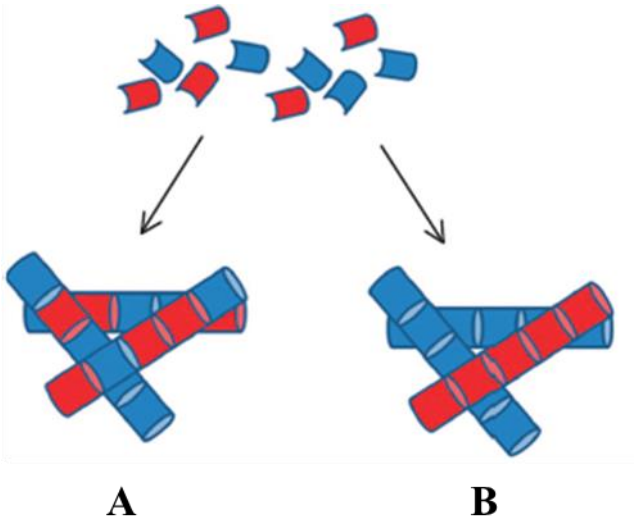

Figure 100. Schematic representation of possible assembly of **AlkyVal$_6$** and **HOAzTzVal$_6$** into fibres: A: orthogonal self-assembly, B: co-assembly.[27]

5.3. Conclusion

The formation of a fluorescent gel product on a fluorescent catalytic gel network was successfully detected by fluorescence confocal microspectroscopy. The fluorescent product resulted from the reaction of 7-diethylamino-3-azidocoumarine with an initial two-component gel network, composed by a reactant gelator and a fluorescent gelator. It was observed that the formation of the product clearly occured in the zones where the catalytic fluorescent network was initially detected, suggesting that the product aggregates grow on the interception points between the network of the alkyne reactant and the one of the catalytic fluorescent gel network.

This heterogeneous catalytic system highlights the importance of multicomponent interpenetrating gel networks on the formation of new functional materials. The obtained two-component fluorescent material could be used in cell imaging, as a potential scaffold for better visualization of interaction between substrates and cells.[18,28]

5.4. References

[1] Nayak MK, Kim BH, Kwon JE, Park S, Seo J, Chung JW, Park SY. Gelation-induced enhanced fluorescence emission from organogels of salicylanilide-containing compounds exhibiting excited-state intramolecular proton transfer: synthesis and self-assembly. Chemistry – A European Journal 2010; 16: 7437-7447.

[2] Ajayaghosh A, Praveen VK, Vijayakumar C. Organogels as scaffolds for excitation energy transfer and light harvesting. Chemical Society Reviews 2008; 37: 109-122.

[3] Babu SS, Prasanthkumar S, Ajayaghosh A. Self-assembled gelators for organic electronics. Angewandte Chemistry 2012; 51: 1766-1776.

[4] Leong WL, Tam AYY, Batabyal SK, Koh LW, Kasapis S, Yam VWW, Vittal JJ. Fluorescence enhancement of coordination polymeric gel. Chemical Communications 2008; 3628-3630.

[5] Zimmermann J, Zeug A, Roder B. A generalization of the Jablonski diagram to account for polarization and anisotropy effects in time-resolved experiments. Physical Chemistry Chemical Physics 2003; 5: 2964-2969.

[6] Lichtman JW, Conchello JA. Fluorescence microscopy. Nature Methods 2005; 2: 910-919.

[7] Ji X, Shi B, Wang H, Xia D, Jie K, Wu ZL, Huang F. Supramolecular construction of multifluorescent gels: Interfacial assembly of discrete fluorescent gels through multiple hydrogen bonding. Advanced Materials 2015; 27: 8062-8066.

[8] Zhao Z, Lam JWY, Tang BZ. Self-assembly of organic luminophores with gelation-enhanced emission characteristics. Soft Matter 2013; 9: 4564-4579.

[9] George SJ, Ajayaghosh A. Self-assembled nanotapes of Oligo(*p*-phenylene vinylene)s: Sol-gel-controlled optical properties in fluorescent π-electronic gels. Chemistry – A European Journal 2005; 11: 3217-3227.

[10] Del Guerzo A, Olive AG, Reichwagen J, Hopf H, Desvergne JP. Energy transfer in self-assembled [*n*]-acene fibers involving ≥100 donors per acceptor. Journal of the America Chemical Society 2005; 127: 17984-17985.

[11] Giasante C, Raffy G, Shäfer C, Rahma H, Kao MT, Olive AG, Del Guerzo A. White-light-emitting self-assembled nanofibers and their evidence by microspectroscopy of individual objects. Journal of the American Chemical Society 2011; 133: 316-325.

[12] Bastiaens PIH, Squire A. Fluorescence lifetime imaging microscopy: spatial resolution of biochemical processes in cells. Trends in Cell Biology 1999; 9: 48-52.

[13] Boens N, Qin W, Barasic N, Hofkens J, Ameloot M, Pouget J, Lefèvre J, Valeur B, Gratton E, vandeVen M, Silva ND, Engelborghs Y, Willaert K, Silien A, Rumbles G, Phillips D, Visser AJWG, van Hoeck A, Lakowicz JR, Malak H, Gryczynski I, Szabo AG, Krajcarski DT, Tamai N, Miura A. Fluorescence lifetime standards for time and frequency domain fluorescence spectroscopy. Analytical Chemistry 2007; 79: 2137-2149.

[14] Suhling K, French PM, Phillips D. Time-resolved fluorescence microscopy. Photochemical and Photobiological Sciences 2005; 4: 13-22. Analytical Chemistry 2007; 79: 2137-2149.

[15] Vandeven M, Ameloot M, Valeur B, Boens N. Pitfalls and their remedies in time-resolved fluorescence spectroscopy and microscopy. Journal of Fluorescence 2005; 15: 377-413.

[16] Axelrode D. Carbocyanine dye orientation in red cell membrane studied by microscopic fluorescence polarization. Biophysics Journal 1979; 26: 557-573.

[17] Piston DW, Rizzo MA. FRET by fluorescence polarization microscopy. Methods in Cell Biology 2008; 85: 415-430.

[18] Ji W, Liu G, Xu M, Dou X, Feng C. Rational design of coumarin-based supramolecular hydrogelators for cell imaging. Chemical Communications 2014; 50: 15545-15548.

[19] Draper ER, McDonald TO, Adams DJ. Photodimerisation of a coumarin-dipeptide gelator. Chemical Communications 2015; 51: 12827-12830.

[20] Kislukhin AA, Hong VP, Breitenkamp KE, Finn MG. Relative performance of alkynes in copper-catalyzed azide-alkyne cycloaddition. Bioconjugate Chemistry 2013; 24: 684-689.

[21] Aliprandi A, Mauro M, De Cola L. Controlling and imaging biomimetic self-assembly. Nature Chemistry 2016, 8: 10-15.

[22] Sivakumar K, Xie F, Cash BM, Long S, Barnhill HN, Want Q. A fluorogenic 1,3-dipolar cycloaddition reaction of 3-azidocoumarins and acetylenes. Organic Letters 2004; 6: 4603-4606.

[23] Xing B, Yu CW, Chow KH, Ho PL, Fu D, Xu B. Hydrophobic interaction and hydrogen bonding cooperatively confer a vancomycin hydrogel: A potential candidate for biomaterials. Journal of the American Chemical Society 2002, 124: 14846-14847.

[24] Wang C, Zhang D, Xiang J, Zhu D. New organogels based on an anthracene derivative with one urea group and its photodimer: Fluorescence enhancement after gelation. Langmuir 2007; 23: 9195-9200.

[25] Mukherjee A, Chakrabarty R, Ng SW, Patra GK. The synthesis, characterizations, X-ray crystal structures and properties of Cu(I) complexes of a bis-bidentate schiff base ligand. Inorganica Chimica Acta 2010, 363: 1707-1712.

[26] Brege JJ, Gallaway C, Barron AR. Fluorescence quenching of single-walled carbon nanotubes with transition-metal ions. The Journal of Physical Chemistry C 2009; 113: 4270-4276.

[27] Morris KL, Chen L, Raeburn J, Sellick OR, Cotanda P, Paul A, Griffiths PC, King SM, O'Reilly RK, Serpell LC, Adams DJ. Chemically programmed self-sorting of gelator networks. Nature Communications 2013; 4: 1480-1485.

[28] Goktas M, Cinar G, Orujalipoor I, Ide S, Tekinay AB, Guler MO. Self-assembled peptide amphiphile nanofibers and PEG composite hydrogels as tunable ECM mimetic microenvironment. Biomacromolecules 2015; 16: 1247-1258.

5.5. Supporting Information

5.5.1. Gelation Procedures

5.5.1.1. Gel AlkyVal$_6$

The gelator **AlkyVal$_6$** was heated in a 4 mL screw-capped vial in the presence of 400 µL of solvent, until complete dissolution (~30 sec). The resultant hot solution was then sonicated for 1 min, resulting in the formation of a gel which was allowed to stabilize for 20 minutes at room temperature.

5.5.1.2. General procedure for the gels RAzTzVal$_6$

The gelator **RAzTzVal$_6$** was heated at 300 ºC in a 4 mL screw-capped vial in the presence of 400 µL of solvent, until complete dissolution (~2 min). The resultant hot solution was then sonicated for 20 seconds, resulting in the formation of a gel which was allowed to stabilize for 20 minutes at room temperature. For the formation of the metallogels, the gelator was heated together with the copper salt $[Cu(MeCN)_4]PF_6$ in a 2:1 molar ratio, following a similar gelation procedure.

5.5.1.3. Two-component gel HOAzTzVal$_6$/Et$_2$NAzTzVal$_6$

The gelators **HOAzTzVal$_6$** (1.94 mg; $2.2x10^{-3}$ mmol) and **Et$_2$NAzTzVal$_6$** (2.18 mg; $2.2x10^{-3}$ mmol) were heated together at 300 ºC in a 4 mL screw-capped vial in the presence of 400 µL of octanol, until complete dissolution (~2 min). The resultant hot solution was then sonicated for 20 seconds, resulting in the formation of a gel which was allowed to stabilize for 20 minutes at room temperature.

5.5.1.4. Gel Cu(I)-PhTzVal$_6$

The **PhTzVal$_6$** gelator and the copper salt $[Cu(MeCN)_4]PF_6$ in a 2:1 molar ratio were heated together in a 4 mL screw-capped vial in the presence of 400 µL of solvent, until complete dissolution (~1 min). The resultant hot solution was then sonicated for 40 seconds, resulting in a gel which was subsequently allowed to stabilize for 20 minutes at room temperature.

5.5.2. Microscopy Studies

5.5.2.1. Instrumentation

Confocal microscopy was performed on a Picoquant Microtime 200 with two MPD SPADs and a 375 nm pulsed laser diode delivering 90-300 ps pulses at 5 MHz. A 80% T/20% R spectrally flat beam splitter was used in combination with a microscope objective (100x UPLSAPO, NA 1.4), suitable interferential filters, a 50 µm pinhole, and, when specified, a polatizing beam splitter and two Glan-Thompson polarizers. For polarization microscopy, the instrumental G-factor was measured in solution using DDOA for the blue spectral range and diethylamino substituted azidocoumarine soluble analogue for the cyano blue emission range. Typical laser powers of 30 W/cm^2 at 385 nm and ~130 W/cm^2 have been used. Emission spectra were acquired with an Andor SR303i spectrometer equipped with a Newton EMCCD system. The spectra were intensity corrected for instrumental response, measuring suitable reference samples that cover the whole spectral range.

5.5.2.2. General preparation of the samples

The gelator(s) was heated in a 4 mL screw-capped vial in the presence of 400 µL of deoxygenated octanol, until complete dissolution. The resultant hot solution was then sonicated for 15 seconds and 100 µL of the resultant semi-viscous solution was carefully transferred to the sample holder and allowed to age for 20 minutes at room temperature. For the formation of the metallogels, the gelator was heated together with the copper salt $[Cu(MeCN)_4]PF_6$ in a 2:1 molar ratio, following a similar procedure as the one for the native gels.

5.5.2.3. Catalytic experiments

5.5.2.3.1. Reaction system with Cu(I)-PhTzVal$_6$ catalyst

The gelator **PhTzVal$_6$** (1.63 mg; $2.2x10^{-3}$ mmol) and the copper salt $[Cu(MeCN)_4]PF_6$ (0.42 mg; $1.1x10^{-3}$ mmol) were heated together in a 4 mL screw-capped vial in the presence of 400 µL of octanol, until complete dissolution (~1 min). In a separate vial, the **AlkyVal$_6$** (2.7 mg; $5.6x10^{-3}$ mmol) was heated in parallel in a 4 mL screw-capped vial, in the presence of 400 µL of octanol and for a similar period of time. The resultant hot vials were opened and 100 µL of each hot solution were rapidly transferred to the sample holder. After aging for 20 minutes, 100 µL of a $2.93x10^{-2}$

mM dimethylamine-azidocoumarine solution, prepared in 400 µL of octanol, were carefully added at the top of the two-component gel and allowed to react for 16h.

5.5.2.3.2. Reaction system with fluorescent Cu(I)-HOAzTzVal$_6$ catalyst

The first step for the preparation of the reaction system consisted in the formation of the two-component gel **Cu(I)-HOAzTzVal$_6$/AlkyVal$_6$**. Briefly, the gelator **Cu(I)-HOAzTzVal$_6$** (1.91 mg; $2.2x10^{-3}$ mmol) and the copper salt $[Cu(MeCN)_4]PF_6$ (0.42 mg; $1.1x10^{-3}$ mmol) were heated together at 300 ºC in a 4 mL screw-capped vial containing presence of 400 µL of octanol, until complete dissolution (~2 min). The resultant hot solution was sonicated for 15 seconds, giving a semi-viscous solution, from which 100 µL were taken using a 100-1000 µL micropipette and rapidly transferred to a 1 mL syringe equipped with a needle on the bottom and without elbow. The addition was done by the top of the syringe plastic tube and the semi-viscous solution was allowed to stabilize on the tube for 10 minutes until the formation of a gel. In a separate 4 mL screw-capped vial, the reactant **AlkyVal$_6$** (2.7 mg; $5.6x10^{-3}$ mmol) was heated in the presence of 400 µL of octanol until complete dissolution (~30 sec). The resultant hot solution was sonicated for 15 seconds and 100 µL of the remaining semi-viscous solution were rapidly transferred to the top of the previously formed **Cu(I)-HOAzTzVal$_6$** metallogel. After 20 minutes, 2 mL of octanol were added on the top of the resultant two-component metallogel **Cu(I)-HOAzTzVal$_6$/AlkyVal$_6$** and allowed to diffuse through it in order to remove possible uncoordinated copper or unaggregated gelator molecules that could have remained in solution. After washing, the syringe plastic tube was cut and the two-component gel carefully transferred to the sample holder. Finally, 100 µL of a $2.93x10^{-2}$ mM diethylamino-azidocoumarine solution, prepared in 400 µL of octanol, were carefully added to the sample holder and allowed to react for 16h.

5.5.3. General characterization methods

5.5.3.1. Minimum gel concentration

For retrieving the minimum gel concentration, the native gels, or the corresponding metallogels, were formed in 4 mL screw-capped vials in concentrations ranging from 8 mg/mL to 2.5 mg/mL, using 400 µL of the desired solvent. Each gel was formed following the gelation procedure

previously described. The minimum concentration at which the gel withstands gravity upon inversion of the vial was considered as the minimum gelation concentration (m.g.c).

5.5.3.2. Fluorescence spectroscopy

A $5x10^{-6}$ M solution of the desired compound was prepared in degassed octanol and emission spectra acquired at λ_{exc}= 385 nm on a Horia Jobin-Yvon Fluorolog spectrofluorimeter, using a quartz cell with a 1 cm path length.

5.5.3.3. Ultraviolet-Visible Spectroscopy

A $5x10^{-6}$ M solution of the desired compound was prepared in degassed octanol and absorption spectra was measured on a Cary 5000 UV-Vis spectroscope, using a quartz cell with a 1 cm path length.

5.5.3.4. Wide-angle X-ray Diffraction

The obtained gels/metallogels were dried on air or by lyophilization (Telstar LyoQuest), depending on the nature of the gel (organogel or hydrogel), and the resultant powder resuspended in hexane. The suspension was applied into the glass sample holder and the solvent allowed to evaporate. The resultant powdered sample was analysed by X-ray diffraction (XRD) at room temperature using a Bruker D4 Endeavor X-ray powder diffractometer with Cu-K_α radiation. Data were collected for 2θ values between 2 and 40º with a step size of 0.03º and a time step of 10 s.

5.5.3.5. Transmission Electron Microscopy

A small portion of the gel/metallogel was placed on a nickel grid coated with carbon and allowed to dry on air. Images were recorded in a JEOL 2100 microscope.

5.5.4. Synthesis and Characterization

All reagents, starting materials and solvents (p.a. grade) were purchased from commercial suppliers and used as received without further purification. ^{1}H and ^{13}C NMR spectra measurements were recorded in a Varian Mercury 300 MHz spectrometer at 30 ºC.

5.5.4.1. Synthesis of azidocoumarines

The azidocoumarines were synthesized as previously reported,[22] following the reaction schemes represented in **Figure 101**.

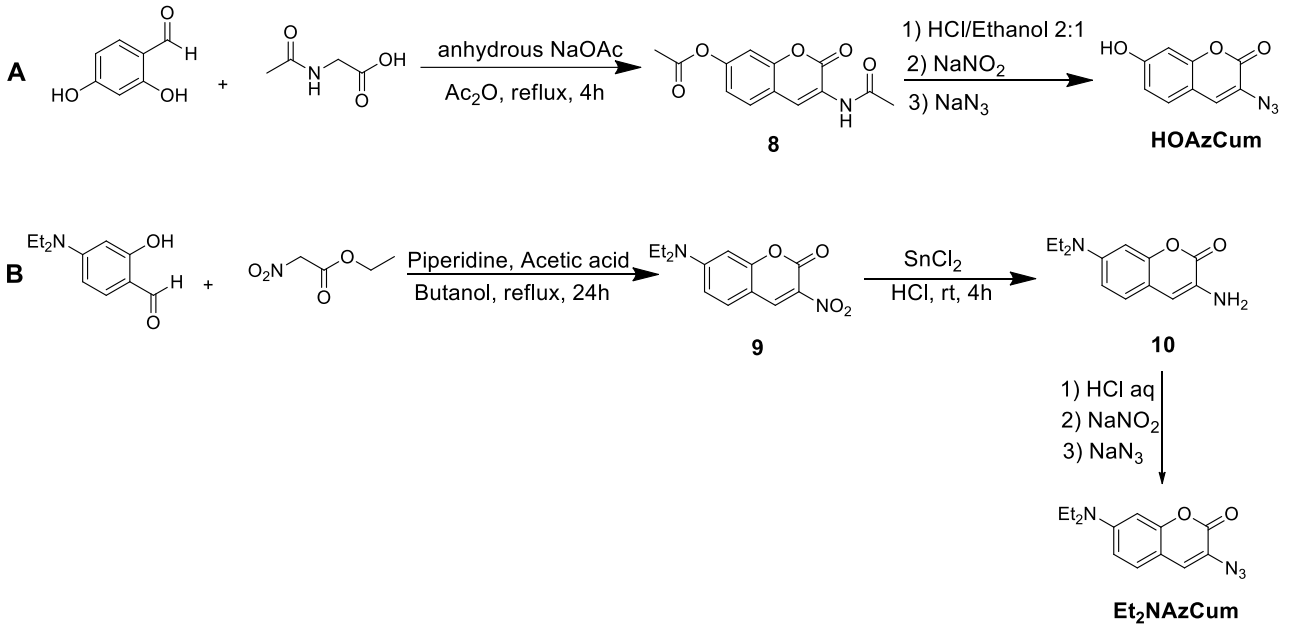

Figure 101. Synthesis of azidocoumarine fragments.

5.5.4.1.1. Synthesis of compound 8

A mixture of 2,4-dihydroxybenzaldehyde (9 g; 65.10 mmol), N-acetylglycine (7.63 g; 65.10 mmol), anhydrous sodium acetate (16.04 g; 196 mmol) in acetic anhydride (18 mL) was refluxed under stirring for 4h. The reaction mixture was poured onto ice to give a yellow precipitate, which was filtered and washed with ice cold water (3x 5 mL). The obtained product was dried under vacuum overnight, giving a pale yellow solid (1.8 g; 11%). Characterization: ^{1}H NMR (300 MHz, d_6-DMSO): δ (ppm) 9.71 (s, Coumarin-N<u>H</u>COCH$_3$, 1H), 8.59 (s, Coumarin-<u>H</u>, 1H), 7.72 (d, *J* = 8.5 Hz, Coumarin-<u>H</u>, 1H), 7.25 (s, Coumarin-<u>H</u>, 1H), 7.11 (d, *J* = 7.4 Hz, Coumarin-<u>H</u>, 1H), 2.28 (s, C<u>H</u>$_3$COO-Coumarin, 3H), 2.15 (s, Coumarin-NHCOC<u>H</u>$_3$, 3H).

5.5.4.1.2. Synthesis of compound HOAzCum

Compound **8** (1.785 g; 6.83 mmol) was refluxed in a mixture 2:1 conc. HCl:EtOH (100 mL) for 1h. Then, ice cooled water (130 mL) was added to dilute the solution, which was cooled in an ice bath before the addition of $NaNO_2$ (0.94 g; 13.66 mmol). After stirring for 10 min, NaN_3 (1.34 g; 20.58 mmol) was carefully added in portions. After stirring for more 15 min, the resulting precipitate was filtered, washed with water, and dried under vacuum to afford a brown solid (1.09 g; 75%). Characterization: ^{1}H NMR (300 MHz, d_6-DMSO): δ (ppm) 10.49 (s, HO-Coumarin, 1H), 7.57 (s, Coumarin-H, 1H), 7.46 (d, *J* = 8.5 Hz, Coumarin-H, 1H), 6.78 (m, Coumarin-H, 2H).

5.5.4.1.3. Synthesis of compound 9

A mixture containing n-butanol (84 mL), 4-diethylamino salicylaldehyde (6 g; 31.05 mmol), ethyl nitroacetate (4.13 g; 31.05 mmol; 3.45 mL), molecular sieves 4 Å (1 g), piperidine (0.37 g; 4.32 mmol) and acetic acid (0.86 mL) was refluxed for a period of 48h. Upon cooling to room temperature, a bright yellow solid formed, which was collected and dissolved in DMF (10 mL) at 80 ºC, and filtered again to remove the molecular sieves. Upon addition of ice to the filtrate, a precipitate formed, which was washed with cold n-butanol (10 mL) and water (20 mL) to give the product as a bright yellow solid (4.68 g; 58%). Characterization: ^{1}H NMR (300 MHz, $CDCl_3$): δ (ppm) 8.71 (s, Coumarin-H, 1H), 7.43 (d, *J* = 9.1 Hz, Coumarin-H, 1H), 6.70 (m, Coumarin-H, 1H), 6.48 (d, *J* = 2.4 Hz, Coumarin-H, 1H), 3.50 (q, *J* = 7.2 Hz, $(CH_2CH_3)_2N$-, 4H), 1.27 (t, *J* = 7.2 Hz, $(CH_2CH_3)_2N$-, 6H).

5.5.4.1.4. Synthesis of Compound 10

In a 25 mL round bottom flask equipped with a magnetic stirrer, were placed in order, 37% HCl (95 mL) and stannous chloride (25.1 g; 32.4 mmol). To this suspension, compound **9** (4.67 g; 17.84 mmol) was added at room temperature in small portions and over a period of 30 min. Stirring was continued for 4h, before the solution was poured onto ice and made alkaline with a 5M NaOH solution, at 15 ºC using an ice bath. The resultant suspension was extracted with diethyl ether (2 x 50 mL) the organic layer was washed with water (100 mL), dried over anhydrous NaSO4 and concentrated to a pasty residue, which upon triturating using hexane yielded the desired product as a pale yellow solid (3.31 g; 80%). Characterization: ^{1}H NMR (300 MHz, $CDCl_3$): δ (ppm) 7.11 (d, *J* = 8.6 Hz, Coumarin-H, 1H), 6.69 (s, Coumarin-H, 1H), 6.56 (m, Coumarin-H, 2H), 3.85 (br s,

Coumarin-N$\underline{H}_2$, 2H), 3.37 (q, *J* = 7.1 Hz, (C$\underline{H}_2$CH$_3$)$_2$N-, 4H), 1.18 (t, *J* = 7.1 Hz, (CH$_2$C$\underline{H}_3$)$_2$N-, 6H).

5.5.4.1.5. Synthesis of Et$_2$NAzCum

Compound **10** (2.02 g; 8.70 mmol) was slowly dissolved in HCl aq. (17%; 78 mL) at room temperature. Upon cooling to 0-5 ºC and addition of $NaNO_2$ (0.6 g; 8.70 mmol), the reaction mixture was stirred for 1 h maintaining the same temperature. This was followed by the addition of NaOAc (40 g; 48.76 mmol) dissolved in water (100 mL) to adjust the pH of the resulting solution to 4. Sodium azide (1.16 g; 17.83 mmol) was added in portions at 0-5 ºC and the mixture stirred for another 5h maintaining the same temperature. The precipitated product was then filtered, washed with ice cold water (20 mL) and dried under vacuum. The resultant green solid was purified by preparative thin-layer chromatography (CH_2Cl_2) giving a yellow solid (2.01 g; 89%). Characterization: ^{1}H NMR (300 MHz, $CDCl_3$): δ (ppm) 7.19 (d, *J* = 8.8 Hz, Coumarin-$\underline{H}$, 1H), 7.10 (s, Coumarin-$\underline{H}$, 1H), 6.59 (d, *J* = 8.8 Hz, Coumarin-$\underline{H}$, 1H), 6.51 (s, Coumarin-$\underline{H}$, 1H), 3.85 (br s, Coumarin-N$\underline{H}_2$, 2H), 3.41 (q, *J* = 7.1 Hz, (C$\underline{H}_2$CH$_3$)$_2$N-, 4H), 1.21 (t, *J* = 7.1 Hz, (CH$_2$C$\underline{H}_3$)$_2$N-, 6H).

5.5.4.2. Synthesis of RAzTzVal$_6$ gelators

The synthetic route to obtain the **RAzTzVal$_6$** fluorescent gelators is represented in **Figure 102**.

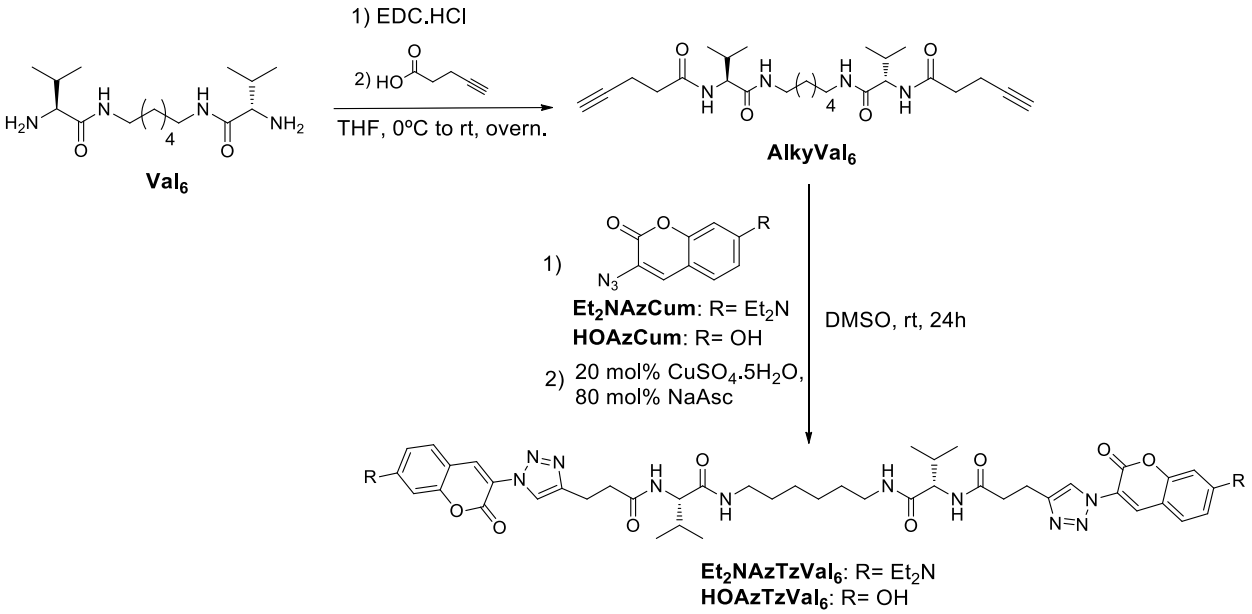

Figure 102. Scheme for the synthesis of **RAzTzVal$_6$** gelators.

5.5.4.2.1. Synthesis of compound AlkyVal$_6$

A suspension of 4-pentynoic acid (1.09g; 11.14 mmol) and EDC.HCl (2.14 g; 11.14 mmol) in THF (40 mL) was allowed to stir for 20 min at room temperature. After cooling to 0 ºC, the mixture was treated dropwise with a solution of compound 2 (1.4 g; 4.45 mmol) in THF (20 mL) and allowed to stir for 1h30 at room temperature. The resultant mixture was concentrated in the rotavapor and the precipitate filtered, washed with 0.1 M NaOH (15 mL) and water (30 mL), giving a white solid (1.82 g; 86%). Characterization: ^{1}H NMR (300 MHz, d_6-DMSO): δ (ppm) 7.83 (m, -CON<u>H</u>CH + -CON<u>H</u>CH$_2$, 2H), 4.09 (t, *J* = 7.6 Hz -CONHC<u>H</u>, 1H), 2.04 (m, -CONHC<u>H$_2$</u>, 2H), 2.70 (s, C<u>H</u>CCH$_2$CH$_2$CH$_2$-, 1H), 2.33 (m, CHCC<u>H$_2$</u>C<u>H$_2$</u>-, 4H), 1.90 (m, C<u>H</u>(CH$_3$)$_2$, 1H), 1.35 (m, -CH$_2$C<u>H$_2$</u>CH$_2$, 2H), 1.23 (br s, -CH$_2$CH$_2$C<u>H$_2$</u>, 2H), 0.81 (d, *J* = 6.7 Hz, -CH(C<u>H$_3$</u>)$_2$, 6H). ^{13}C (75 MHz, d_6-DMSO): δ (ppm) 171.15, 170.69, 84.27, 71.66, 58.22, 34.39, 30.93, 29.41, 26.43, 19.63, 18.69, 14.73. ESI-MS (m/z) = 497.3104 $[M+Na]^+$; $C_{26}H_{42}N_4O_4$. Calculated for $C_{26}H_{42}N_4O_4$: 497.3104.

5.5.4.2.2. Synthesis of Et$_2$NAzTzVal$_6$

To a solution of **AlkyVal$_6$** (0.35 g; 0.74 mmol) and **Et$_2$NAzCum** (0.42 g; 1.62 mmol) in DMSO (55 mL) were added $CuSO_4 \cdot 5H_2O$ (0.036 g; 0.15 mmol) and sodium ascorbate (0.117 g; 0. 59 mmol). After stirring for 24h at room temperature, the mixture was poured with ice. The resultant precipitate was filtered, washed with cold CH_2Cl_2 (2x 10 mL) and dried under vacuum. The product was then filtered in alumina type II and eluted with 50:50 AcOEt: MeOH, yielding a green solid (0.69 g; 96%). Characterization: ^{1}H NMR (300 MHz, d_6-DMSO): δ (ppm) 8.38 (s, triazole-<u>H</u>, 1H), 8.23 (s, Coumarin-<u>H</u>, 1H), 7.88 (m, -CON<u>H</u>CH + -CON<u>H</u>CH$_2$, 2H), 7.60 (d, *J* = 9.1 Hz, Coumarin-<u>H</u>, 1H), 6.80 (d, *J* = 9.2 Hz, Coumarin-<u>H</u>, 1H), 6.63 (s, Coumarin-<u>H</u>, 1H), 4.08 (**t**, *J* = 7.6 Hz, -CONHC<u>H</u>, 1H), 3.43 (m, (C<u>H$_2$</u>CH$_3$)$_2$N- + triazole-C<u>H$_2$</u>CH$_2$CH$_2$, 6H), 2.97 (m, triazole-C<u>H$_2$</u>CH$_2$ + -CONHC<u>H$_2$</u>, 4H), 2.59-2.57 (m, triazole-CH$_2$C<u>H$_2$</u>, 2H), 1.89 (m, -C<u>H</u>(CH$_3$)$_2$, 1H), 1.33 (m, -CH$_2$C<u>H$_2$</u>CH$_2$, 2H), 1.13 (t, *J* = 6.9 Hz, (CH$_2$C<u>H$_3$</u>)$_2$N- + -CH$_2$CH$_2$C<u>H$_2$</u>, 8H), 0.77 (d, *J* = 5.0 Hz, -CH(C<u>H$_3$</u>)$_2$, 6H). ^{13}C (75 MHz, d_6-DMSO): δ (ppm) 171.58, 171.23, 157.09, 155.99, 146.60, 136.83, 123.26, 116.73, 110.42, 106.90, 96.76, 58.31, 34.80, 30.75, 29.42, 26.42, 21.77, 19.60, 18.61, 12.74. ESI-MS (m/z) = 991.5527 $[M+H]^+$; $C_{42}H_{60}N_{10}O_4$. Calculated for $C_{42}H_{60}N_{10}O_4$: 991.5518.

5.5.4.2.3. Synthesis of HOAzTzVal$_6$

To a solution of **AlkyVal$_6$** (0.5 g; 1.05 mmol) and **HOAzCum** (0.45 g; 2.21 mmol) in DMSO (80 mL), were added $CuSO_4.5H_2O$ (0.051 g; 0.21 mmol) and sodium ascorbate (0.167 g; 0.84 mmol). After stirring for 24h at room temperature, the resulting mixture was poured onto ice. The precipitate was filtered, washed with cold ethyl acetate (2 x 5mL) and dried under vacuum. The product was then purified by column chromatography (90:10 to 50:50 AcOEt: MeOH), yielding a green solid (0.85 g; 93%). Characterization: ^{1}H NMR (300 MHz, d_6-DMSO): δ (ppm) 8.43 (s, triazole-H, 1H), 8.23 (s, Coumarin-H, 1H), 7.88 (m, -CONHCH + -CONHCH$_2$, 2H), 7.62 (d, *J* = 8.6 Hz, Coumarin-H, 1H), 6.77 (d, *J* = 8.3 Hz, Coumarin-H, 1H), 6.67 (s, Coumarin-H, 1H), 4.08 (t, *J* = 7.6 Hz, -CONHCH, 1H), 3.03-2.90 (m, triazole-CH$_2$CH$_2$ + -CONHCH$_2$, 4H), 2.58 (m, triazole-CH$_2$CH$_2$, 2H), 1.89 (m, -CH(CH$_3$)$_2$, 1H), 1.31 (m, -CH$_2$CH$_2$CH$_2$, 2H), 1.17 (br s, -CH$_2$CH$_2$CH$_2$, 2H), 0.78 (d, -CH(CH$_3$)$_2$, 6H). ^{13}C (75 MHz, d_6-DMSO): δ (ppm) 171.57, 171.21, 156.90, 155.58, 146.65, 136.67, 131.30, 123.32, 118.05, 109.29, 102.50, 58.28, 34.78, 30.76, 29.39, 26.41, 21.75, 19.60, 18.60. ESI-MS (m/z) = 903.3781 $[M+Na]^+$; $C_{44}H_{52}N_{10}O_{10}$. Calculated for $C_{44}H_{52}N_{10}O_{10}$: 903.3766.

5.5.4.3. Synthesis of the azidocoumarine soluble analogue for the determination of g-factor

The synthetic route to obtain the non-aggregating molecule for determination of g-factor is represented in **Figure 103**.

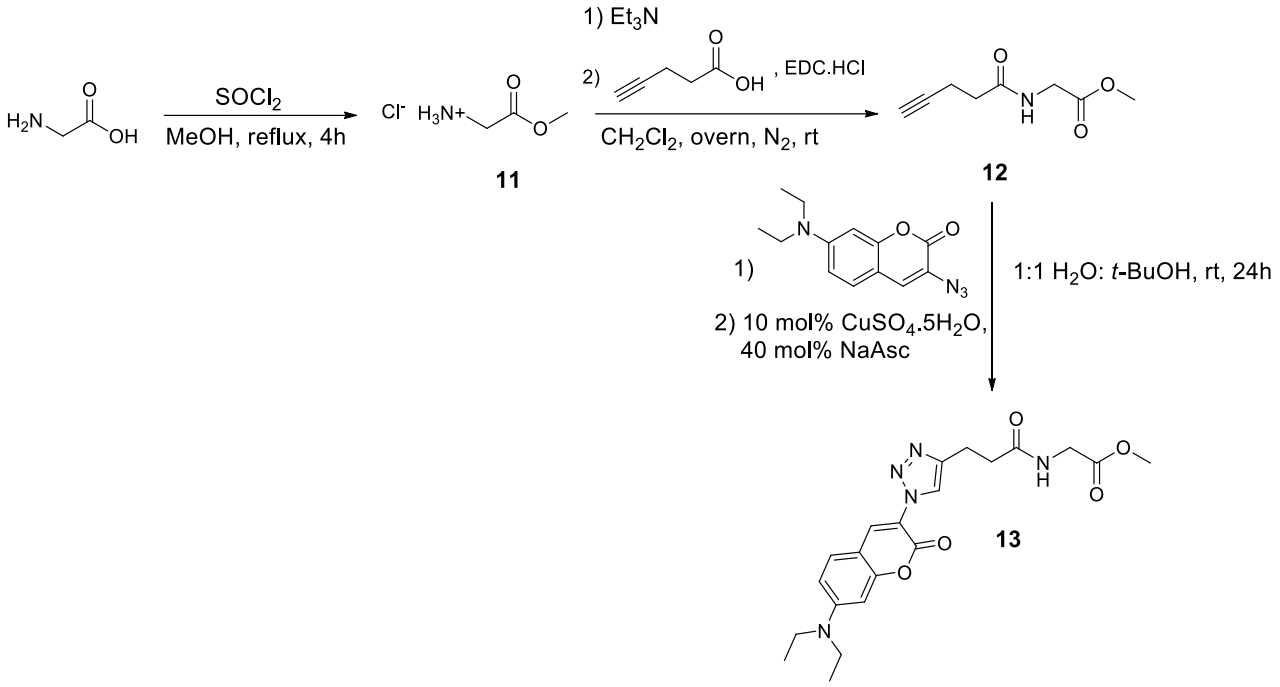

Figure 103. Synthesis of soluble molecule for determination of g-factor.

5.5.4.3.1. Synthesis of compound 11

A suspension of glycine (5 g; 66.6 mmol) in anhydrous methanol (67 mL) was treated dropwise with $SOCl_2$ (9.51 g; 79.93 mmol; 5.81 mL) at 0 ºC under N_2. After stirring at 0ºC for 15 minutes, the mixture was heated at 65 ºC and allowed to react for 4h under N_2. After completion of the reaction (TLC $CHCl_3$:MeOH 8:2), the solvents were evaporated on the rotavapor. The residue was then dissolved in MeOH (30 mL) and the solvent evaporated on the rotavapor. After repeating this last procedure for four times, the resultant product was washed with diethyl ether (10 mL) and dried under vacuum, giving a white solid (8.14 g; 98%). ^{1}H NMR (300 MHz, d_6-DMSO): δ (ppm) 8.59 (s, $N\underline{H}_3^+$, 3H), 3.77 (s, $C\underline{H}_2CO$, 2H), 3.63 (s, $COOC\underline{H}_3$, 3H).

5.5.4.3.2. Synthesis of compound 12

A suspension of 4-pentynoic acid (1.2 g; 12.23 mmol) and EDC.HCl (2.345 g; 12.23 mmol) in THF (20 mL) was allowed to react for 20 min at room temperature under N_2. The reaction was then cooled to 0 ºC and treated dropwise with a solution of **11** (1.28 g; 10.20 mmol) and trimethylamine (4.54 g; 44.86 mmol; 6.26 mL) in THF (10 mL). After 16h stirring at room temperature, the crude was concentrated on the rotavapor and the precipitate washed with 0.1 M NaOH (2 x 10 mL), water

(2 x 20 mL) and 0.1 M HCl (1 x 10 mL), and dried under vacuum to yield a white solid (0.38 g; 22%). Characterization: ^{1}H NMR (300 MHz, $CDCl_3$): δ (ppm) 6.25 (br s, -CONH, 1H), 4.04 (d, *J* = 5.0 Hz, -CONHCH_2CO, 2H), 3.73 (s, COOCH_3, 3H), 2.47 (m, -CH_2CH_2CO, 4H), 1.98 (**s**, CHCCH_2, 1H). ^{13}C (75 MHz, $CDCl_3$): δ (ppm) 171.13, 170.39, 82.74, 69.41, 52.43, 41.26, 34.93, 14.65. ESI-MS (m/z) = 245.1400 $[M+H]^+$; $C_8H_{11}NO_3$. Calculated for $C_8H_{11}NO_3$: 245.1402

5.5.4.3.3. Synthesis of compound 13

To a solution of **12** (0.065 g; 0.38 mmol) in 3:1 *t*-BuOH:H_2O (4 mL) were added **Et$_2$NAzCum** (0.104 g; 0.40 mmol), $CuSO_{4.5}H_2O$ (0.019 g; 0.077 mmol) and sodium ascorbate (0.054 g; 0.306 mmol), and the resultant mixture allowed to stir for 24h at room temperature. The crude mixture was concentrated in the rotavapor before the addition of EtOAc (10 mL). The organic phase was washed with a saturated solution $NaHCO_3$ (3 x 5 mL) and brine (2 x 5 mL). The organic extractions were dried over anhydrous $MgSO_4$ and the solvents removed on the rotavapor. The obtained solid was washed with cold diethyl ether (5 mL) and dried under vacuum. Characterization: ^{1}H NMR (300 MHz, d_6-DMSO): δ (ppm) 8.44 (br s, triazole-H + -CONHCH_2, 2H), 8.28 (s, Coumarin-H, 1H), 7.63 (d, *J* = 8.8 Hz, Coumarin-H, 1H), 6.83 (d, *J* = 8.1 Hz, Coumarin-H, 1H), 6.67 (s, Coumarin-H, 1H), 3.86 (d, *J* = 5.6 Hz, -CONHCH_2CO, 2H), 3.63 (s, -COOCH_3, 3H), 3.49 (m, (CH_2CH_3)$_2$N-, 4H), 2.95 (t, *J* = 7.2 Hz, Triazole-CH_2, 2H), 2.59 (t, *J* = 7.5 Hz, Triazole-CH_2CH_2, 2H), 1.15 (**s**, (CH_2CH_3)$_2$N-, 6H). ^{13}C (75 MHz, d_6-DMSO): δ (ppm) 172.16, 170.93, 157.19, 156.05, 151.83, 146.45, 136.99, 130.94, 123.34, 116.82, 110.45, 106.97, 96.82, 52.13, 44.68, 34.74, 21.52, 12.77. ESI-MS (m/z) = 428.1929 $[M+H]^+$; $C_{21}H_{25}N_5O_5$. Calculated for $C_{21}H_{25}N_5O_5$: 428.1934.

Chapter 6

A Dynamic Catalytic Self-assembled System

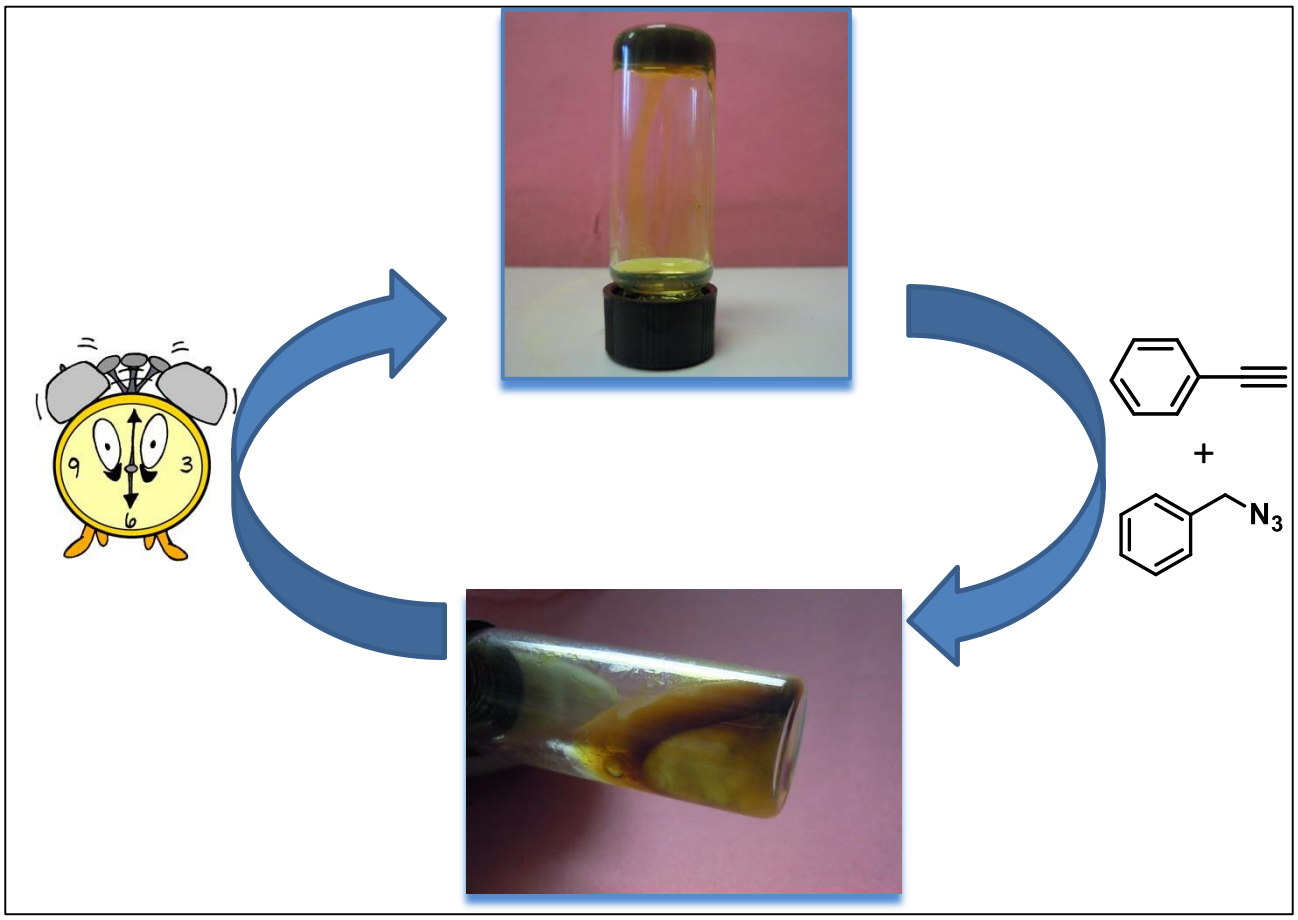

In this chapter, a catalytic self-assembled system for the model 'click' reaction is presented. The conditions required to promote displacement of the system out of the equilibrium were investigated, as well as the consequent catalytic activity. Focusing on a greener approach of the use of heterogeneous catalysts, the recyclability of the catalytic system has also been investigated.

6.1. Introduction

Materials found in nature combine many inspiring properties such as sophistication, miniaturization, hierarchical organization, hybridization, resistance and adaptability. Hierarchical constructions on a scale ranging from nanometres, micrometres to millimetres are characteristic of biological structures and allow them to answer physical and chemical demands imposed by the environment.[1]

Self-assembly has always been regarded as nature's preferred way to build these three dimensional complex materials. DNA strands self-assemble into a double helix that stores genetic information, several proteins organize into multiprotein complex which enable transcription, translation, TNA splicing, signalling, exocytosis, RNA interference, and numerous other cellular processes; cellular membranes self-assemble from phospholipids, cholesterol, glycolipids, and protein building blocks to delineate cell's boundary, cells spontaneously organize into tissues, bacteria into colonia and higher organisms into swarms, schools or flocks.[2]

A clear example of nature's adaptability is the ability of living systems to change their structures in response to changing situations, mainly through molecular assembly and disassembly via competing catalytic pathways and under the influence of chemical fuels.[3] In real cells, tissues and organisms, self-assembly builds dynamic aggregates that change and function only if energy is delivered to them, either chemical or by external fields. Thus, it is worthwhile to say that most biological forms of adaptive or intelligent behaviour are based on dynamic self-assembly (DYSA) processes, where the mode of organization is intimately related with the amount of energy supplied to the system.[2]

Unlike most traditional materials, which are locked into global or local thermodynamic minima, dynamic materials should be displaced from the equilibrium and be able to reside in multiple metastable states between which they could be interconverted.[4] Although metastable and dynamic aggregates are both considered out-of-equilibrium self-assembled structures, one distinguishes from the other due to their capacity of assembling into temporarily ordered structures, whose lifetime is monitored by a continuous supply and dissipation of energy.[5] For a more chemically precise definition, it can be considered that metastable structures are static and kinetically trapped, existing because the available thermal energy is not sufficient to overcome the activation barrier required to transform them into the most thermodynamically stable state. On the other hand, dissipative structures are dynamic and require the active and continuous input of energy to push the system out of equilibrium.[6,7]

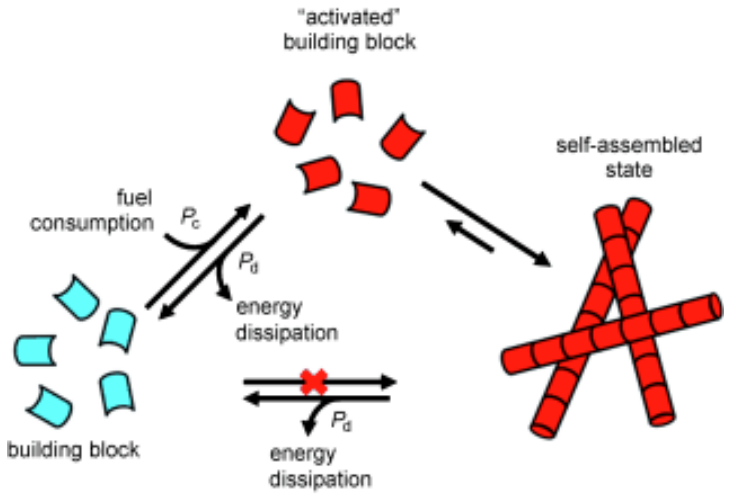

Figure 104. Schematic representation of dissipative self-assembly.[9]

The most famous example of this kind of dissipative structures in nature is the microtubules formed by tubulin dimers activated by the interaction with guanosine-5'-triphosphate (GTP). These activated building blocks are hydrolysed over time to guanosine diphosphate (GDP), resulting in microtubule collapse. Upon depolymerisation, the released tubulin units can exchange GDP by GTP (energy source), undergoing another round of polymerization. This specific behaviour allows this cytoskeletal polymer to be highly dynamic, capable of polymerizing, depolymerizing and moving within the cytoplasm on a time scale from seconds to minutes.[8]

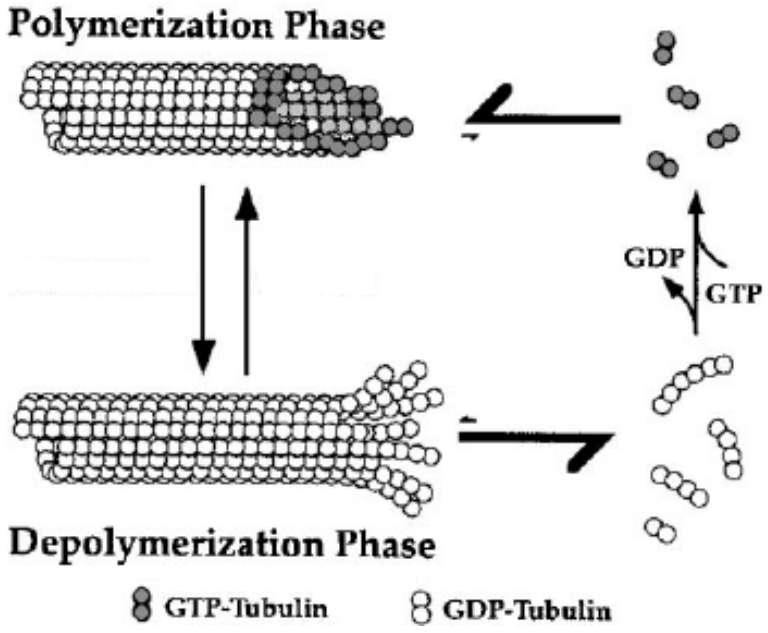

Figure 105. Tubulin microtubule dynamic instability.

Active self-assembled materials such as actin networks and microtubules distinguish themselves from equilibrium self-assembled materials by their ability to use free energy provided by the

conversion of fuel to achieve transient structure formation and carry out work, being their behaviour controlled by kinetics of fuel consumption rather than thermodynamic stability. The development of dynamic materials may provide a range of functions that are not obtained in static, equilibrium materials, such as multifunctionality, adaptability, reconfigurability and self-repairing.[4] Attracted by the multiple properties of these kinds of systems, scientists used nature as a school to try to develop similar artificial dynamic systems.

A very interesting example of this kind of artificial dissipative self-assembled systems was reported by van Esch and co-workers, who presented the first example of a molecular gel that is temporarily formed by dynamic self-assembly and using a chemical fuel.[9] The dissipative self-assembly system was based on dibenzoyl-(*L*-)-cystine (DBC), which assembles in elongated fibres when the pH of the medium is below its *pKa* (~ 4.5), and in DBC-dimethyl ester, which is known to self-assemble independently of the pH. The addition of methyl iodide to the reaction medium at pH= 7 and 35 ºC promoted the alkylation of DBC, converting the water soluble dicarboxylate into the corresponding dimethyl ester, activating the self-assembly process (**Figure 106**).

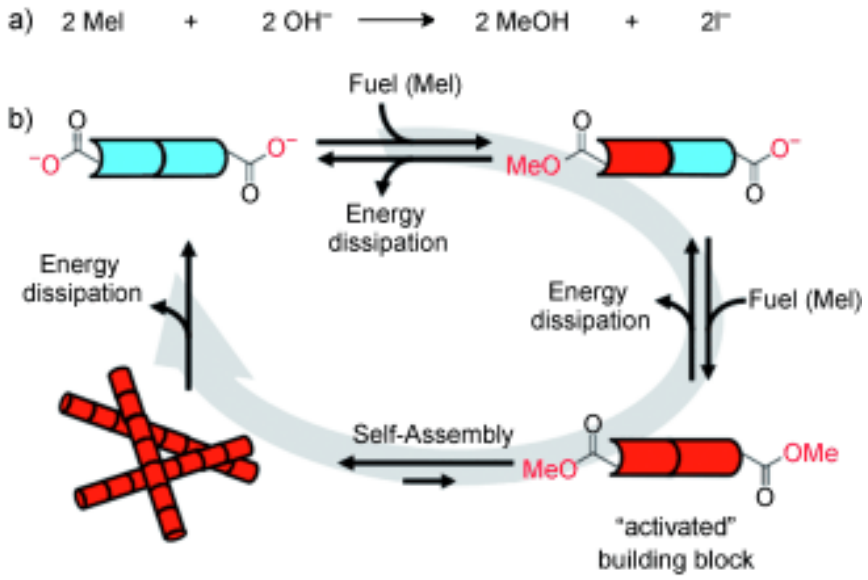

Figure 106. Reaction cycle of the dissipative system.[9]

However, upon consumption of the fuel, the system is hydrolysed back to the diacid in an energy-dissipating step, returning to its thermodynamically stable non-aggregating state. In a relatively similar dynamic self-assembled system, the same authors used dimethylsulfate (DMS) as fuel to promote the alkylation, and consequent gelation, of carboxylate functionalized molecules.[10] The authors observed that parameters such as lifetime, stiffness and regenerative behaviour of the gels could be tuned by the kinetics of fuel consumption.

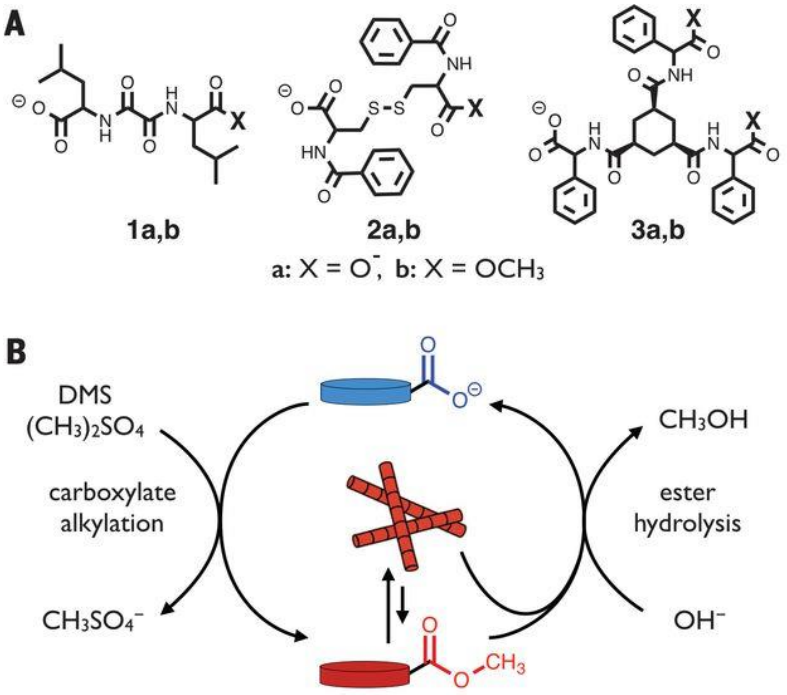

Figure 107. (A): Chemical structure of tested gelators **1**, **2** and **3**. (B): Reaction cycle of dissipative self-assembled system.[10]

In this chapter, a dynamic catalytic system has been developed using an amphiphilic gelator functionalized with an azidocoumarine fragment. The difference in respect to the abovementioned dissipative self-assembled systems is that the gelator is able to transform into a different physical state without suffering any chemical modification on its structure. The dynamic behaviour of this system is supported by the model 'click' reaction between benzylazide and phenylacetylene, where the reactants act as fuels by promoting the disassembly of the gel. In addition, the transient disassembly behaviour of the system provide the gelator with temporary high catalytic activity towards the model 'click' reaction.

6.2. Results and Discussion

6.2.1. Design and Synthesis

The *L*-valine azidocoumarinetriazolyl (**Et$_2$NAzTzVal$_n$**) amphiphilic gelators have been synthesized in a similar way to the bolaamphiphilic fluorescent gelators presented in **Chapter 5**, but using propyl or dodecylamine instead of an alkylidenediamine. Briefly, the synthetic procedure involved simple peptide coupling of the pentynoic acid to propyl or dodecylamine, using EDCI·HCl as a coupling agent. The obtained alkyne *L*-valine derivative was then coupled to the synthesized

azidocoumarines through a copper catalysed azide-alkyne cycloaddition, resulting in the compounds **Et$_2$NAzTzVal$_3$** and **Et$_2$NAzTzVal$_{12}$**.

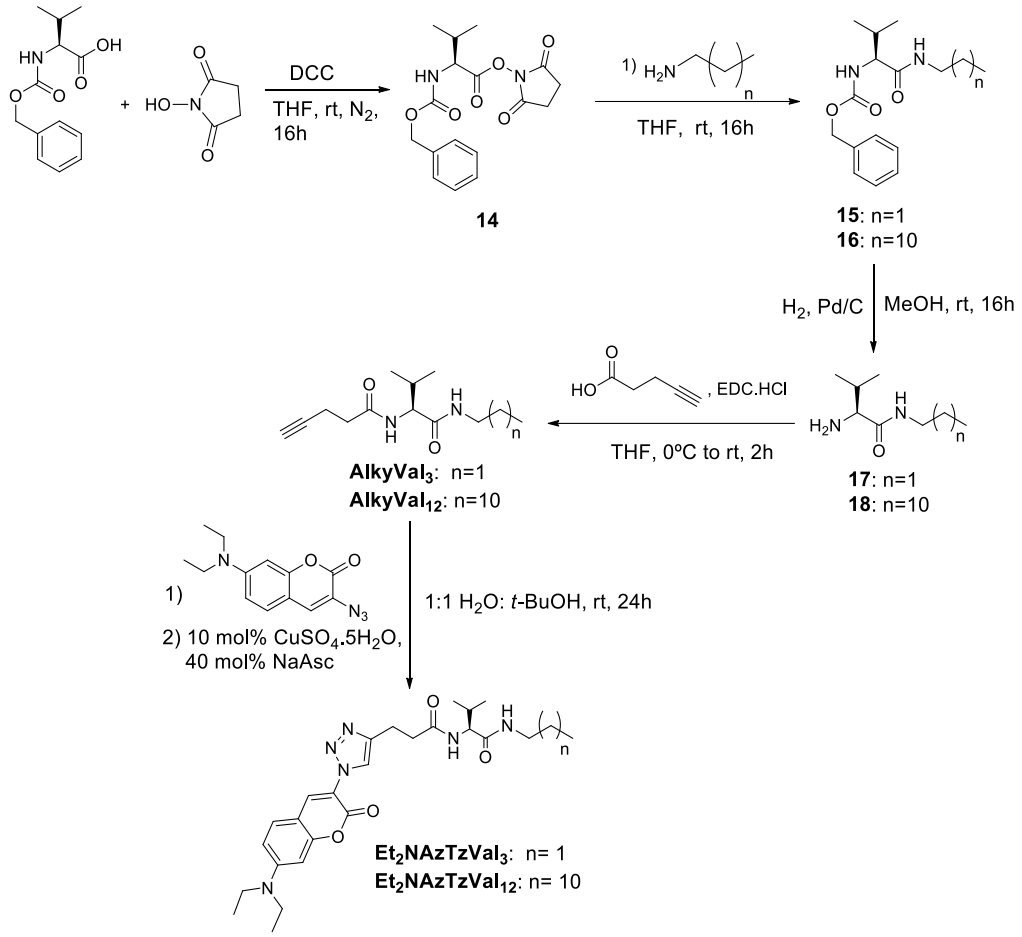

Figure 108. Synthesis of the amphiphilic gelators **Et$_2$NAzTzVal$_n$**.

6.2.2. Self-assembly behaviour

The ability of the amphiphilic compounds **Et$_2$NAzTzVal$_3$** and **Et$_2$NAzTzVal$_{12}$** to form gels was evaluated in the typical solvent mixture for 'click' reactions 1:1 H_2O:*t*-BuOH and in high boiling point alcohols (**Table 18**).

Table 18. Gelation experiments of compounds **Et$_2$NAzTzVal$_n$**[a].

Solvent	Et$_2$NAzTzVal$_3$	Et$_2$NAzTzVal$_{12}$	Aspect
n-BuOH	S	S	-
H_2O:*t*-BuOH (1:1)	S	G	Opaque
t-BuOH	S	S	-
Octanol	S	S	-

[a] S: Soluble, G: Gel; *c* = 8 mg/mL.

The obtained results suggest that the amphiphilic compounds exhibit a considerably lower gelation performance than the bolaamphiphilic gelators studied in **Chapters 3** and **5**, which were able to form gels or aggregates in the majority the tested solvents. These results were quite expected, since the symmetrical bolaamphiphilic compounds have twice as many amide bonds in comparison with the amphiphilic ones, favouring the gelation by intermolecular H bonding between amide groups. However, it is important to highlight the successful gelation of the amphiphilic compound **Et$_2$NAzTzVal$_{12}$** in the typical solvent for 'click' reactions 1:1 H_2O:*t*-BuOH. The absence of one extra amide bond in this amphiphilic compound is compensated by the presence of a long carbon chain in its structure, which promotes gelation by hydrophobic interactions. The absence of such long carbon tail in the compound **Et$_2$NAzTzVal$_3$** resulted in an increased solubility observed in all the tested solvents.

The minimum gel concentrations of the compound **Et$_2$NAzTzVal$_{12}$** and of the corresponding metallogel **Cu(I)-Et$_2$NAzTzVal$_{12}$**, were found to be 10.7 mM and 7.1 mM in the mixture 1:1 H_2O:*t*-BuOH. The lower m.g.c. registered in the presence of the metal suggest some contribution from the metal centre on the gelation process, although it is not the main driving force for gelation. The compound **Et$_2$NAzTzVal$_3$** was discarded from these studies due to its inability to form gels.

6.2.3. Structural and morphologic characterization of the gels

The structural arrangement of the gel **Et$_2$NAzTzVal$_{12}$** and of the corresponding metallogels was accessed by wide angle x-ray diffraction (WAXD).

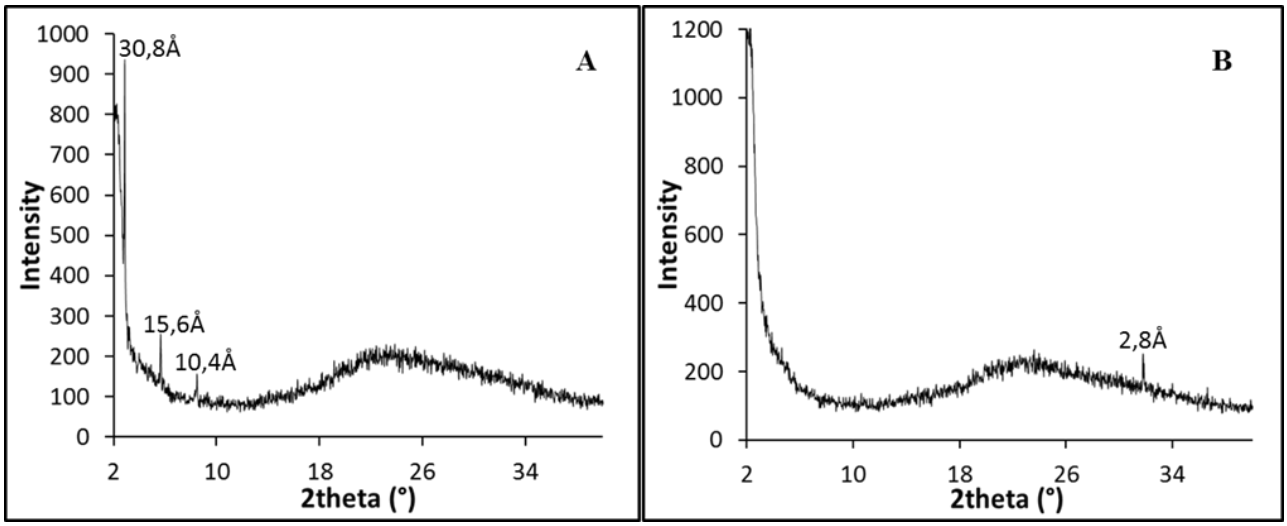

Figure 109. WAXD of gels **Et$_2$NAzTzVal$_{12}$** (A) and **Cu(I)-Et$_2$NAzTzVal$_{12}$** (B).

The molecules of the amphiphilic gelator **Et$_2$NAzTzVal$_{12}$** seem to follow a semi-amorphous packing during the self-assembly process, guiding to a final structural arrangement exhibiting some

short-range order and periodicity. This is particularly evidenced by the appearance of peaks around 2θ= 2º, 5º and 7º, suggesting the presence of repeating units at distances 30.8Å, 15.6Å and 10.4Å that may correspond to side-to-side (horizontal) repetition of piles of **Et$_2$NAzTzVal$_{12}$** molecules, whose self-assembly is supported by intermolecular hydrogen bonding between the different amide groups (**Figure 109A** and **Figure 110**). Such type of self-assembly resembles the one proposed in a recent publication for the analogue gelator functionalized with a *L*-proline fragment.[11]

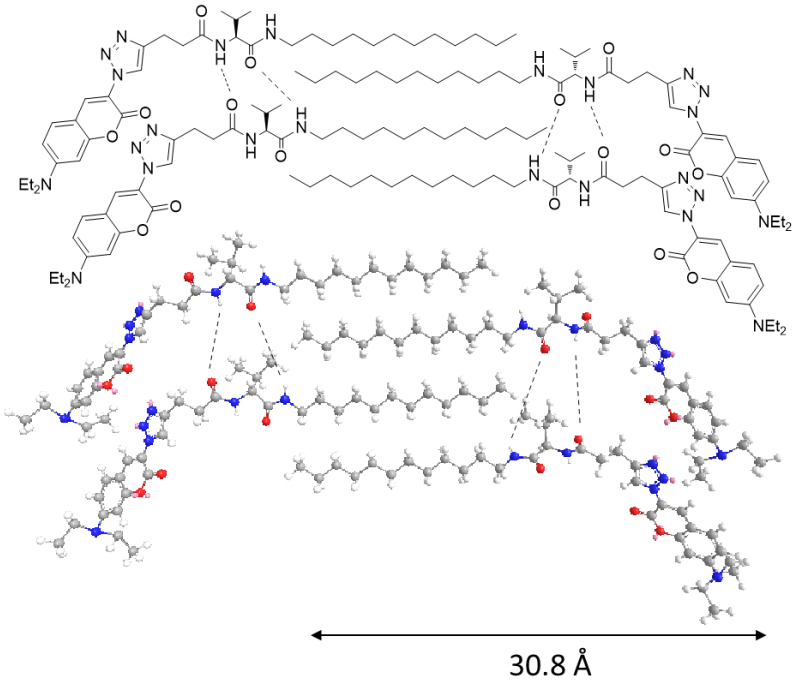

Figure 110. Proposed molecular packing for the gelator **Et$_2$NAzTzVal$_{12}$**.

However, in the case of the metallogel **Cu(I)-Et$_2$NAzTzVal$_{12}$,** the presence of the metal appears to introduce some disorder in the self-assembling process, probably due to the required organization of four molecules of **Et$_2$NAzTzVal$_{12}$** near the metal centre to form a tetrahedral coordination complex (**Figure 109B**).

Further insights on the structural arrangement of the amphiphilic gelator **Et$_2$NAzTzVal$_{12}$** in absence and in the presence of copper(I) were obtained by circular dichroism spectroscopy. The obtained spectra showed that the presence of copper(I) did not introduce remarkable conformational changes on the resultant gel. Both **Et$_2$NAzTzVal$_{12}$** and **Cu(I)-Et$_2$NAzTzVal$_{12}$** gelators are characterized by the presence of a positive band around λ= 370 nm, followed by a negative band at λ= 230 nm (**Figure 111**). In the gel without metal, this band is splitted into another minimum at λ= 215 nm and followed by a negative band at λ= 195 nm.

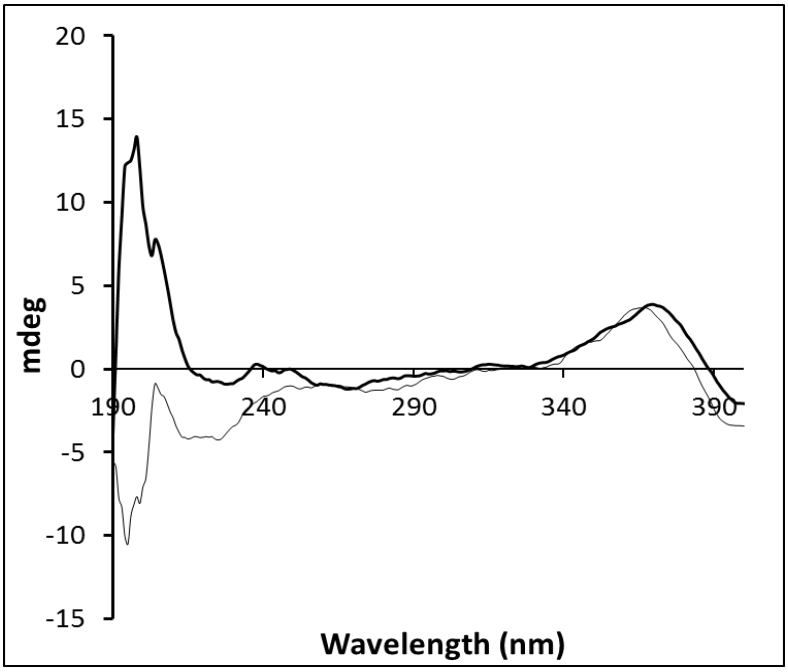

Figure 111. Circular dichroism spectra of the gel **Et$_2$NAzTzVal$_{12}$** (grey) and of the corresponding metallogel **Cu(I)-Et$_2$NAzTzVal$_{12}$** (black).

When copper(I) is present, it is possible that the coordination geometry of the metal center induce a twist into the fiber orientation, self-assembling in a structure that resembles the double-helix with characteristic negative band at λ= 230 nm followed by an intense positive lobe at λ= 195 nm.[12] This twisted morphology of the metallogel fibres is also supported by the corresponding TEM pictures, acquired without staining the samples (**Figure 112C-D**).

The relatively similar morphology between the fibres belonging to the pure gel and the ones of the corresponding metallogel is in good agreement with the WAXD analysis, where it has been observed that the presence of the metal has not induced critical changes in the structural arrangement of the gel. The presence of copper(I) is well observed by the white contrast of the fibres in STEM picture and supported by EDS analysis (**Figure 112E-F**).

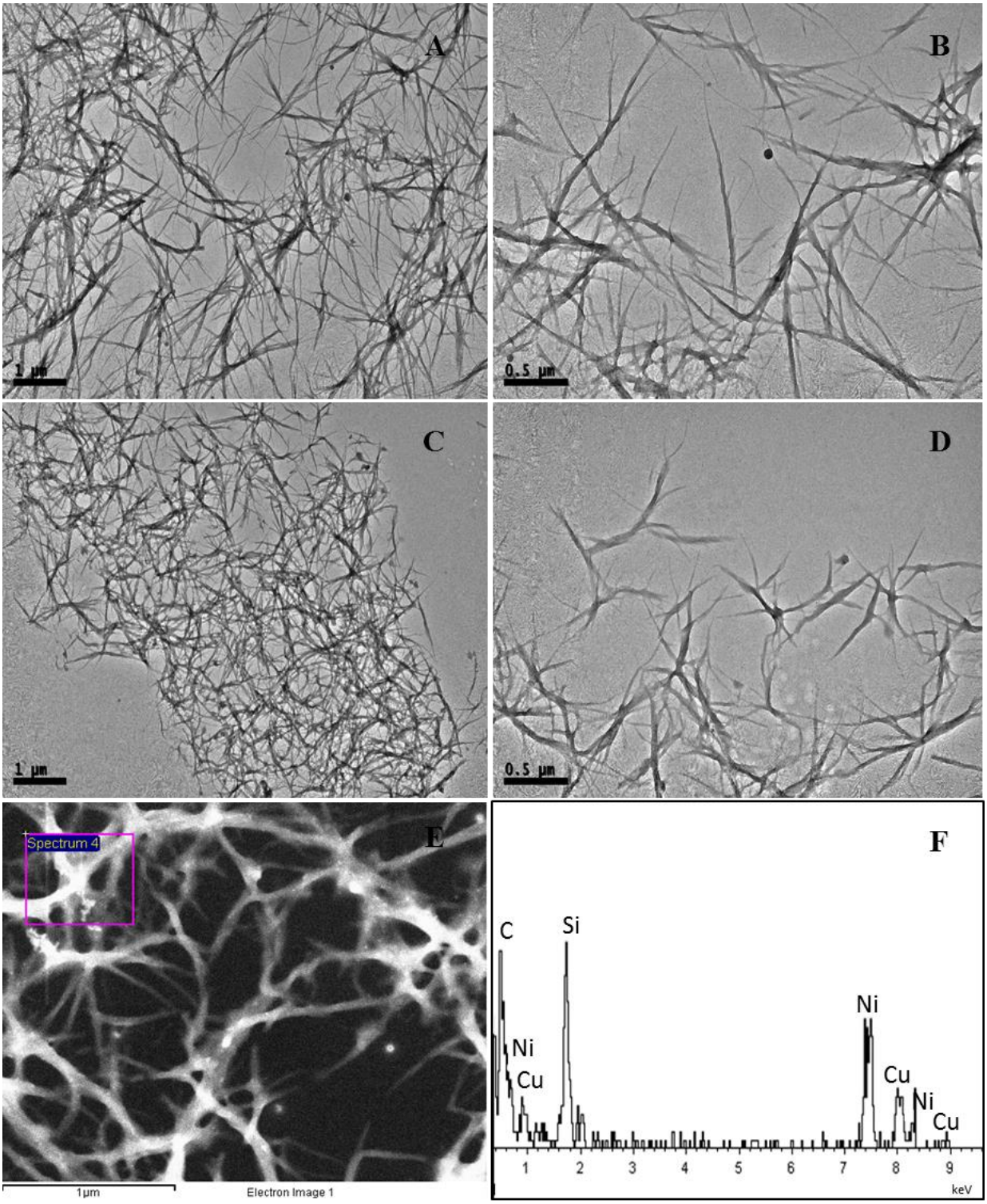

Figure 112. TEM pictures of the gel **Et_2NAzTzVal$_{12}$ (A-B)** and the corresponding metallogel (**C-D**). STEM-EDS analysis of the metalogel **Cu(I)-Et_2NAzTzVal$_{12}$** (**E-F**) without staining.

6.2.4. Photophysical properties

Although it was not fundamental for the scope of the work, the fluorescent nature of the gelator motivated the study of its photophysical properties in the presence and absence of the copper(I).

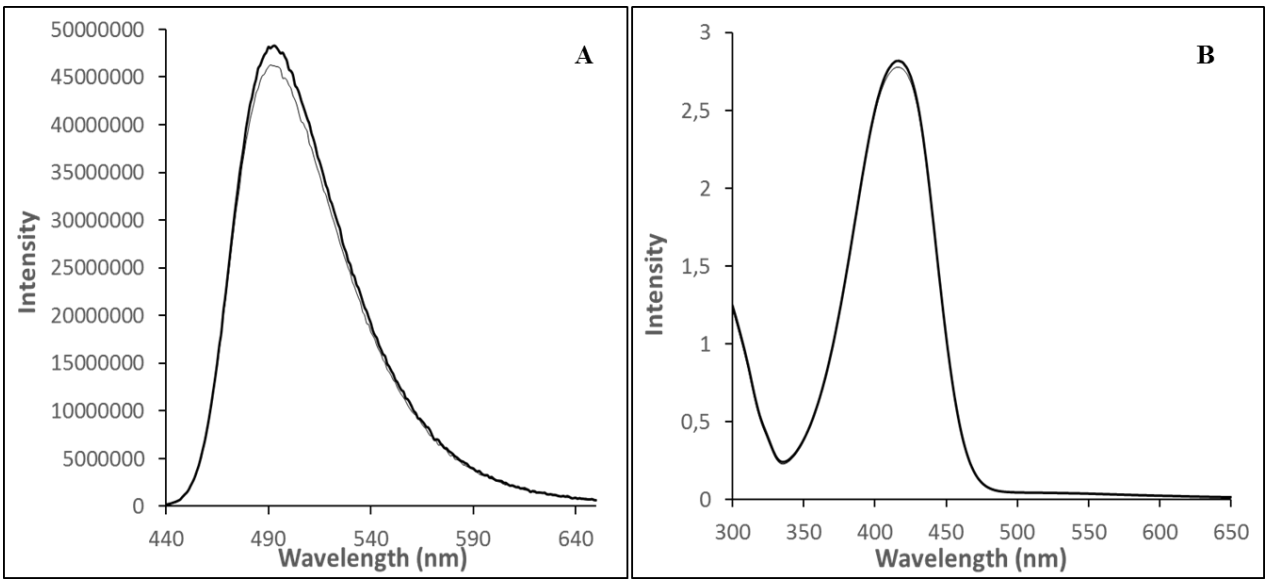

Figure 113. Emission (A) and absorption (B) spectra of the gel **Et_2NAzTzVal$_{12}$** (black) and of the corresponding metallogel **Cu(I)-Et_2NAzTzVal$_{12}$** (grey). Absorption and emission (λ_{exc}= 385 nm) spectra measured in solution at a concentration $1x10^{-4}$ M.

In the case of the amphiphilic gelator, the presence of copper(I) did not influence the photophysical properties of the gel. Both gels present an absorption maximum at λ= 420 nm and an emission maximum at λ= 490 nm, exhibiting a high fluorescence intensity. This was different to what has been observed in **Chapter 5** for the bolaamphiphilic gelators functionalized with azidocoumarine, where a high quenching of fluorescence in the presence of the metal has been detected. This finding suggests that different self-assembly processes occur depending on the amount of triazole ligands present in the molecule.

6.2.5. Catalysis model 'click' reaction

As done for the bolaamphiphilic gelators in **Chapter 3**, the catalytic performance of the amphiphilic metallogel **Cu(I)-Et_2NAzTzVal$_{12}$** was tested in the model 'click' reaction between benzylazide and phenylacetylene.

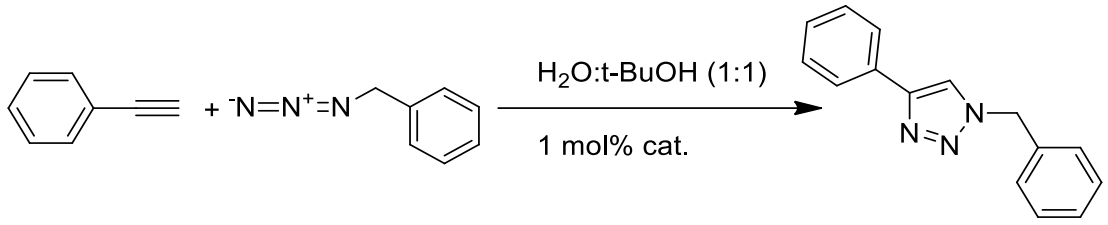

Figure 114. Huisgen's 1,3-dipolar cycloaddition between phenylacetylene and benzylazide.

The reaction was performed in a 1:1 *t*-BuOH:H_2O mixture in the presence of the metallogel catalyst (1 mol%), in air and at rt, for periods between 3 to 8h and using as copper source the complex $[Cu(MeCN)_4]PF_6$. For the same reaction, blank experiments were carried in the presence of the copper salt and/or of the non-aggregating benzyltriazole derivative **BzTzAPropyl**, synthesized in **Chapter 3**. For comparative purposes, catalytic experiments were also carried in the presence of the bolaamphiphilic metallogel **Cu(I)-Et$_2$NAzTzVal$_6$**, initially synthesized in **Chapter 5**. This gelator was able to form self-sustainable gels in 1:1 *t*-BuOH:H_2O at a concentration of $2.4x10^{-2}$ mM.

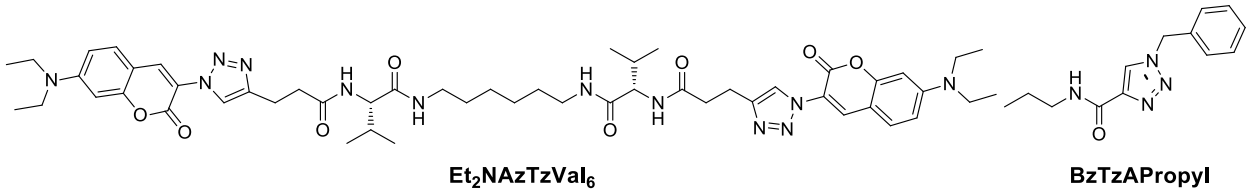

Et$_2$NAzTzVal$_6$ **BzTzAPropyl**

Figure 115. Structures of the bolaamphiphilic gelator **Et$_2$NAzTzVal$_6$** and of the non-aggregating benzyltriazole derivative **BzTzAPropyl**.

The gelator **Cu(I)-Et$_2$NAzTzVal$_{12}$** has shown to be an effective heterogeneous gel catalyst for the model 'click' reaction, achieving 92% conversion after 8h reaction (**Table 19A**). For a similar period of time, 54% and 66% conversion have been obtained for the blanks, although it can be observed that no significant difference was found between these values and the ones obtained after 6h reaction (41% and 53%, respectively). Contrary to expectations, the presence of the triazole fragment in the non-aggregating compound **Cu(I)-BzTzAPropyl** did not result in a substantially higher catalytic performance in comparison with the copper salt $[Cu(MeCN)_4]PF_6$. The lowest obtained performance was attributed to the reaction carried in the presence of the bolaamphiphilic gelator **Cu(I)-Et$_2$NAzTzVal$_6$**, achieving no more than 30% conversion in 8h. In this specific case, it is possible that diffusion problems of the reactants into the gel phase might be on the source of such lower conversion values.

Table 19. Catalytic activity of the gelators and the blanks in 1:1 t-BuOH:H_2O

Entry	Catalyst	Conversion at 3h (%)[a]	Conversion at 6h (%)[a]	Conversion at 8h (%)[a]
A	**Cu(I)-Et_2NAzTzVal$_{12}$**	71	84	92
B	**Cu(I)-Et_2NAzTzVal$_6$**	1.5	22	30
C	**[Cu(MeCN)$_4$]PF_6**	13	41	54
D	**Cu(I)-BzTzAPropyl**	9	53	66

[a] Catalytic experiments were performed at room temperature without stirring, using 400 µL of 1:1 H_2O:*t*-BuOH as solvent medium. The reactants in stoichiometric proportion (0.21 mmol) were mixed and added directly at the top of the metallogel catalyst (1 mol%) composed by the gelator (5.34 mg; $8.4x10^{-3}$ mmol) and the copper salt [Cu(MeCN)$_4$]PF_6 (0.80 mg; $2.1x10^{-3}$ mmol). At the end of the experiment, the products were directly extracted with 700 µL $CDCl_3$. The organic phase was dried over anhydrous $MgSO_4$ and the conversion determined by ^{1}H-NMR.

Similarly to what was observed for the gelators studied in **Chapter 3**, the catalytic performance of the metallogel **Cu(I)-Et_2NAzTzVal$_{12}$** was considerably higher in the first 3h reaction, where 71% of conversion could be obtained, a value which is 60% higher than the ones registered in the presence of the blanks [Cu(MeCN)$_4$]PF_6 and **BzTzAPropyl,** (**Table 19C-D**). However, it is important to highlight that this catalytic ability of the gel **Cu(I)-Et_2NAzTzVal$_{12}$** was considerably higher than the one observed for the bolaamphiphilic families **Cu(I)-PhTzVal$_n$** and **Cu(I)-BzTzVal$_n$** investigated in **Chapter 3**, whose conversions were not more than 15% higher in comparison with the ones registered for the blanks.

To better understand the significant difference between the conversions achieved for the fluorescent amphiphilic and bolaamphiphilic compounds, the amount of copper(I) coordinated to both gelators was determined by ICP-MS.

Table 20. Amount of copper coordinated by the amphiphilic and bolaamphiphilic fluorescent gelators.[a]

Compound	% Cu coordinated
Cu(I)-Et_2NAzTzVal$_{12}$	45.0
Cu(I)-Et_2NAzTzVal$_6$	96.0

[a] The amount of copper coordinated was determined in the mixture 1:1 H_2O:*t*-BuOH, in the presence of the gelator (5.34 mg; $8.4x10^{-3}$ mmol) and the copper salt [Cu(MeCN)$_4$]PF_6 (0.80 mg; $2.1x10^{-3}$ mmol).

It is interesting to see that the best catalytic performance was exhibited by the gel presenting the worst copper loading, coordinating only 45% of copper initially present in solution. Despite the excellent coordination ability of the bolaamphiphilic gelator, its catalytic performance for the model 'click' reaction was relatively poor. This mismatch between the copper loading capacity and the catalytic activity of the gels motivated a deeper investigation on the catalytic performance exhibited

by the amphiphilic fluorescent gel **Cu(I)-Et$_2$NAzTzVal$_{12}$**.

6.2.6. Transient self-assembly derived catalytic activity

It was initially proposed that such high catalytic activity exhibited by the amphiphilic gelator could be related with the presence of a long carbon tail in its structure. In an analogy to the amphiphilic gelator **ProValDoc** studied in **Chapter 4**, the high hydrophobicity of the pending carbon chain would contribute not only for the gelation of the compound but also to facilitate the migration of the hydrophobic reactants to the closely packed bilayer structure, reacting in close proximity with the catalytic site. This would result in an increase in the reaction kinetics, as reported for the **ProValDoc** gelators applied to the direct aldol reaction between *p*-nitrobenzaldehyde and cyclohexanone.[16]

Besides this structural arrangement that could be on the basis of the improved catalytic activity of the gelator **Cu(I)-Et$_2$NAzTzVal$_{12}$**, another interesting finding is the dynamic behaviour of this self-assembled system, which is able to disassemble and undergo into solution once it is fed with reactants benzylazide and phenylacetylene. This dynamic system resembles the dissipative systems published by van Esch and co-workers,[9,10] although in this case the gelator molecule is not subjected to any chemical transformation during the whole process. One of the main novelties in this system is that the far from equilibrium behaviour of the gel **Cu(I)-Et$_2$NAzTzVal$_{12}$** is not controlled by the consumption of the fuel by the gelator, but by the occurrence of the model 'click' reaction (**Figure 116**).

As summarized in **Figure 116**, at the beginning the gel is formed by heating until complete dissolution, followed by cooling in ultrasounds for 1 minute. The reactants benzylazide and phenylalkyne (defined as fuel) are then added on the top of the gel and after 10 min, the formation of a biphasic mixture is observed. Looking at the UV lamp at a λ=365 nm, it appears that the gelator has disassembled and migrated to the top phase of a biphasic solution, which should be the organic phase considering the lower density of *t*-BuOH (0.78 g/cm^3) in comparison with water. After some time of reaction, the gelator assembles again together with the product of the reaction, forming an entangled network that entraps the solvent leading to an opaque gel. This dynamic self-assembled system can be reactivated by further addition of the reactants, promoting the disassembling of the gel and consequent phase separation.

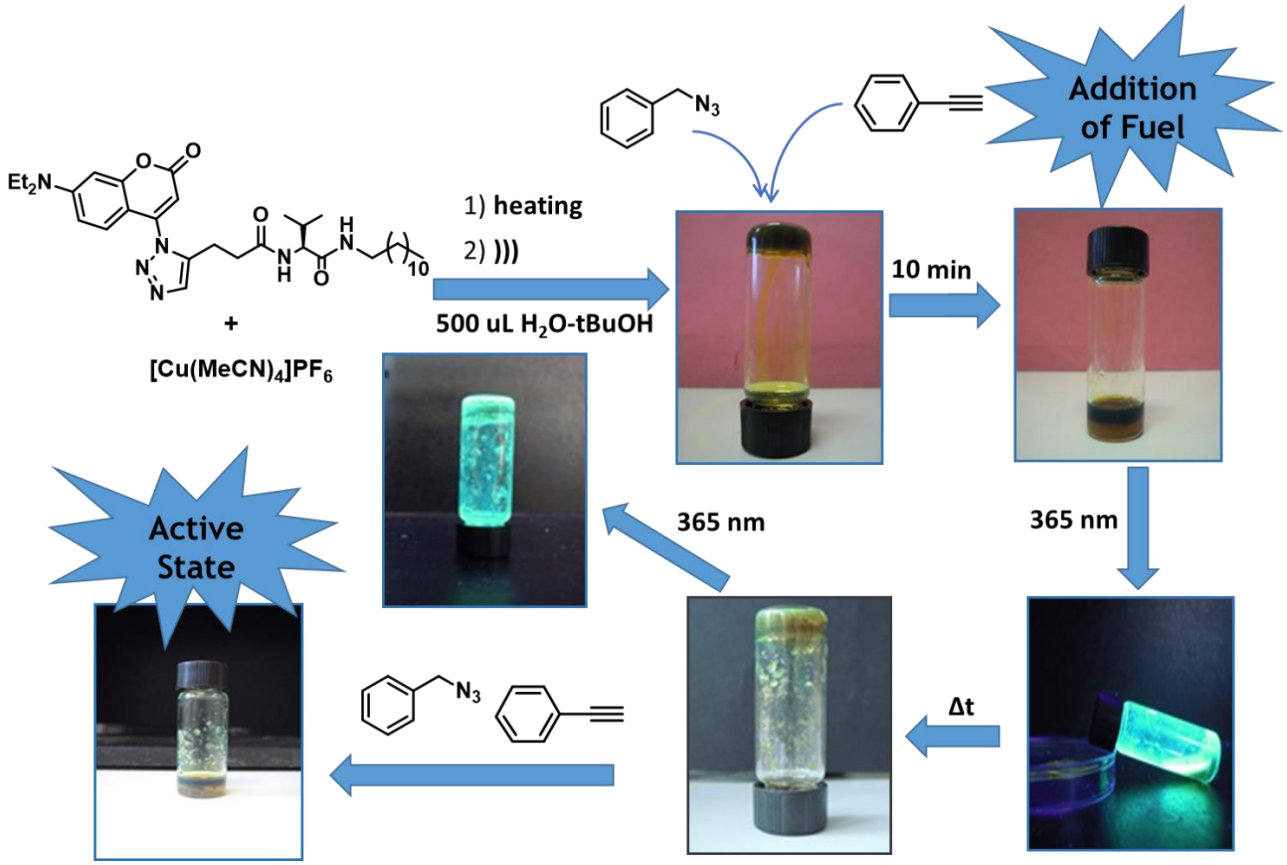

Figure 116. Dynamic self-assembly behaviour of the fluorescent gelator **Cu(I)-Et$_2$NAzTzVal$_{12}$** in the catalysis of the model 'click' reaction between phenylacetylene and benzylazide.

Such transient self-assembly behaviour is possible not only due to the characteristic metastability of the gels, allowing reversible transitions from gel to solution and vice-versa, but also due to the input of energy provided by the addition of the reactants, which create a hydrophobic environment that forces the gelator to go into the apolar organic phase. The consumption of the reactants due to the occurrence of the model 'click' reaction lowers the hydrophobic nature of the medium, promoting the reassembly of the gel. Thus, this non-equilibrium dynamic system can be defined as hydrophobicity/solubility-driven dynamic self-assembly.

To better understand if the dynamic behaviour of the gelator is directly responsible for the high catalytic activity, a series of catalytic experiments with constant amount of catalyst but decreasing amount of reactants were performed. By decreasing the amount of reactants added to the reaction medium, the proportion of catalyst is theoretically increasing (**Table 21**). Such experiments would also help to evaluate the minimum concentration of reactants needed to promote the disassembly of the gel.

Table 21. Initial amount of reactants and conversions achieved by the metallogel **Cu(I)-Et$_2$NAzTzVal$_{12}$** in the model 'click' reaction[a].

Entry	Initial amount (mmol) of catalyst Cu(I)-Et$_2$NAzTzVal$_{12}$ (mol ratio 4:1 Cu)	Amount BnN_3 (mmol)	Amount Phenylacetylene (mmol)	Calculated amount of catalyst (mol%)	Conversion after 6h (%)[a]
A	0.0042	0.21	0.21	0.5	46
B	0.0042	0.10	0.10	1	64
C	0.0042	0.05	0.05	2	26

[a] Catalytic experiments were performed at room temperature without stirring, using 500 µL of 1:1 H_2O-*t*BuOH as solvent medium. Briefly, the reactants in stoichiometric proportion were mixed and added directly at the top of the metallogel catalyst, composed by the gelator (2.67mg; $4.2x10^{-3}$ mmol) and the copper salt $[Cu(MeCN)_4]PF_6$ (0.40 mg; $1.05x10^{-3}$ mmol) in a 4:1 molar ratio. At the end of the experiment, the products were directly extracted with 700 µL $CDCl_3$. The organic phase was dried over anhydrous $MgSO_4$ and the conversion determined by ^{1}H-NMR.

The obtained results suggest an uncommon trend in the catalytic activity of the gelator **Cu(I)-Et$_2$NAzTzVal$_{12}$**, taking into account that the lowest conversion was obtained in the presence of 2 mol% catalyst. However, the visual inspection of the vials at t= 10 min and t= 6h of reaction, belonging to the experiments carried in the presence of 0.5 mol% and 2 mol% catalyst, where 0.24 mmol and 0.06 mmol of each reactant were added, respectively, allow a better understanding of the phenomenon taking place during the catalytic process.

While in **Figure 117A,** after 10 minutes of reaction, it could be clearly observed the catalytic gelator **Cu(I)-Et$_2$NAzTzVal$_{12}$** in contact with the reaction medium, in **Figure 117B,** where a higher amount of fuel was present, the gelator disassembled and migrated to the top organic phase, leaving a biphasic heterogeneous solution.

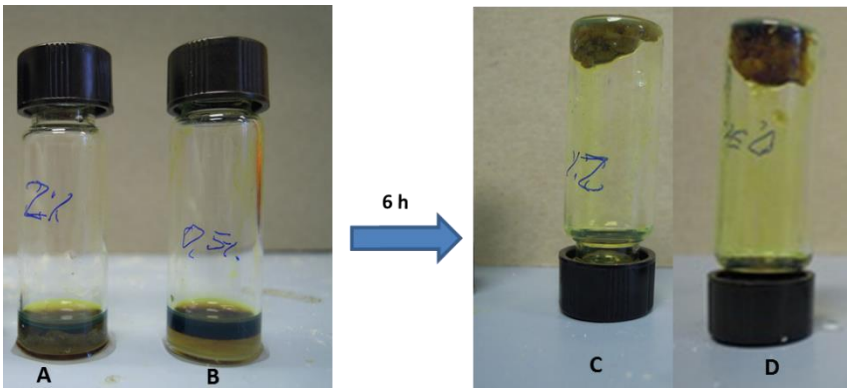

Figure 117. Physical appearance of the model 'click' reaction at t= 10 min (A; B) and at t= 6h (C; D), carried in the presence of the gelator **Cu(I)-Et$_2$NAzTzVal$_{12}$** (0.0048 mmol) and after addition of 0.24 mmol (A, D) and 0.06 mmol (B, C) of reactants.

After 6h of reaction, the formation of a self-sustained gel was observed in both vials (**Figure 117C** and **Figure 117D**), although no disassembling process has been detected in the presence of 2

mol% catalytic gel along all the reaction. On the other hand, when the reaction was carried in the presence of 0.5 mol% gel catalyst, corresponding to a higher amount of fuel, a dynamic self-assembly behaviour has been observed, where the gel disassembled after 10 minutes reaction (**Figure 117B**), to further reassemble together with some precipitated product (**Figure 117D**). It is curious to observe that higher conversions have been obtained for the reactions carried with 0.5 mol% and 1 mol% catalyst, 46% and 64%, respectively, than in the presence of 2 mol% catalyst, where the achieved conversion was not higher than 26% (**Table 21**). It is also important to highlight that in the presence of 1 mol% catalytic gel, a similar disassembly/self-assembly behaviour has been observed along the reaction.

The fact that higher conversions have been obtained for the reaction carried in the presence of lower amounts of catalyst, allow us to conclude that this dynamic self-assembly behaviour is responsible for the catalytic ability of the gel **Cu(I)-Et$_2$NAzTzVal$_{12}$**. Furthermore, it can be concluded that the reactants have a fundamental role on promoting this dynamic behaviour of the metallogel catalyst, creating a favourable hydrophobic environment for the migration of the gelator through a disassembling process. Moreover, these experiments suggest that the ideal reactant/metallogel molar ratio necessary to promote the disassembly of the catalytic gel is between 25 and 50. However, it is still not clear if the gel completely solubilizes in the organic phase or if it just forms nanoaggregates that migrate to the interface of the biphasic solution.

In an attempt to clarify this issue, the catalysis of the model 'click' reaction in the presence of 0.5 mol% **Cu(I)-Et$_2$NAzTzVal$_{12}$** was repeated and after 10 minutes, the top layer of the biphasic solution was taken with a syringe, filtered through a 0.22 μm filter, evaporated and analysed by ^{1}H NMR. The obtained spectrum (**Figure 118**) indicate that the organic phase arising from the biphasic solution is mainly composed by the catalyst and the product, since the reactants benzylazide and phenylacetylene are volatile and should have been evaporated together with the solvent in the rotavapor. However, it seems to be clear that the catalyst solubilizes in the organic phase and acts as a temporary homogeneous catalyst, reassembling latter in a mixed product-gel phase.

To further confirm this hypothesis, the model 'click' reaction was performed using only *t*-BuOH as solvent media and in the presence of 0.5 mol% catalyst. In this solvent the catalyst **Cu(I)-Et$_2$NAzTzVal$_{12}$** was completely soluble and 67% conversion was achieved after 24h. This result supports that the model 'click' reaction is catalysed in solution due to the dynamic behaviour of the metallogel **Cu(I)-Et$_2$NAzTzVal$_{12}$**.

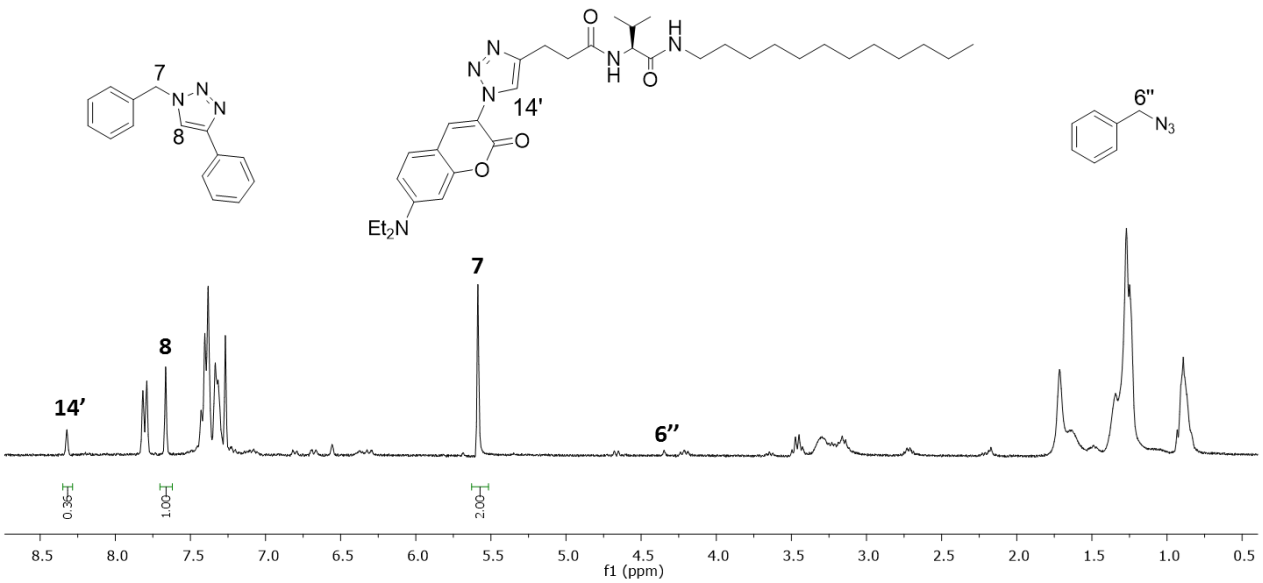

Figure 118. ^{1}H NMR spectrum of the top phase from the biphasic mixture formed after 10 minutes of the model 'click' reaction in the presence of 0.5 mol% gel catalyst.

However, it is still unclear how this dynamic behaviour affects the final structure of the gel. To better understand this issue, the reaction was repeated for 24h, changing the proportion of catalyst and the amount of 1:1 *t*-BuOH:H_2O (**Table 22**). The aim of this study was to investigate the structural arrangement of the gel and gel/product mixtures after the reaction by WAXD analysis.

Table 22. Conversions and model 'click' reaction conditions using the gelator Cu**(I)-Et$_2$NAzTzVal$_{12}$** as catalyst.

Entry	Amount catalyst (%mol)	Amount BnN3 (mmol)	Amount Phenylacetylene (mmol)	Amount solvent (mL)	Conversion after 24h (%)[a]
B	0.5	0.21	0.21	0.5	65
C	5	0.21	0.21	0.5	48
D	5	0.21	0.21	2.5	5.7

[a] Catalytic experiments were performed at room temperature without stirring, using 500 µL of 1:1 H_2O:*t*-BuOH as solvent medium. Briefly, the reactants in stoichiometric proportion (0.21 mmol) were mixed and added directly at the top of the metallogel catalyst, composed by the gelator and the copper salt $[Cu(MeCN)_4]PF_6$ in a 4:1 molar ratio. At the end of the experiment, the products were directly extracted with 700 µL $CDCl_3$. The organic phase was dried over anhydrous $MgSO_4$ and the conversion determined by ^{1}H-NMR.

Similarly to what has been observed in previous experiments, a higher conversion was obtained when using a lower amount of catalyst, where a dynamic self-assembly behaviour has been observed (**Table 22B**). Comparing the reactions carried in the presence of 5 mol% metallogel **Cu(I)-Et$_2$NAzTzVal$_{12}$**, a higher conversion was obtained in the reaction where a lower volume of 1:1 *t*-BuOH:H_2O (0.5 mL) has been used (**Table 22C**). This was rather expected, since the reactants

are more concentrated, creating a stronger hydrophobic environment to promote the disassembly of the gel. However, it is important to highlight that when 0.5 mL of solvent was used together with 5 mol% catalyst, it seems that only a partial amount of gelator disassembled and migrated into solution, which was rather expected since the molar ratio reactants/catalyst used was 5 to 10 times lower than one established as ideal, determined based on the conversions obtained in **Table 21**.

At the end of each reaction, the obtained gel/product precipitate was analysed by WAXD and the obtained diffractograms compared with the one of the native gel **Et$_2$NAzTzVal$_{12}$** (**Figure 119**). This experiment would provide information about possible structural changes occurring in the gel catalyst due to its dynamic self-assembly behaviour.

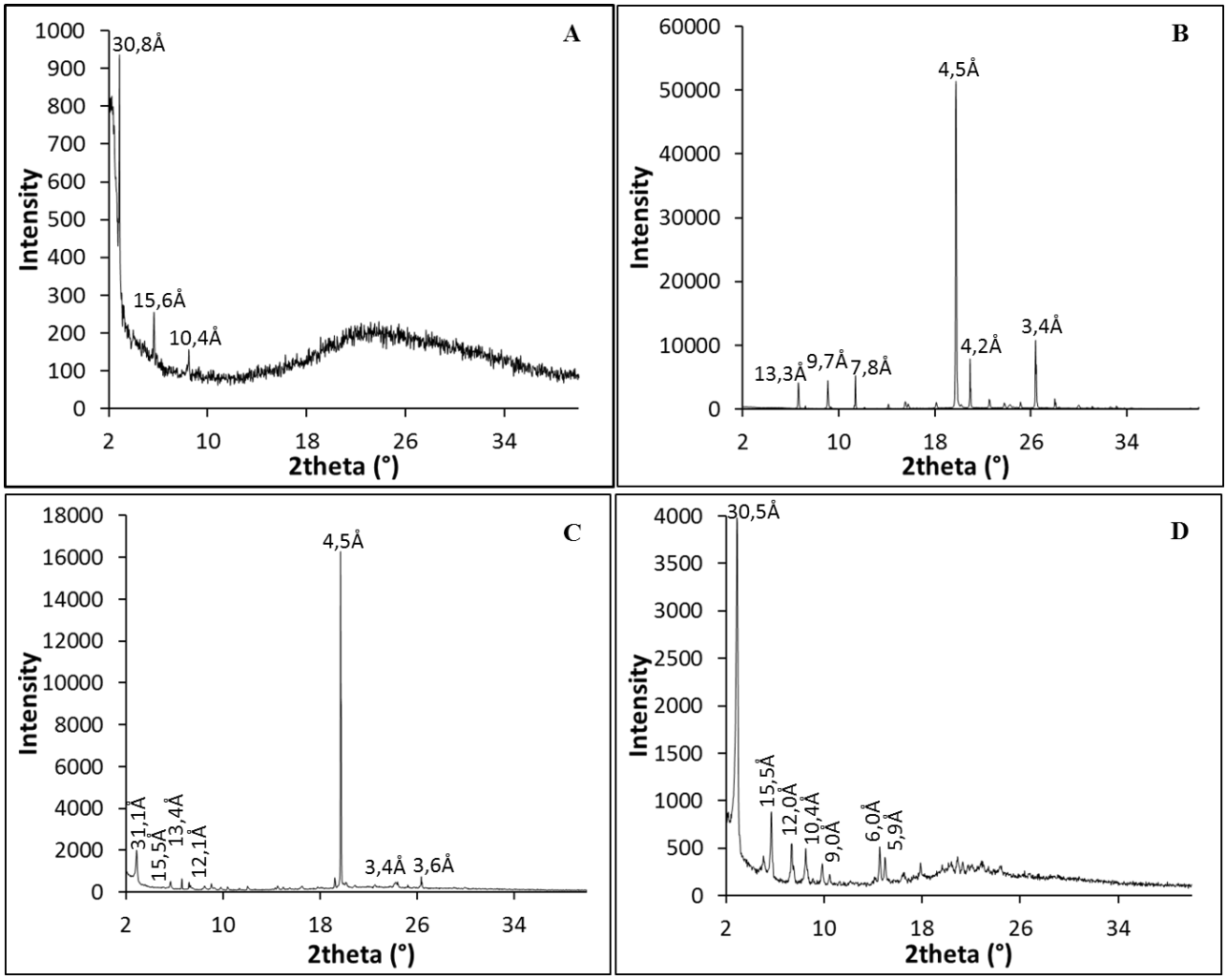

Figure 119. Diffractograms of the native gelator **Et$_2$NAzTzVal$_{12}$** and of the precipitate resultant from the model 'click' reaction catalysed for 24h by 0.5 mol% (B) and 5 mol% (C, D) of catalyst using 500 µL (B, C) and 2.5 mL (D) of 1:1 t-BuOH:H_2O. The conversions achieved were 65% (B), 48% (C) and 5.7% (D).

The conversions achieved during these experiments (**Table 22**) are consistent with the obtained diffractograms (**Figure 119**). By comparing the conversions and conditions used in the catalysis of

the model 'click' reaction with the obtained diffractograms, it can be suggested that the crystalline structure represented in **Figure 119B** belongs mainly to product of reaction, considering that 65% conversion has been achieved using 0.5 mol% of catalyst (**Table 22B**). The small amount of catalyst compared with the high quantity of final product makes the catalyst practically undetectable by WAXD.

On the other hand, when the amount of catalyst is increased to 5 mol%, maintaining the volume of solvent (**Table 22C**), the obtained precipitate seems to be composed by a mixture of phases (**Figure 119C**). In this diffractogram, it is possible to observe lattice distances similar to the ones represented in **Figure 119B** (13.4 Å, 4.5 Å and 3.6 Å), which are attributed to pure product, and in **Figure 119D** (31.1 Å, 15.5 Å, 12.1 Å), which in turn are relatively similar to the ones observed for the native gel in **Figure 119A** (30.8 Å and 15.4 Å). Thus, the diffractogram in **Figure 119C** correspond to a mixture of product and native gel.

The diffractogram represented in **Figure 119D** appears to be composed by a single crystalline phase corresponding to the gel catalyst after reaction, since no characteristic peaks of the final product (**Figure 119B**) could be observed, probably due to the low conversion achieved (**Table 22D**). In the diffractogram of **Figure 119D** it is clearly evident the presence of peaks characteristic of the initial gel at 2θ= 2.9º, 5.7º and 8.5º together with a new peak at 2θ= 7.3º, that is also common to the diffractogram of **Figure 119C** and thus may probably correspond to a transient structural arrangement of the catalytic gel. Additionally, there are also some peaks at 2θ= 9.9º, 14.6º and 15.0º which are not common neither to diffractogram of the native gel (**Figure 119A**) nor to the diffractogram characteristic of the final product of the reaction (**Figure 119B**), suggesting that they could be related with a new structural arrangement of the gel arising from its reassembling process. Thus, it can be suggested that the dynamic self-assembly behaviour of the catalyst promote a rearrangement of the gel in a more ordered and compacted crystalline structure, although some distances between the lattice plans such as d= 30.5 Å, 15.5 Å and d= 10.4 Å are similar to the ones obtained for the native gel (**Figure 119A**).

TEM analysis (without staining) performed on an aliquot of the reaction taken from the interface at t=10 minutes, just after the formation of a biphasic solution, revealed the presence of fibres with 10 nm width (**Figure 120C-D**). At this point, the engangled network of helical fibres initially observed for the pure metallogel **Cu(I)-Et$_2$NAzTzVal$_{12}$** seems to transform into small extended thin fibres with linear conformation, supporting the disassembly of the gel.

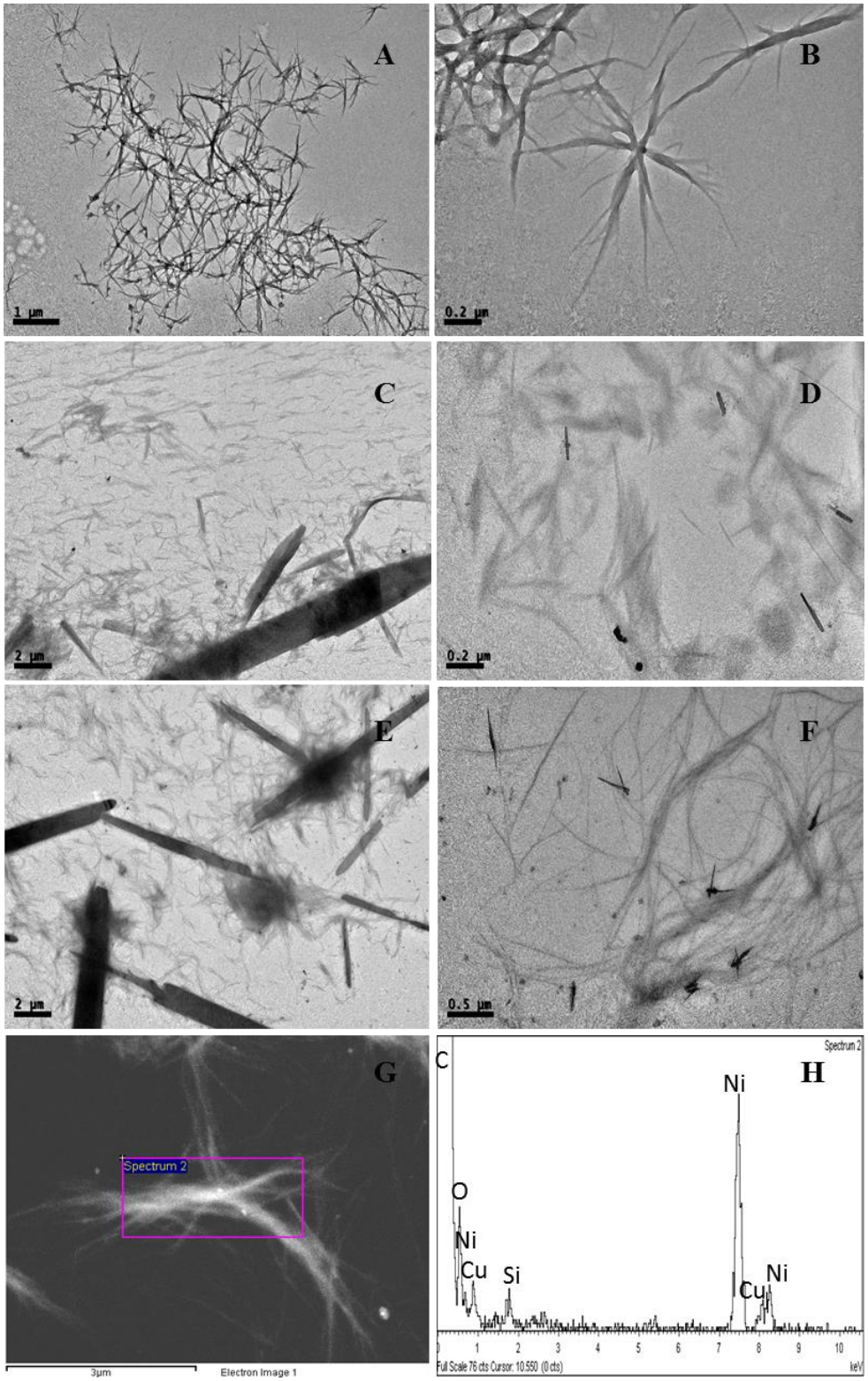

Figure 120. TEM images of metallogel **Cu(I)-Et$_2$NAzTzVal$_{12}$** before reaction (A-B), at t= 10 min (C-D) and at t=24h (E-F). STEM picture of **Cu(I)-Et$_2$NAzTzVal$_{12}$** at t= 24h (G) and corresponding EDS spectrum (H). Magnifications are 2500x (A), 1000x (C-D), 5000x (F), 10000x (B-G).

At the end of the reaction, the gel tends to reassemble, rebuilding an entangled network of thin fibres that entraps large crystals of final product in its structure (**Figure 120E-F**). The

morphological differences between these new fibres and the ones observed for the initial metallogel **Cu(I)-Et$_2$NAzTzVal$_{12}$** is in well accordance with the appearance of new peaks in the diffractogram corresponding to the final gel-product mixture (**Figure 119D**). It is important to highlight that after reassembly, the fibres still have the contrast characteristic of the coordination of the metal, whoose the presence is confirmed by EDS analysis.

These findings confirm that the catalytic ability is consequence of a series of events including:

- the disassembly of the metallogel **Cu(I)-Et$_2$NAzTzVal$_{12}$** promoted by the addition of the hydrophobic reactants benzylazide and phenylalkyne
- the migration to the organic phase, where the catalysis occurs
- Posterior reassembly of the gel into a more ordered and crystalline structure.

Furthermore, the dynamic catalytic system can also behave as a visual indicator of the progress of the reaction, since the reassembly of the gel occurs when the conversion is approximately 50%.

6.2.7. Recyclability

One of the most important characteristics that distinguishes the heterogeneous catalysts is the possibility of recovering and reusing them in consecutive catalytic cycles, resulting in a higher economic return. Thus, the recycling performance of the heterogeneous catalytic system **Cu(I)-Et$_2$NAzTzVal$_{12}$** was investigated on the model 'click' reaction.

The dynamic self-assembly behaviour of the system allowed to carry these studies with continuous feed of reactants, i.e., each 24h reaction, a batch of reactants was added in the same vial at the top of the mixed gel-product precipitate, promoting the formation of a biphasic solution and consequent reactivation of the catalyst.

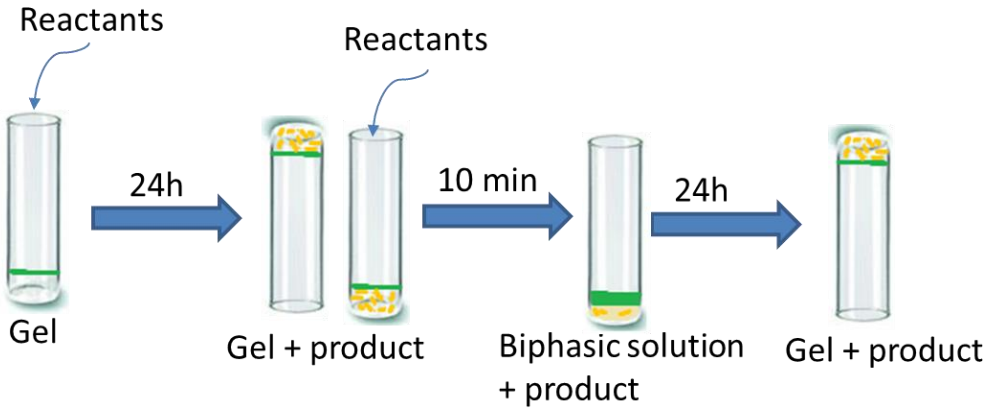

Figure 121. Schematic representation of stepwise-activated recycling experiments.

This method is regarded as a greener, efficient and time-saving procedure, since there is no need of recovering the catalyst after each run. The conversions obtained after each catalytic cycle are

represented in **Table 23**.

Table 23. Stepwise-activated recycling tests performed on the catalytic metallogel **Cu(I)-Et$_2$NAzTzVal$_{12}$** (0.5 mol%) in the model 'click' reaction. A new batch of reactants was added every 24h.

Run	Amount BnN_3 (mmol)	Amount product (mmol)	Conversion after 24h (%)[a]
1	0.210	0.121	58
2	0.210	0.085	40
3	0.210	0.049	24

[a] The reactants phenylacetylene (21.9 mg; $2.14x10^{-1}$ mmol; 23.5 µL) and benzylazide (28.5 mg; $2.14x10^{-1}$ mmol; 26.7 µL) were directly added at the top of the catalytic gel composed by the gelator **Et$_2$NAzTzVal$_{12}$** (2.67 mg; $4.29x10^{-3}$ mmol) and the copper salt $[Cu(MeCN)_4]PF_6$ (0.40 mg; $1.07x10^{-3}$ mmol) in 500 µL 1:1 H_2O:*t*-BuOH and the mixture allowed to react at room temperature and without stirring for periods from 24 to 72h. A new batch of reactants was introduced every 24h, without intermediate recovery of the catalytic gel. The reactions were done in triplicate in order to evaluate the conversion of the two remaining vials after each run. For this, the crude mixture was directly extracted with 700 µL $CDCl_3$ and the organic phase dried over anhydrous $MgSO_4$. The conversions were determined by ^{1}H-NMR in $CDCl_3$.

Although in the first run 58% conversion has been achieved, it was observed that the catalyst loses 16-18% of catalytic activity after each run. The precipitation of a growing amount of product together with the catalyst, after each run, may negatively influence the migration of the gelator **Cu(I)-Et$_2$NAzTzVal$_{12}$** to the organic phase, introducing a decay in the catalytic activity.

Thus, new recycling experiments were carried, but this time the reactants were added in periods of 3h, before the reassembling process of the catalytic gel and formation of the mixed product-gel network. In this case, it would be expected that the catalyst is maintained in its active form through the continuous supply of reactants before it returns to its self-assembled state.

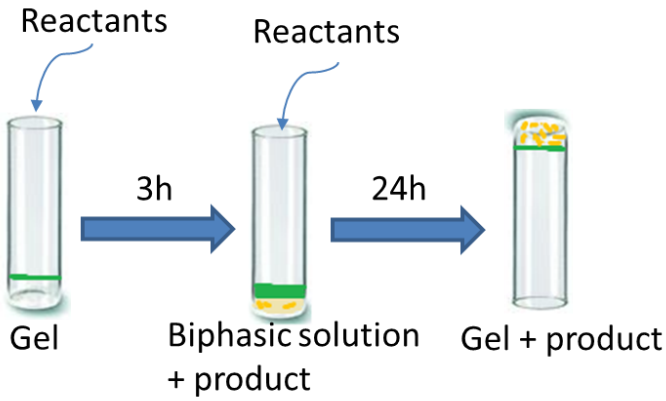

Figure 122. Schematic representation of continuously-activated recycling experiments.

The conversion was determined after 24h counting from the addition of the last batch of reactants.

As done for the previous recycling experiments, these reactions were also performed in triplicate and two vials were treated after each run to check the corresponding conversion.

Table 24. Continuously activated recycling tests performed on the catalytic metallogel **Cu(I)-Et$_2$NAzTzVal$_{12}$** (0.5 mol%) in the model 'click' reaction.

Run	Amount BnN_3 (mmol)	Amount product (mmol)	Conversion at 24h (%)
1	0.21	0.121	58
2	0.42	0.125	59
3	0.63	0.051	24

[a] The reactants phenylacetylene (21.9 mg; $2.14x10^{-1}$ mmol; 23.5 µL) and benzylazide (28.5 mg; $2.14x10^{-1}$ mmol; 26.7 µL) were directly added at the top of the catalytic gel composed by the gelator **Et$_2$NAzTzVal$_{12}$** (2.67 mg; $4.29x10^{-3}$ mmol) and the copper salt $[Cu(MeCN)_4]PF_6$ (0.40 mg; $1.07x10^{-3}$ mmol) in 500 µL 1:1 H_2O:*t*-BuOH, and the mixture allowed to react at room temperature without stirring. The reactants were added consecutively in intervals of 3h until a total of 9h, and the mixture allowed to react for further 24h counting from the addition of each batch. The reactions were done in triplicate in order to evaluate the conversion of the two remaining vials after each run. For this, the crude mixture was directly extracted with 700 µL $CDCl_3$ and the organic phase dried over anhydrous $MgSO_4$. The conversions were determined by ^{1}H-NMR in $CDCl_3$.

The obtained results show that if the reactants are added while the gel is still in its active form (before its reassembly), the gelator **Cu(I)-Et$_2$NAzTzVal$_{12}$** can be used for two consecutive runs maintaining its catalytic activity. However, after a third run, the gelator loses around 50% of its catalytic performance, probably due to a saturation of the catalytic sites and/or due to the presence of a considerable amount of precipitated product in the reaction medium. Nevertheless, comparing the conversions obtained in **Table 23** and **Table 24** for the first two runs, it can be concluded that the presence of precipitated product entrapped in the network of the catalytic gel is responsible for a decay on its recycling performance, probably by interfering in the disassembling step.

6.3. Conclusion

A dynamic self-assembled catalytic system activated by the model 'click' reaction was successfully developed. The addition of the reactants benzylazide and phenylacetylene (fuels) to the reaction medium resulted in the disassembly of the gel, acquiring a transient catalytically active form. The dynamic behaviour of this system provided the gel with catalytic activity for the model 'click' reaction, obtaining conversions of 71% in the first three hours of reaction and in the presence of 1 mol% catalyst. Additionally, this self-assembled transient system may also be used as a visual indicator of the progress of the reaction, since it reassembles once 50% of conversion is achieved,

returning to its thermodynamically favoured metastable state. Finally, the system could be continuously reused for two consecutive runs without losing its catalytic activity. The dynamic self-assembly behaviour of this catalytic system allows the consecutive addition of batches of reactants without the need of isolating the catalyst after each run, providing a greener and less time-consuming approach.

6.4. References

[1] Sanchez C, Arribart H, Guille MMG. Biomimetism and bioinspiration as tools for the design of innovative materials and systems. Nature materials 2005; 4: 277-288.

[2] Fialkowski M, Bishop KJ, Klajn R, Smoukov SK, Campbell CJ, Grzybowski BA. Principles and implementations of dissipative (dynamic) self-assembly. Journal of Physical Chemistry B 2006; 110: 2482-2496.

[3] Pappas CG, Sasselli IR, Ulijn RV. Biocatalytic pathway selection in transient tripeptide nanostructures. Angewandte Chemistry International Edition 2015 ; 54 : 8119-8123.

[4] Warren SC, Guney-Altay O, Grzybowski BA. Responsive and nonequilibrium nanomaterials. The Journal of Physical Chemistry Letters 2012; 3: 2103-2111.

[5] Davey S. Self-assembly: Supramolecular sustenance. Nature Chemistry 2010.

[6] Kumar DK, Steed JW. Supramolecular gel phase crystallization: orthogonal self-assembly under non-equilibrium conditions. Chemical Society Reviews 2014; 43: 2080-2088.

[7] Mattia E, Otto S. Supramolecular systems chemistry. Nature Nanotechnology 2015; 10: 111-119.

[8] Desai A, Mitchison TJ. Microtubule polymerization dynamics. Annual Reviews on cell and developmental biology 1997; 13: 83-117.

[9] Boekhoven J, Brizard AM, Kowgli KN, Koper GJ, Eelkema R, van Esch JH. Dissipative self-assembly of a molecular gelator by using a chemical fuel. Angewandte Chemistry International Edition 2010; 49: 4825-4828.

[10] Boekhoven J, Hendriksen WE, Koper GJ, Eelkema R, van Esch JH. Transient assembly of active materials fuelled by a chemical reaction. Science 2015; 349: 1075-1079.

[11] Berdugo C, Miravet JF, Escuder B. Substrate selective catalytic molecular hydrogels: the role of the hydrophobic effect. Chemical Communications 2013; 49: 10608-10610.

[12] Yu G, Xuzhou Y, Chengyou H, Huang F. Characterization of supramolecular gels. Chemical Society Reviews 2013; 42: 6697-6722.

6.5. Supporting Information

6.5.1. Gelation Procedure

The gelator **$Et_2NAzTzVal_{12}$** (2.67 mg; $4.2x10^{-3}$ mmol) was heated in a 4 mL screw-capped vial in the presence of 500 μL of solvent, until complete dissolution (~30 sec). The resultant hot solution was then sonicated for 20 seconds, resulting in the formation of a gel which was allowed to stabilize for 20 minutes at room temperature. For the formation of the metallogels, the gelator was heated together with the copper salt $[Cu(MeCN)_4]PF_6$ in a 4:1 molar ratio, following a similar gelation procedure.

6.5.2. Catalytic experiments

Catalytic experiments were performed at room temperature without stirring, using 400 μL of 1:1 H_2O:*t*-BuOH as solvent medium. Briefly, the reactants in stoichiometric proportion were mixed and added directly at the top of the metallogel catalyst (1 mol%), composed by the gelator and the copper salt $[Cu(MeCN)_4]PF_6$ in a 4:1 molar ratio. At the end of the experiment, the products were directly extracted with 700 μL $CDCl_3$. The organic phase was dried over anhydrous $MgSO_4$ and the conversion determined by ^{1}H-NMR.

6.5.3. Recycling experiments

6.5.3.1. Stepwise-activated recycling experiments

The reactants phenylacetylene (21.9 mg; $2.14x10^{-1}$ mmol; 23.5 μL) and benzylazide (28.5 mg; $2.14x10^{-1}$ mmol; 26.7 μL) were directly added at the top of the catalytic gel composed by the gelator $Et_2NAzTzVal_{12}$ (2.67 mg; $4.29x10^{-3}$ mmol) and the copper salt $[Cu(MeCN)_4]PF_6$ (0.40 mg; $1.07x10^{-3}$ mmol) in 500 uL 1:1 H_2O:*t*-BuOH, and the mixture allowed to react at room temperature and without stirring for periods from 24h (1st run) to 72h (3rd run). A new batch of reactants was introduced every 24h, without intermediate recovery of the catalytic gel. The reactions were done in triplicate in order to evaluate the conversion of the two remaining vials after each run. For this, the crude mixture was directly extracted with 700 μL $CDCl_3$ and the organic phase dried over anhydrous $MgSO_4$. The conversions were determined by ^{1}H-NMR in $CDCl_3$.

6.5.3.2. Continuously-activated recycling experiments

The reactants phenylacetylene (21.9 mg; $2.14x10^{-1}$ mmol; 23.5 μL) and benzylazide (28.5 mg; $2.14x10^{-1}$ mmol; 26.7 μL) were directly added at the top of the catalytic gel composed by the

gelator **$Et_2NAzTzVal_{12}$** (2.67 mg; $4.29x10^{-3}$ mmol) and the copper salt $[Cu(MeCN)_4]PF_6$ (0.40 mg; $1.07x10^{-3}$ mmol) in 500 µL 1:1 H_2O:*t*-BuOH, and the mixture allowed to react at room temperature without stirring. The reactants were added consecutively in intervals of 3h until a total of 9h, and the mixture allowed to react for further 24h counting from the addition of each batch. The reactions were done in triplicate in order to evaluate the conversion of the two remaining vials after each run. For this, the crude mixture was directly extracted with 700 µL $CDCl_3$ and the organic phase dried over anhydrous $MgSO_4$. The conversions were determined by ^{1}H-NMR in $CDCl_3$.

6.5.4. General Characterization Methods

6.5.4.1. Minimum gel concentration

For retrieving the minimum gel concentration, the native gels, or the correspondent metallogels, were formed in 4 mL screw-capped vials in concentrations ranging from 8 mg/mL to 2.5 mg/mL, using 400 µL of the desired solvent. Each gel was formed following the gelation procedure previously described. The minimum concentration at which the gel withstands gravity upon inversion of the vial was considered as the minimum gelation concentration (m.g.c.).

6.5.4.2. Quantification of Coordinated copper

After the formation of the catalytic metallogel, 100 µL of surrounding solution were collected with a 1 mL syringe and filtered through a 0.22 µm filter. The filter was washed with a solution of 5% HNO_3 (2x1 mL) in Milli-Q water to remove remaining uncoordinated copper. A 25 mL solution of the sample in 5% HNO_3 was prepared and the concentration of copper(I) determined by inductively coupled plasma-mass spectrometry (ICP-MS) using a Varian 710-ES.

6.5.4.3. Wide-angle X-ray Diffraction

The obtained gels/metallogels were dried on air or by lyophilization (Telstar LyoQuest), depending on the nature of the gel (organogel or hydrogel), and the resultant powder resuspended in hexane. The suspension was applied into the glass sample holder and the solvent allowed to evaporate. The resultant powdered sample was analysed by X-ray diffraction (XRD) at room temperature using a Bruker D4 Endeavor X-ray powder diffractometer with Cu-K_α radiation. Data were collected for 2θ values between 2 and 40º with a step size of 0.03º and a time step of 10 s.

6.5.4.4. Circular Dichroism

Circular Dichroism spectra were carried out in pressed pellets composed by 1 (%m/m) lyophilized gel:KBr on a Jasco J-810 spectropolarimeter.

6.5.4.5. Transmission Electron Microscopy

A small portion of the gel/metallogel was placed on a nickel grid coated with carbon and allowed to dry on air. Images were recorded in a JEOL 2100 microscope without using any stain.

6.5.4.6. Nuclear Magnetic Resonance

^{1}H and ^{13}C NMR spectra measurements were recorded in a Varian Mercury 300 MHz spectrometer at 30 ℃.

6.5.5. Synthesis and Characterization

The diethylamino substituted azidocoumarine **Et_2NAzCum** was reacted with *L*-valine propanamine and dodecylamine derivative, yielding the amphiphilic family of fluorescent compounds **Et_2NAzTzVal$_n$** (**Figure 123**).

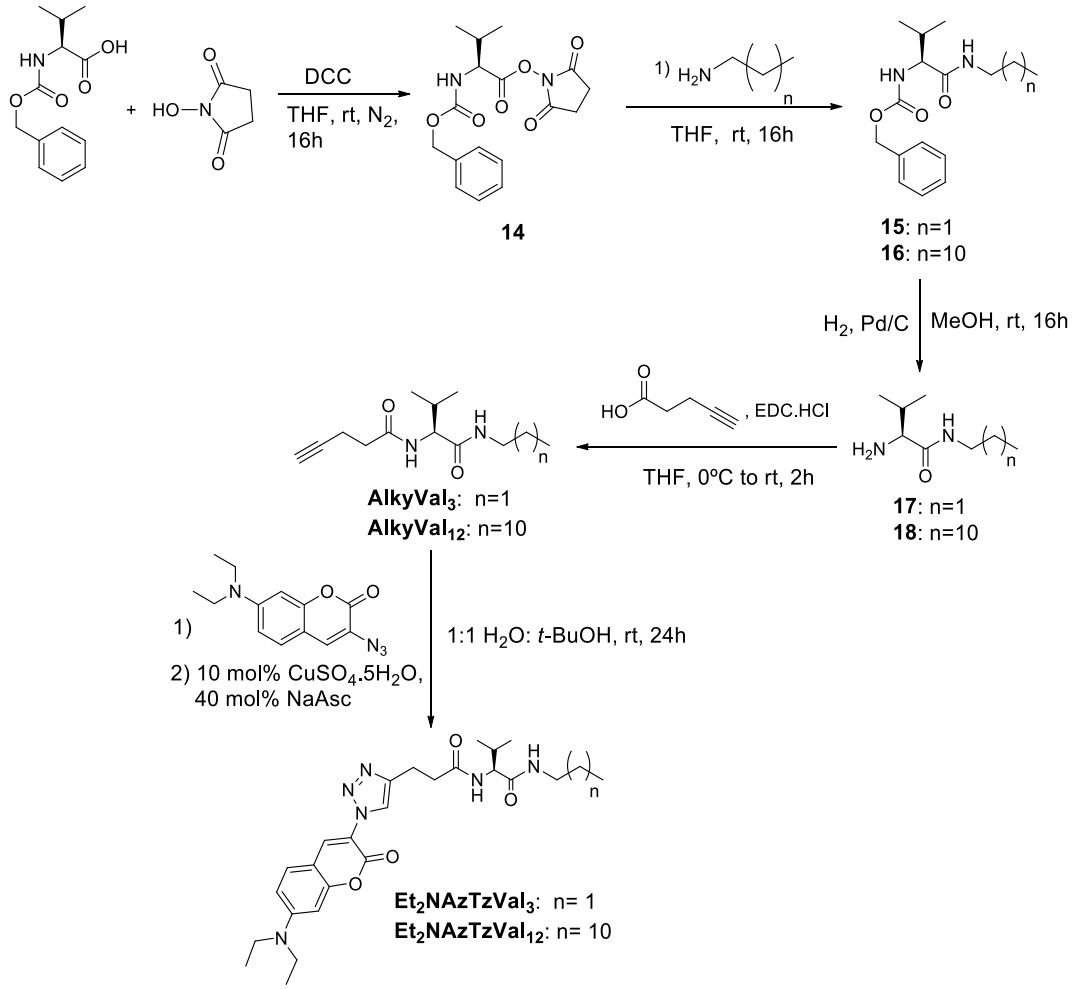

Figure 123. Synthesis of compounds **$Et_2NAzTzVal_n$**.

6.5.5.1. Synthesis of compound 14

A solution of *N,N*-dicyclocarbodiimide (DCC) (9.39 g; 45.5 mmol) in THF (25 mL) was added dropwise to a clear solution of carbobenzyloxy-*L*-valine (11.31 g; 45 mmol) and N-hydroxysuccinimide (5.18 g; 45 mmol) in THF (180 mL) under N_2 at 0 ºC. The resultant mixture was allowed to stir overnight between 0-5 ºC. The resultant white precipitate was filtered and the filtrate concentrated to half and put into the freezer (- 20 ºC) overnight. The remaining dicyclohexylurea was filtered again and the resultant solution evaporated. The precipitate was recrystallized from 2-propanol, giving a white solid (15.64 g, 99%). Characterization: ^{1}H NMR (300 MHz, d_6-DMSO): δ (ppm) 7.35 (m, Ph-H, 5H), 5.27 (d, *J* = 9.0 Hz, -OCONH, 1H), 5.14 (s, $PhCH_2$, 2H), 4.68 (t, *J* = 9.0, -CONHCHCO 1H), 2.83 (s, $-COCH_2CH_2CO$, 4H), 2.33 (m, $-CH(CH_3)_2$, 1H), 1.05 (s, $-CH(CH_3)_2$, 6H).

6.5.5.2. General Procedure Synthesis compounds 15-16

A solution of commercially available alkylamine (14.35 mmol) in anhydrous THF (60 mL) was added dropwise to a solution of compound **14** (5 g; 14.35 mmol) in anhydrous THF (90 mL) under N_2 at 25 ºC, and the resultant mixture stirred overnight at room temperature. The resultant pasty mixture was filtered, washed with 0.1M HCl (15 mL), water (30 mL) and dried under vacuum at 60 ºC.

Compound **15** was obtained as a white solid (4.04 g; 96%). Characterization: ^{1}H NMR (300 MHz, d_6-DMSO): δ (ppm) 7.85 (br s, CONHCH$_2$, 1H), 7.34 (m, Ph-H, 5H), 7.16 (d, *J* = 8.7 Hz, -OCONH, 1H), 5.02 (s, PhCH$_2$, 2H), 3.76 (t, *J* = 7.9, -CONHCHCO, 1H), 2.99 (m, -CONHCH$_2$, 2H), 1.90 (m, -CH(CH$_3$)$_2$, 1H), 1.39 (m, - CH$_2$CH$_2$CH$_3$, 2H), 0.83 (s, -CH(CH$_3$)$_2$ + -CH$_2$CH$_3$, 9H). ^{13}C (75 MHz, d_6-DMSO): δ (ppm) 171.44, 156.55, 137.59, 128.79, 128.221, 128.091, 65.79, 60.85, 30.68, 22.74, 19.67, 18.74, 11.84. ESI-MS (m/z) = 283.1859 $[M+H]^+$; $C_{16}H_{24}N_2O_3$. Calculated for $C_{16}H_{24}N_2O_3$: 283.1865.

Compound **16** was synthesized as a white solid (5.84 g; 97%). Characterization: ^{1}H NMR (300 MHz, d_6-DMSO): δ (ppm) 7.82 (br s, CONHCH$_2$, 1H), 7.34 (m, Ph-H, 5H), 7.15 (d, *J* = 8.8 Hz, -OCONH, 1H), 5.02 (s, PhCH$_2$, 2H), 3.76 (t, *J* = 7.9, -CONHCHCO, 1H), 3.03 (m, -CONHCH$_2$, 2H), 1.91 (m, -CH(CH$_3$)$_2$, 1H), 1.30 (m, - CH$_2$(CH$_2$)$_{10}$CH$_3$, 20H), 0.83 (s, -CH(CH$_3$)$_2$ + -(CH$_2$)$_{10}$CH$_3$, 9H). ^{13}C (75 MHz, d_6-DMSO): δ (ppm) 171.38, 156.53, 137.58, 128.78, 128.21, 128.08, 65.78, 60.83, 31.77, 30.68, 29.43, 29.17, 26.76, 22.56, 19.65, 18.73, 14.42. ESI-MS (m/z) = 419.3269 $[M+H]^+$; $C_{25}H_{42}N_2O_3$. Calculated for $C_{25}H_{42}N_2O_3$: 419.3274.

6.5.5.3. General Procedure Synthesis compounds 17-18

Palladium catalyst (10% Pd/C) was suspended in methanol (100 mL) and stirred at room temperature for 10 min. Then, a solution of compound **15/16** (6.98 mmol) in methanol (30 mL) was added, and the reaction mixture allowed to stir under H_2 for 16h. The black reaction mixture was filtered over celite and the filtrate concentrated on the rotavapor. The resultant oily product was dried under vacuum.

Compound 17 was obtained as a white solid (1.09g; 99%). Characterization: ^{1}H NMR (300 MHz, d_6-DMSO): δ (ppm) 7.76 (br s, CONHCH$_2$, 1H), 3.02 (m, -CONHCH$_2$, 2H), 2.89 (d, *J* = 5.1 Hz, -CHCO, 1H), 1.83 (m, -CH(CH$_3$)$_2$, 1H), 1.40 (m, - CH$_2$CH$_2$CH$_3$, 2H), 0.81 (m, -CH(CH$_3$)$_2$ + -

$CH_2C\underline{H}_3$, 9H).

Compound 18 was synthesized as a white solid (1.95 g; 98%). Characterization: ^{1}H NMR (300 MHz, d_6-DMSO): δ (ppm) 7.71 (br s, CON$\underline{H}CH_2$, 1H), 3.04 (m, -CONHC$\underline{H}_2$, 2H), 2.87 (d, *J* = 5.0 Hz, -C$\underline{H}$CO, 1H), 1.82 (m, -C$\underline{H}(CH_3)_2$, 1H), 1.30 (m, - $CH_2(C\underline{H}_2)_{10}CH_3$, 20H), 0.83 (dd, *J* = 23.0 Hz, 6.5 Hz, -CH(C$\underline{H}_3)_2$ + -$(CH_2)_{10}C\underline{H}_3$, 9H). ^{13}C (75 MHz, d_6-DMSO): δ (ppm) 174.87, 60.55, 38.65, 32.12, 31.78, 29.66, 29.49, 29.19, 26.85, 22.57, 19.99, 17.58, 14.40. ESI-MS (m/z) = 285.2910 $[M+H]^+$; $C_{17}H_{36}N_2O_4$. Calculated for $C_{17}H_{36}N_2O_4$: 285.2906.

6.5.5.4. General Procedure Synthesis compounds AlkyVal$_n$

A suspension of 4-pentynoic acid (4.28 mmol) and EDC.HCl (4.28 mmol) in THF (30 mL) was stirred under N_2 at room temperature. After cooling to 0 ºC, the mixture was treated dropwise with a solution of compound **17/18** (3.42 mmol) in THF (40 mL) and allowed to stir for 2.5h at room temperature. The resultant mixture was concentrated in the rotavapor, filtered and washed with 0.1 M NaOH (10 mL) and water (20 mL). The resultant product was dried under vacuum.

Compound **AlkyVal$_3$** was obtained as a white solid (0.37 g; 45%). Characterization: ^{1}H NMR (300 MHz, d_6-DMSO): δ (ppm) 7.86 (br s, CON$\underline{H}CH_2$, 1H), 4.09 (t, *J* = 8.0 Hz, -CONHC$\underline{H}$CO, 1H), 2.99 (m, -CONHC$\underline{H}_2$, 2H), 2.71 (s, C$\underline{H}$C, 1H), 2.34 (br s, -CC$\underline{H}_2C\underline{H}_2$, 4H), 1.91 (m, -C$\underline{H}(CH_3)_2$, 1H), 1.39 (m, - $CH_2C\underline{H}_2CH_3$, 2H), 0.82 (m, -CH(C$\underline{H}_3)_2$ + -$CH_2C\underline{H}_3$, 9H). ^{13}C (75 MHz, d_6-DMSO): δ (ppm) 171.24, 170.75, 84.29, 71.68, 58.27, 34.42, 30.93, 22.74, 19.66, 18.70, 14.75, 11.85. ESI-MS (m/z) = 239.1753 $[M+H]^+$; $C_{13}H_{22}N_2O_2$. Calculated for $C_{13}H_{22}N_2O_2$: 239.1760.

Compound **AlkyVal$_{12}$** was synthesized as a white solid (1.18 g; 95%). Characterization: Characterization: ^{1}H NMR (300 MHz, d_6-DMSO): δ (ppm) 7.84 (br s, CON$\underline{H}CH_2$, 1H), 4.08 (t, *J* = 7.8 Hz, -CONHC$\underline{H}$CO, 1H), 3.01 (m, -CONHC$\underline{H}_2$, 2H), 2.70 (s, C$\underline{H}$C, 1H), 2.33 (br s, -CC$\underline{H}_2C\underline{H}_2$, 4H), 1.88 (m, -C$\underline{H}(CH_3)_2$, 1H), 1.29 (m, - $CH_2(C\underline{H}_2)_{10}CH_3$, 20H), 0.81 (m, -CH(C$\underline{H}_3)_2$ + -$CH_2C\underline{H}_3$, 9H). ^{13}C (75 MHz, d_6-DMSO): δ (ppm) 171.12, 170.65, 84.24, 71.64, 58.21, 34.40, 31.76, 29.50, 29.42, 26.76, 22.55, 19.62, 18.67, 14.73, 14.40. ESI-MS (m/z) = 365.3162 $[M+H]^+$; $C_{22}H_{40}N_2O_2$. Calculated for $C_{22}H_{40}N_2O_2$: 365.3168.

6.5.5.5. General Procedure Synthesis of compounds $Et_2NAzTzVal_n$

To a solution of **$AlkyVal_n$** (1.51 mmol) in a mixture 3:1 *t*-BuOH:H_2O (60 mL) were added **$Et_2NAzCum$** (0.43 g; 1.66 mmol), $CuSO_4.5H_2O$ (0.074 g; 0.302 mmol) and sodium ascorbate (0.239 g; 1.208 mmol), and the resultant mixture allowed to stir for 24h at room temperature. The crude mixture was concentrated in the rotavapor before the addition of EtOAc (30 mL). The organic phase was washed with a saturated solution $NaHCO_3$ (3 x 15 mL) and brine (2 x 15 mL). The organic extractions were dried over anhydrous $MgSO_4$ and the solvents removed on the rotavapor. The obtained solid was washed with cold diethyl ether (10 mL) and dried under vacuum.

Compound **$Et_2NAzTzVal_3$** was obtained as a brown solid (0.74 g; 99%). Characterization: Characterization: ^{1}H NMR (300 MHz, d_6-DMSO): δ (ppm) 8.40 (s, triazole-H, 1H), 8.24 (s, Coumarin-H, 1H), 7.89 (m, -CONHCH + -CONHCH$_2$, 2H), 7.61 (d, *J* = 7.7 Hz, Coumarin-H, 1H), 6.81 (d, *J* = 9.3 Hz, Coumarin-H, 1H), 6.65 (s, Coumarin-H, 1H), 4.09 (t, *J* = 7.6 Hz, -CONHCH, 1H), 3.47 (m, (CH$_2$CH$_3$)$_2$N-, 4H), 2.98 (m, triazole-CH$_2$CH$_2$ + -CONHCH$_2$, 4H), 2.57 (m, triazole-CH$_2$CH$_2$, 2H), 1.89 (m, -CH(CH$_3$)$_2$, 1H), 1.36 (m, -CH$_2$(CH$_2$)$_{10}$CH$_2$ + (CH$_2$CH$_3$)$_2$N-, 26H), 0.79 (br s, -CH(CH$_3$)$_2$ + -CH$_2$CH$_3$, 9H). ^{13}C (75 MHz, d_6-DMSO): δ (ppm) 171.63, 171.32, 157.14, 156.03, 151.83, 136.88, 130.96, 123.30, 116.76, 110.46, 106.94, 96.80, 58.34, 44.69, 34.83, 30.77, 22.74, 21.79, 19.63, 18.62, 12.75, 11.81. ESI-MS (m/z) = 497.2879 $[M+H]^+$; $C_{26}H_{36}N_6O_4$. Calculated for $C_{26}H_{36}N_6O_4$: 497.2876.

Compound **$Et_2NAzTzVal_{12}$** was obtained as a green solid (0.45 g; 48%). Characterization: ^{1}H NMR (300 MHz, d_6-DMSO): δ (ppm) 8.39 (s, triazole-H, 1H), 8.23 (s, Coumarin-H, 1H), 7.92 (m, -CONHCH + -CONHCH$_2$, 2H), 7.60 (d, *J* = 8.8 Hz, Coumarin-H, 1H), 6.80 (d, *J* = 8.4 Hz, Coumarin-H, 1H), 6.63 (s, Coumarin-H, 1H), 4.07 (t, *J* = 7.6 Hz, -CONHCH, 1H), 3.45 (m, (CH$_2$CH$_3$)$_2$N-, 4H), 2.97 (m, triazole-CH$_2$CH$_2$ + -CONHCH$_2$, 4H), 2.55 (m, triazole-CH$_2$CH$_2$, 2H), 1.88 (m, -CH(CH$_3$)$_2$, 1H), 1.20 (m, -CH$_2$(CH$_2$)$_{10}$CH$_2$ + (CH$_2$CH$_3$)$_2$N-, 26H), 0.79 (m, -CH(CH$_3$)$_2$ + -CH$_2$CH$_3$, 9H). ^{13}C (75 MHz, d_6-DMSO): δ (ppm) 171.58, 171.10, 157.16, 155.04, 136.78, 130.94, 123.26, 116.73, 110.50, 107.05, 96.70, 58.36, 34.76, 31.74, 29.44, 22.55, 26.80, 21.83, 19.60, 18.59, 14.39, 12.73. ESI-MS (m/z) = 623.4279 $[M+H]^+$; $C_{35}H_{54}N_6O_4$. Calculated for $C_{35}H_{54}N_6O_4$: 623.4285.

Chapter 7

Final Conclusions

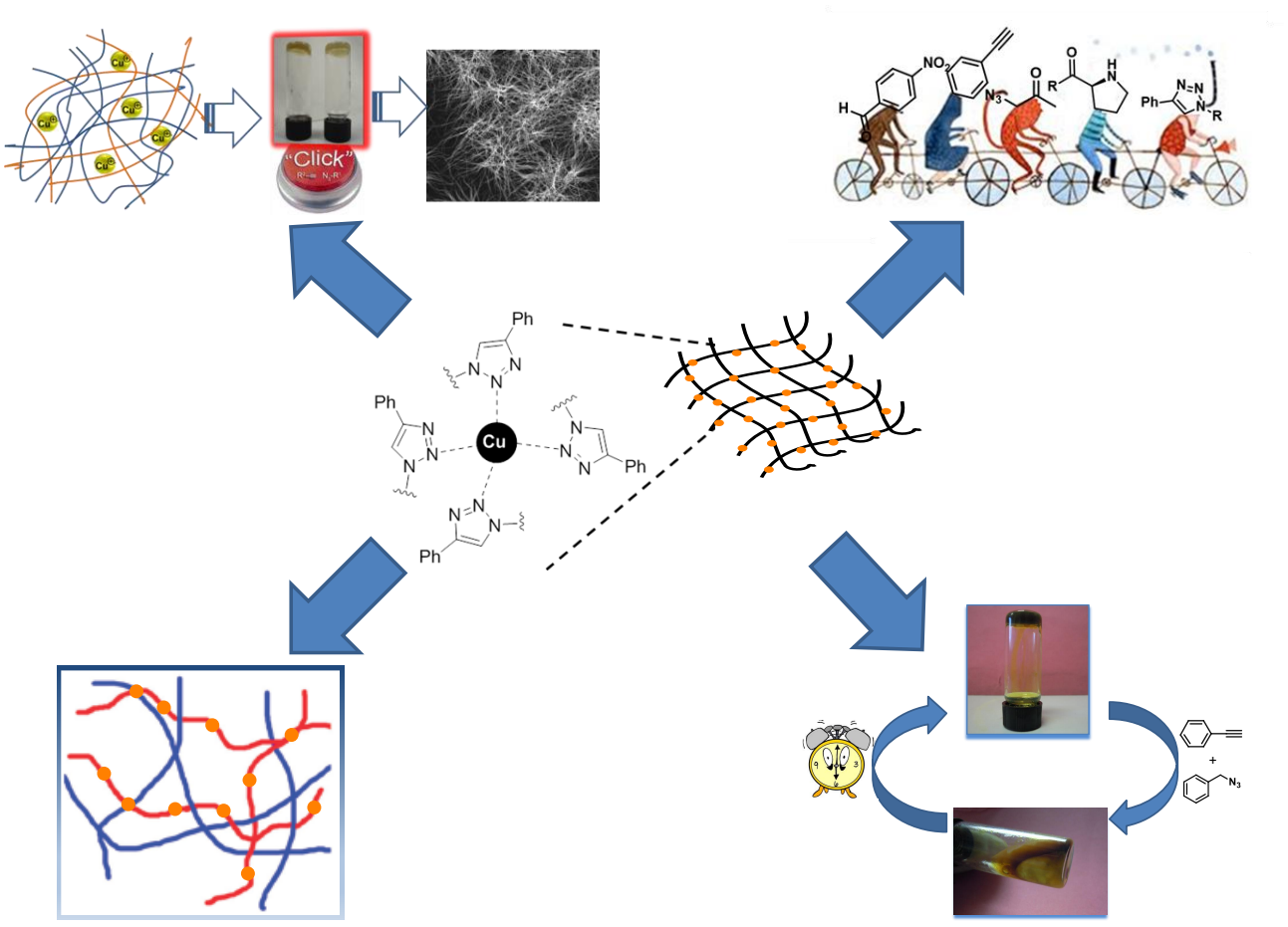

The thesis aims the design, synthesis and characterisation of molecular gels that could be applied as heterogeneous catalysts for 'click' reactions, namely in the Huisgen 1,3-dipolar cycloaddition. Inspired by the copper catalysed variant of this reaction, the *L*-valine derived compounds were functionalized with triazole fragment to provide them with coordination ability.

The presence of the metal did not have a remarkable influence on the self-assembly of the gelators, although it has been observed a pronounced reinforcement of the gels **PhTzVal$_3$** and **PhTzVal$_8$**, probably due to cross-linking provided by the metal centre. In the gels having a three carbon chain length, the coordination to the metal resulted in the formation of more crystalline and organised closely-packed structures, to which it was attributed the lower autocatalytic activity of the gel **PhTzVal$_3$**. All the gels of **PhTzVal$_n$** family were able to coordinate more than 99% of copper in solution, evidencing that the way in which the gelator self-assembles before and along the reaction is a determinant factor for the different autocatalytic ability of the gelators.

The ability of **PhTzVal$_3$** to form gels in water allowed its use as a tandem catalyst for a click-aldol reaction system. The metallogel was able to catalyse both the click and aldol reactions, achieving the final 'clicked'-aldol products in 62% yield in 2d. The catalysis appears to follow a mechanism similar to typeII-aldolases, where the coordination of the substrate to the metal centre together with an aggregation effect of the metallogel seem to be on the source of its good catalytic activity.

Our studies were also directed to the synthesis of functional multicomponent materials. Although we were not capable of revealing the self-assembly process of a multicomponent fluorescent gel by following its formation using fluorescence confocal microscopy, it was proven that the formation of a multicomponent reactant-catalytic gel network could be a useful methodology for the design of new multifunctional gel materials. The product of the reaction was formed exactly on the same place were the catalytic fibers were present, revealing the fundamental role of these heterogeneous catalytic gel materials.

Following from this work, a new triazole functionalized amphiphilic fluorescent gel with catalytic activity for the model click reaction has been obtained. The dynamic behaviour of this system was well represented by the ability of this gel to change between transient self-assembled states. The reactants were responsible for the activation of the gel consequent catalytic activity. The gel could also be applied as a sensor to measure the progress of the reaction, since it was able to reassemble around 50% conversion. Furthermore, it could be used two consecutive times without loss of catalytic activity in a continuous recycling mode. The fact that it do not need to be isolated

between each catalytic cycle evidences the green an environmentally-friendly behaviour of this catalytic gel.

In summary, this thesis highlights the versatility and dynamic behaviour of organometallic gel systems, suggesting their application as potential heterogeneous catalysts for CuAAC. High copper loading capacity, ability to form gels in water, easy functionalization using traditional synthetic procedures, together with their aminoacid derived nature constitute clear advantages for the application of these heterogeneous systems in the catalysis of bioconjugation 'click' reactions, constituting a valuable alternative for the use of strain-promoted catalysis with cyclooctines.

Despite the mentioned achievements, there are some issues that should be improved such as the catalytic activity of the bolaamphiphilic gelators to the model 'click' reaction. Additionally, the use of a fluorescent alkyne reactant in **Chapter 5** coupled with a lower background emission would be advantageous on the moment of visualizing the network of the initial two-component gels and following the self-assembly process. Last but not least, the recyclability of the gel catalyst presented in **Chapter 6** should be improved in order to obtain a "greener" and economically valuable heterogeneous catalyst.

Conclusiones finales

La tesis tiene como principal objetivo el diseño, síntesis y caracterización de geles moleculares y su aplicación como catalizadores heterogéneos para reacciones 'click', principalmente en la reacción de cicloadición Huisgen 1,3-dipolar. Partiendo de la variante de esta reacción catalizada por cobre, gelantes derivados de *L*-valina fueron funcionalizados con triazol para que actúen como ligandos de cobre (I).

La presencia del metal no influye significativamente en el auto-ensamblaje de los gelantes, aunque haya sido observado un refuerzo de la estructura de los geles de la familia **PhTzVal$_n$**, probablemente debido a la habilidad de "cross-linking" aportada por el centro metálico. En los geles bolaanfifilicos donde los dos fragmentos de *L*-valina están separados por una cadena de 3 átomos de carbono, la coordinación del metal favorece la formación de geles más cristalinos y organizados en estructuras más empaquetadas, los cuales revelaron una peor actividad autocatalítica. Todos los geles de la familia **PhTzVal$_n$** revelaron una buena afinidad por el metal, siendo capaces de coordinar más del 99% del cobre (I), comprobando que su diferente actividad catalítica depende principalmente de la forma como el gelante se auto-ensambla antes y durante la reacción.

La habilidad del compuesto **PhTzVal$_3$** para formar geles en agua permitió su utilización como un catalizador tándem en un sistema reacción 'click'-aldol. El metalogel ha sido capaz de catalizar tanto la reacción 'click' como la adición aldólica, obteniéndose los aldoles-'clickados' en 2 días con un rendimiento de 62%. La catálisis puede seguir un mecanismo similar al de las aldolasas de tipo II, donde la coordinación del sustrato al centro metálico y la agregación del metalogel parecen contribuir a una buena actividad catalítica.

La síntesis de materiales multicomponente funcionales también ha merecido una especial atención durante la realización de este trabajo doctoral. Aunque no se haya conseguido seguir el proceso de auto-ensamblaje de un gel multicomponente fluorescente utilizando la técnica de microespectroscopia confocal de fluorescencia, se ha observado que la formación de una red multicomponente formada por un gel reactivo y otro catalítico podrá constituir una importante metodología para el desarrollo de nuevos geles multifuncionales.

En el seguimiento de esto estudio, un nuevo gel anfifilico fluorescente funcionalizado con un fragmento de triazol ha sido desarrollado. El comportamiento dinámico de este sistema está bien representado en la capacidad de este gel para cambiar entre diferentes estados auto-ensamblados

transitorios. La adición de reactivos a este sistema resulta en la activación del gelante y en su consecuente actividad catalítica. Dicho gel podría también ser utilizado como un sensor para medir el rendimiento de la reacción 'click' modelo entre la bencilazida y el fenilacetileno, aprovechando el hecho de que el gel vuelve a auto-ensamblarse cuando el rendimiento de la reacción está en torno al 50%. Además, el gel puede ser utilizado dos veces consecutivas sin perder su actividad catalítica y sin necesidad de ser aislado entre cada ciclo catalítico, evidenciando el comportamiento sostenible de esto nuevo gel catalítico.

En resumen, esta tesis resalta la versatilidad y el comportamiento dinámico de los geles organometálicos, demostrando su aplicación como potenciales catalizadores de la CuAAC. La combinación de factores como la buena capacidad de coordinación al cobre(I), habilidad para formar geles en agua, sencilla funcionalización utilizando procesos sintéticos tradicionales y el hecho que deriven de amino ácidos, constituyen importantes ventajas para la aplicación de estos sistemas como catalizadores heterogéneos de reacciones 'click' de bioconjugación, pudiendo funcionar como una alternativa viable a la catálisis utilizando ciclooctinos.

Aunque se hayan alcanzado resultados bastante satisfactorios, hay todavía algunos aspectos que se pueden mejorar, uno de ellos la actividad catalítica de los gelantes bolaanfifilicos en la reacción 'click' modelo. Adicionalmente, el uso de un gel alquino fluorescente en el Capítulo 5 acoplada a una emisión más baja del fondo constituirían importantes ventajas no solo a la hora de visualizar la red del gel de dos componentes, sino también a la hora de seguir su proceso de auto-ensamblaje por microscopia. Por último, pero no menos importante, la reciclabilidad del gel descrito en el Capítulo 6 deberá ser mejorada de cara a obtener un catalizador heterogéneo sostenible y económicamente ventajoso.

Annex

NMR spectra of selected compounds

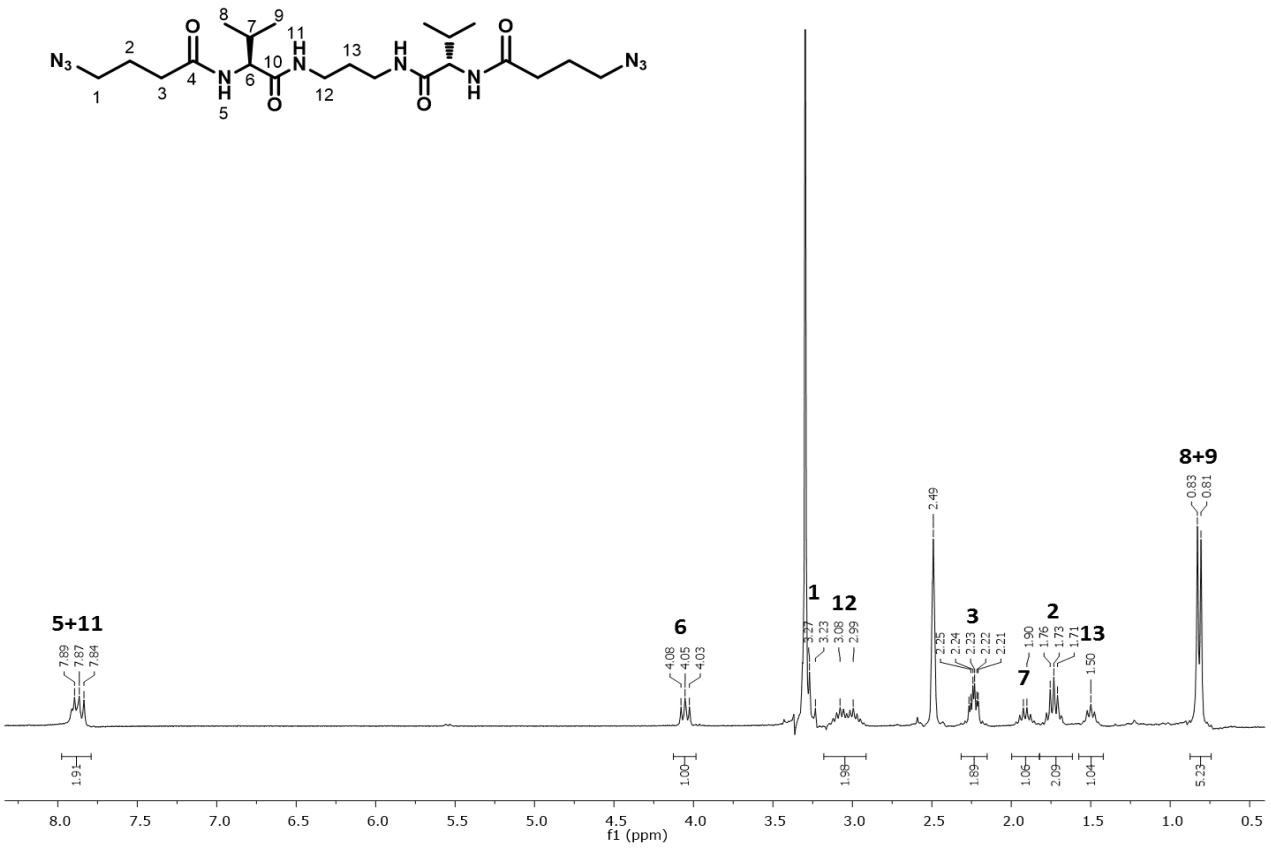

Figure 124. ^{1}H-NMR spectrum of compound **$N_3Val_3N_3$** (300 MHz, d_6-DMSO).

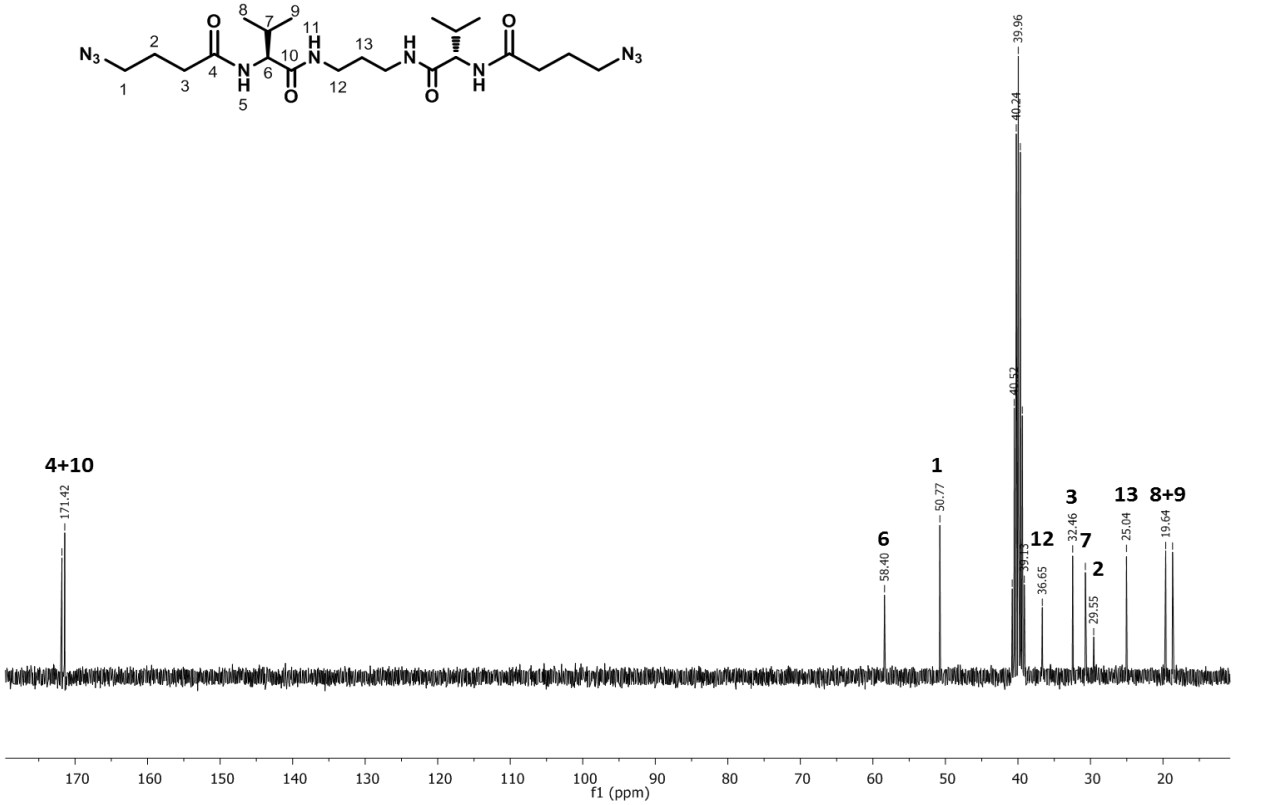

Figure 125. ^{13}C-NMR spectrum of compound **$N_3Val_3N_3$** (300 MHz, d_6-DMSO).

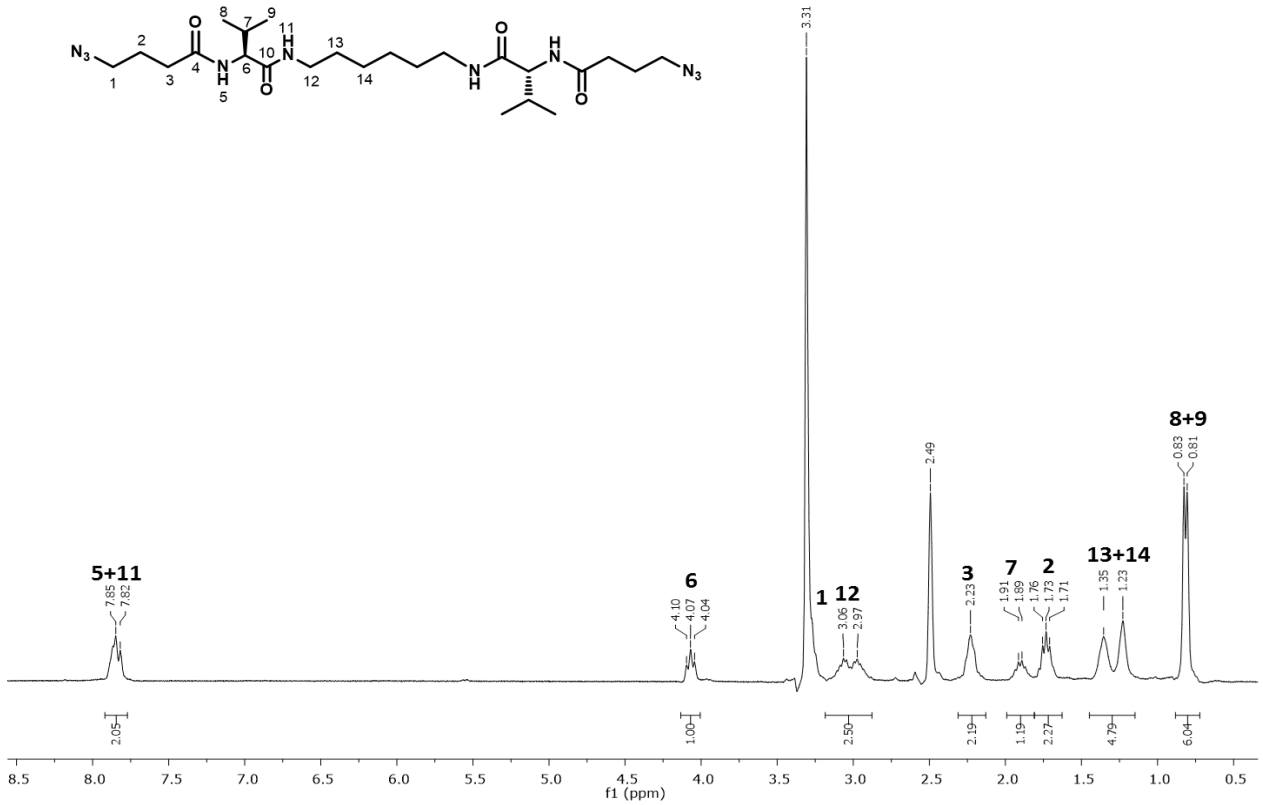

Figure 126. ^{1}H-NMR spectrum of compound **$N_3Val_6N_3$** (300 MHz, d_6-DMSO).

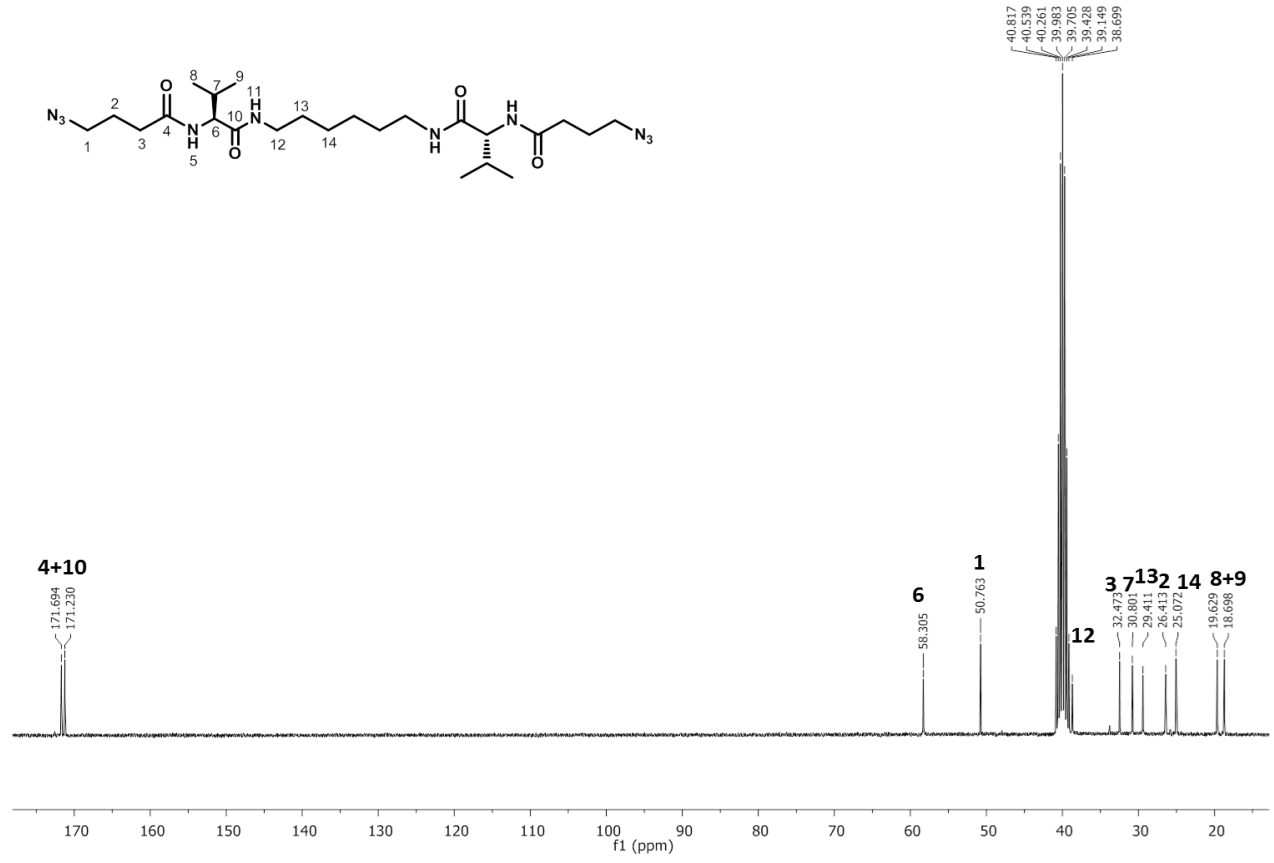

Figure 127. ^{13}C-NMR spectrum of compound **$N_3Val_6N_3$** (300 MHz, d_6-DMSO).

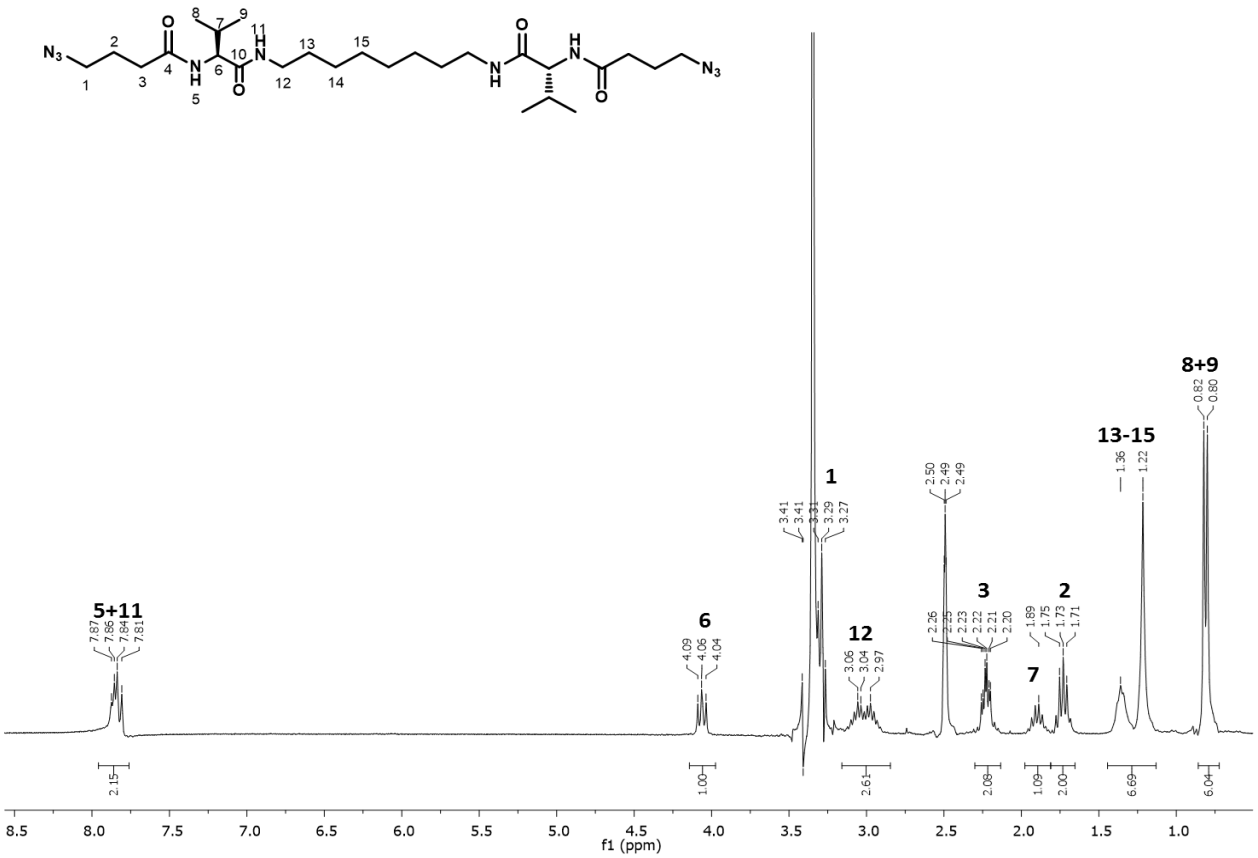

Figure 128. ^{1}H-NMR spectrum of compound **$N_3Val_8N_3$** (300 MHz, d_6-DMSO).

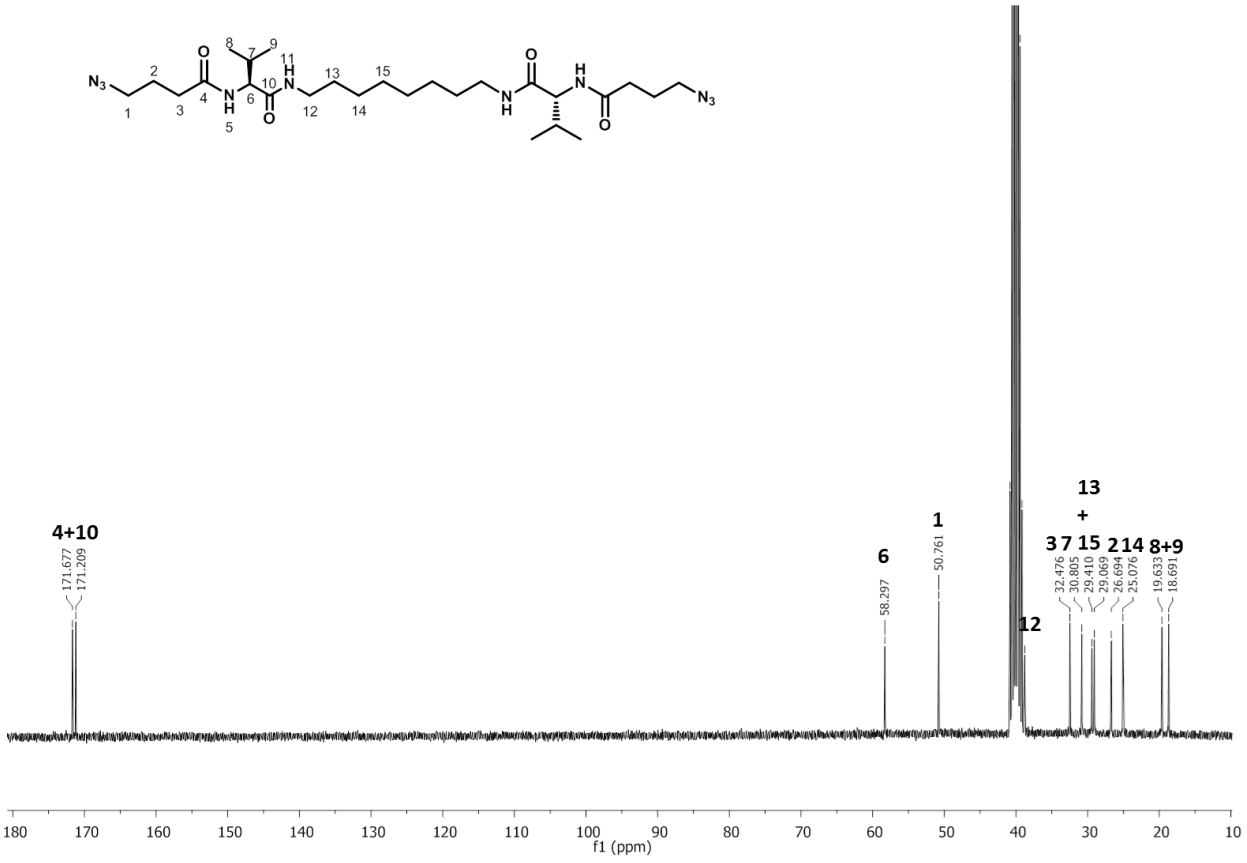

Figure 129. ^{13}C-NMR spectrum of compound **$N_3Val_8N_3$** (300 MHz, d_6-DMSO).

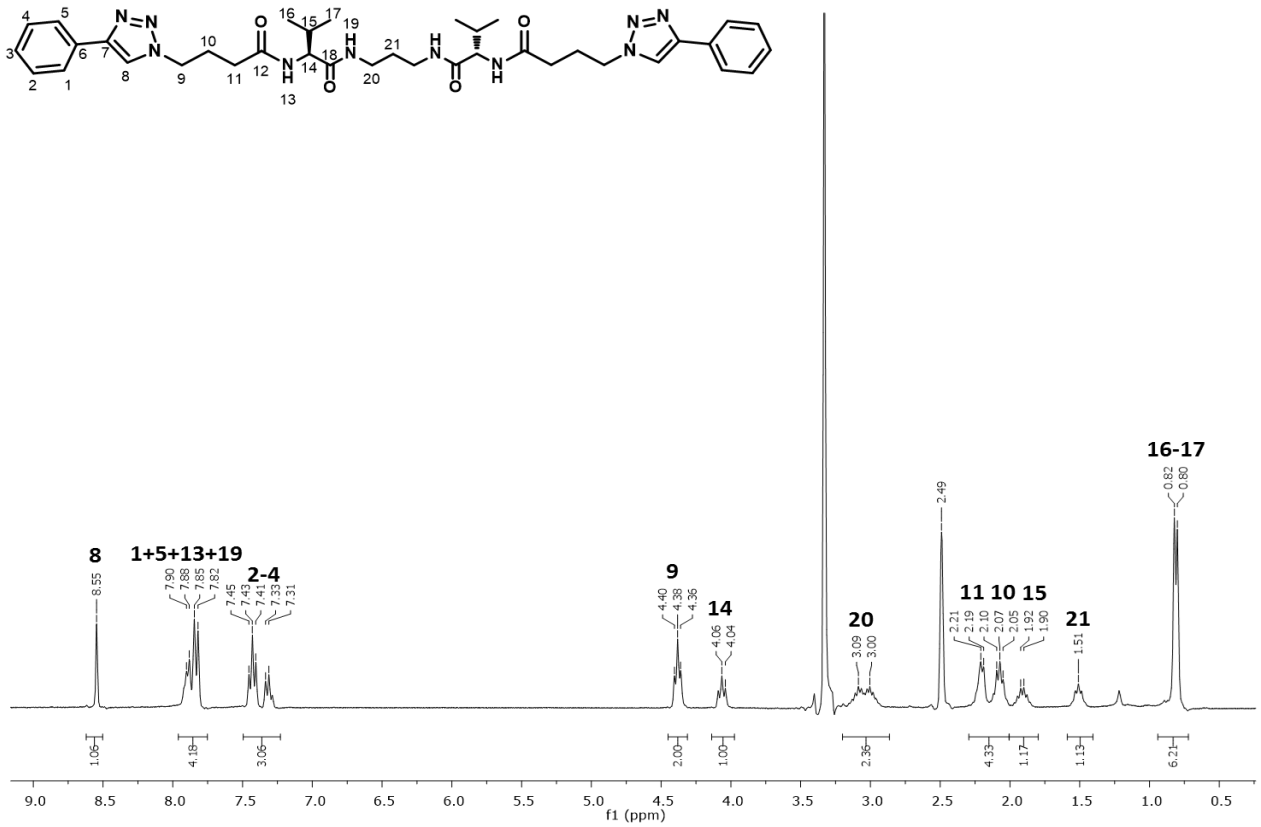

Figure 130. ^{1}H-NMR spectrum of compound **PhTzVal$_3$** (300 MHz, d_6-DMSO).

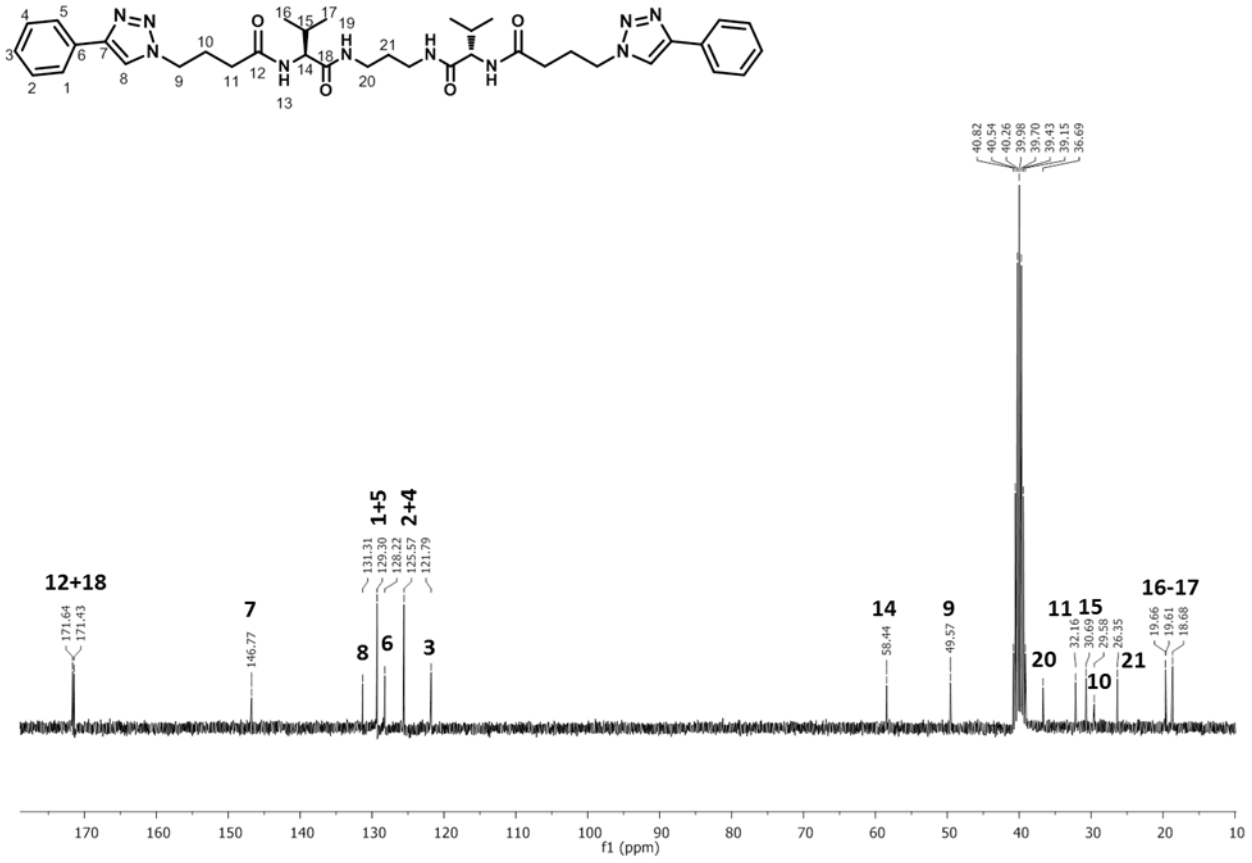

Figure 131. ^{13}C-NMR spectrum of compound **PhTzVal$_3$** (300 MHz, d_6-DMSO).

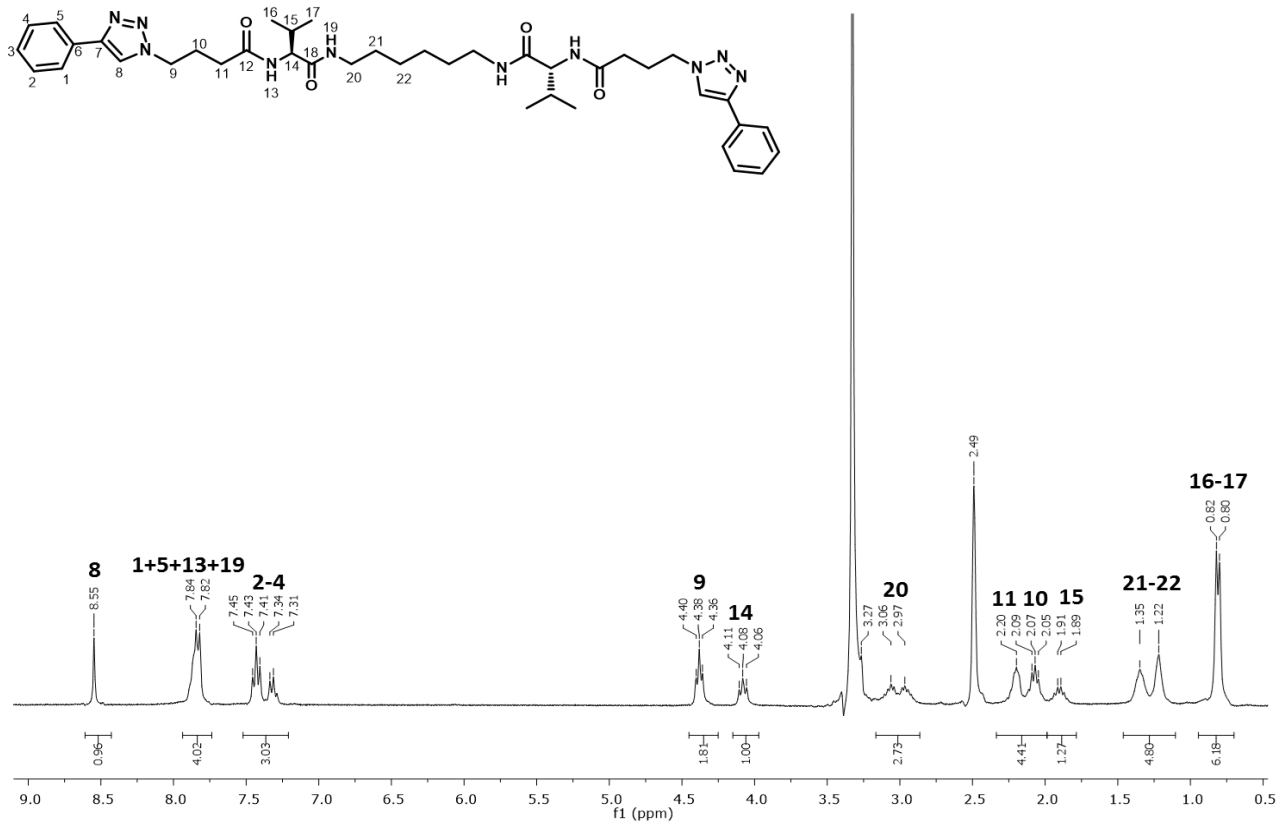

Figure 132. ^{1}H-NMR spectrum of compound **PhTzVal$_6$** (300 MHz, d_6-DMSO).

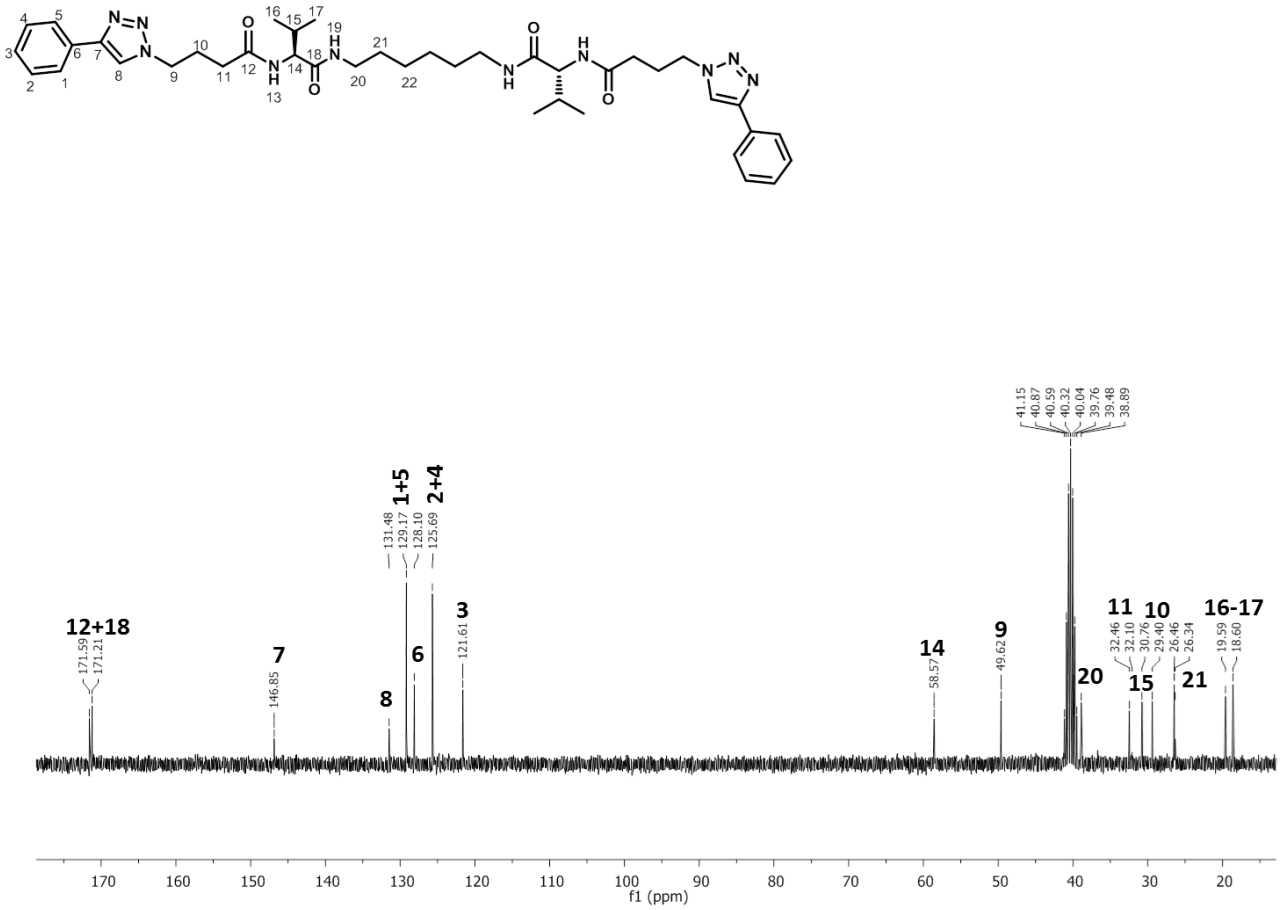

Figure 133. ^{13}C-NMR spectrum of compound **PhTzVal$_6$** (300 MHz, d_6-DMSO).

Figure 134. [1]H-NMR spectrum of compound **PhTzVal$_8$** (300 MHz, d_6-DMSO).

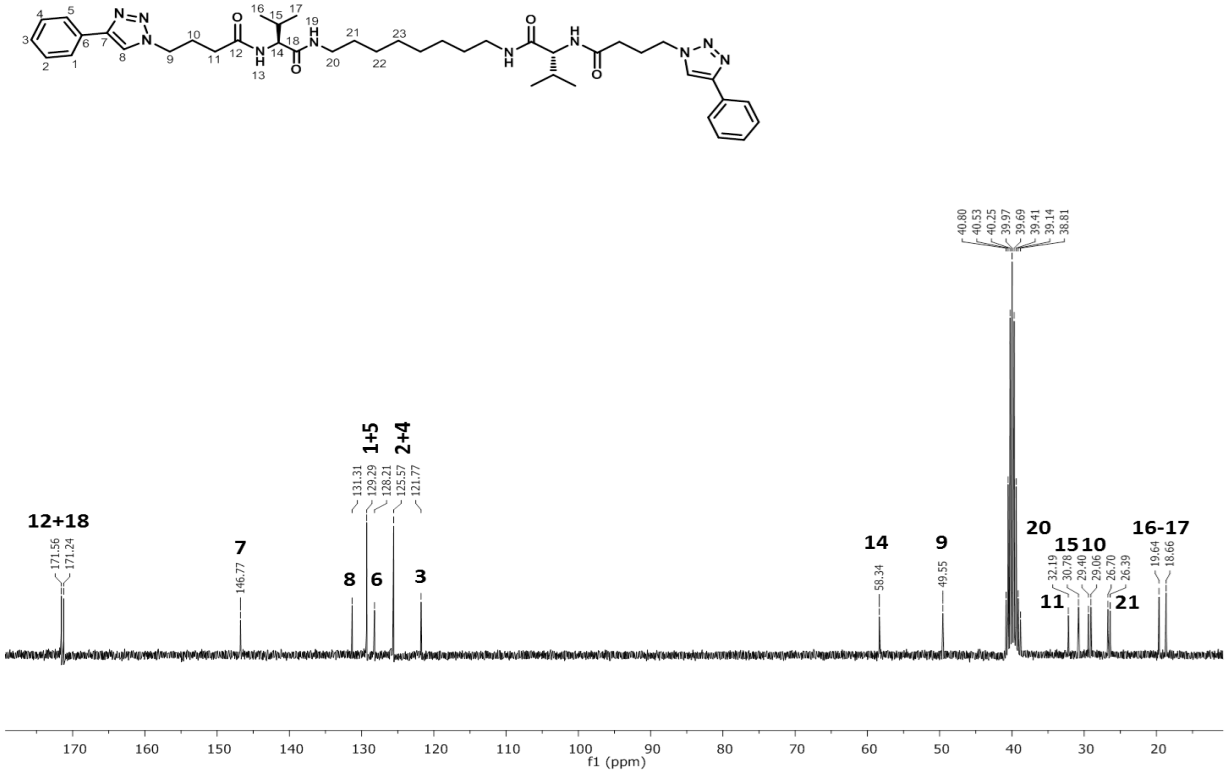

Figure 135. [13]C-NMR spectrum of compound **PhTzVal$_8$** (300 MHz, d_6-DMSO).

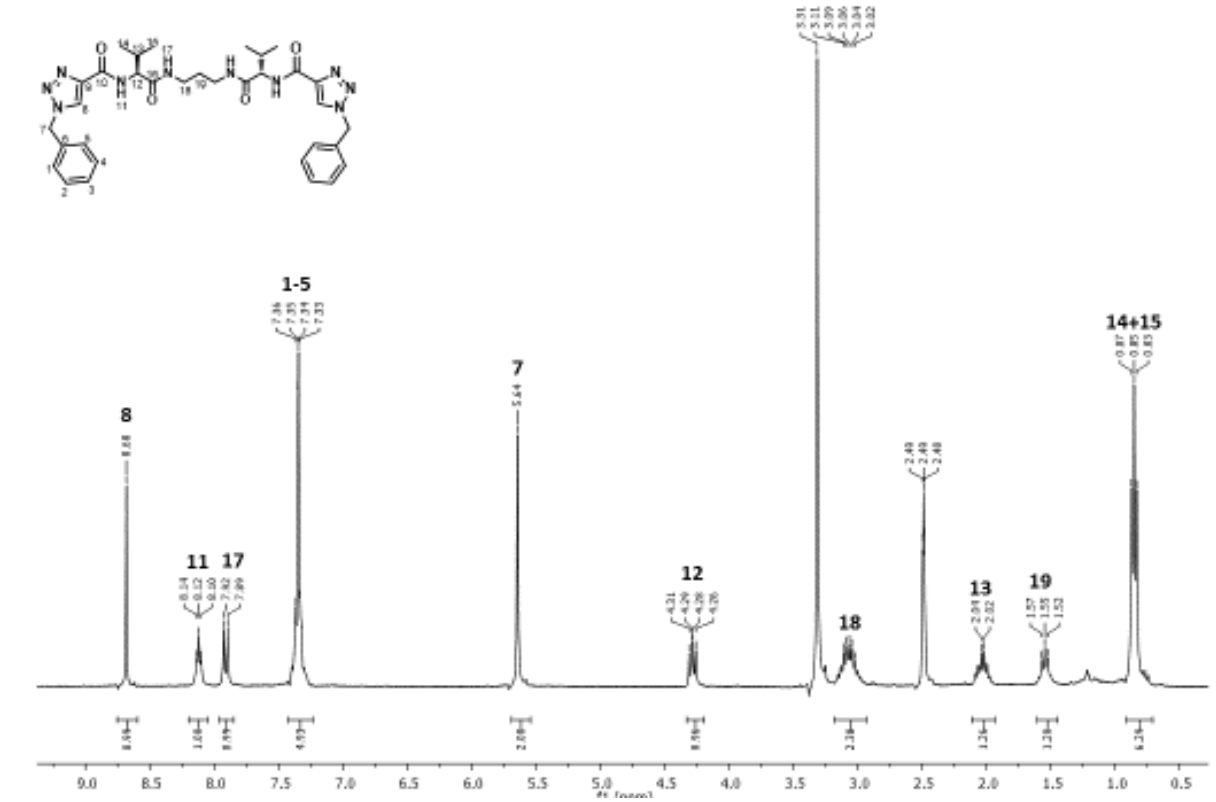

Figure 136. ^{1}H-NMR spectrum of compound **BzTzAVal$_3$** (300 MHz, d_6-DMSO).

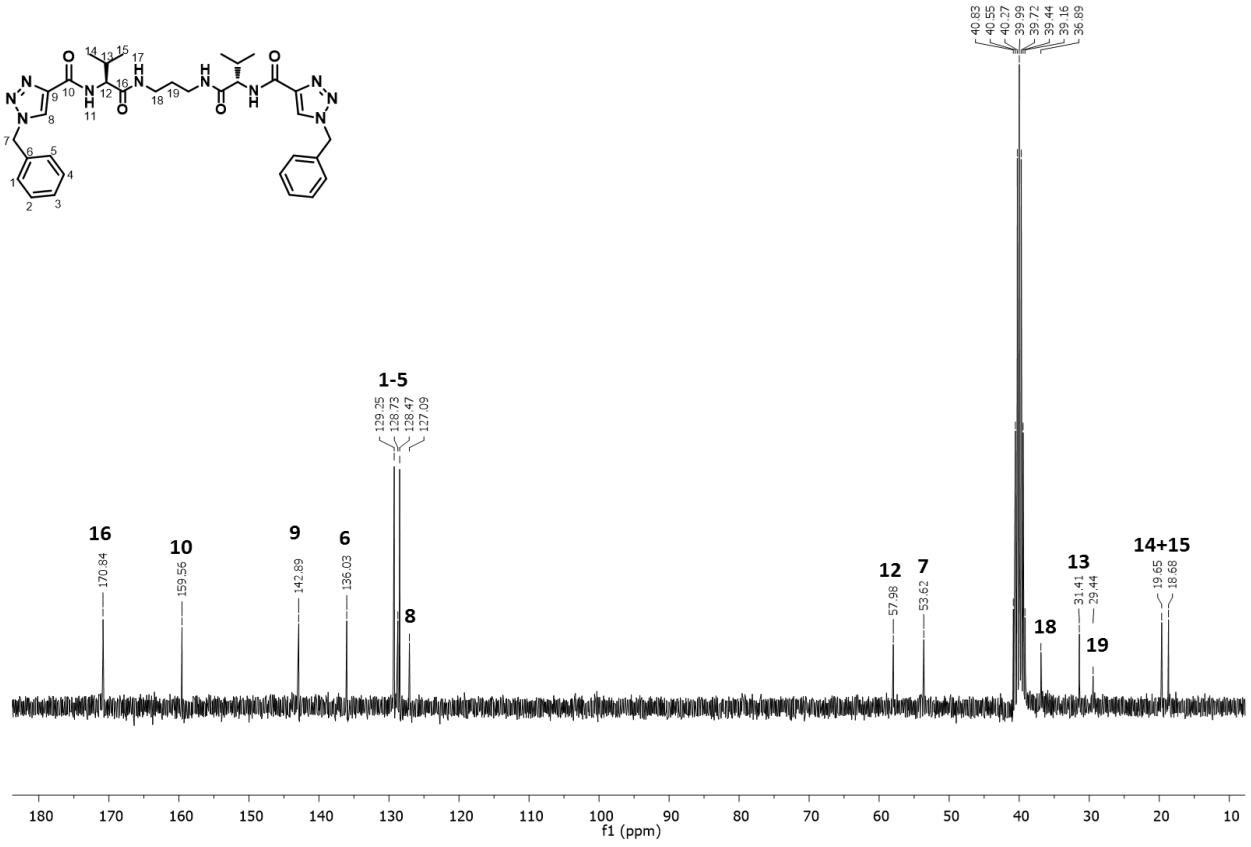

Figure 137. ^{13}C-NMR spectrum of compound **BzTzAVal$_3$** (300 MHz, d_6-DMSO).

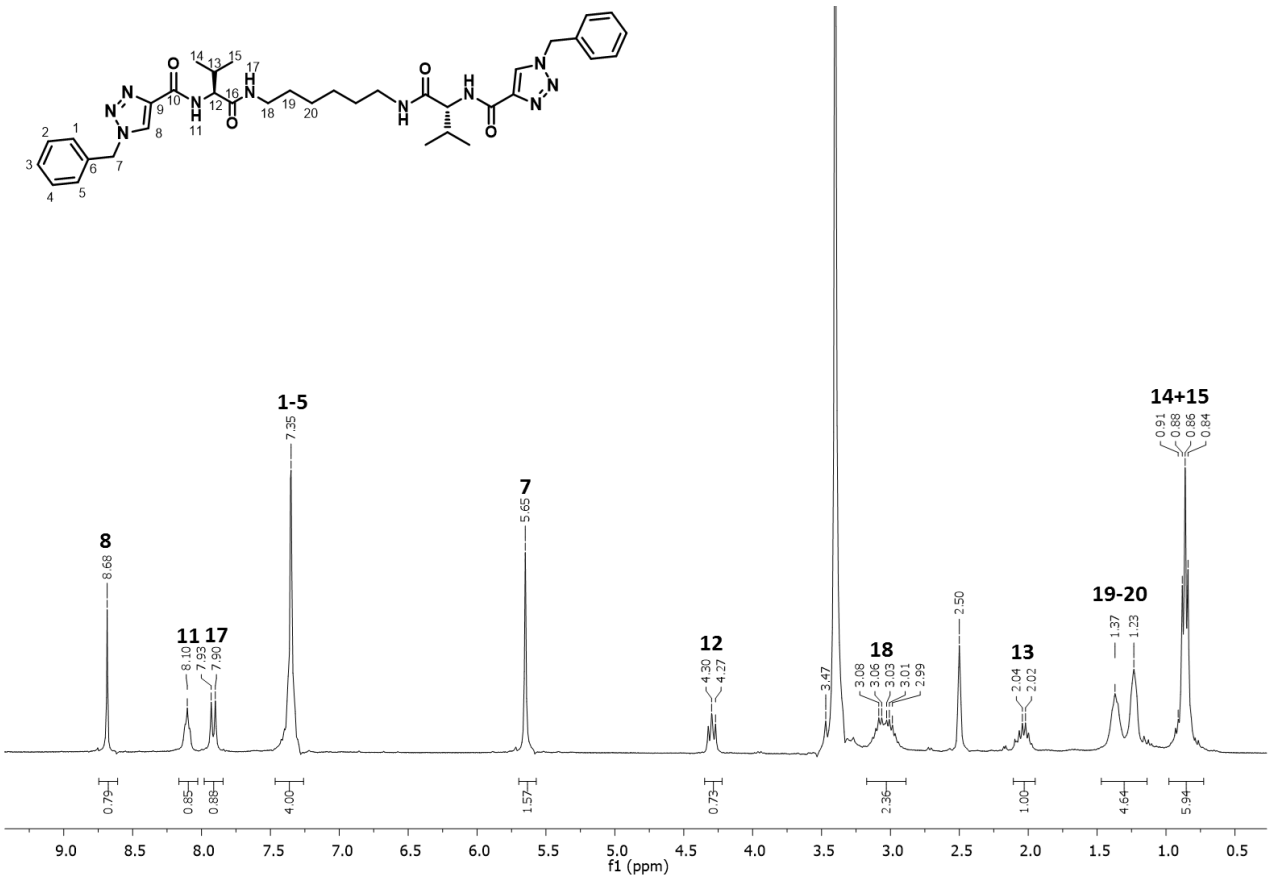

Figure 138. ^{1}H-NMR spectrum of compound **BzTzAVal$_6$** (300 MHz, d_6-DMSO).

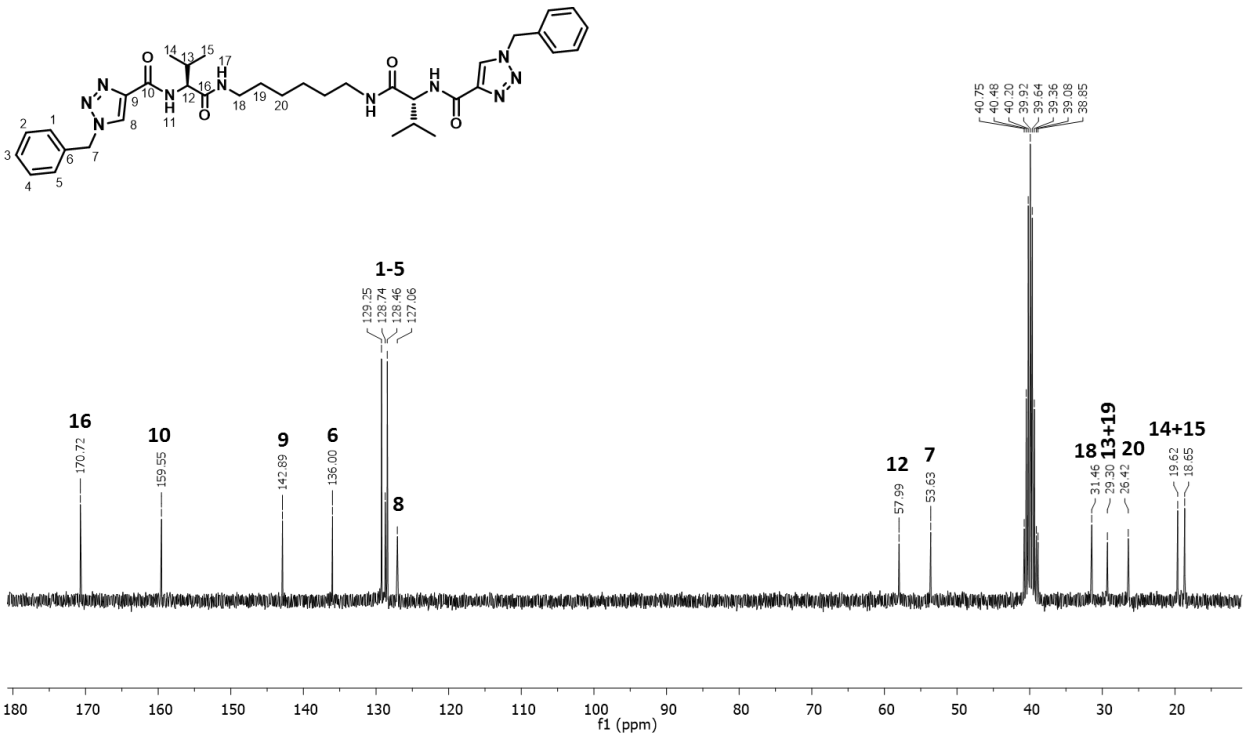

Figure 139. ^{13}C-NMR spectrum of compound **BzTzAVal$_6$** (300 MHz, d_6-DMSO).

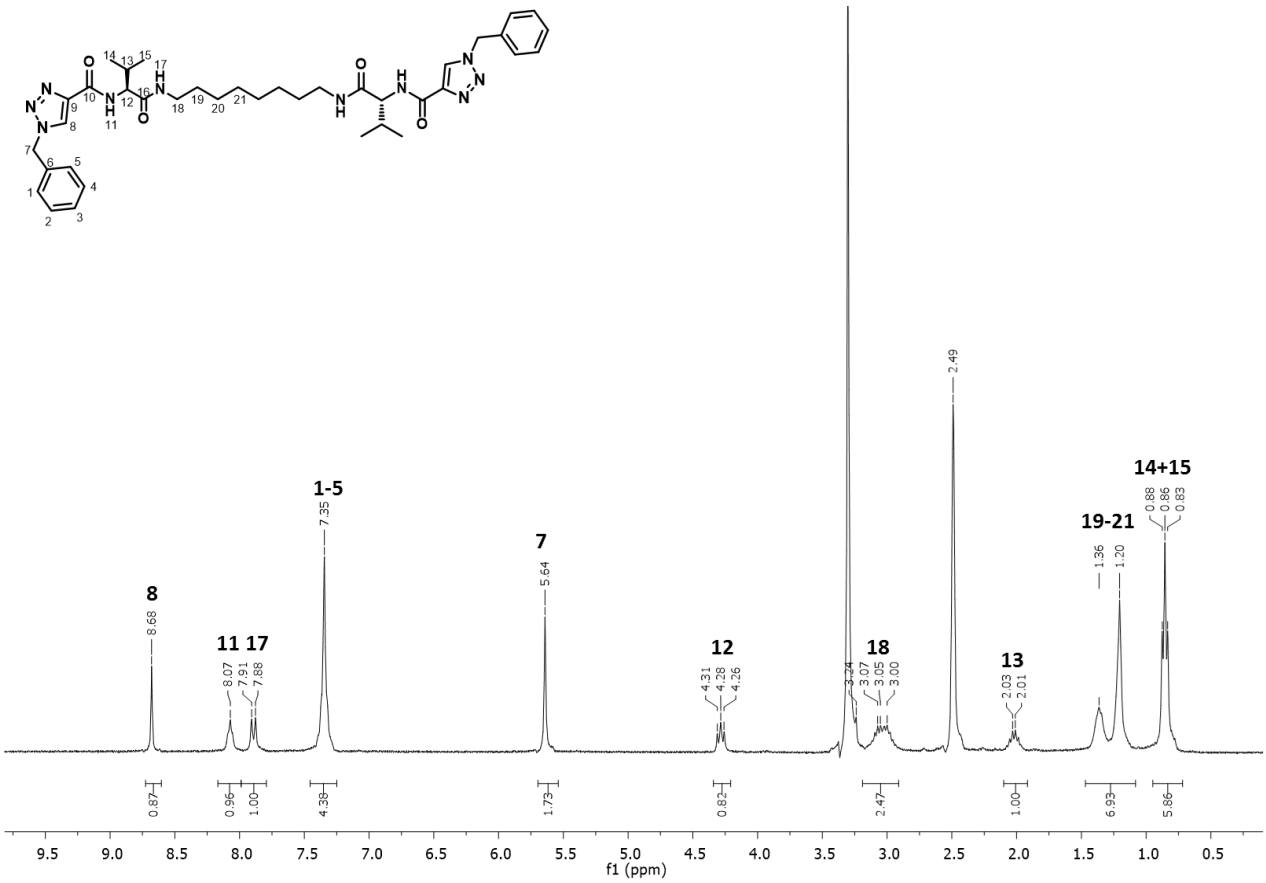

Figure 140. [1]H-NMR spectrum of compound **BzTzAVal$_8$** (300 MHz, d_6-DMSO).

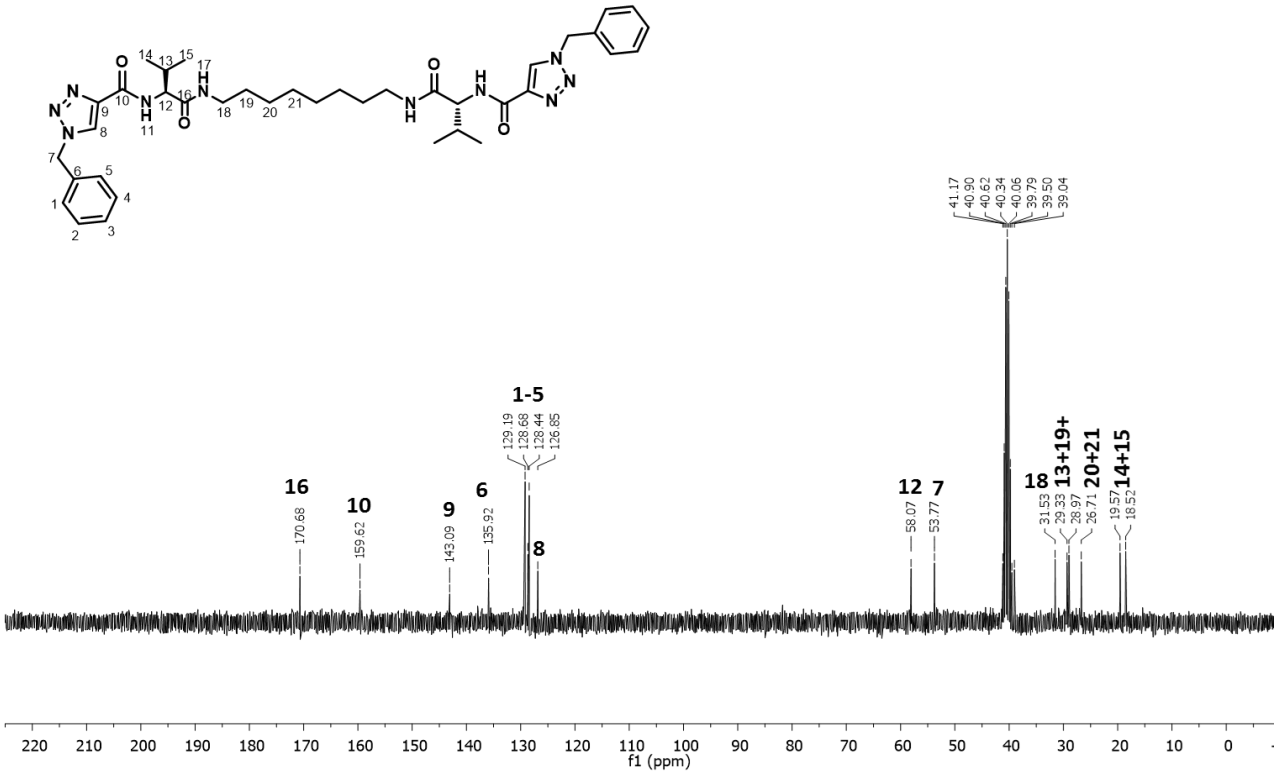

Figure 141. [13]C-NMR spectrum of compound **BzTzAVal$_8$** (300 MHz, d_6-DMSO).

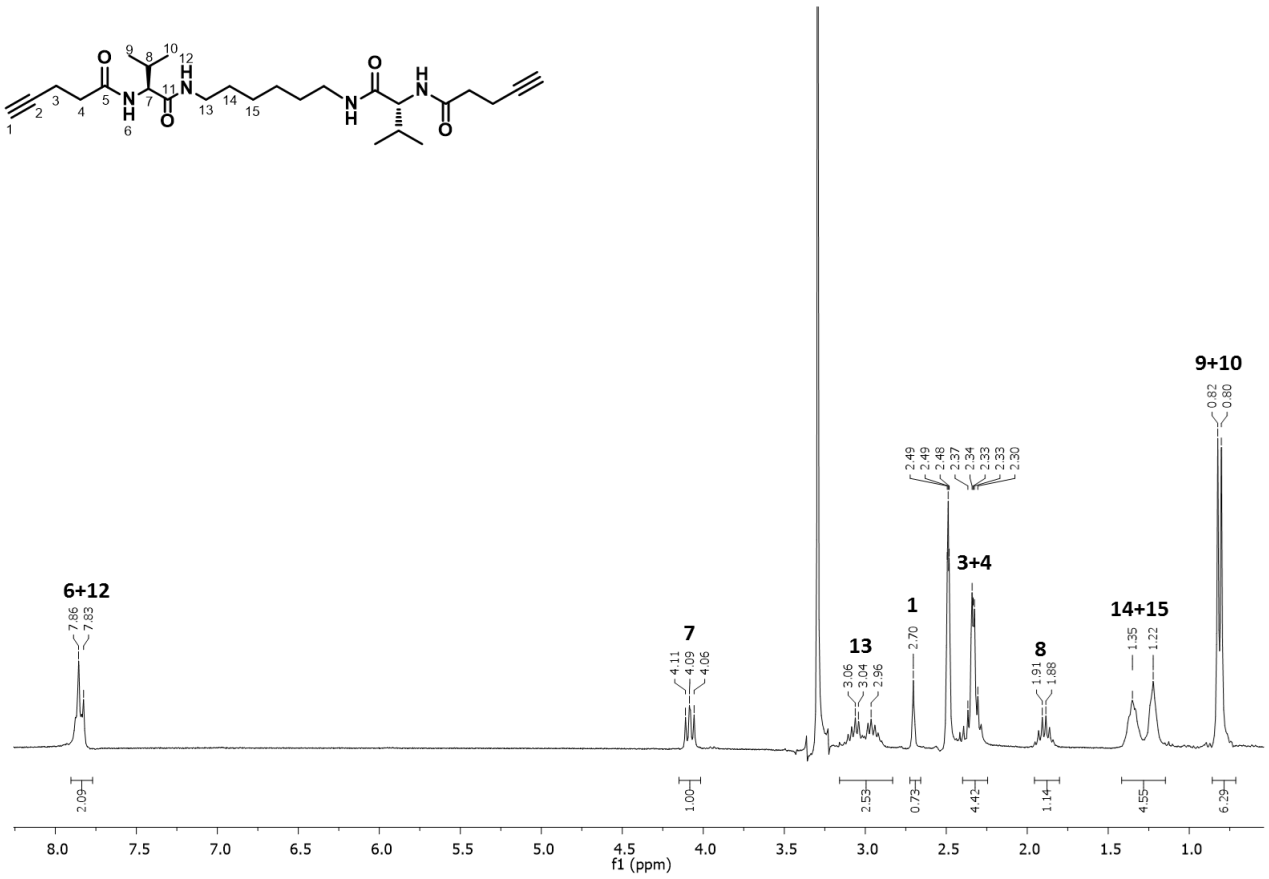

Figure 142. ^{1}H-NMR spectrum of compound **AlkyVal$_6$** (300 MHz, d_6-DMSO).

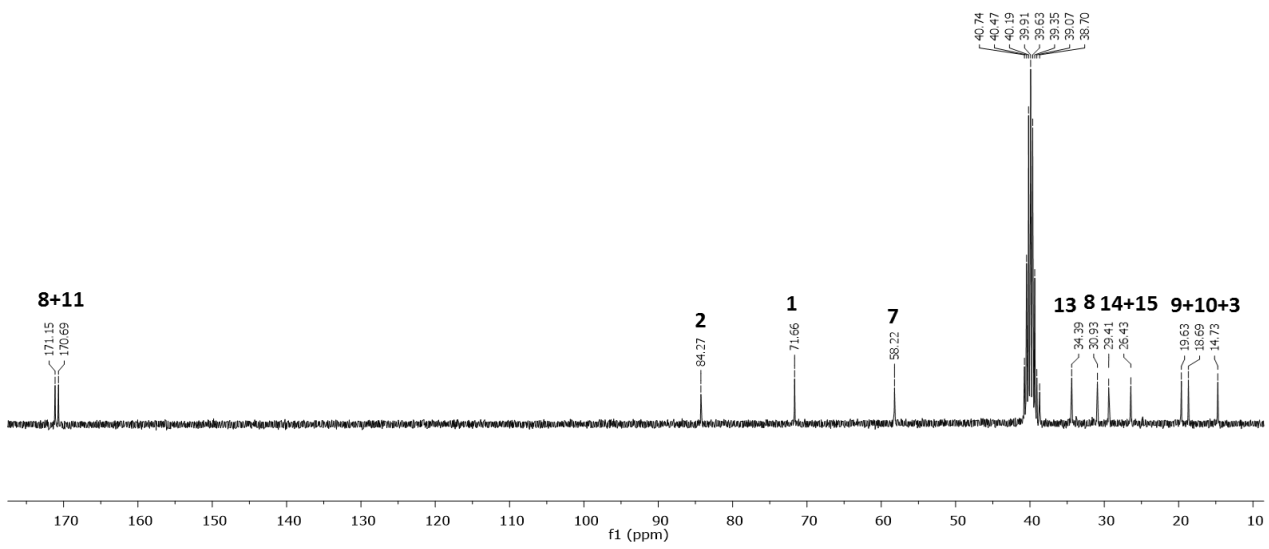

Figure 143. ^{13}C-NMR spectrum of compound **AlkyVal$_6$** (300 MHz, d_6-DMSO).

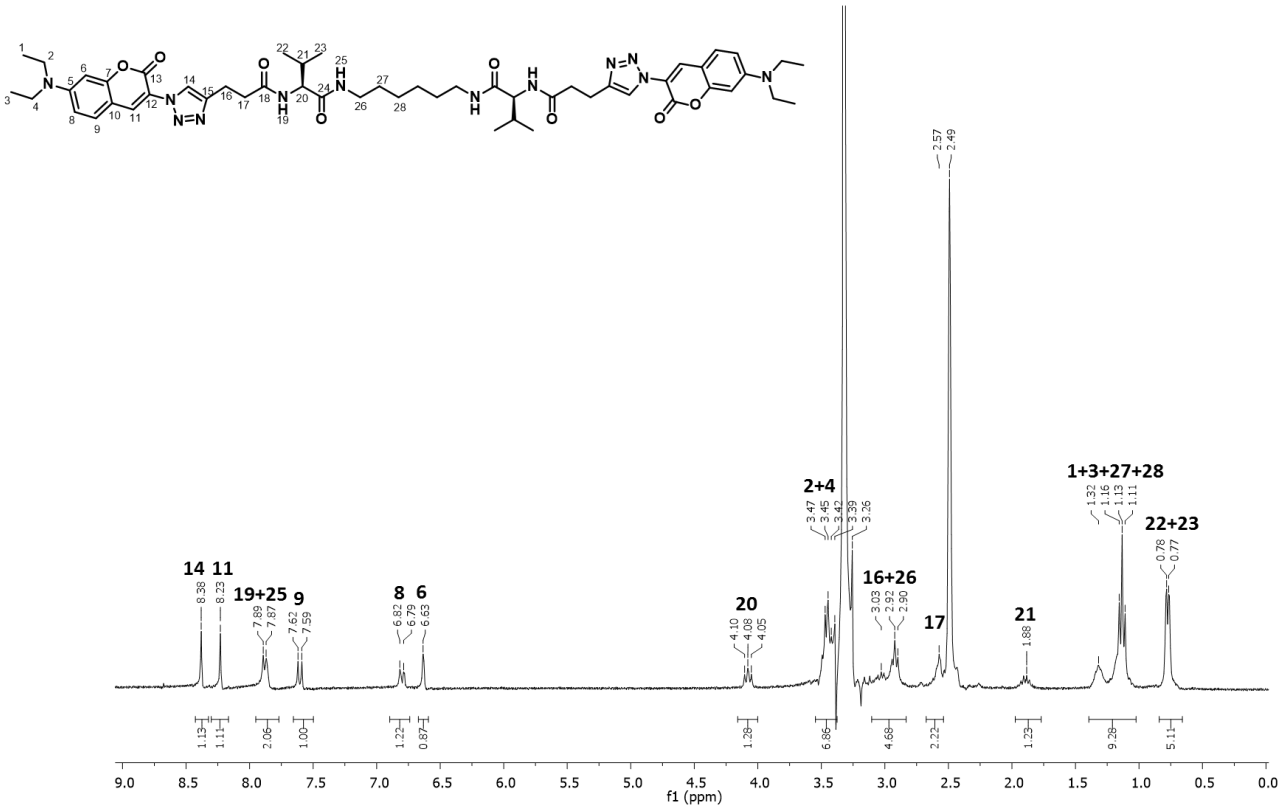

Figure 144. ^{1}H-NMR spectrum of compound **Et$_2$NAzTzVal$_6$** (300 MHz, d$_6$-DMSO).

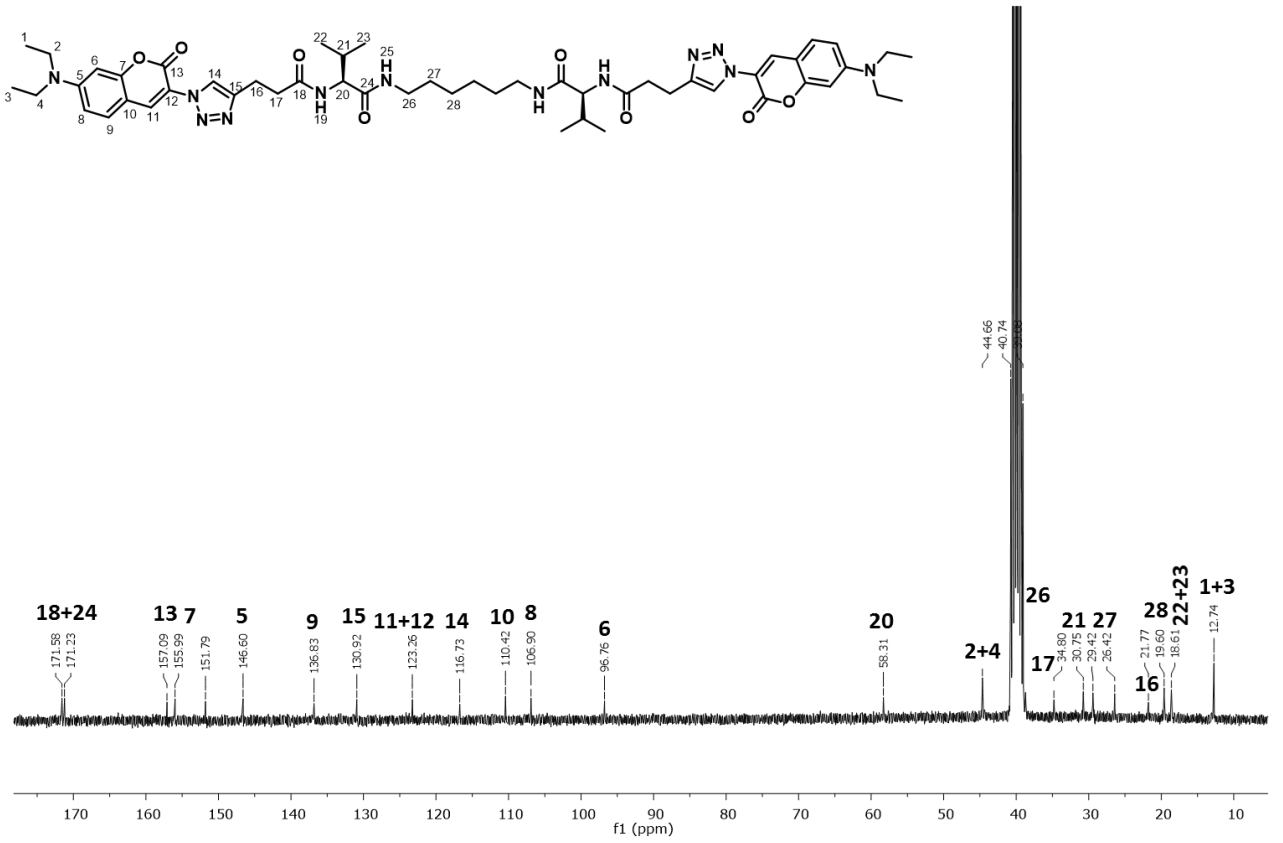

Figure 145. ^{13}C-NMR spectrum of compound **Et$_2$NAzTzVal$_6$** (300 MHz, d$_6$-DMSO).

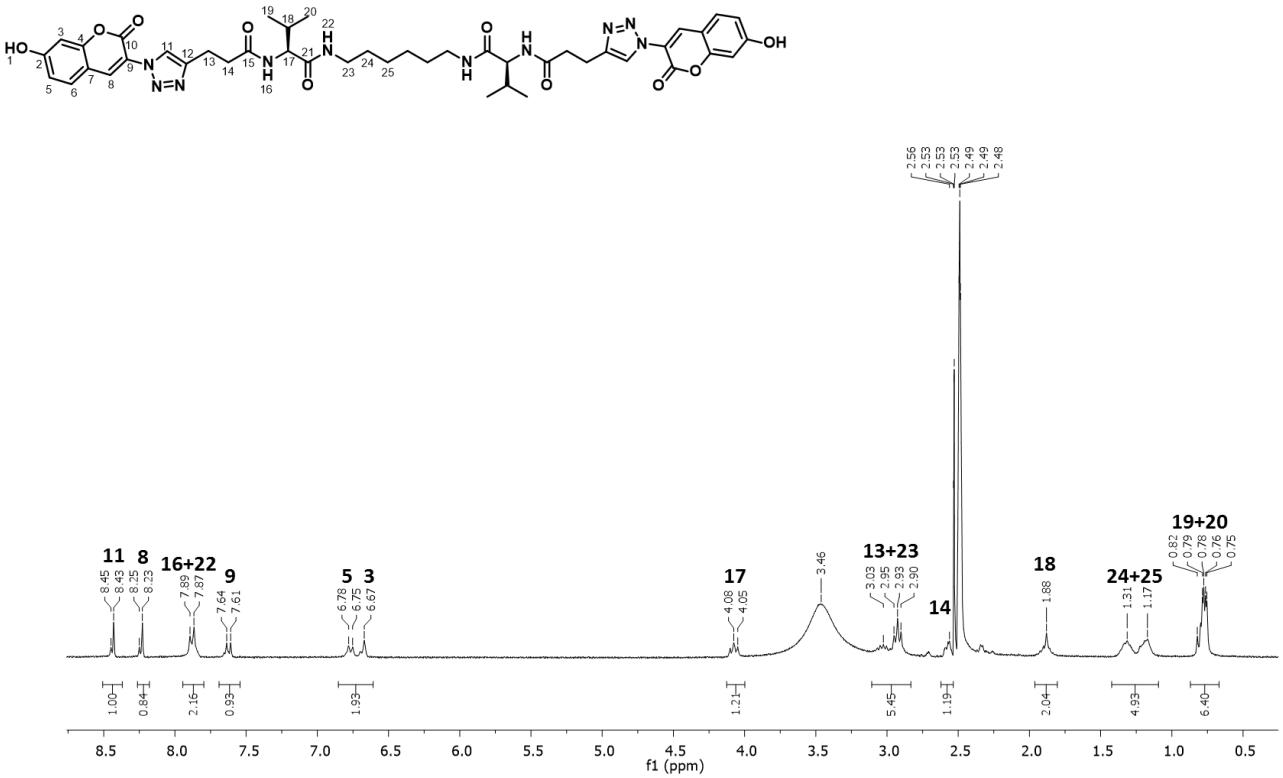

Figure 146. [1]H-NMR spectrum of compound **HOAzTzVal$_6$** (300 MHz, d_6-DMSO).

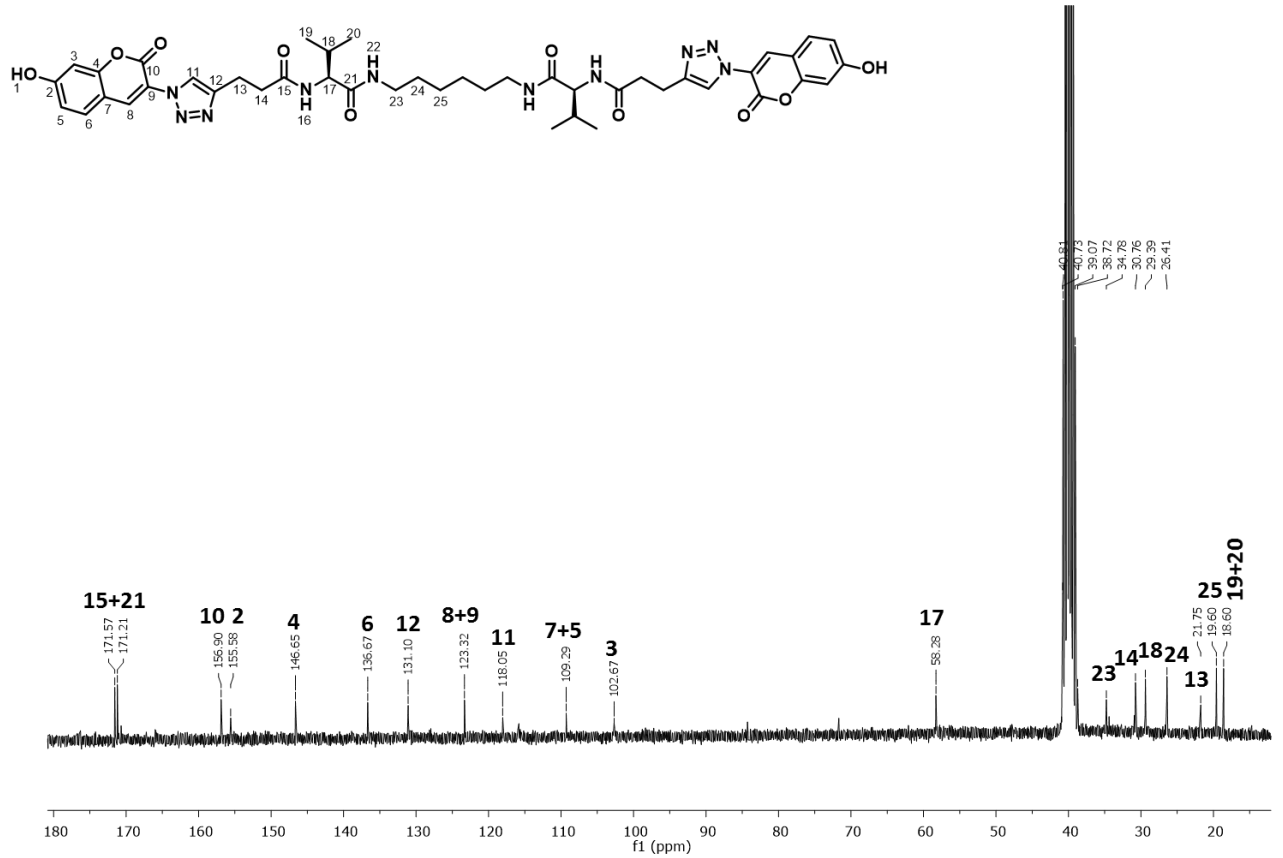

Figure 147. [13]C-NMR spectrum of compound **HOAzTzVal$_6$** (300 MHz, d_6-DMSO).

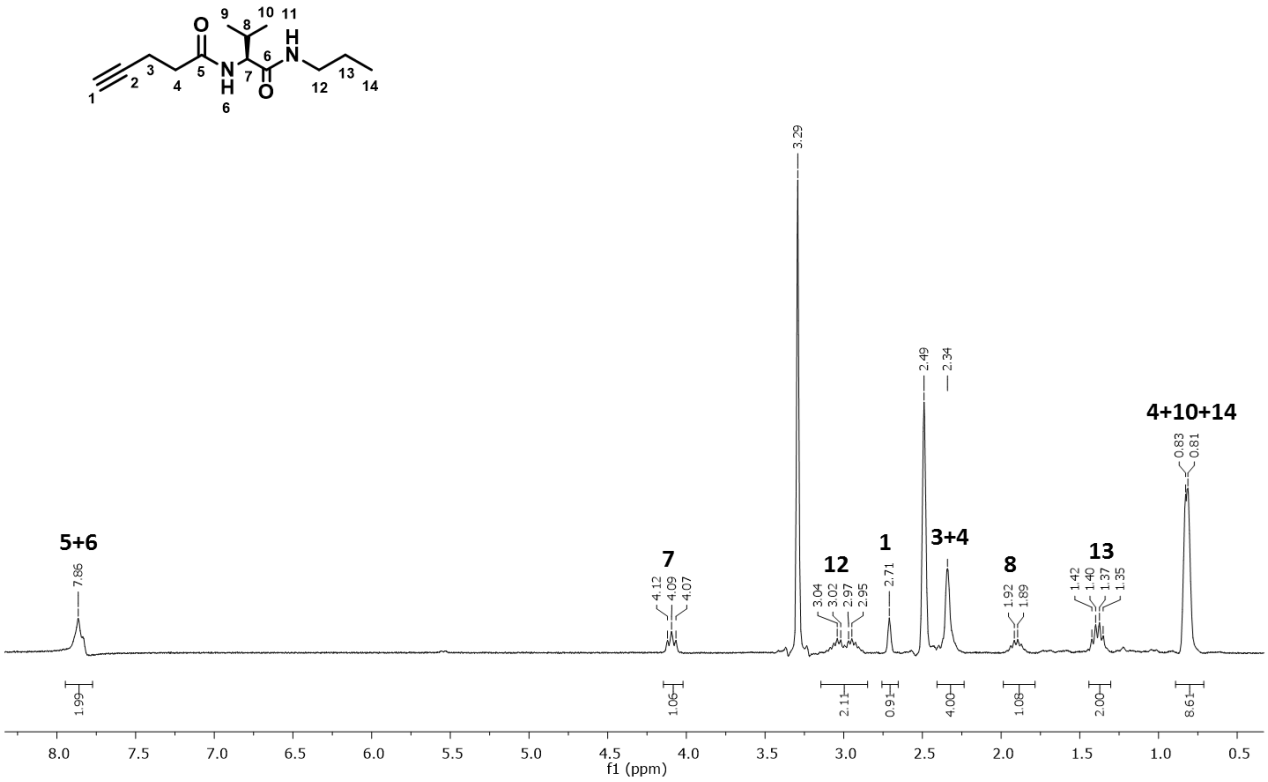

Figure 148. ^{1}H-NMR spectrum of compound **AlkyVal$_3$** (300 MHz, d_6-DMSO).

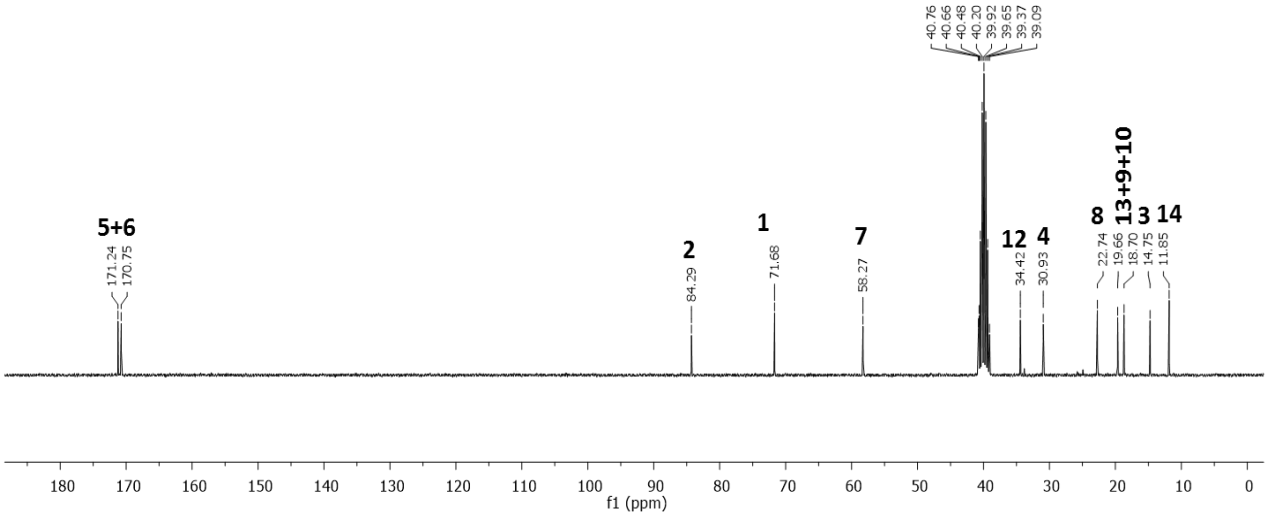

Figure 149. ^{13}C-NMR spectrum of compound **AlkyVal$_3$** (300 MHz, d_6-DMSO).

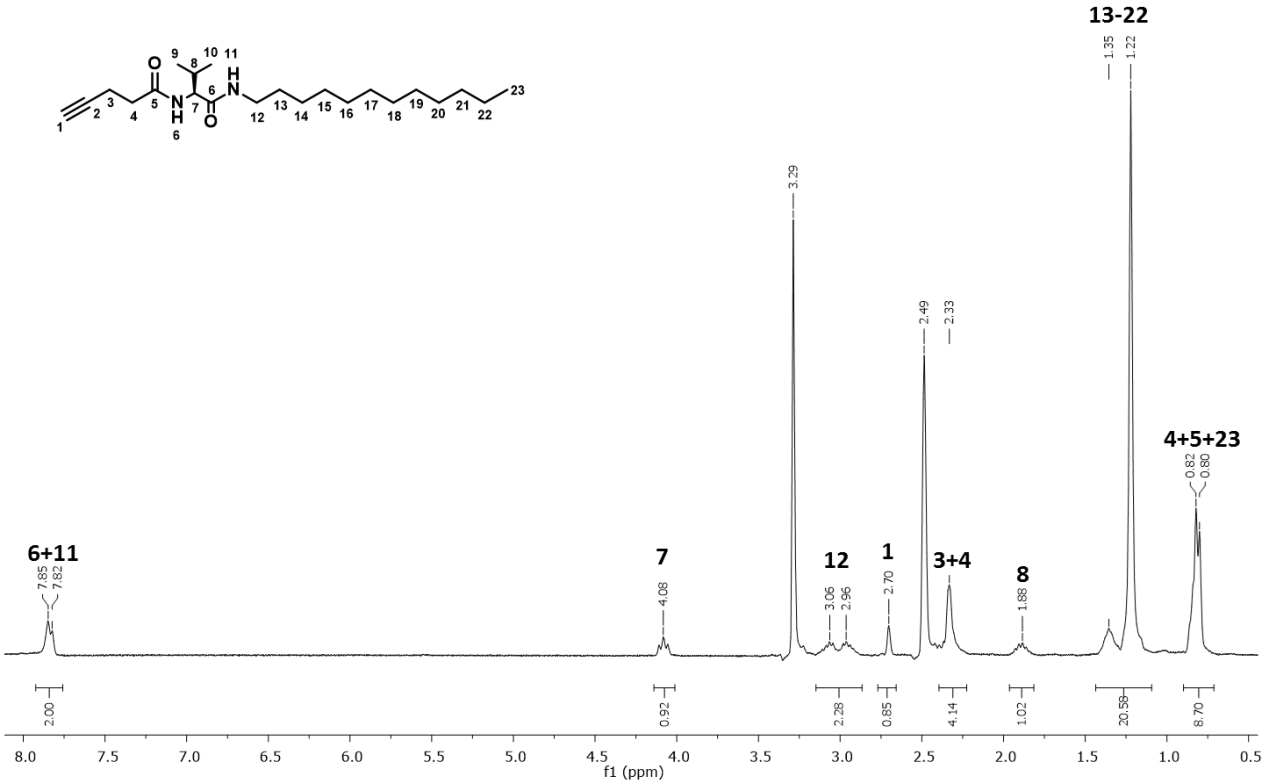

Figure 150. ^{1}H-NMR spectrum of compound **AlkyVal$_{12}$** (300 MHz, d$_6$-DMSO).

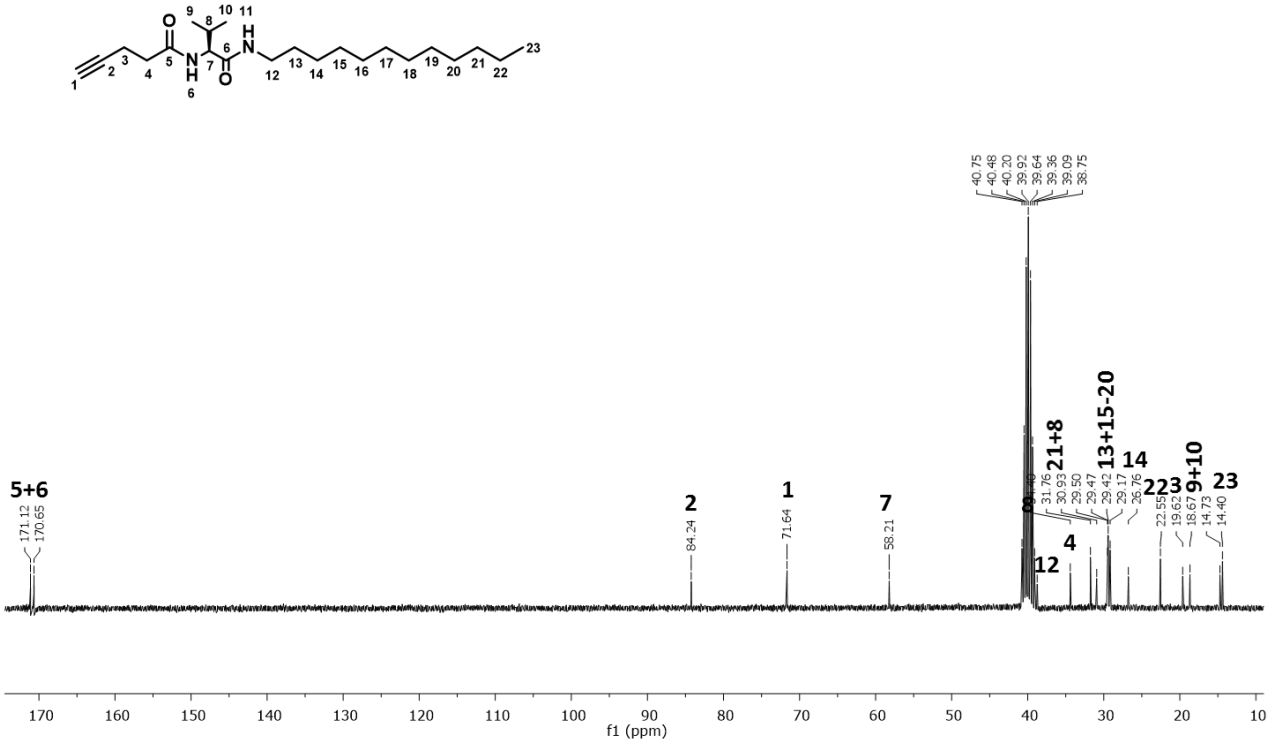

Figure 151. ^{13}C-NMR spectrum of compound **AlkyVal$_{12}$** (300 MHz, d$_6$-DMSO).

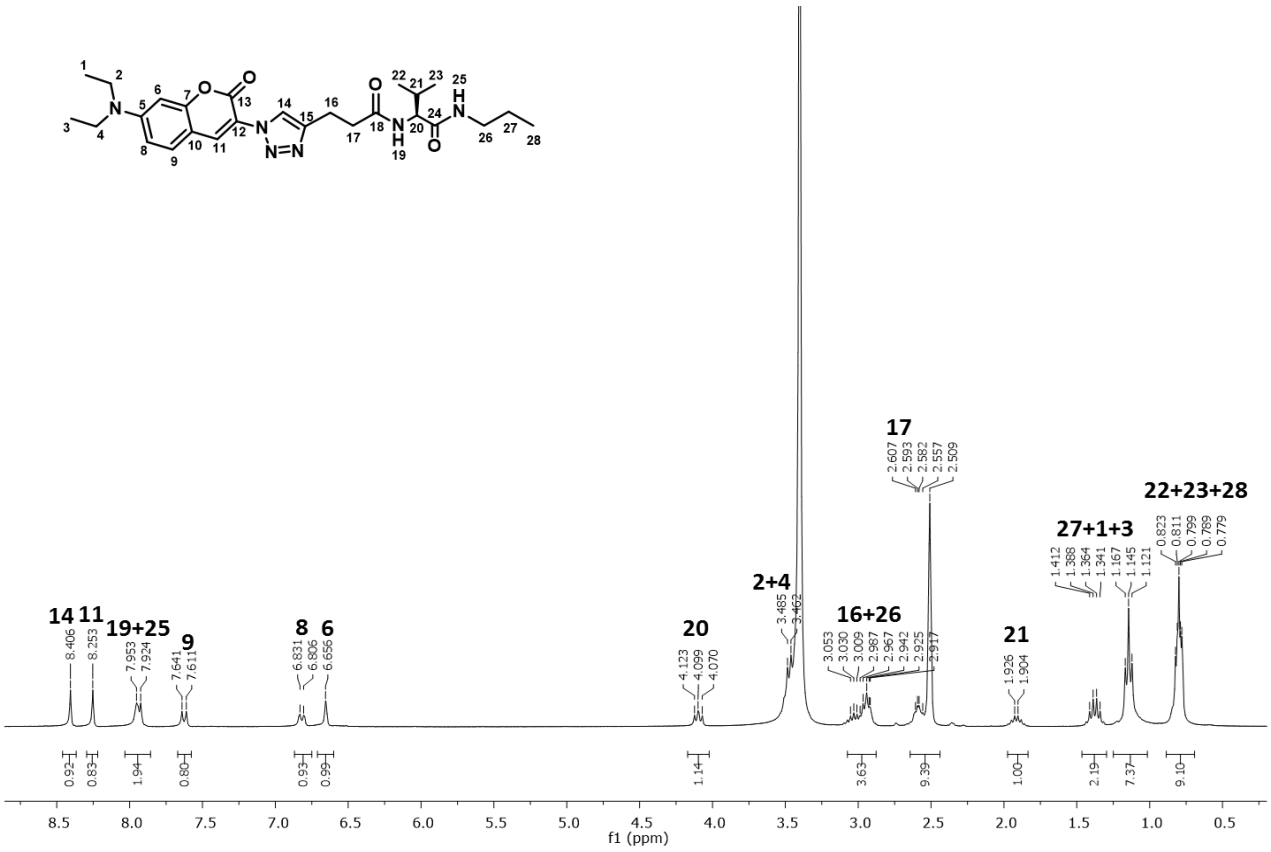

Figure 152. ^{1}H-NMR spectrum of compound **Et_2NAzTzVal$_3$** (300 MHz, d_6-DMSO).

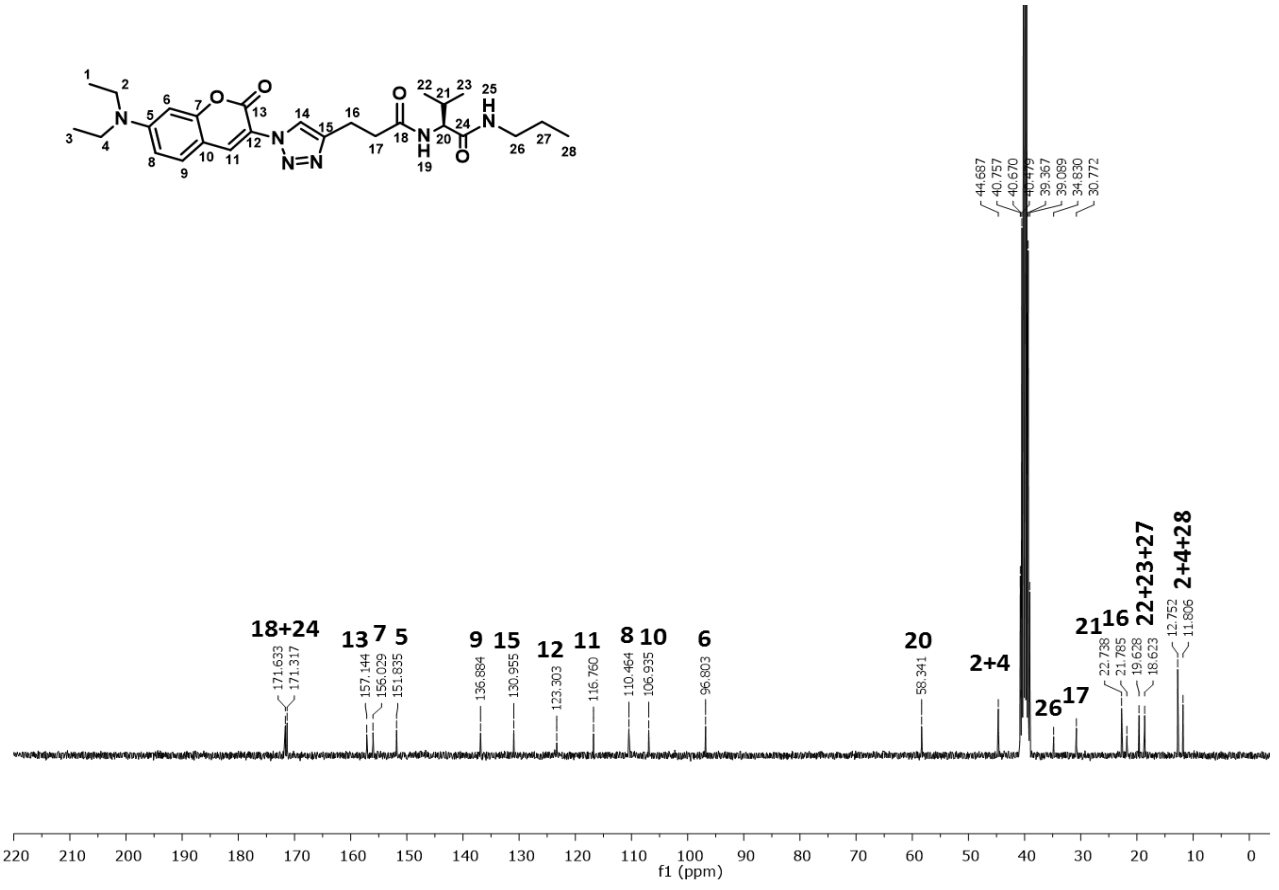

Figure 153. ^{13}C-NMR spectrum of compound **Et_2NAzTzVal$_3$** (300 MHz, d_6-DMSO).

Figure 154. [1]H-NMR spectrum of compound **Et$_2$NAzTzVal$_{12}$** (300 MHz, d_6-DMSO).

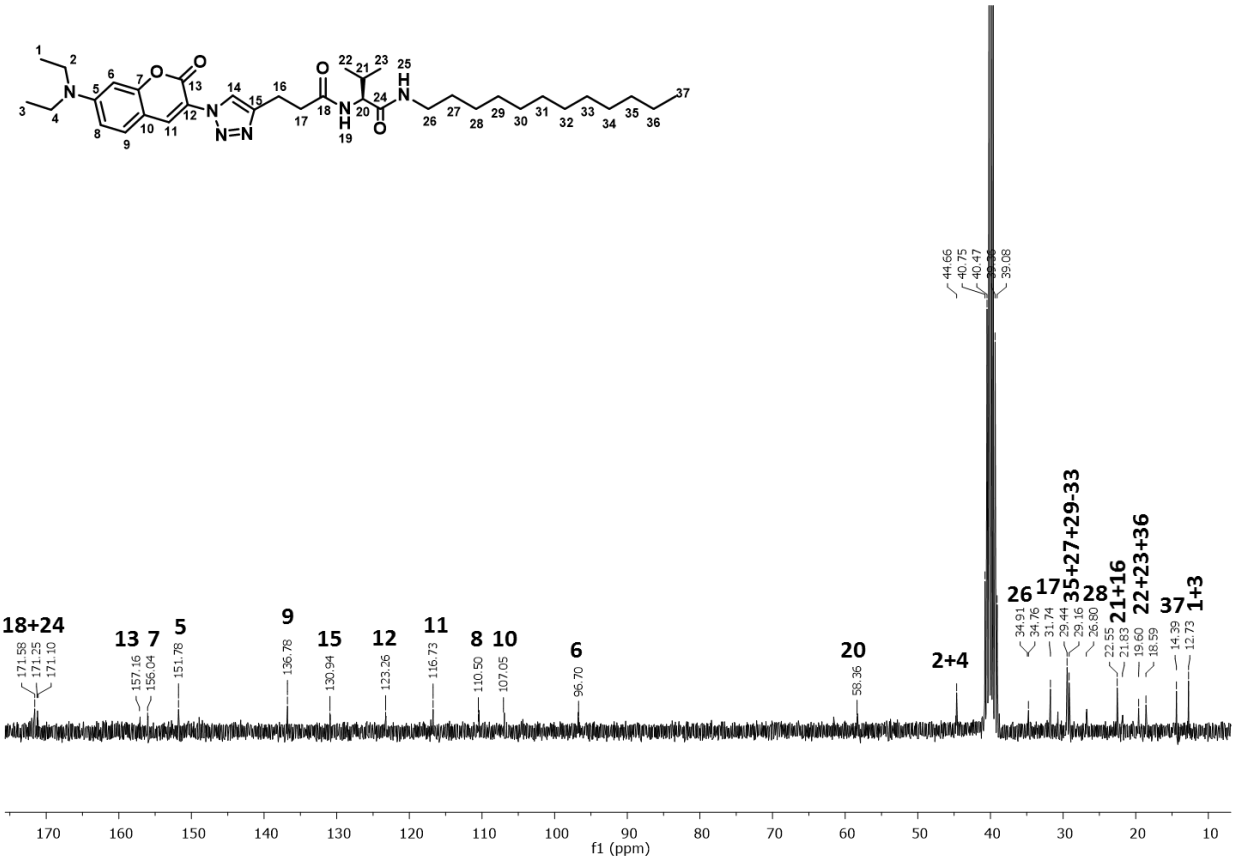

Figure 155. [13]C-NMR spectrum of compound **Et$_2$NAzTzVal$_{12}$** (300 MHz, d_6-DMSO).